UNIVERSITY OF SOUTHAMPTON

Faculty of Natural and Environmental Sciences

Ocean and Earth Sciences

On the fate of plumes from deep-sea oil well blowouts, and their effects on sediment communities

by

Charlotte E. Main

Thesis for the degree of Doctor of Philosophy

April 2015

ABSTRACT

Little is known about the fate of subsurface hydrocarbon plumes from prolonged oil well blowouts, and their effects on deep-sea sediment communities. As deepwater drilling expands in the Faroe-Shetland Channel (FSC), oil well blowouts are a possibility, and the complex ocean circulation of this region presents challenges to understanding possible subsurface oil pathways. Here, questions on the fate and effects of subsurface oil plumes were addressed with experiments and modelling. Experiments were performed on uncontaminated deep-sea sediments from a site remote from the FSC. A three dimensional ocean general circulation model (GCM) was used with a Lagrangian particle tracking algorithm to study patterns of subsurface oil distribution from a release in the FSC for the period 1994 – 2009.

Deep-sea sediment microcosms were incubated in the presence of water accommodated fraction of crude oil (WAF) at low to high (5 % to 50 % by water volume) treatment levels, with sediment community oxygen consumption (SCOC) measured and compared to controls. Sediment macrofauna and bacteria were studied using measures of biomass. The microbial community was further studied using relative abundance and stable carbon isotope ratios ($\delta^{13}C$ values) of phospholipid fatty acids (PLFAs).

Oxygen demand increased significantly at higher treatment levels (25% to 50% WAF). Treatment effects on macrofauna biomass were non-significant. However, there was significant WAF-driven reduction in bacteria biomass, and clear changes in microbial community composition. There were non-significant shifts in the $\delta^{13}C$ values of PLFAs.

Release depth of modelled subsurface plumes affected both the direction and extent of their transport and there was both seasonal and interannual variability. Plumes that were advected into overflow water were carried the furthest (>2500 km in June 2008); westwards through the Faroe Bank Channel towards the Iceland basin, reaching as far as southern Greenland, the Labrador Sea and the Northwest Atlantic. An index of temperature-controlled oxygen consumption rate (simulating oil respiration) indicated that large areas of the subsurface ocean (>50,000 km^2 in 300 m depth water after one month) would be impacted by increased oxygen consumption in the event of a prolonged oil well blowout and the seafloor footprint beneath the plumes could be up to 100,000 km^2. Quantifying impacts of any potential future spill in the FSC will benefit from these investigations on the distribution and effects of subsurface oil in this region.

Table of Contents

Chapter 2: Deep-sea macrofauna and sediment community oxygen consumption rates in the presence of hydrocarbons

Chapter 3: Hydrocarbon contamination effects on deep-sea SCOC and microbial community composition

Chapter 4: Simulating trajectories of subsurface oil using a 3D GCM

Chapter 5: General Discussion

List of tables

Chapter 2

Chapter 3

Chapter 4

List of figures

Chapter 1

Chapter 2

Chapter 3

square = 19:1(n-6); open triangle = 17:1(n-8). (d) square = 15:0; upward pointing triangle = 15:0ai; downward pointing triangle = 16:0; circle = 16:0i; diamond = 18:0; crossed square = 18:1(n-7).

Chapter 4

DECLARATION OF AUTHORSHIP

I, Charlotte E. Main

declare that this thesis and the work presented in it are my own and has been generated by me as the result of my own original research.

On the fate and effects of plumes from deep-sea oil well blowouts, and their effects on sediment communities

I confirm that:

1. This work was done wholly or mainly while in candidature for a research degree at this University;
2. Where any part of this thesis has previously been submitted for a degree or any other qualification at this University or any other institution, this has been clearly stated;
3. Where I have consulted the published work of others, this is always clearly attributed;
4. Where I have quoted from the work of others, the source is always given. With the exception of such quotations, this thesis is entirely my own work;
5. I have acknowledged all main sources of help;
6. Where the thesis is based on work done by myself jointly with others, I have made clear exactly what was done by others and what I have contributed myself;
7. Parts of this work are published as: Main, C. E., Ruhl, H. A., Jones, D. O. B., Yool, A., Thornton, B. and Mayor, D. J. (2015) Hydrocarbon contamination affects deep-sea benthic oxygen uptake and microbial community composition. Deep-Sea Research I.

Signed: .....

Date: .....

Acknowledgements

My list of thanks is typically long, and must start with my supervisors, Henry Ruhl, Andrew Yool and Dan Jones, who I have enjoyed working with immensely. I hope that this will be the start of a long professional association and also friendship. I had the pleasure of working in the field with all of my three supervisors on different occasions, usually involving either copious amounts of mud or some highly technical piece of equipment that didn't want to work, or both. I also benefitted greatly from the wealth of experience that Adrian Martin and Martin Solan brought as panel chairs. The research was funded primarily by the Natural Environment Research Council, through the University of Southampton and Serpent Project.

Dan Mayor became a helpful mentor and supervisor for the experimental part of the project and deserves huge thanks and credit for helping with my education.

Barry Thornton, Maureen Procée and Gillian Martin provided lab support and excellent tuition at the James Hutton Institute in Aberdeen.

Colette Cheng, Alice Horton and Josh Pedar were all tireless assistants onboard the research cruises where the experiments were performed. Also, it is difficult to see how the experiment could have been possible without the immense help and technical assistance of Duncan Mathew. Thanks also to the other scientists and ships' crew from JC062 and D377, and to Ben Boorman, who designed and built much of the experimental apparatus.

Steve Rider from SGS provided the crude oil for my experiments. At the time when I needed the oil, I was living over the road from a BP oil terminal and called over one day to see what they could do. Unfortunately, there was such an enormous amount of 'red tape' involved with dealing with BP at that time that things started to look bleak. Then some helpful contacts I had made through the Hamble Conservation Volunteers put me in touch with SGS, who test the oil as it comes out of the pipeline from Wytch Farm.

I would like to thank Katya Popova for introducing me to Ariane and Yevgeny Aksenov and Christian Florindo Lopez for advice on extracting sections from the NEMO output

for model validation. Penny Holliday also provided valuable advice for the model validation. I gratefully acknowledge the assistance of Jeff Blundell and Josie Robinson with various technical and network issues.

The University of Southampton has been incredibly supportive over the years, providing me not only with PhD support and education but also funding a fantastic opportunity to suspend my project and work at Woods Hole Oceanographic Institution in the Chris Reddy lab. Speaking of education, the bacteria *Bordetella pertussis* taught me that I am no longer invincible as I was preparing for my upgrade assessment, shortly before I left for the USA. I suppose I should in some way be grateful for learning that, though I didn't much enjoy the 100 days they spent in my lungs.

Some other friends of mine who deserve particular thanks are:

Julie Black, Marianne James and Mike Reading for proofreading; Debby Besford for being there on the end of a phone or train line at some of the more mentally taxing moments, Kirsty Robson and Helen Smith also for providing me refuge, and Greg Blaeford for simply 'getting me.'

During this project I have had the great fortune to be able to fulfil other long-held ambitions, including an ascent of the Old Man of Hoy. Although maintaining any kind of sensible work-life balance through fieldwork and thesis writing has got the better of me on many an occasion, I can hardly imagine a place on this planet where I could feel more enthralled than on rock near to ocean. So for me, the words of Friedrich Nietzsche surely sum up these kinds of endeavours the best, be they theses, or seastacks:

"On the mountains of truth you can never climb in vain: either you will reach a point higher up today, or you will be training your powers so that you will be able to climb higher tomorrow."

Table of Acronyms

DM	Darwin Mounds
DWH	Deepwater Horizon
EEL	Extended Ellett Line
EIA	Environmental Impact Assessment
FAME	Fatty acid methyl ester
FBC	Faroe Bank Channel
FSC	Faroe-Shetland Channel
FSCBW	Faroe-Shetland Channel Bottom Water
GCM	Ocean general circulation model
GLS	Generalised least squares models
IAEA	International Atomic Energy Agency
ISOW	Iceland Scotland Overflow Water
LADCP	Lowered Acoustic Doppler Current Profiler
LME	Linear mixed effects models
MNAW	Modified North Atlantic Water
NAC	Norwegian Atlantic Current
NADW	North Atlantic Deep Water
NAO	North Atlantic Oscillation
NSAIW	Norwegian Sea Arctic Intermediate Water
NSDW	Norwegian Sea Deep Water
NEMO	Nucleus of European Modelling of the Oceans

PLFA	Phospholipid fatty acid
RDA	Redundancy analysis
SAC	Special Area of Conservation
SCOC	Sediment community oxygen consumption
SPE	Solid phase extraction
WAF	Water accommodated fraction
WTR	Wyville-Thomson Ridge

Chapter 1: General Introduction

1.1 Context

Modern societies remain largely dependent on crude oil as a material and energy resource. This has pushed the frontiers of oceanic oil drilling to exploit previously inaccessible reserves, for example those found on the continental slope.

The 2010 Macondo oil well blowout was the largest accidental input of hydrocarbons into the deep sea from a single incident (DHSG, 2011), resulting in a prolonged (87 days) release of crude oil and gas into the deep (~1600 m) waters of the Gulf of Mexico. When the oil well was finally capped in July 2010, some estimates for the total amount of oil spilled had reached 4.9 million barrels[1] (McNutt *et al.*, 2011). There was uncertainty around the true amount of oil spilled, where it went and what effects it had on biota in the deep sea. This was because it became clear that a large amount of oil never reached the surface (Ryerson *et al*., 2011; Reddy *et al*., 2011). Much of this subsurface oil, as well as that from surface slicks, ultimately contaminated the seabed (Montagna *et al*., 2013; Fisher *et al*., 2014). Although some of the environmental impacts of this oil at the deep-sea floor have been documented (White *et al*., 2012) the true extent of its distribution and effects remains uncertain (Valentine *et al*., 2014).

The Macondo spill made history, being widely regarded as the worst accidental oil spill to date, with the highest estimates of hydrocarbons entering the ocean as a result of a single release. In addition, chemical dispersants were injected at the leaking well head for the first time as part of the incident response, as well as being applied at the surface. Science and technology were mobilised in order to try and begin to understand the pathways that oil had entered in the deep sea. For example, an autonomous underwater vehicle was used to map large subsurface oil plumes that became entrained into deep water currents (Camilli *et al*., 2010). State-of-the-art ocean general circulation models were used to simulate transport of oil at and below the surface, to compare with satellite

[1] One 'barrel' of crude oil is approximately equivalent to 120 litres at atmospheric pressure and 20°C.

imagery of slick extent (Liu *et al*., 2011a). Subsequently, work has also been done to model the evolution of the plume of oil from the leaking well (Socolofsky *et al*., 2011), the dispersal of dissolved and neutrally buoyant plumes (Adcroft *et al*., 2010) and their potential effects on deep ocean biota (Valentine *et al*., 2012). The Gulf of Mexico has become one of the most intensely studied ocean regions on the planet, with a globally significant research initiative set up around understanding the effects of what became known as the 'Deepwater Horizon' spill (DWH) - after the drilling rig that sank at the well during the disaster.

A six month moratorium declared by the U.S. Department of the Interior on 30th May 2010 prevented drilling in water deeper than 150 m in the USA for a period following the DWH spill. Despite this, drilling deep has progressed unimpeded in many other parts of the world. In 2011, around eight million barrels of oil per day were being produced from deep water reserves beyond the continental shelf-edge break at about 250 m water depth (Leffer *et al*., 2011). Companies are now keen to exploit deeper oil reserves, despite clear evidence that the burning of fossil fuels has caused dramatic increases in atmospheric carbon dioxide levels (Keeling *et al*., 2005) that has led to alarming global climate change (IPCC, 2014). Nevertheless, as reserves beneath shallow water become depleted and it becomes more economically viable to drill deeper, countries such as the UK, Faroe Islands, New Zealand, Norway, Canada, Angola and Brazil all have, or are developing, plans for deep water drilling programmes. The distribution and effects of oil from a large spill would be highly influenced by the oceanic conditions present at any of these drilled locations.

In this study, experiments and models were used in novel ways to address some of the questions surrounding the potential dispersal of subsurface oil, and its effects on biological processes of deep-sea benthic communities. The work draws on what has been published so far in the emerging field of deep water oil pollution research, much of which has been addressed at understanding the DWH spill.

1.2 Evolution and persistence of subsurface plumes of hydrocarbons from a leaking well

Oil and natural gas that leaked from the Macondo well entered the deep ocean as a high pressure jet at temperatures around 100°C warmer than the surrounding water (Reddy *et al*., 2011). Large quantities of the oil and gas were propelled rapidly towards the surface. However, as the main column of oil, gas and droplets rose through the water, very small (<100 µm diameter) droplets of oil were able to form a neutrally buoyant layer of hydrocarbons that remained at between 800 to 1300 m water depth (Socolofsky *et al*., 2011). Soluble compounds, including natural gas and monoaromatic hydrocarbons; benzene, toluene, ethyl-benzene and xylene (collectively: BTEX) also dissolved in the seawater. Dispersants were used at the well head to further encourage the formation of small droplets and slow the progression of oil to the surface, thus contributing to the formation of large, neutrally buoyant, subsurface plumes of hydrocarbons (Figure 1.1.).

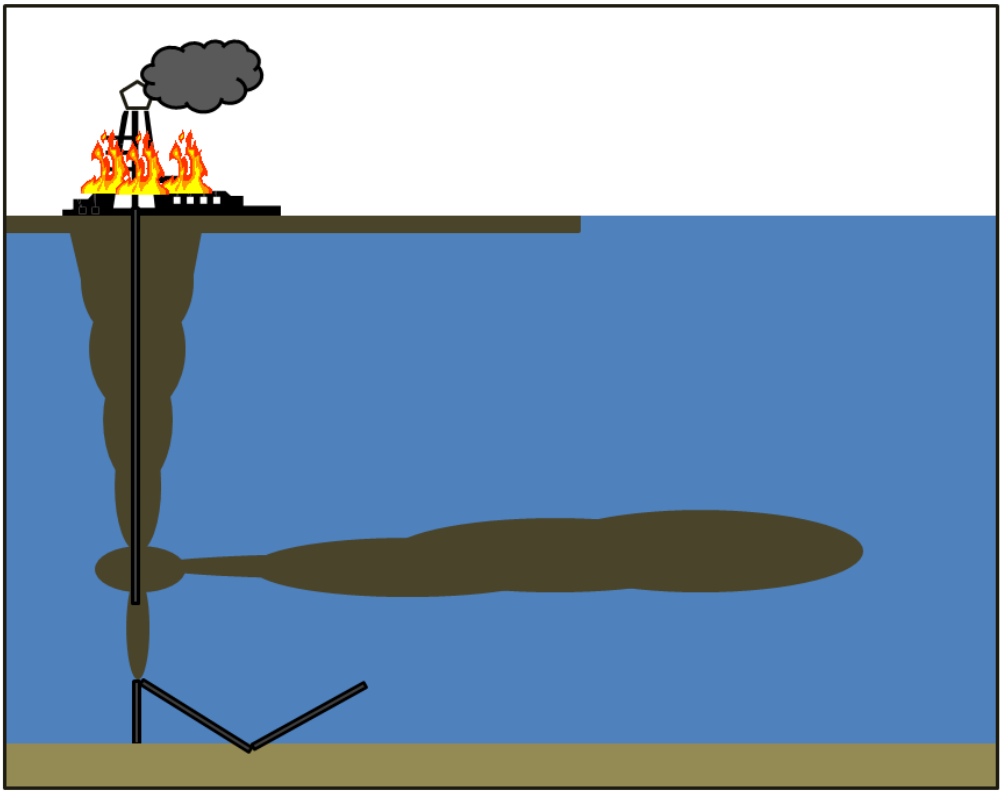

Figure 1.1. Plume formation in the deep Gulf of Mexico following the 2010 Macondo oil well blowout.

These plumes were entrained into the deep water currents of the Gulf of Mexico where they persisted for months. Camilli *et al*. (2010) used an autonomous underwater vehicle to map trajectories of the plumes. They detected hydrocarbon layers of dissolved BTEX and naphthalene peaking at around 1100 to 1300 m water depth. They also measured depletions in oxygen concentration within the plumes. It was not technically possible to ascertain the true extent of the plumes, but one was mapped to the southwest of the leaking well for over 35 km in June 2010 (Camilli *et al*., 2010). The plumes were composed mainly of methane, ethane and propane in dissolved and gas hydrate forms; dissolved hydrocarbons (BTEX) and small oil droplets of unknown composition (Camilli *et al*., 2010; Ryerson *et al*., 2011; Reddy *et al*., 2011).

Various reports were issued on the levels of hydrocarbon degradation that took place within the plumes. These included 'not substantial' degradation rates in plumes composed largely from BTEX (Camilli *et al*., 2010). In contrast, large depletions of ethane and propane relative to methane were attributed to microbial respiration by Valentine *et al*. (2010).

The plumes triggered blooms of indigenous deep-sea bacteria including γ-Proteobacteria, a group that are related to petroleum degraders (Hazen, *et al*., 2010). The response of deepwater bacteria communities was strong enough to cause appreciable local oxygen anomalies as they respired dissolved methane (Kessler *et al*., 2011), propane and ethane (Valentine *et al*., 2010). The relatively cool temperatures of the deep sea (~ 4°C in the deep Gulf of Mexico) appeared to favour certain genera (*Oceanospirillales*, *Colwelia* and *Cycloclasticus*) that were found at depth but not in surface slicks of oil (Redmond & Valentine, 2011). *Colwelia*, in particular, was adapted to the colder temperatures of the deep Gulf of Mexico, and experiments with benzene labelled with the heavy isotope ^{13}C confirmed that these bacteria were able to use benzene as a carbon source (Redmond & Valentine, 2011). In other experiments, colonies of *Colwelia* sp. and *Oceanospirillales* formed bacterial flocs in mixtures of MC252 oil and Corexit 9500 dispersant, degrading up to ~ 60% of the oil in microcosms during 20 days of incubation, and preferentially targeting straight chain compounds such as alkanes Bælum *et al*. (2012).

There were further processes that led to the entrainment of oil beneath the ocean surface in addition to these water-borne plumes. A 'dirty blizzard' of aggregates composed oil

and sinking marine snow (Passow *et al*., 2012) formed layers of Macondo oil contamination in deep-sea sediments within 25 km of the Macondo well head (Montagna *et al*., 2013). Recent evidence has found that there was contamination caused by fallout from the plumes. White *et al*. (2012) documented an oily sludge at the seabed beneath the path of a plume that was traced to hydrocarbons from MC252 oil from the Macondo well. An area estimated at 3,200 km^2 of seabed around the Macondo well was contaminated by fallout from plumes (Valentine *et al*., 2014). A further hypothesis, the 'toxic bathtub ring', has been suggested to have resulted in hydrocarbons in the plumes contacting the seabed through their advection over a slope. The possible routes of hydrocarbons reaching the seafloor warrants further study, as do their effects on deep sea biota and processes.

1.3 Deep-sea sediment communities

Below the euphotic zone, energy input to heterotrophic marine biota is mainly via a downward flux of particulate organic carbon (POC, Billet *et al*., 1983). This POC is made up from a mixture of labile and refractory lipids deriving from organic phytodetritus and zooplankton faecal pellets (Laureillard *et al*., 2004). As it sinks through the water column, POC, or 'marine snow,' is largely remineralised, mainly by marine bacteria (Azam *et al*., 1983). However, a small fraction of the total POC sinks out of the water column to the deep-sea floor. Organic detritus arriving at the seabed is processed by the sediment community, of which megafauna (Smith, 1992); macrofauna (Sun *et al*., 1999); foraminifera (Gooday, 1988) and bacteria (Lochte & Turley, 1988; Witte *et al.*, 2003) are important constituents. The relative fraction of organic carbon that is processed by different components of the deep-sea benthic community, whether respired or incorporated into biomass has been assessed experimentally *ex situ* and measured *in situ* and depends on, for example: detritus composition; feeding strategies of the benthos; depth or temperature (Lohse *et al*., 1998; Heip *et al*., 2001; Gontikaki *et al*., 2011a; Gontikaki *et al*., 2011b; Hughes *et al*., 2011).

The linkages between detrital flux, its consumption and utilisation by deposit feeders are complex. In the deep-sea most of the organic carbon arriving at the seabed is respired, either by free-living sediment bacteria or by metazoans directly. However,

since much of the organic carbon is refractory in nature and thus hard to digest, it has been recently proposed that much of the organic carbon needs to be first ingested by deposit feeding metazoans harbouring specialised bacteria in their guts (Rowe & Deming, 2011). It is quite possible – as with shallow water benthos, where spatial orientation of food resources can result in niche differentiation between bacteria and macrofauna (van Nugteren *et al*., 2009) – that this mechanism could also operate in the deep-sea. Deep-sea benthic communities respond to changes in food supply as shown by evidence of community change in the abyssal North Atlantic (Ruhl & Smith, 2004) and discrepancies in measurements of benthic oxygen consumption rates in the North Pacific (Smith *et al*., 1992).

In relation to the water column above them, deep-sea sediments are responsible for only a small amount of remineralisation of carbon and macronutrients. However, their role is nevertheless important for biogeochemical cycling. For example, biotic processes in the deep sea carry out and mediate long-term burial of carbon. Hence they therefore play a part in overall ecosystem functioning (Middelburg & Meysman, 2007).

Ecosystem functioning relies on the transfer of organic matter, its decomposition and nutrient regeneration by living organisms and is thought to depend on biodiversity of communities both in terrestrial (Naeem *et al*., 1994) and marine environments (Danovaro *et al*., 2008). Ecosystem functioning in the deep sea has becoming an area of concern in terms of anthropogenic impacts (Danovaro *et al*., 2008; Ruhl & Smith, 2004; Ramirez-Llodra *et al*., 2011).

1.4 Dissolved hydrocarbons and their study in experimental aquatic systems

Monoaromatic hydrocarbons[2] (MAHs) are among the few hydrocarbons that are slightly water-soluble, and made up a large proportion of the neutrally buoyant plumes following the DWH spill (Reddy *et al*., 2011). Monoaromatic hydrocarbons have generated previous interest in terms of oil pollution (Rowland *et al*., 2001; Smith *et al*., 2001) and are among the more toxic hydrocarbons found in crude oil (Neff *et al*., 2000). They are considered to be very harmful to humans, for example, benzene (Figure 1.2) is considered to be highly carcinogenic (Delore & Borgomano, 1928; Yardley-Jones *et al*., 1991; Li *et al*., 2014). As a result, the measurement of BTEX is carried out routinely in pollution assessments where, for example, there is concern over contamination of groundwater by hydrocarbons (Doherty & Otitoloju, 2013).

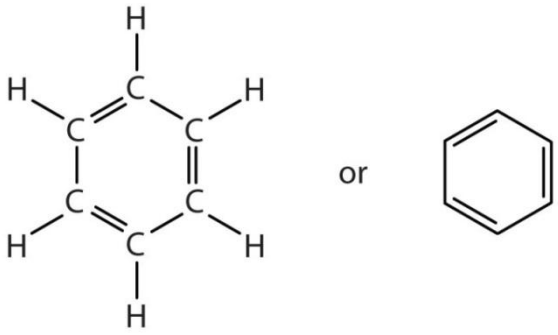

Figure 1.2. The chemical structure of benzene represented explicitly (left) and diagrammatically (right).

The study of oil pollution is challenged by the complexity of its composition. Crude oil is a complex mixture of many different hydrocarbon compounds. Its chemical

[2] Monoaromatic hydrocarbons possess one benzene ring. Benzene is an organic compound with the formula C_6H_6. A benzene ring is an arrangement of six carbon atoms; three with double bonds. The electrons forming the double bonds are actually shared, such that the double bonds can be considered to be formed in any alternating arrangement. Other monoaromatic hydrocarbons are compounds similar to benzene that have similar properties. For example, toluene, C_7H_8, has one benzene ring with one methyl group (CH_3) attached to a carbon atom.

composition is impossible to fully resolve, leading to an unresolved complex mixture of hydrocarbons (UCM) responsible for the toxicity of whole oil (Scarlett et al., 2007a). The composition of crude oil also varies according to extraction location (Hahn-Weinheimer & Wirner, 1980). It has been difficult to develop standardised methods for the addition of crude oil to aquatic experimental systems, not least because most of the hydrocarbons that make up bulk crude oil are insoluble in water. Also, the lighter, more volatile fractions (e.g. BTEX) readily evaporate, meaning that bulk composition of oil continually changes when in contact with air. Consequently, many studies have utilised a solution containing hydrocarbons as a proxy for bulk oil because of the possibility of standardising production of a solution that can easily and reproducibly be used as a treatment relating to a specific crude oil.

A water accommodated fraction of crude oil (WAF) is a laboratory-prepared solution made by low energy mixing of crude oil and water. The mixture must be stirred for a long enough duration (at least 24 hours) that a stable composition of solutes is achieved (Coelho & Aurand, 1997; Faksness *et al*., 2008). A WAF is not filtered, technically distinguishing it from the water soluble fraction of crude oil (WSF), which has also been used in toxicity studies (Faksness *et al*., 2012). The effects of WAF and WSF on aquatic invertebrate fauna have been extensively studied through acute (Long & Holdway, 2002; Bejarano *et al*., 2006) and chronic (Scarlett et al., 2007b) toxicity testing. Dissolved hydrocarbons have also been employed to study crude oil exposure effects on reproductive success (Lewis *et al*., 2008) and larval development (Neff *et al*., 2000). The composition of WAF is directly related to that of the parent crude oil from which it is produced, with resulting differences in toxicity levels of WAF produced from different parent oils (Hokstad *et al*., 1999).

1.5 Measuring impacts of oil pollution on benthic communities

Observational studies have aided the development of conceptual models to study pollution-induced disturbance of benthos. For example, Pearson and Rosenberg (1978) proposed a conceptual model of macrobenthic succession along a gradient of organic enrichment (hereafter, the P-R model). The P-R model suggested that profiles of species numbers, abundance and biomass of an invertebrate community followed characteristic patterns in relation to one another in response to a disturbance and through their subsequent recovery. The P-R model was based on benthic datasets from a study of organic enrichment from sewage sludge. However, Grassle and Grassle (1974) drew upon some of the key concepts of the model to study a coastal oil spill. In particular, they noted a characteristic succession in terms of re-colonisation of the area following the spill, with small, short-lived, opportunistic species being the first to reappear in large number, followed by larger, longer-lived species that were more characteristic of the community prior to the disturbance. The P-R model has not always held up in quantitative analyses (Maurer *et al*., 1993; Gray *et al*., 2002). However, its concepts have endured as the basis for ecological disturbance investigation in some cases (e.g. Magni *et al*., 2009).

A range of studies have measured the composition of macrobenthic species assemblages in order to evaluate chronic impacts of oil industry operations on the continental shelf (e.g. Gray *et al*., 1990; Daan *et al*., 1994) and their recovery from oil industry disturbance (Mair *et al*., 1987). Benthic community composition has also been used to evaluate the severity and recovery of oil spills (Dauvin 1998; Feder & Blanchard, 1998; Dauvin, 2000). Macrofauna and meiofauna diversity and abundance were used to define the benthic footprint of contamination of the 2010 DWH spill (Montagna *et al*., 2013).

It has been suggested that taxonomic level does not necessarily need to be resolved to species level in order to detect pollution stress (Olsgard *et al*., 1997). For instance, some studies have utilised photographic surveys of clearly visible megafauna (animals > 1 cm in any dimension) to assess disturbance (e.g. Jones *et al*., 2007; Hughes *et al*., 2010) and recovery (Gates *et al*., 2012). Photographic surveys may be useful in situations

where it is not possible to collect sufficient replicates of macrofauna or meiofauna for the statistical analysis change in benthic communities.

Certain species and groups of macrofauna and meiofauna have been proposed as bio-indicators of benthic pollution disturbance, for example, foraminifera (Denoyelle *et al*., 2010; Hess *et al*., 2013).

The response of macrofauna to organic enrichment can also be assessed using the Infaunal Trophic Index (ITI, Word, 1979). The ITI compares the abundance of individuals from four macrofaunal groups, defined on the basis of their trophic mode (i.e. suspension feeders, and sediment surface/subsurface deposit feeders).

Phylum-specific adaptations (e.g. shell closing in bivalves; Tran *et al*., 2003) may make particular animals less susceptible to oil pollution. In contrast, certain genera of amphipods (e.g. *Ampelisca*) are particularly susceptible to oil toxicity (Dauvin, 1998). As a result, the response of a whole benthic community to spilled oil depends on the proportion of susceptible species present (Dauvin 1998, 2000).

1.6 Oxygen consumption measurements in ecology

1.6.1 Sediment community oxygen consumption

Environmental disturbance of individuals, species or functional groups can be evaluated by measuring sediment oxygen dynamics in association with biology (Smith & Teal, 1973; Hyland *et al*., 2005; Glud, 2008).

Respiration, the chemical reaction on which all heterotrophic biology depends for an energy supply, relies heavily on oxygen as the terminal electron acceptor (TEA). While anaerobic respiration using alternative TEAs is possible, the energetic returns using these can be considerably lower. Beneath the oceanic euphotic zone, the energy input to heterotrophic marine biota is mainly via a downward flux of particulate organic carbon (POC, Billett *et al*., 1983) composed of a mixture of labile and refractory lipids deriving from organic phytodetritus and zooplankton faecal pellets (Laureillard *et al*., 2004). A large proportion of POC generated in the euphotic zone is respired (or ‘remineralised’) as it sinks through the water column, mainly by marine microorganisms (Azam *et al*.,

1983). However, a small fraction sinks out of the water column to the deep-sea floor, where it can be rapidly processed by resident fauna and bacteria (Lochte & Turley, 1988; Gooday, 1988; Witte *et al*., 2003). Hence, strong links, or 'pelagic-benthic coupling' exist between processes happening at the surface, in the water column and at the deep-sea floor (Graf, 1989). Oxygen consumption rate is directly related to the rate of carbon remineralisation, according to the assumption that the amount of oxygen consumed is approximately equal to the amount of carbon dioxide respired (Hargrave, 1973). This means that rates of carbon remineralisation at depth can be used to estimate rates of food supply from the euphotic zone (Jahnke, 1996). The relationship between biomass and food supply has been used with inverse modelling to establish potential differences in the roles of labile detritus versus non-labile detritus in the support of an abyssal depth food web (van Oevelen *et al*., 2012).

At continental slope depths (~1000 m) of the North Atlantic, Heip *et al.* (2001) reported that macrofauna and bacteria were important contributors to sediment community oxygen consumption and hence carbon remineralisation. However, the remineralisation rate attributed to bacteria was not directly measured – merely estimated by subtraction from total SCOC the proportion attributed to other groups including macrofauna and meiofauna.

1.6.2 Respiration rate changes in response to stress

Changes in respiration rate have been measured in a range of studies on stress of both individuals and communities of benthos because of the role of this process in ecosystem functioning. For example, respiration and heart rate increased in Arctic spider crabs, *Hyas araneus*, exposed to polycyclic aromatic hydrocarbons (PAHs) in the laboratory (Camus *et al*., 2002). The total oxygen demand of an entire sediment community of bacteria and fauna (hereafter sediment community oxygen consumption, SCOC) has also been used to indicate whole community metabolism in relation to stress. For example, Olsen *et al*. (2007a) who used slurry experiments to compare sediment oxygen demand of Arctic and temperate sediments in the presence of oil, found that Arctic sediments consumed significantly more oxygen over experimental incubations of 21 days at ambient temperature. Oxygen consumption rate of organisms has been used

previously to indicate health status though measures such as the 'scope for growth' (Widdows *et al*., 1995). Hence, elevated respiration rates in Arctic sediments exposed to oil (Olsen *et al*., 2007a) may indicate that these sediments were comparatively more sensitive to oil pollution than the temperate sediments.

While oil can cause stress in both metazoans and also bacteria (Griffin and Calder, 1977) it can additionally be used by hydrocarbon-degrading bacteria as a metabolic substrate, as was indicated by microbial respiration of the DWH plumes (Valentine *et al*., 2010; Kessler *et al*., 2011). The use of oil as an energy source has also been studied experimentally in relation to the bioremediation of oil spills. For example, Lapham *et al*. (1999) matched the stable carbon isotope ratio of bacterial respired CO_2 to that of orimulsion (a form of heavy oil fuel) in slurry experiments, showing that the bacteria had used the oil as a metabolic substrate.

1.7 Investigating bacterial responses to oil using biomarkers and stable isotopes

The use of biomarkers with stable isotope analysis can facilitate the study of interactions between xenobiotic agents and biological systems. There are various working definitions of the term, 'biomarker' in use in geochemical and environmental investigations (see Peters *et al*., 2005) with a key difference in usage between geological and biological studies being that, in geology, the term is applied to molecules that remain stable over geological time, whereas in biological investigations biomarkers are sought that turnover rapidly enough on death to be associated only with living biomass. The study of biological biomarkers with stable carbon isotope analysis can provide information on the identity of microbial populations, their biomass and their nutrition source (Boschker & Middelburg, 2002).

The natural stable isotopes of carbon include carbon-12 (^{12}C, about 98.89% of carbon, globally) and carbon-13 (^{13}C, about 1.11% of carbon, globally). There are also trace quantities, relatively, of the naturally occurring radioactive isotope, carbon-14, as well as other, heavier isotopes of carbon that are also unstable. Stable isotope ratios of ^{12}C

and ^{13}C can be compared against an international standard[3] to report a deviation relative to that standard (reported in parts per thousand using the notation, δ). Hence, if a sample is depleted in ^{13}C the ratio will be negative relative to the standard. Organic matter that has undergone diagenesis to form petroleum is appreciably depleted in ^{13}C (e.g. Hahn-Weinheimer & Hirner, 1980) and ^{14}C is not found in oil because the half-life of this isotope (5700 years) is short in comparison to the age of oil. Isotopic fractionation, carried out by biochemical processes of living organisms, shifts $\delta^{13}C$ values (DeNiro & Epstein, 1978; Peterson & Fry, 1987). Therefore, many heterotrophic bacteria have a carbon isotopic ratio that is attributable to their food source (Blair *et al*., 1985; Coffin *et al*., 2012; Hullar *et al*., 1996). Analysing stable isotopes in target lipid molecules can therefore lead to insightful studies of microbial ecology and a range of molecule types can be used as biomarkers, including phospholipid fatty acids (PLFAs), sterols, ether lipids, D-amino acids and other molecules (Boschker & Middelburg, 2002).

Phospholipid fatty acids are a class of lipids consisting of a glycerol molecule ($C_3H_8O_3$) with two fatty acid molecules attached. A further group containing phosphate (PO_4^{3-}) is in place of a third fatty acid. This distinguishes PLFAs from true fats, which have three fatty acid chains attached to the glycerol group. Fatty acids are long-chain molecules of carbon and hydrogen possessing a carboxylic acid group (CO_2H) at one end. Phospholipids are highly polar molecules, possessing a 'head' (the part consisting of glycerol and phosphate) that has a high affinity for water, whereas the tail (fatty acid chains) does not. This chemical structure of phospholipids results in the property that allows them to easily form lipid bilayer membranes in cells, as they will tend to align themselves with their hydrophobic tails inwards and their hydrophilic head outwards (Figure 1.3).

[3] Historically, fossilised Pee-Dee Belemnite was used as the international standard for carbon isotopes, and this has been largely replaced by international reference carbon dioxide gas.

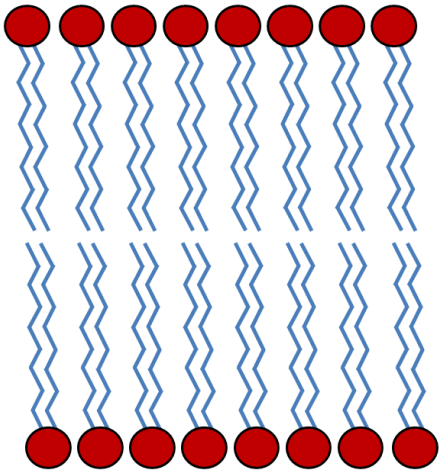

Figure 1.3. Schematic representation of a phospholipid membrane bilayer. Long-chain fatty acid molecules are denoted by lines. The glycerol and phosphate head is represented by circles.

The hydrocarbon chain tail of phospholipids can be saturated, therefore containing only single bonds, or unsaturated; with double bond(s). Additional methyl groups may be present. Certain types of PLFA such as odd-chain saturated fatty acids (e.g. pentadecanoic acid) are mostly synthesised by bacteria. Unsaturated fatty acids disrupt the alignment of the molecules, thus allowing a function of increased permeability of the membrane. The advantage of analysing PLFAs as biomarkers is that they degrade rapidly in dead and decaying matter, and are thus easily attributable to living biota (White *et al*., 1979) and estimate microbial biomass (Zelles *et al*., 1992; Guezennec & Fiala-Medioni 1996). Hence they have been useful for measuring change in sediment microbial communities (Guckert *et al*., 1985). Certain groups of bacteria can be distinguished from one another by measuring profiles of phospholipids (Lechevalier *et al*., 1977).

Quantifying and comparing isotopes of carbon between samples can be used to trace uptake of hydrocarbons by bacteria. For example, Cowie *et al*. (2010), working on soil bacteria, found that bacteria PLFA biomarkers in hydrocarbon-contaminated soil were depleted in the heavy isotope of carbon, ^{14}C. Slater *et al*. (2006) also used ^{14}C to indicate metabolism of oil, showing that bacteria had used anthropogenically spilled oil on a rocky intertidal shore as a source of carbon, incorporating the petroleum

hydrocarbon into mono-unsaturated PLFAs and therefore depleting these PLFAs in ^{14}C relative to uncontaminated samples. Syakti *et al*. (2006) incubated sediment contaminated with crude oil in microcosms and compared PLFAs of sediment bacteria in treatments and controls for incubation times of up to 21 days. Results indicated that biodegradation had taken place in the oil-contaminated sediment, although there had been a non-specific increase in the bacteria, with both heterotrophic bacteria and petroleum biodegraders increasing in abundance.

Bacteria are among the few organisms that possess the enzymes necessary to carry out oil biodegradation; the process of breaking large, complicated hydrocarbon molecules into smaller units until simple sugars are formed that can easily be metabolised. Biodegraders are therefore essential to the process of bioremediation: the removal of contaminants by living organisms. Biodegradation was thought to have consumed oxygen in appreciable quantities in DWH plumes in the deep Gulf of Mexico, though not so high as to contribute significantly towards hypoxia (Joint Analysis Group, 2010). As with many other metabolic processes in living organisms, biodegradation rates are affected strongly by temperature (Atlas, 1975, 1981) and temperature-mediated decay rates have been applied in simulations of the spread of oil at depth in the Gulf of Mexico (Adcroft *et al*., 2010).

1.8 Modelling oil spills

The progression of oil and gas erupting from a sub-sea oil well blowout is difficult to predict. Studies modelling the fate of oil and gas from subsea blowouts consider, to varying degrees, the influence of a range of initial oil properties and the effect of chemical and biological weathering over time. Operational, commercially available oil-spill modelling tools such as the Oil Spill Contingency and Response model, OSCAR (Reed *et al*., 1995) make use of multiple parameters that consider the chemical and physical behaviour of oil in seawater, including weathering. Deep water oil spill models have also been developed, for example, 'DeepBlow' (Johansen, 2000) is a Lagrangian[4]

[4] The term 'Lagrangian' refers to the tracking of objects or water along the course of their travel, as opposed to 'Eulerian' measurements of the passage of water/objects past one point.

plume model specifically considering multiphase components of oil and gas and applying these to deep-sea conditions. Detailed models of oil behaviour such as this one are effective at modelling oil in the near field, as it emerges from an irrupting well head into seawater. Plumes of oil and gas from deep water oil well blowouts may behave quite differently to those in shallow water, because of effects of the pressure and temperature regime on, for example, the proportion of dissolved gas, gas hydrate formation, oil droplet size and hence resulting plume buoyancy (Johansen, 2003; Dasanayaka & Yapa, 2009) and dynamics (Yapa & Dasanayaka, 2008). The DeepBlow model, which was validated with a unique, planned oil spill experiment in the sea, 'DeepSpill' (Johansen, 2003), indicated that for deep releases of oil (700 to 1500 m depth) the formation of gas hydrates is important for limiting plume buoyancy and thus vertical transport. These models are technologically advanced but are industry-led and therefore not readily available to publicly funded institutions in order to test scenarios or research questions.

In addition to the properties of the leaking oil and gas, the effects of ocean currents on transport are also important. Ocean general circulation models (GCMs) represent the state-of-the-art in simulating ocean currents and their use as tools to help simulate the Lagrangian transport of oil has been adopted in operational oil spill situations (Liu *et al*., 2011b). Ocean GCMs have been developed to resolve ocean currents on large geographic scales. They employ an understanding of ocean physics in order to improve our understanding of the transport of seawater and its constituent parts. This is used to study the oceans on scales where detailed sampling of the subsurface ocean is not possible. The applications of such models have been diverse, including studies of the pathways of major current systems (Koch-Larrouy *et al*., 2008), thermohaline circulation (Blanke *et al*., 1999) and ocean transport of pollutants (Nakano and Povinec, 2012). There are also examples involving the study of biogeochemistry on ocean basin scales (Popova *et al*., 2010) and the effects of climate change on lower trophic levels and their contribution to carbon export (Yool *et al*., 2013).

Ocean GCMs were applied in the context of the DWH spill to consider questions such as the possible role of plume depth on horizontal transport. Dissolved and neutrally buoyant hydrocarbons were modelled by Adcroft *et al*. (2010) using a high resolution (1/8°) ocean GCM, with a simple, temperature-dependent decay rate embedded to allow estimation of the persistence of oil along transport pathways. They found that depth and

decay rate were both important determinants in the lateral transport of plumes, and this had implications for the level of exposure a particular depth horizon received. An estimation of oxygen consumption as a result of microbial oxidation of hydrocarbons along the trajectories indicated that regionally significant oxygen depletions could result in the deep sea. Oxygen depletions would consequently affect ecosystem functioning, if severe enough to limit remineralisation.

1.9 Research aims and objectives

Given that there are various possible routes through which hydrocarbons from an oil well blowout can remain subsurface in plumes or reach the seafloor (Section 1.2), there is need for further study on the effects of oil on deep-sea biota and processes.

The main research aims and objectives of this study were:

1. To study natural deep-sea sediment communities experimentally in the presence of added hydrocarbons from crude oil, measuring their oxygen consumption rate in response to oil.

The toxic effects of crude oil on invertebrate macrofauna have been well studied in the laboratory. However, experiments performed on natural, deep-sea benthic communities of macrofauna are lacking from the literature. This will be addressed in Chapter 2, where experimenting with oil was carried out on microcosms formed from deep-sea sediments collected directly from an uncontaminated area far from industry activity.

Null hypotheses tested were as follows:

- There is no effect of hydrocarbons in WAF on SCOC in a natural deep-sea benthic community of macrofauna and bacteria;
- There is no effect of other appropriate explanatory variables on SCOC;
- There is no effect of oil on the distribution of macrofauna biomass among sediment layers.

2. To investigate changes in the composition and stable carbon isotope ratios of phospholipid fatty acids in response to oil.

On the continental slope, the contribution of bacteria to remineralisation represents around half of the total oxygen demand of sediments (Heip *et al*., 2001). Their interaction with macrofauna, for example through spatial differentiation of resources (van Nugteren *et al*., 2009) provides function to biogeochemical cycles of carbon and nutrients. Since bacteria are known to be of importance in the shallow water bioremediation of oil spills (Slater *et al*., 2006) it is also important to better understand their response to oil in the deep sea. In Chapter 3, microcosm experiments were used to expose a natural, deep-sea benthic community to oil. Sediment phospholipid fatty acids were chosen as biomarkers to indicate bacteria biomass, community composition, and stable isotope ratios of carbon ($\delta^{13}C$ values). These were used to assess changes in the microbial community in response to oil.

Null hypotheses tested were as follows:

- There is no effect of hydrocarbons on deep-sea sediment microbial community composition or biomass.
- There is no effect of hydrocarbons on deep-sea sediment microbial community $\delta^{13}C$ values.

3. To utilise a 3-D ocean general circulation model to simulate possible trajectories of oil from a release in the Faroe Shetland Channel and explore spatial and temporal patterns in its dispersal and potential remineralisation.

Contemporary near-field plume modelling for oil spills in deep water considers multiple parameters that are important in the consideration of oil behaviour. The depth of establishment of a plume depends on the conditions specific to a scenario e.g. the gas to oil ratio of leaked hydrocarbons, the depth of release and the water temperature. Once a neutrally-buoyant plume has been established from an oil well blowout, ocean currents become important in determining transport. Therefore, models representing ocean currents are of interest in studying patterns in transport over ocean-basin scales, such as could occur following a prolonged release from an oil well blowout. In Chapter 4, a

state-of-the-art three-dimensional ocean general circulation model was used to study pathways of oil transport from a prolonged release from a drilled site in the Faroe-Shetland Channel, considering the 16 year period 1994 to 2009. Seasonal and interannual patterns in transport pathways were considered in relation to the depth of establishment of modelled subsurface plumes (represented by release depth). The possible biogeochemical implications in terms of increased pelagic oxygen consumption and the extent of seafloor contact were also considered.

Chapter 2: Deep-sea macrofauna and sediment community oxygen consumption rates in the presence of hydrocarbons

2.1 Introduction

Macrofauna contribute to the biotic mediation of ecosystem functioning through their physical and physiological activities. They are important contributors to benthic respiration, which remineralises organic detritus at the seabed (Smith & Teal, 1973; Heip *et al*., 2001). Bioturbation of macrofauna allows processing and incorporation of organic carbon into sediments (Blair *et al*., 1996; Sun *et al*., 1999; Biles *et al*., 2002). Bioturbation can hence also regulate the distribution of contaminants arriving there (Hedman *et al*., 2008). The burrowing activities of macrofauna also mediate microbial communities in the sediment (Laverock *et al*., 2010; Ashforth *et al*., 2011) and faunal-bacteria interactions are therefore likely to be important in the biogeochemical cycling of both organic matter and macronutrients in the oceans (Hunter *et al*., 2012). Through the mixing of sediments by faunal bioturbation, a portion of organic carbon exported from the euphotic zone becomes buried (van Weering *et al*., 1998).

The bioturbating activities of macrofauna are important for the remediation of ocean floor habitats where oil exploration and production cause chronic impacts. Drill cuttings are produced when drilling an oil well, and are redistributed back into the ocean close to drilled sites. The cuttings consist of lubricating mud, rock and sediment that has been extracted from the seabed as part of the drilling and oil extraction process. Recolonisation by macrofauna (Daan & Mulder, 1996; Trannum *et al*., 2011) and megafauna (Gates *et al*., 2012) of areas previously covered by drill cuttings allows for the material to eventually be processed back into the seabed fabric.

Effects of contaminants on benthic invertebrate fauna have been studied from the cellular level up to individual species, populations and communities. At the cellular level, toxic hydrocarbons from crude oil induce regulatory mechanisms in marine

invertebrates that may affect their metabolism. For example, the compensatory extrusion of sodium was hypothesised by Aunaas *et al*. (1991) to have led to an increase in the respiration rate of the amphipod *Gammarus oceanicus* exposed to water soluble fraction of crude oil. Olsen *et al*. (2007b) also reported changes in respiration rate and energy usage by Arctic benthic fauna in response to oil. Changes in respiration rate could be the result of the up regulation of mechanisms to cope with stress or detoxify cells in response to toxic compounds. This requires the activation of energy reserves. Stress may therefore necessitate an increase in heart rate (Camus *et al*., 2002). However, depending on the adaptations of individual species, respiration rates can also be maintained or reduced in relation to stress (Camus *et al*., 2003; Olsen *et al*., 2007b). Studies at the cellular level of biological organisation can give important insights into the possible mechanisms of toxic effects (Hahn, 2011).

When considering effects of pollutants on whole organisms, median lethal concentration (LC_{50}) tests are performed to indicate acute toxicity, with the end point (50% mortality rate in the test population) providing a way of standardizing the test against levels and periods of exposure. Acute toxicity has been studied for a variety of organisms, for example lobster larvae (Wells and Sprague, 1976); mussels (Fernández *et al*., 2006; Reineke *et al*., 2006); echinoderms (Neff *et al*., 2000) and corals (Negri & Heyward, 2000). Mortality can be difficult to assess visually, and alternatively, behavioural or developmental abnormalities can be used as the test end point (e.g. Neff *et al*., 2000).

The use of LC_{50} tests alone for monitoring or predicting the effects of oil pollution has drawn criticism (Moles, 2000). This is because animals that survive lethal tests may on the other hand show significant chronic effects, such as reduced growth and reproduction (Scarlett et al., 2007b); behavioural effects such as reduced burrowing activity (Scarlett et al., 2007c) or reduced feeding rate (Reineke *et al*., 2006; Georgiades *et al*., 2003). Mixtures of oil and chemical dispersants can be more toxic to marine invertebrates than crude oil alone and dispersants themselves are also acutely toxic to some organisms (Negri & Heyward, 2000; Shafir *et al*., 2007). Other studies have reported reduced overall toxicity of oil with the application of dispersants (Aunaas *et al*., 1991).

At the community level, chronic impacts of oil industry activities have often been measured by assessing changes in species assemblages of benthic invertebrates in response to pollution (e.g. Gray *et al*., 1990; Daan *et al*., 1994) and during recovery

from disturbance (Mair *et al*., 1987). Detailed analysis of community structure at the species level is of great interest, yet is time consuming in comparison to other whole community measures that can also indicate status e.g. sediment community oxygen consumption (SCOC, the consumption of oxygen by all living biota within a sediment community). Total oxygen uptake rate of sediments is thus indicative of whole community metabolism (Smith and Teal 1973; Glud, 2008) and through the relationship with organic carbon remineralisation, oxygen utilisation rates can be included with indicators of stress to study impacts on marine benthos (Hyland *et al*., 2005). Rates of SCOC are inversely correlated with depth in the deep ocean (Rowe *et al*., 2008) and are correlated with organic input by POC (Jahnke, 1996; Smith *et al*., 2001).

Effects of hydrocarbons on benthic respiration rates have previously been studied experimentally, where oxygen demand of shallow (200-300m) Arctic marine sediment communities increased in response to high concentrations of crude oil slurry (Olsen *et al*., 2007a). Degradation of organic compounds present in drill cuttings has caused increases in benthic respiration in chronically-impacted areas of oil industry activity, resulting in changes to the structure and functioning of benthic communities (Schaanning *et al*., 2008; Trannum *et al*., 2011).

Increase in respiration rate can be caused by a physiological response to pollution stress in some invertebrates. Changes in the energy budget of invertebrate fauna exposed to hydrocarbons have previously indicated that compensatory mechanisms are upregulated in response to contaminants. For example, physiological responses in mussels, *Mytilus edulis*, that had high tissue levels of hydrocarbons, resulted in lower scope for growth of these animals (Widdows *et al*., 1995). Cellular energy allocation, a biomarker indicating the net energy budget at the cellular level was altered in response to water accommodated fraction of crude oil (WAF) in experimental systems with an Arctic amphipod, *Gammarus setosus*, (Olsen *et al*., 2007b). The net available energy available to cells was decreased because of increased energy consumed by respiration. However, in the same study, the amphipod *Osinimus litoralis* and the bivalve *Liocyma fluctuosa* were not as susceptible to WAF.

Toxicity of crude oil depends on its composition and the degree of weathering undergone. The relatively light fractions of crude oil, such as monoaromatic hydrocarbons (MAHs), are generally more toxic than most polycyclic aromatic hydrocarbons (PAHs, Neff *et al*., 2000). Deep-sea plumes of dissolved hydrocarbons

are likely to form following a deep water oil well blowout (Camilli *et al*., 2010; Socolofsky *et al*., 2011). Such plumes are likely to contain mainly the more soluble, yet highly toxic fractions of crude oil and gas, such as monoaromatic hydrocarbons (benzene, toluene, ethyl-benzene and isomers of xylene, BTEX) and methane (Reddy *et al*., 2011). Hence, contact with plumes could cause stress or mortality to macrofauna, with resulting changes in SCOC.

The introduction of oil into aquatic experimental systems is difficult to standardise. A water accommodated fraction (WAF) of crude oil has been used in a range of previous studies to facilitate introduction of hydrocarbons into meso- and micro-cosms, for example, to assess hydrocarbon toxicity (e.g. Scarlett *et al.*, 2007b; Bejarano *et al*., 2006; Lewis *et al*., 2008). This is partly because the composition of fresh crude oil varies according to the reservoir of extraction (e.g. Hahn-Weinheimer & Wirner, 1980). Fresh oil that is open to the atmosphere will change in composition over time the lighter fractions evaporate. In many studies of the effects of oil on aquatic organisms, the soluble fractions of crude oil are used as a proxy, since it is possible to standardise the preparation of these treatment solutions and form a relatively stable mixture of hydrocarbons and water. A water accommodated fraction of crude oil is produced by low-energy mixing of fresh bulk oil with seawater for at least 24 hours (Faksness *et al*., 2008). Monoaromatic hydrocarbons (BTEX), which are slightly soluble in seawater, and these make up the large majority of hydrocarbons in WAF. The absence of filtering of WAF distinguishes it, technically, from the laboratory-prepared water soluble fraction (Singer *et al*., 2000). Previously, experimental studies have been used to measure various toxic effects of WAF, including effects on invertebrate behaviour (Georgiades *et al*., 2003); chronic toxicity including delayed mortality (Scarlett *et al*., 2007b); reproductive effects (Lewis *et al*., 2008) and lethal effects (Faksness *et al*., 2012).

Bulk crude oil is less dense than seawater (crude oil is ~800 kg m^{-3}, compared to ~1025 kg m^{-3} of seawater at atmospheric pressure). Therefore, a large proportion of crude oil emitted from a seabed oil well blowout will be propelled towards the ocean surface to form slicks. However, as was observed following the 2010 Macondo oil well blowout, oil that is emitted as a high pressure jet at high temperature (~100°C at the Macondo well, Reddy *et al*., 2011) atomises to form small droplets that may be further reduced in size by the application of dispersants (Masutani & Adams, 2000; Socolofsky *et al*.,

2011). Hence, vast plumes of these dissolved hydrocarbons and small droplets are able to persist in the deep sea for many months (Camilli *et al*., 2010). Oil was documented on the seafloor beneath the passage of large plumes of hydrocarbons in the Gulf of Mexico following the Macondo oil well blowout (White *et al*., 2012) and subsequently a footprint of Macondo oil contamination of up to 3200 km^2 was reported by Valentine *et al*., 2014). Evidence of oil and marine snow aggregates, also in the Gulf of Mexico (Passow *et al*., 2012; Ziervogel *et al*., 2014) provide further evidence that hydrocarbons reach the seafloor from oil well blowouts.

Here, the effect of hydrocarbons on deep-sea SCOC was studied in an *ex situ* microcosm experiment that was performed using natural sediment communities collected from the seafloor of the European continental margin of the North Atlantic. The effects of WAF on SCOC were measured at three treatment levels in relation to controls and thus provided potential indications of physiological responses including stress. Treatment levels ranged from 0% WAF (controls) to 25% WAF (as a percentage of the estimated overlying water present). The density, biomass and taxonomic classes of the extant macrofaunal communities were quantified for half of the replicate microcosms. Null hypotheses investigated in this study were:

- There is no effect of WAF on sediment community oxygen consumption.

Stress induced changes in metabolic rate by macrofauna could result in increases or decreases in SCOC.

- There is no effect of other non-collinear explanatory variables on SCOC.

The explanatory variables of temperature and macrofauna biomass were assessed.

- There is no effect of WAF treatment on the distribution of macrofauna biomass in the sediment.

Macrofauna could respond to oil-induced stress by either burrowing deeper or by shoaling in the sediment. This could lead to a difference in biomass between the same sediment horizons of treated versus control microcosms.

2.2 Methods

The study location, an area of the North Atlantic continental slope known as the Goban Spur (49° 35.5' N, 011° 50.9' W), is a non-drilled site at ~995 m (Figure 2.1), assumed to be free of anthropogenically spilled oil because of its distance (> 100 km) from industry activity.

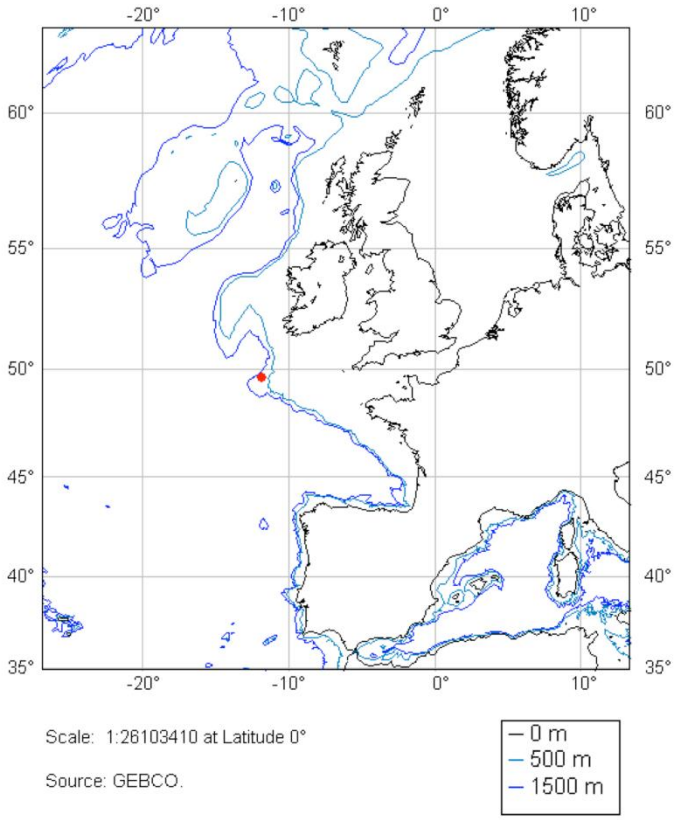

Figure 2.1. Map showing the location of the Goban Spur study site.

Near-bottom currents at the Goban Spur are relatively high (up to 35 cm s^{-1}, Flach, *et al.*, 1998). Sediments of the Goban Spur have an organic carbon content of approx 0.5% by weight (Lohse *et al.*, 1998); somewhat lower than at adjacent sites of the North Atlantic, e.g. the nearby Whittard Canyon (0.9 – 1.1% by weight, Duineveld *et al.*,

2001). Total SCOC is accounted for approximately equally by bacteria and by deposit feeding macrofauna (Heip *et al*., 2001).

Sediment cores were collected from the continental slope of the Goban Spur during August 2011 at the positions and depths shown in Table 2.1. The ambient bottom water temperature was 8.6°C.

Table 2.1. Details of sediment cores collected for the incubation experiment.

Core	Treatment (% WAF)	Station	Date	Depth (m)	Latitude (N)	Longitude (W)	Observations
51	5	135	25/08/2011	993	49˚ 35.630’	011˚ 50.802’	TDM
52*	0	135	25/08/2011	993	49˚ 35.630’	011˚ 50.802’	TDM
53*	15	135	25/08/2011	993	49˚ 35.630’	011˚ 50.802’	TDM
54*	25	135	25/08/2011	993	49˚ 35.630’	011˚ 50.802’	TDM
55	25	135	25/08/2011	993	49˚ 35.630’	011˚ 50.802’	TDM
56	0	135	25/08/2011	993	49˚ 35.630’	011˚ 50.802’	TDM
57*	5	136	25/08/2011	994	49˚ 35.631’	011˚ 50.798’	
58*	25	136	25/08/2011	994	49˚ 35.631’	011˚ 50.798’	
59*	0	136	25/08/2011	994	49˚ 35.631’	011˚ 50.798’	
60	15	136	25/08/2011	994	49˚ 35.631’	011˚ 50.798’	
61*	15	136	25/08/2011	994	49˚ 35.631’	011˚ 50.798’	
62	25	137	25/08/2011	994	49˚ 35.632’	011˚ 50.804’	
63	0	137	25/08/2011	994	49˚ 35.632’	011˚ 50.804’	
64	5	137	25/08/2011	994	49˚ 35.632’	011˚ 50.804’	
65*	5	138	25/08/2011	994	49˚ 35.631’	011˚ 50.802’	
66*	0	138	25/08/2011	994	49˚ 35.631’	011˚ 50.802’	
67	15	138	25/08/2011	994	49˚ 35.631’	011˚ 50.802’	
68*	15	138	25/08/2011	994	49˚ 35.631’	011˚ 50.802’	
69*	25	139	26/08/2011	996	49˚ 35.630’	011˚ 50.804’	
70	25	139	26/08/2011	996	49˚ 35.630’	011˚ 50.804’	
71	5	139	26/08/2011	996	49˚ 35.630’	011˚ 50.804’	
72	0	139	26/08/2011	996	49˚ 35.630’	011˚ 50.804’	
73	15	139	26/08/2011	996	49˚ 35.630’	011˚ 50.804’	
74*	5	139	26/08/2011	996	49˚ 35.630’	011˚ 50.804’	

TDM = touch down mark on core sediment surface.

* Cores for which macrofauna data were obtained (n = 3 for each treatment level and controls).

2.2.1 Preparation of water accommodated fraction of crude oil

Seawater was collected from immediately above the seabed at the study location prior to coring operations. This seawater was used to prepare a WAF using fresh crude oil from the Wytch Farm oilfield (Dorset, UK, obtained in February 2011). A standard low-speed mixing procedure was used to prepare WAF (Anderson *et al*., 1974; Hokstad *et al*., 1999) bottle at 8 °C (close to the ambient seabed water temperature). In brief, 20 L of seawater and 613 ml fresh crude oil (613 mL; the density of Wytch Farm crude oil[5] is 0.8162 kg L^{-1}) were combined in a glass aspirator to produce an oil loading rate of 25 g L^{-1} (Faksness *et al*., 2008). Low energy stirring of this solution, with no vortex present in the surface slick, was carried out for approximately 24 hours. Samples of WAF were taken at intervals to check consistency of its composition (see Section 2.2.3). The resulting WAF was composed mainly of the monoaromatic hydrocarbons: benzene; toluene; ethyl benzene and isomers of xylene (BTEX) and remained stable throughout the time when it was being used as a treatment solution for the microcosms (Table 2.2).

Table 2.2. Concentration (mg L^{-1}) of analytes in WAF (analysis performed by ERT Fugro, UK). Sample S1 was preserved after 32 hours of low energy stirring. Sample S2 was preserved after 48 hours of low energy stirring.

	Sample S1	Sample S2
Benzene	0.9	1.1
Toluene	1.1	1.3
Ethyl Benzene	0.1	0.1
m,p-xylene	0.3	0.3
o-xylene	0.1	0.2
Oil total	5	4.7
BTEX total	2.5	3

[5]BP official documentation:
http://www.bp.com/liveassets/bp_internet/bp_crudes/bp_crudes_global/STAGING/local_assets/downloads_pdfs/Wytch_Farm_Mar10.xls

2.2.2 Sediment core collection

A total of 24 sediment cores (10 cm internal diameter) and overlying water were collected using a Bowers and Connelly megacorer (Barnett *et al*., 1984) and immediately transferred to an incubator set at the ambient bottom water temperature (8.6˚C). Cores were acclimated to experimental conditions for approximately 24 hours in the dark.

2.2.3 Treating sediment cores with WAF

Sediment cores were contaminated with WAF at three treatment levels of hydrocarbons (six replicates per treatment) based on the estimated volume of core overlying water (5%, 15% and 25% overlying water volume). Six cores formed controls that were not contaminated with WAF. During the treatment period, samples of WAF were collected from the preparation vessel and preserved with 50 mL hydrochloric acid of specific gravity 1.18. This was done approximately half way through the cores' treatment period (after 32 hours of stirring) and after 48 hours of stirring to provide an estimate of hydrocarbon concentrations in treatments and check consistency of the WAF composition (Table 2.2). All glassware and the various components of the microcosms were acid washed with 10% hydrochloric acid and rinsed with ultra-pure water before use in the experiment. The sediment surface of the microcosms was photographed immediately following collection and at the end of the experiment.

2.2.4 Incubation of microcosms

Following treatment, the sediment cores were immediately sealed without a headspace and were incubated at the ambient seabed water temperature (8.6˚C). Core overlying water in the microcosms was stirred manually for approximately 10 seconds every two hours and for 10 seconds preceding measurement of oxygen (a schematic diagram of the cores incubations experimental apparatus is presented in figure A1.1). Incubations were

ceased when (or before) core overlying water oxygen concentration reached ~80% of starting levels (approximately 2.5 days) so as to ensure that the system remained oxic. Oxygen concentration in the overlying water was measured at approximately regular intervals (every ~12 hours). Water samples of 32 mL were extracted at intervals from a sample port in the microcosm lid using a glass syringe and a thick gauge stainless steel needle, immediately following manual stirring of the core water. The volume of water removed from the core was compensated for by gradual insertion of a cylinder through the lid (Figure A1.1). This ensured that head space of air was kept at or as close to zero throughout the incubation. Water volumes removed were corrected for in calculations of total oxygen concentration. On extraction from the cores, the water samples were transferred carefully to a glass beaker and an optode sensor (Aandera, model 3830) was placed into the sample such that the level of the water rose to above the level of the sensing foil and the temperature sensor. The sensor was left for three minutes in the sample with gentle agitation to allow the sensor to stabilise, and the reading of oxygen concentration was taken at two minutes. Before use, the optode was calibrated to saturated and zero values of oxygen concentration as follows. For the saturated calibration point, a reading was taken with the optode submerged in aerated seawater at known temperature (8 °C). For the zero oxygen concentration calibration point, the optode was submerged in 500 mL seawater containing 5 g anhydrous sodium sulfite. Carbon remineralisation rates were estimated from rates of oxygen consumption assuming a respiratory quotient of 1 (moles of oxygen consumed equals moles of carbon dioxide evolved). This was done to allow for the fact that the respiratory substrate was technically unknown.

2.2.5 Macrofauna density and biomass

At the end of the incubation period, the top 0-1 cm layer of sediment from three of the replicates from each treatment level was preserved in buffered 4% formaldehyde. The other three replicates from each treatment level were frozen at -80°C for subsequent prokaryote analyses. Sediment samples that were frozen were later lost as a result of technical problems, leaving only the formaldehyde-preserved samples for analysis. These were used to quantify macrofauna biomass and abundance by taxonomic class.

Macrofauna were removed from the sediment sections by gently washing with seawater on a 500 μm mesh sieve. The animals were stained with Rose Bengal and sorted under a reflecting microscope. Density (estimated number of individuals m^{-2}) of each represented class was estimated by scaling numbers in each sediment sample up by a factor of 127 to give estimated density per square metre. Animals were weighed together in classes. The wet weight was used to give an estimate of macrofauna biomass (mmol C m^{-2}), assuming 12.4% carbon content for nematodes (Jensen, 1984) and 4.3% carbon content for all other animals (Rowe, 1983) except ophiuroids and echinoids (1.9% carbon content).

Macrofauna biomass data were available from an additional incubations experiment investigating treatment effects of WAF on deep-sea sediment communities (see methods in Chapter 3). Wet weight of macrofauna biomass caught on a 500 μm sieve were used from sediment horizons 0 – 1 cm; 1 – 2 cm; 2 – 5 cm; 5 – 10 cm. The treatment levels of WAF in this additional experiment were 25 % and 50 % by volume of core overlying water (4 replicates at each treatment level, and 4 replicate controls).

2.2.6 Data analysis

Data exploration and analysis was conducted using the statistical programming language R (R Core Team, 2013) with the 'nlme' package (Pinheiro and Bates, 2013). Graphical data exploration was used to assess the data for outliers and instances of colinearity, and to help with appropriate selection of non-collinear explanatory variables (Zuur *et al*., 2010). Oxygen concentration was measured repeatedly from the same individual cores, forming temporally auto-correlated data. This violates the assumption that error estimates are independent. Hence, linear mixed effects models (LME), which are able to account for that fact, were used to examine whether oxygen concentration in the cores overlying water was affected by exposure to WAF. The techniques and statistical theory behind linear mixed effects models are described in detail by Pinheiro and Bates (2000) and Zuur *et al*., (2009).

Linear mixed effects models were fitted to total oxygen concentration data from all microcosms (n=6 for each treatment and controls), in which the effect of time was specified as fixed and individual core identity as random. This allowed line intercepts to vary with core identity and so accounted for the range in starting concentrations of the microcosms. The *a priori* assumption that core identity should be specified as a random affect was tested by comparing models with and without the random effects using a likelihood ratio test. The modifying effect of treatment on oxygen consumption rate was tested by fitting linear mixed effects models with and without the interaction term and compared using a likelihood ratio test with a restricted maximum likelihood method (REML).

Oxygen data were further explored in relation to other explanatory variables with LME. Graphical data exploration indicated that macrofaunal biomass and density variables were highly collinear. The variance of macrofauna biomass was heteroscedastic among oil treatments and there was increasing variance in the oxygen data with increasing time in the experiment. The full model to explain oxygen concentration prior to backwards selection included, as explanatory variables: additive effects of macrofaunal biomass (mmol C m^{-2}), treatment, time and temperature, and interactive effects of treatment and time and biomass and temperature. There was a significant effect of core identity, leading to the inclusion of core identity as a random effect in the model. A combined structure for variance was allowed for by including an exponential function to be fitted to the variable of core duration (time) and variance covariates for macrofaunal biomass. Using a backwards selection protocol (Pinero and Bates 2000), models were run with the sequential removal of terms and comparison of model fits with p-values at each step.

Biomass data from an additional experiment (Chapter 3) were analysed using generalized least squares models, to investigate the null hypothesis that there were no WAF treatment effects on distribution of biomass down to 10 cm. The variance of macrofauna biomass was heteroscedastic among oil treatments. The full model to explain macrofauna biomass contained macrofauna biomass as the response variable. Additive effects of treatment and an interaction of treatment with depth were investigated using linear modeling and a backwards selection model fitting procedure (Pinheiro and Bates, 2000).

2.3 Results

2.3.1 Treatment effects on SCOC

Oxygen concentration in the microcosms reduced linearly over time (Figure 2.2). The random effect of core identity was highly significant (df = 1; L. ratio = 41.1; $p < 0.0001$). There was a non-significant treatment × time interaction (df = 1, L. ratio = 4.70; p = 0.19). Hence there were not significant treatment effects of the oil on SCOC and the null hypothesis of no treatment effects on SCOC could not be rejected. The optimal model for oxygen consumption contained only the effect of time. Model parameters and diagnostics are presented in the Appendix (Tables A1.1 and A1.2).

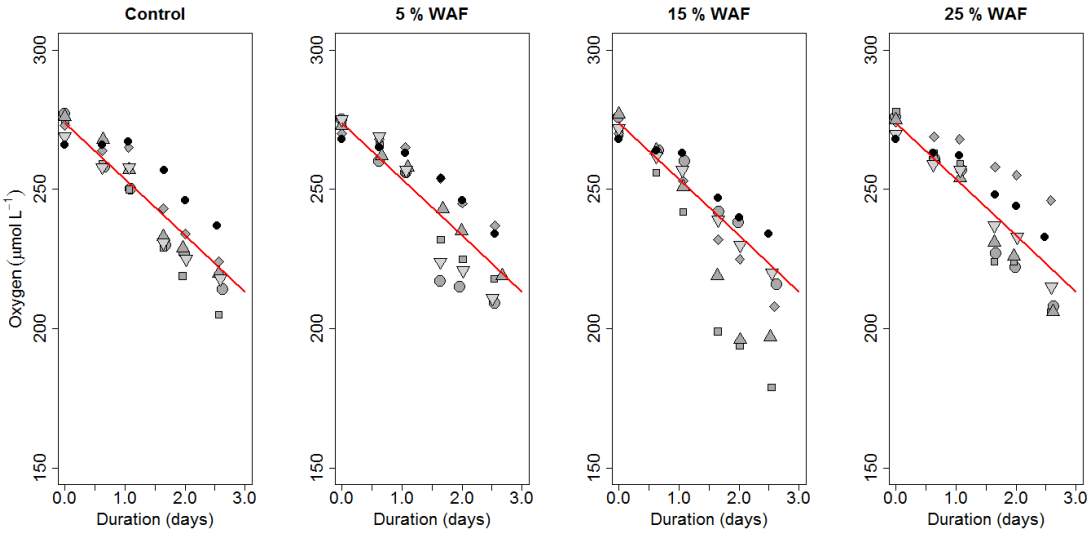

Figure 2.2. Oxygen concentration over the course of the ~2.5 day incubations. Symbols indicate data from individual cores, with six replicate cores at each treatment level. Predictions from the optimal model of oxygen concentration over time are indicated by straight lines.

2.3.2 Exploring SCOC in relation to macrofauna biomass, composition, and temperature

SCOC was further explored in relation to the macrofauna present in cores for which those data were obtained (n = 3 at each treatment level). A backwards selection model fitting protocol indicated that total macrofaunal biomass, temperature and the interaction of these variables were all significant predictors of oxygen consumption rate (Table 2.3) in the replicate cores for which these data were all available (n = 3 at each treatment level).

Table 2.3. Results of statistical modeling of oxygen in response to macrofauna biomass, temperature and the interaction of these variables

Model term	df	L. ratio	p value
Total macrofauna biomass	1	4.17	0.0412
Temperature	1	6.20	0.0127
Biomass × temperature	1	15.0	< 0.0001

Macrofaunal density (individuals m^{-2}) and biomass (mmol C m^{-2}) were quantified from six phyla in the sediment surficial layer. Estimated total density of macrofauna in the surfical layer was on average 2844 numbers m^{-2}. Polychaetes and nematodes were typically the most numerous of the represented groups (Figures 2.3, 2.4). Polychaetes, bivalves and nematodes tended to dominate both density and total estimated biomass (Figures 2.3, 2.4, 2.5). The standard error in estimates of density and biomass were both generally high (Table 2.4).

Table 2.4. Estimated macrofauna density and biomass present in the sediment surface layer (0-1 cm).

Treatment (% WAF)	Density (numbers m^{-2})	Average ± standard error	Biomass (mmol C m^{-2})	Average ± standard error
0	1783		3.94	
0	3565	2334 ± 616	18.22	8.11 ± 5.08
0	1655		2.17	
5	3947		6.67	
5	2419	3268 ± 449	4.89	5.70 ± 0.52
5	3438		5.54	
15	2419		18.72	
15	1910	3226 ± 1071	2.33	10.55 ± 4.56
15	5348		11.25	
25	2801		1.38	
25	4202	2546 ± 1037	9.15	7.27 ± 2.58
25	637		2.97	

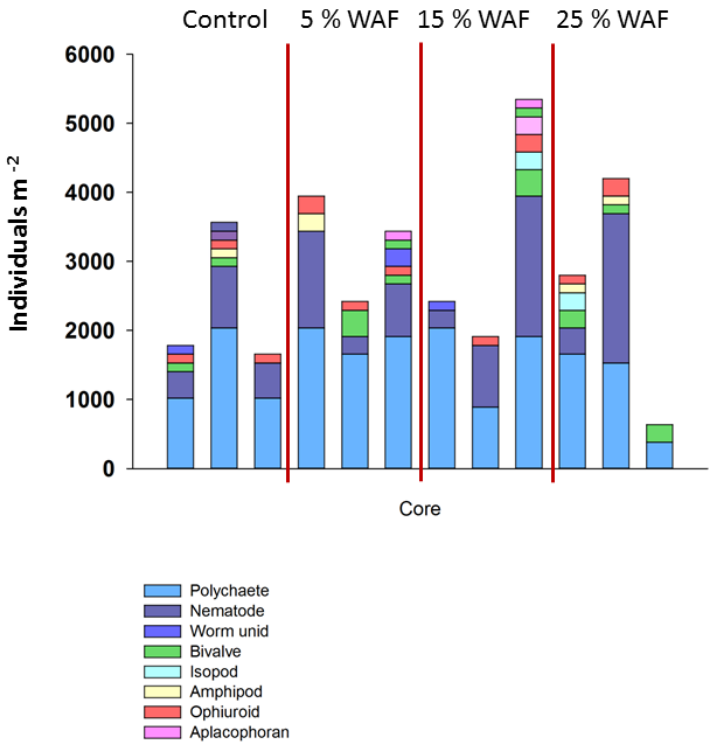

Figure 2.3. Estimated density of each taxonomic class in the 12 sediment cores preserved for faunal analyses.

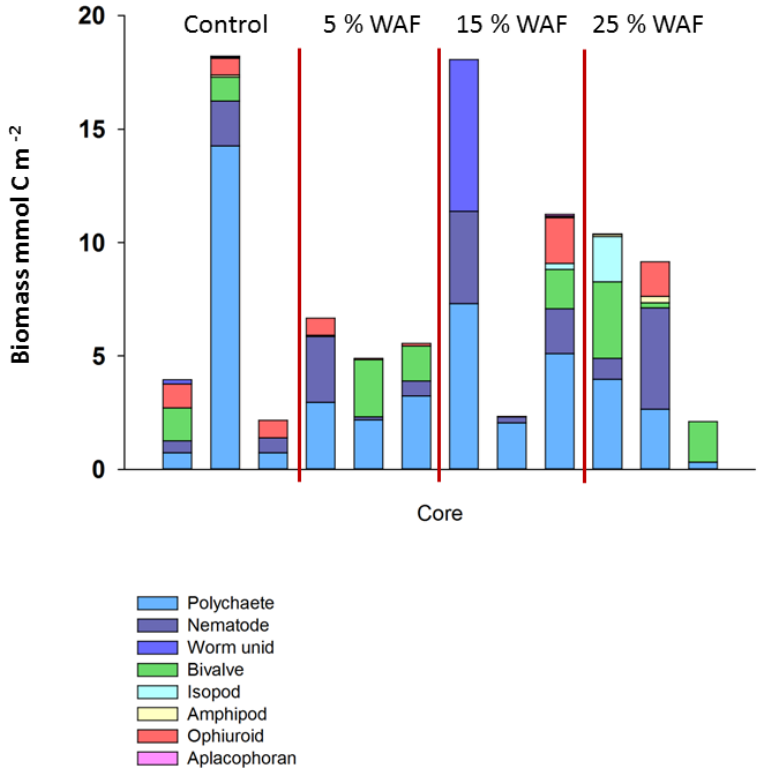

Figure 2.4. Biomass of each taxonomic class in the 12 sediment cores preserved for faunal analyses.

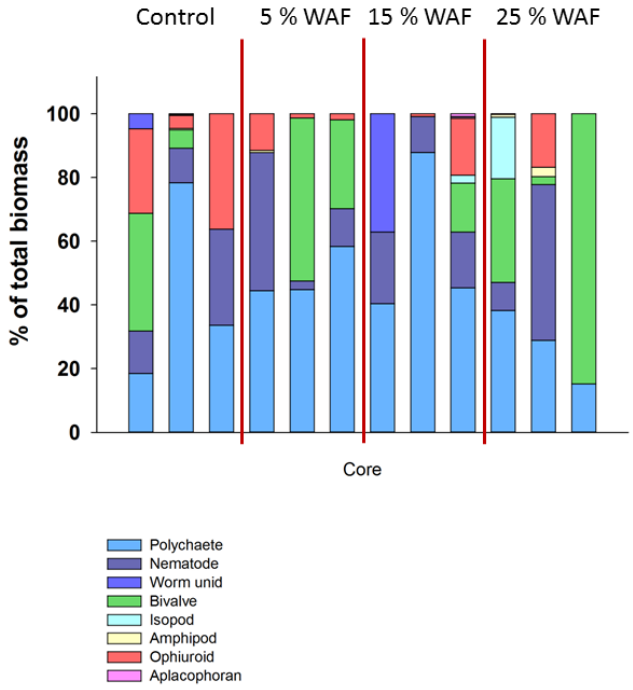

Figure 2.5. Macrofauna class as a percentage of total biomass (mmol C m^{-2}) present in each core.

Oxygen data from each sediment core are shown in relation to the estimated total macrofauna biomass (mmol C m^{-2}) present in the 0 – 1 cm layer (Figure 2.6). Points falling well below the model line in the 15% WAF plot (Figure 2.6) belonged to two cores: i) a core with low biomass in the 0 – 1cm layer; and ii) a core for which biomass data were not estimated.

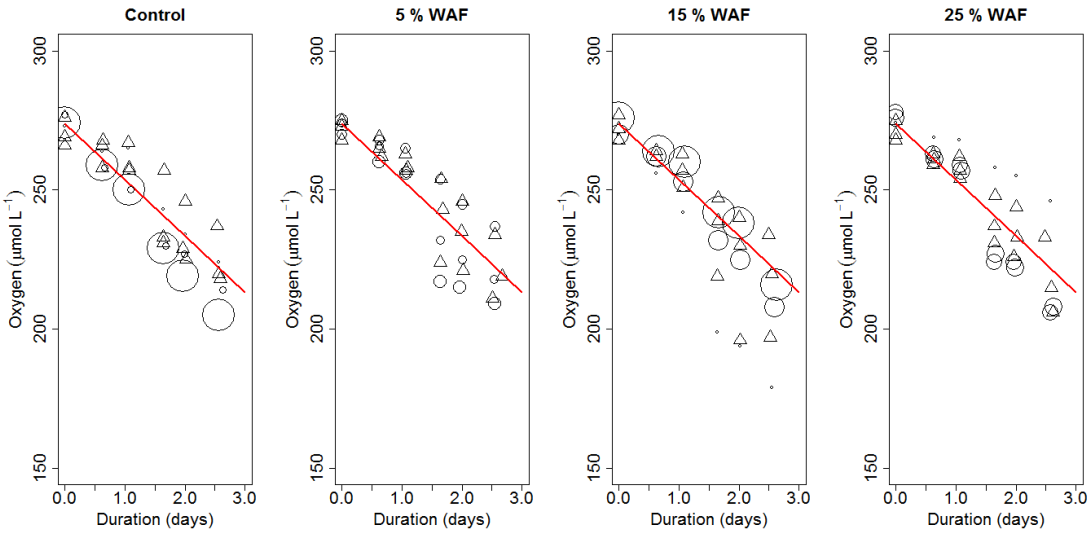

Figure 2.6. Oxygen concentration over the course of the ~2.5 day incubations. Circle symbols indicate oxygen data from cores for which macrofauna biomass data were estimated in the surficial layer. Circular symbols are scaled in size to total macrofauna biomass (mmol C m^{-2}) in the relevant core. Triangle symbols indicate oxygen data from cores for which no biomass data were estimated. Model–predicted oxygen concentrations for the optimal model of oxygen concentration over time are indicated by red lines.

A temperature gradient of approximately 2°C was observed across the incubator in which the experiment was performed (Table 2.5). The temperature experienced at either end of the incubator was ~1°C either side of the value at a temperature probe connected to a thermostat that was located in the centre of the chamber (the thermostat was set at 8.6°C: ambient bottom water temperature at time of core collection). Remineralisation rates were estimated for each core from the slope of the linear change in oxygen concentration (Table 2.5). Rates estimated for the warmer end of the incubator were

between 6.13 and 7.66 mmol C m^{-2} d^{-1} whereas rate estimates for the cooler end were between 4.85 and 6.23 mmol C m^{-2} d^{-1} (Table 2.5).

Table 2.5. Estimated temperature of cores positioned at either end of incubator and measured rates of carbon remineralisation from the experiment

Core ID	Treatment (% WAF)	Estimated temperature (°C)	Remineralisation mmol C m^{-2} day^{-1}	Average rate ± standard error
74	5	7.6	5.68	
68	15	7.6	6.23	5.6 ± 0.4
69	25	7.6	4.85	
64	5	9.6	7.33	
60	15	9.6	7.66	7.0 ± 0.5
70	25	9.6	6.13	

The average rate of carbon remineralisation was ~26% higher in cores located at the warmer end of the incubator. This is supported by Q_{10} theory, which would imply that, using a Q_{10} of 2 (common in biological systems), a 10°C rise in temperature results in a doubling of the rate of reaction.

Photographs of the microcosms' sediment surface taken before and after the experiment indicated that burrowing activity and bioturbation had taken place over the course of the incubations. This was visible at all treatment levels (see photographs Figures A1.2 – A1.9, Appendix 2). Evidence of macrofauna activity included new ophiuroid burial marks in control cores (e.g. Figure A1.3) and treated cores (Figure A1.7, 15% WAF treatment). Also, new tracks were formed during the course of the experiment in control cores (e.g. Figure A1.3) and treated cores (e.g. Figure A1.5, 5% treatment level; Figure A1.7, 15% treatment level; Figure A1.9, 25% treatment level). Some new burrows were also formed (Figure A1.7, 15% treatment level).

Effects of WAF on possible burrowing behaviour were further investigated using data from an additional experiment (Chapter 3) and linear modeling. There was a non-significant effect of sediment depth on total macrofaunal biomass (df = 3; L. ratio = 4.44; p = 0.22; Figure 2.7). There were also non-significant WAF treatment effects on

biomass (df = 2; L. ratio = 1.86; p = 0.39) and a non-significant interaction of WAF treatment with depth (df = 9; L. ratio = 10.2; p = 0.33). A large individual present in one of the 2-5 cm cores made the variance of biomass at the 50 % WAF treatment level high (Figure 2.7), but the overall interpretation remained that WAF did not affect biomass at these depth horizons.

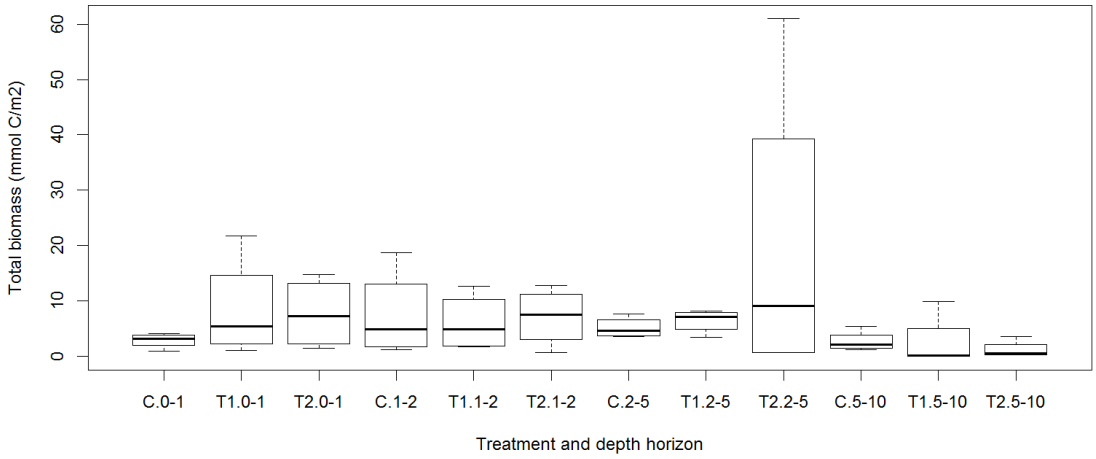

Figure 2.7. Total wet weight macrofaunal biomass caught on a 500 µm sieve at four depth horizons and two treatment levels of WAF (25 % and 50 % of overlying water volume) compared to controls. C = control; T1 = 25% WAF; T2 = 50% WAF. Sediment layers are indicated by: 0 – 1 = 0 to 1 cm layer; 1 – 2 = 1 to 2 cm layer; 2 – 5 = 2 to 5 cm layer; 5 – 10 = 5 to 10 cm layer.

2.4 Discussion

This study found no significant effect of WAF on the SCOC in natural deep-sea sediment microcosms incubated *ex situ*. Chosen treatment levels of WAF ranged from 5% to 25% of overlying water volume. Significant reductions in oxygen concentration were measured in the microcosms at all treatment levels, indicating that, broadly speaking, the experiment had operated as expected despite the lack of a treatment × time interaction. The biomass of the macrofauna present in the surficial layer at the end of the experiment was found to be a significant explanatory variable for SCOC. Other

potentially significant explanatory variables, such as bacteria were not measured (this will be returned to in Chapter 3). A temperature gradient measured across the incubator may also have contributed to the lack of a clear effect of oil treatment on oxygen consumption rate and this variable had a significant interaction with macrofauna biomass in explaining oxygen consumption rate. The macrofauna present in the microcosms were active in all WAF treatments and controls.

Respiration rates have previously been studied in relation to oil-induced stress of individual organisms (Camus *et al*., 2002a; Camus *et al*., 2002b) and whole sediment communities (Olsen *et al*., 2007a). Hydrocarbons can cause stress-induced changes in respiration and cellular energy allocation of benthic invertebrates, although species (and hence their individual modes of feeding and behaviour) are likely determinants of oil-sensitivity and hence whether respiration rate could rise or remain unaffected (Olsen *et al*., 2007b). Other effects of contaminants on invertebrates include changes in behaviour, for example, burrowing avoidance of amphipods has been observed in experimentally-contaminated sediments (Scarlett et al., 2007c).

It cannot be ruled out that the non-significant effect of treatment on SCOC may indicate that there was no response to the hydrocarbons by the sediment community. However, an observed temperature gradient across the incubator explained a significant proportion of variance when backwards selection of linear mixed effects models was considered in detail. It was impossible to disentangle entirely what could be responsible for non-significant treatment effects. However, warmer temperatures at the end of the incubator, where the highest SCOC rates were observed, were supported by metabolic theory. Thus, rates at the incubator's warmer end were on average 26% higher than those in (2°C) cooler temperatures. Warmer water temperatures could have elevated the metabolic rate of animals (Brown *et al*., 2004). Furthermore, oxygen solubility is inversely related to temperature. Clearly, temperature control is of critical importance in incubator studies involving the measurement of oxygen, and this should be better managed in future experimental work.

The macrofaunal community present in the surface (0-1cm) layer of the microcosms was typically dominated by polychaetes. Other motile fauna e.g. ophiuroids were also well represented in several of the cores. The observed macrofaunal activity, indicated

by the formation of new tracks, burrows and burial marks was present across all treatments and therefore cannot necessarily be explained by stress-induced behaviour (e.g. decreased burrowing, Scarlett et al., 2007c) in relation to the added oil. Future work could consider in more detail the effect of oil on burrowing activities of macrofauna, as it is possible that toxicity-induced stress might induce either shoaling or burrowing away from the sediment surface. A non-significant effect of WAF treatment on the distribution of total macrofauna biomass was found here. However, greater taxonomic resolution might enhance the interpretation of this result

The ecological relevance of studying a community with microcosms has its limitations (Carpenter, 1996). The microcosms used in this experiment were designed to replicate as close as practicable the conditions present at the seafloor. With shallow water studies it is feasible to control the number of individuals or species of macrofauna present in each microcosm (e.g. Ieno *et al*., 2006; Mayor, *et al*., 2013). However, intertidal fauna are by necessity relatively tolerant and so may be reasonably resistant to careful handling. The sediment cores used in the present study were handled as quickly and carefully as possible so as to avoid any artefacts caused by undue warming of the cores, and randomisation was employed at every step in the experiment to eliminate bias.

Mortality (either acute or delayed) was not measured in the experiment. In this study it was also not possible to predict mortality in relation to the WAF treatments with confidence as the toxicity of crude oil to deep water invertebrates is not well known. Deep-sea ecotoxicological research is generally lacking and there are very few examples of studies that address the impact of oil on macrofauna in this context (Vevers *et al*., 2010). It is likely that as with shallow water species some will be more tolerant than others, possibly related to their feeding mode. There is a large range of LC_{50} values reported in the literature for shallow water organisms, with some organisms being very tolerant e.g. median lethal concentrations as high as 13.9 mg L^{-1} (total petroleum hydrocarbons, TPH) 48 hour LC_{50} for the polychaete *Neanthes arenaceodentata* exposed to WAF (Rossi *et al*., 1976). In contrast, a relatively low exposure of 0.95 mg L^{-1} (TPH) elicited acute mortality (24 hour LC_{50}) in the decapod *Pandalus danae* (Rice *et al*., 1976). Acute mortality tests have been developed to standardise the assessment of pollution across gradients of exposure. However, the susceptibility of individual organisms in acute LC_{50} tests does not account for the diversity of exposure modes

present to an entire macrofaunal community (e.g. deposit feeders vs filter feeders). Also, acute mortality tests do not measure delayed mortality, which may occur days, weeks or months after exposure to a contaminant (Brodersen, 1987; Scarlett et al., 2007b).

The carbon remineralisation rate in the control cores was estimated as 24.5 mg C m^{-2} d^{-1} assuming a respiratory quotient of 1 (i.e. moles of oxygen consumed = moles of CO_2 evolved). Although the benthic community may have changed over time, as has been observed elsewhere in the deep ocean (Ruhl & Smith, 2004) the result found here compares well to previous measurements of benthic remineralisation at the Goban Spur. Heip *et al*., (2001) measured rates of 22 mg C m^{-2} d^{-1} in undisturbed conditions of the Goban Spur area at approximately the same depth and also in summer, attributing approximately half of this quantity of remineralisation to the macrofauna. By subtraction, Heip *et al.* (2001) therefore attributed almost half of the benthic remineralisation on the continental slope at this site to bacteria. Bacteria are typically large contributors to benthic respiration at both continental slope (Heip *et al*., 2001) and abyssal depths (van Oevelen *et al*., 2012). The importance of bacteria as part of the sediment community is addressed in Chapter 3, where the effect of hydrocarbons on bacteria community composition and biomass is studied.

Sediment community oxygen consumption is an easily measured community metric that can be measured in relation to pollution stress (Olsen *et al*., 2007a). An improved understanding of perturbations in rates of SCOC in the presence of contaminants may help to develop a better understanding of ecosystem functioning in relation to disturbance. However, for SCOC to be of most use in impact assessment, background levels need to be established across different sediment types, seasons and disturbance regimes to provide sensible baselines for comparison.

Chapter 3: Hydrocarbon contamination effects on deep-sea SCOC and microbial community composition

3.1 Introduction

Following the Macondo oil well blowout and the subsequent sinking of the Deepwater Horizon drilling rig, the leaking oil and gas entered a range of transport pathways (Ryerson *et al*., 2011). In addition to forming surface slicks and evaporating into the atmosphere, dissolved oil and small droplets formed multiple horizontal intrusions that were entrained into currents in the deep ocean (Camilli *et al*., 2010; Reddy *et al*., 2011; Socolofsky *et al*., 2011). These hydrocarbon 'plumes' persisted for months, triggering blooms of bacteria (Hazen *et al*., 2010) that produced a local, persistent depletion of oxygen in the water column as oil respiration occurred (Kessler *et al*., 2011). Oil persisted at toxic concentrations for months after the initiation of the leak, both in the water column and in sediments on the continental slope (Paul *et al*., 2013).

Mechanisms through which Macondo oil arrived at the seabed have been discussed following the accident. Aggregates of oil with particulate organic matter were observed in the water column that could have been exported from the euphotic zone (Passow *et al*., 2012). Oil in subsurface intrusions could also be advected directly onto a slope according to the so-called 'toxic bathtub ring' hypothesis (Deepwater Horizon Oil Spill Principal Investigator Workshop Final Report, 2012). At the seabed, tidal pumping of pore waters and faunal ventilation of burrow structures may draw oil beneath the sediment surface. Hence, there are multiple pathways through which deep-sea benthos may come into contact with hydrocarbon contaminants following a spill. At the seabed, there was strong evidence that oil from the Macondo well caused stress to benthic fauna (White *et al*., 2012) and the seabed area affected was > 3200 km^2 (Valentine *et al*., 2014).

Impacts of oil industry activities and pollution have commonly been measured by assessing changes in species assemblages of benthic invertebrates in response to pollution (e.g. Gray *et al*., 1990). Other benthic community measures, e.g. sediment community oxygen consumption (SCOC, the consumption of oxygen by all living biota within a sediment community) can also indicate health status, as it provides an index of whole community metabolism (Smith and Teal., 1973; Brown *et al*., 2004; Glud, 2008). Oxygen demand also commonly correlates with indicators of stress in the marine benthos (Hyland *et al*., 2005).

Effects of hydrocarbons on benthic respiration rates have previously been studied experimentally, where oxygen demand of shallow (200-300m) Arctic marine sediment communities increased in response to high concentrations of crude oil slurry (Olsen *et al*., 2007a). Sedimentation by drill cuttings also results in chronic increases in benthic respiration and changes to the structure and functioning of benthic communities (Schaanning *et al*., 2008; Trannum *et al*., 2011). Increases in respiration rates reflect the up-regulation of compensatory mechanisms in response to hydrocarbon contaminants (Widdows *et al*., 1995; Olsen *et al*., 2007b).

Crude oil has known toxic effects in metazoans and it can also cause stress and toxicity in bacteria (Griffin & Calder, 1977). However, for certain groups of hydrocarbon-degrading bacteria, the introduction of oil into a system instead represents a food source (Yakimov *et al*., 2007). Hydrocarbon-degrading bacteria are among the few organisms that possess the enzymes necessary to break up large, complex hydrocarbon molecules, converting them to smaller molecules, until they form simple sugars (Atlas, 1981). Oil-induced stress is however also possible in hydrocarbon-degraders at very high concentrations. For example, inhibitory concentrations of toluene (740 μM) and ethyl-benzene (315 μM) resulted in the production of membrane-protecting phospholipids in oil degraders (Zink and Rabus, 2010).

Biodegradation of crude oil by hydrocarbon-degrading bacteria tends to preferentially targ*et al*kanes and alkenes (Peters *et al*., 2005) and monoaromatic hydrocarbons (Jobson *et al*., 1972; Oudot, 1984; Jechalke *et al*., 2013; Muñoz *et al*., 2007) and as crude oil is biologically weathered, these compounds are removed or altered before the larger, heavier more polar compounds are broken down.

The use of oil as a metabolic substrate by marine sediment bacteria communities has been observed to lead to a shift in the isotope ratio of their respired carbon (Lapham *et al*. 1999). The depletion of evolved CO_2 with respect to ^{13}C in slurry experiments where bacteria were exposed to petroleum products hence demonstrated the ability of bacteria to perform hydrocarbon breakdown. The importance of bacteria for hydrocarbon breakdown, and thus bioremediation of shallow water oil spills has also been demonstrated in the field, where ^{14}C isotope ratios of microbial phospholipid fatty acids (PLFAs) indicated *in situ* biodegradation of alkanes at a beach site (Slater *et al*., 2006).

Microbial membrane PLFAs, which degrade quickly from non-living cells (White *et al*., 1979), have been used to quantify bacteria biomass (Moodley *et al*., 2005) and identify carbon sources of bacteria through measurement of their isotopic signatures (Boschker & Middelburg, 2002). The changing profiles of PLFAs in sediments exposed to hydrocarbons has been used to reflect functioning of the resident bacteria community and show uptake of oil in the process of hydrocarbon degradation (Pelz *et al*., 2001; Aries *et al*., 2001).

Our understanding remains incomplete with respect to the effects of oil on the structure of natural, deep-sea benthic microbial communities, their functioning with respect to respiration rates and their capacity to metabolise hydrocarbon contaminants. Pollution by hydrocarbons and drill cuttings has been shown to increase total oxygen uptake in both Arctic and temperate shallow (200-300 m) marine sediments (Olsen *et al*., 2007b). However, we do not yet have a detailed understanding of the effects of oil on the structure of deep-sea benthic communities and their functioning with respect to respiration rates. Although hydrocarbon degraders bloomed in the water column in response to oil following the Macondo spill (Valentine *et al*., 2010; Redmond & Valentine, 2011; Kessler *et al*., 2011), it was not clear what response might have occurred in the benthic microbial community.

3.1.1 Aims

In order to predict the implications of future oil well blowouts to the functioning of benthic environments, a better understanding of the response of benthic remineralisation rates and microbial communities to oil-induced disturbance is needed. This was studied

here by means of an *ex situ* microcosm experiment on sediments collected directly from an uncontaminated continental slope at ~1000 m water depth. Effects of WAF (water accommodated fraction) at two treatment levels were measured on SCOC, benthic bacterial biomass and community composition. Isotopic signatures of PLFAs ($\delta^{13}C$ values) were examined to investigate whether WAF exposure resulted in uptake of oil by benthic bacteria. The null hypotheses tested here were as follows:

- Addition of hydrocarbons in WAF does not influence benthic respiration rates;
- Bacterial biomass is not affected by WAF;
- Bacteria community structure, or the isotopic composition of individual PLFAs are not affected by WAF.

3.2 Methods

Sediment cores (10 cm internal diameter with overlying water) were collected at the Goban Spur site (described in Chapter 2, section 2.2) on 23rd July 2012 (Table 3.1). The ambient bottom water temperature was 9.2 °C.

Table 3.1. Details of sediment cores collection, treatment and subsequent analysis.

F = cores preserved in formalin for macrofauna biomass quantification; P = cores frozen at -80°C for prokaryote investigation.

Core ID	Station	Latitude	Longitude	Depth (m)	Treatment (% WAF)	Post experiment analyses
110	D377-56	49º 35.517 N	011º 50.872 W	996	25	F
111	D377-56	49º 35.517 N	011º 50.872 W	996	50	P
112	D377-56	49º 35.517 N	011º 50.872 W	996	0	F
113	D377-56	49º 35.517 N	011º 50.872 W	996	25	P
114	D377-57	49º 35.521 N	011º 50.828 W	995	50	F
115	D377-57	49º 35.521 N	011º 50.828 W	995	0	P
116	D377-57	49º 35.521 N	011º 50.828 W	995	0	F
117	D377-57	49º 35.521 N	011º 50.828 W	995	50	P
118	D377-57	49º 35.521 N	011º 50.828 W	995	25	P
119	D377-58	49º 35.424 N	011º 50.733 W	994	0	P
120	D377-58	49º 35.424 N	011º 50.733 W	994	25	P
121	D377-58	49º 35.424 N	011º 50.733 W	994	50	F
122	D377-58	49º 35.424 N	011º 50.733 W	994	0	F
123	D377-58	49º 35.424 N	011º 50.733 W	994	25	F
124	D377-59	49º 35.426 N	011º 50.847 W	992	50	P
125	D377-59	49º 35.426 N	011º 50.847 W	992	50	F
126	D377-59	49º 35.426 N	011º 50.847 W	992	25	F
127	D377-59	49º 35.426 N	011º 50.847 W	992	0	F
128	D377-59	49º 35.426 N	011º 50.847 W	992	0	P
129	D377-60	49º 35.488 N	011º 50.816 W	992	0	P
130	D377-60	49º 35.488 N	011º 50.816 W	992	50	P
131	D377-60	49º 35.488 N	011º 50.816 W	992	50	F
132	D377-60	49º 35.488 N	011º 50.816 W	992	25	F
133	D377-60	49º 35.488 N	011º 50.816 W	992	25	P

3.2.1 Preparation of water accommodated fraction of crude oil

Seawater was collected from immediately above the seabed at the study location prior to coring operations in order to produce WAF (methods as described in Chapter 2, Section 2.2.1) using crude oil from the Wytch Farm oilfield (Dorset, UK, obtained fresh in June

2012). The natural carbon stable isotope ratio, $\delta^{13}C$, of the whole crude oil was determined using a Flash EA 1112 Series Elemental Analyser connected via a Conflo III to a Delta^{Plus} XP isotope ratio mass spectrometer (all Thermo, Bremen, Germany; analysis performed by the James Hutton Institute, Aberdeen). The isotope ratios were calculated using CO_2 reference gas injected with every sample. The isotopic values of this gas was directly referenced using International Atomic Energy Agency (IAEA) reference materials USGS40 and USGS41 (both L-glutamic acid); certified for $\delta^{13}C$ ($‰_{VPDB}$). Long term precision, over several months, for a quality control standard (milled flour) was: $\delta^{13}C$ -25.5 ± 0.29 ‰ (mean ± sd, n = 200).

3.2.2 Sediment core collection

A total of 24 sediment cores (10 cm internal diameter and between 20 and 40 cm sediment height) and overlying water were collected using a Bowers and Connelly megacorer (Barnett *et al*., 1984) and immediately transferred to an incubator set at the ambient bottom water temperature (9.2°C). The temperature of the cores was further controlled by keeping the ambient temperature of the enclosing room constant (also at 9.2°C). Cores were acclimated to experimental conditions for approximately 24 hours in the dark.

3.2.3 Treating sediment cores with WAF

Sediment core tubes were contaminated with WAF at two treatment levels (eight replicates per treatment) and eight cores formed controls. Treatments of WAF were applied at low (25% overlying water volume) and high (50% overlying water volume) levels. In the controls, 25% of the overlying water was exchanged with uncontaminated bottom seawater. Samples of WAF (450 mL) were preserved with 50 mL hydrochloric acid (specific gravity 1.18, 12.2 M) for later laboratory analysis of WAF composition (ERT Fugro, UK). This was done at intervals spanning the cores treatment period in order to monitor stability of the mixture and provide an estimate of hydrocarbon concentrations in treatments (Table 3.2). All experimental apparatus, and the glass aspirator bottle used for WAF preparation on the ship, were cleaned thoroughly and

rinsed with hydrochloric acid followed by deionised water before use in the experiment. All glassware used for subsequent analytical work was combusted at 450 °C before use.

Table 3.2. Concentration (mg L^{-1}) of analytes in WAF (Analysis performed by ERT Fugro, UK). Sample 1 was preserved after 24 hours of low energy stirring. Samples 2 and 3 were preserved after a further 50 and 70 minutes during the process of cores treatment respectively.

	Sample 1	Sample 2	Sample 3
Benzene	0.5	0.4	0.5
Toluene	0.7	0.6	0.8
Ethyl Benzene	0.1	0.1	0.1
m,p-xylene	0.2	0.2	0.3
o-xylene	0.1	0.1	0.2
Oil total	1.8	1.8	4.4
BTEX total	1.6	1.4	1.9

3.2.4 Incubation of microcosms

Following addition of WAF/water, the sediment cores were immediately sealed without a headspace and incubated at the ambient seabed water temperature. Oxygen concentration in the overlying water was measured at intervals of approximately 6 hours using a non-invasive PreSens Fibox oxygen sensor. The oxygen sensor was calibrated at known temperature by taking readings in high (aerated water) and zero concentration water (5 g anhydrous sodium sulfite was added to 500 mL seawater). The overlying water in each core was stirred manually for approximately 10 seconds every two hours and for 10 seconds preceding measurement of oxygen and incubations were ceased when (or before) core overlying water oxygen concentration reached ~80% of starting levels.

3.2.5 Slicing and preserving sediment horizons

All cores were sectioned at depth horizons (0-1 cm; 1-2 cm) at the end of the incubation period. The sediment horizons of four replicates from each treatment and controls were preserved in 4% formaldehyde for later macrofauna analyses. The remaining sediment was frozen at -80°C for subsequent PLFA analyses (details in Table 3.1).

3.2.6 Macrofauna biomass

Macrofauna were removed from the sediment sections following staining with Rose Bengal and washing on a 500 μm sieve. The animals were sorted into phyla under a reflecting microscope (Natural History Museum, London, UK). Total wet weight biomass was then summed and quantified for depth layers. Wet weights were summed for the 0 – 1 cm; 1 – 2 cm; 2 – 5 cm and 5 – 10 cm sediment layers and an estimate of total macrofauna biomass (mmol C m^{-2}) was calculated, assuming 12.4% carbon content for nematodes (Jensen, 1984) and 4.3% carbon content for all other animals (Rowe, 1983) except ophiuroids (1.9% carbon content). For the present chapter, macrofauna biomass data from the 0 – 1 cm and 1 – 2 cm sediment horizons were analysed in relation to the null hypothesis that there were no WAF treatment effects on macrofauna biomass in these depth layers.

Biomass data from all four sediment horizons were used to investigate WAF treatment effects on the distribution of macrofauna biomass in Chapter 2.

3.2.7 Extraction and quantification of PLFAs

Phospholipid fatty acids were extracted from freeze-dried sediment from the 0-1 cm and 1-2 cm horizons. All solvents used were HPLC grade. Following an extraction method modified from Bligh and Dyer (1959), lipids were extracted from 9.0 g freeze-dried sediment for each replicate sample using a single phase mixture of chloroform : methanol : citrate buffer 1 : 2 : 0.8 v:v:v, Frostegård *et al*., (1991). The lipids were fractionated using 6 mL ISOLUTE SI SPE columns (solid phase extraction with silica as the sorbent, International Sorbent Technology Ltd, Hengoed, UK) preconditioned

with 5 mL chloroform. Dry lipid material was taken up in 400 µL chloroform, vortex mixed twice then transferred onto the column. The vial was rinsed three times with 200 µL chloroform then added to the column on each occasion. The sample was then allowed to pass through the column. The columns were washed sequentially with 2 x 3 mL of chloroform then 2 x 3 mL acetone, these eluates were not retained. The column was then washed with a total of 10 mL methanol. All methanol eluates, containing the PLFAs, were collected in a glass vial, slowly evaporated to dryness under nitrogen gas and stored at – 20°C until further processing.

The PLFAs were subsequently derivitised with methanol to yield fatty acid methyl esters (FAMEs). Each sample was taken up in 1 mL of a 1:1 (v:v) mixture of methanol and toluene in a vial. Then, 1 mL of 0.2 M KOH in methanol was added with a known quantity of C19 internal standard, vortex mixed and incubated at 37°C for 15 minutes. After cooling to room temperature 2 mL of isohexane: chloroform (4:1 v:v), 0.3 mL of 1 M ascetic acid and 2 mL deionized water was added to each vial. The solution was vortex mixed, placed on an end over end mixer for 10 minutes, then centrifuged. The organic phase was transferred to a new vial. The aqueous phase was re-extracted with a further 2 mL of isohexane:chloroform (4:1) and centrifuged as before. Both resultant organic phases were combined, evaporated under nitrogen and stored at -20^{o}C. The residue was extracted with 3 x 100 µL isohexane:chloroform (4:1) and transferred to a glass vial. The solvent was evaporated with nitrogen and samples were stored at -20^{o}C. Samples were taken up in isohexane immediately prior to analysis by gas chromatography-combustion-isotope ratio mass spectrometry (GC-C-IRMS).

The isotopic composition and quantification of individual FAMEs was determined using a GC Trace Ultra with combustion column attached via a GC Combustion III to a Delta V Advantage isotope ratio mass spectrometer (all Thermo Finnigan, Bremen, Germany). Samples (2 µL) were injected in splitless mode, via an inlet held at 250 ^{o}C, onto a J&W Scientific HP-5 column, 50 m length, id 0.2 mm with a film thickness of 0.33 µm (Agilent Technologies Inc, Santa Clara, USA). The He carrier gas was maintained at a constant flow rate of 1.5 mL min^{-1}. The GC oven was initially set at 100^{o}C, held for 1 min and then ramped at 20^{o}C min^{-1} to 190^{o}C, then at 1.5^{o}C min^{-1} to 235^{o}C and finally at 20^{o}C min^{-1} to 295^{o}C; where the temperature was held for 15 min. The oxidation reactor on the interface was maintained at 950^{o}C and the reduction reactor at 650^{o}C.

The $\delta^{13}C_{VPDB}$ values (‰) of the FAMEs were calculated with respect to a CO_2 reference gas injected with every sample and traceable to International Atomic Energy Agency reference material NBS 19 TS-Limestone. Isodat 3.0 Gas Isotope Ratio MS Software (Ver 3.0) (ThermoFisher Scientific, Bremen, Germany) was used for data processing, and the final results were exported into Excel, then further processed using in house Visual Basic macros, which enabled the selection of peaks of interest using relative retention time with respect to the internal standard. The macros also corrected $\delta^{13}C$ values of FAMEs for C added as a methyl group during derivatisation using a mass balance approach. Precision of the $\delta^{13}C$ FAME analysis was indicated by the $\delta^{13}C$ values determined for the C19 internal standard added to all samples; $\delta^{13}C$ = -32.44 ± 0.67 ‰ (mean ± sd, n = 23). Measurement of the Indiana University reference material hexadecanoic acid methyl ester #1 (certified $\delta^{13}C_{VPDB}$ value = -30.74 ± 0.01 ‰) gave a value of -30.86 ± 0.17 ‰ (mean ± sd, n = 13). The combined area of all mass peaks (*m/z* 44, 45 and 46) after background subtraction were collected for each individual FAME peak. These combined areas, relative to those of the internal standard, were used to quantify the 18 most ubiquitous FAMEs and subsequently the PLFAs from which they were derived, as described by Thornton *et al*. (2011).

Various nomenclatures describing the composition of individual PLFAs are in common use in the literature. The system adopted in the present study uses a number to indicate the length (in carbon atoms) of the fatty acid chain followed by a colon symbol and the number of double bonds. The position of the double bond from the methyl end of the molecule is indicated by a number in brackets. If a further methyl group is present this appears at the start as 'Me' with its position along the carbon chain (starting at the carboxylic acid end of the molecule).

For example, pentadecanoic acid, $CH_3(CH_2)_{13}COOH$, is denoted as 15:0, and palmitoleic acid, $CH_3(CH_2)_5CH{=}CH(CH_2)_7COOH$, as 16:1(n-7).

Bacterial biomass was estimated from the concentration of the bacterial biomarker PLFAs: 15:0i, 15:0ai and 16:0i (Moodley *et al*., 2005; Mayor *et al*., 2012a,b) assuming that these PLFAs make up 10% of total bacterial PLFAs and that there is 0.0056g C PLFA / g C biomass (Brinch-Iversen and King, 1990). Estimating bacterial biomass on the basis of specific biomarker PLFAs has the potential to over- or under represent particular groups of bacteria (e.g. Gram-negative or Gram-positive), depending on the

relative abundance of biomarkers in these organisms at the study location. Nevertheless, the PLFAs used to estimate bacteria biomass in this study,15:0i, 15:0ai and 16:0i, are widely used across a range of marine benthic ecosystems as generic bacterial biomarkers (Boschker & Middelburg, 2002; Moodley *et al*., 2005; Bouillon & Boschker, 2006) and therefore provide a reasonable approximation for the overall community response.

3.2.8 Data analysis

Data exploration (Zuur *et al*., 2010) and analysis were conducted using the statistical programming language R (R Core Team, 2013). Statistical models were constructed, using the packages 'nlme' (Pinheiro *et al*., 2014) and 'vegan' (Oksanen *et al*., 2013). Oxygen concentration- and benthic biomass data were examined using linear regression techniques (Pinheiro and Bates, 2000; Zuur *et al*., 2009). The effects of time, treatment (Control, 25% WAF and 50% WAF) and a time × treatment interaction on oxygen concentrations in core overlying water were assessed with a linear mixed effects (LME) statistical model. Core identity was included as a random effect (L. ratio = 337, df = 1, $p < 0.001$) to allow for the correlation of data collected within each core (Zuur *et al*., 2009). Treatment effects on the biomass of bacteria and macrofauna were examined using generalised least squares (GLS) models that included variance covariates to account for instances of heterogeneity. Preliminary analyses examining the interaction between treatment and sediment depth revealed strong heterogeneity in the residual plots. GLS models that allowed the residual spread to vary by treatment level were also used to examine treatment effects on the isotopic signatures of individual PLFAs. Biomass data from the 0-1 and 1-2 cm sediment horizons were therefore analysed separately. The optimal structures of all linear models were determined using backwards selection based on the L. ratio test with maximum likelihood estimation.

Relative abundance (mol %) and stable carbon isotope ratios ($\delta^{13}C$) of the 18 identified PLFAs were examined using redundancy analysis (RDA). Both of these datasets differed significantly between the 0-1 cm and 1-2 cm depth horizons (Figures A2.1 and A2.2) and were therefore analysed separately. The significance of treatment effects were examined using a permuted Monte Carlo test (n = 9999; Zuur *et al*., 2007; Mayor

et al., 2013). Redundancy analysis was also performed on the raw PLFA concentration data (Figure A2.3) to check that similar statistical significance was obtained.

3.3 Results

Oxygen concentrations were affected by a highly significant Time × Treatment interaction (Tables 3.3 and A2.1), indicating that the rate of SCOC was significantly increased by WAF treatment (Figure 3.1). Estimated remineralisation rates were calculated as 1.50 mmol C m^{-2} d^{-1} in control cores; 2.66 mmol C m^{-2} d^{-1} in 25% WAF treated cores and 3.08 mmol C m^{-2} d^{-1} in 50% WAF treated cores (assuming a respiratory quotient of 1).

Table 3.3. Summary of results from the statistical tests (LME, linear mixed-effects; GLS, generalized least squares; RDA, redundancy analysis).

Response	Model	Model term	Df	L-ratio	F	p value
Oxygen concentration	LME	Treatment×time	2	69.6		< 0.001
Bacterial biomass (0 - 1 cm)	GLS	Treatment	2	7.78		0.02
Bacterial biomass (1 - 2 cm)	GLS	Treatment	2	9.27		0.01
Macrofaunal biomass (0 - 1 cm)	GLS	Treatment	2	3.67		0.16
Macrofaunal biomass (1 - 2 cm)	GLS	Treatment	2	0.16		0.92
PLFA composition (0 – 1 cm)	RDA	Treatment	2		2.05	0.03
PLFA composition (1 – 2 cm)	RDA	Treatment	2		1.38	0.13
PLFA $\delta^{13}C$ (0 - 1 cm)	RDA	Treatment	2		1.02	0.42
PLFA $\delta^{13}C$ (1 - 2 cm)	RDA	Treatment	2		0.757	0.77

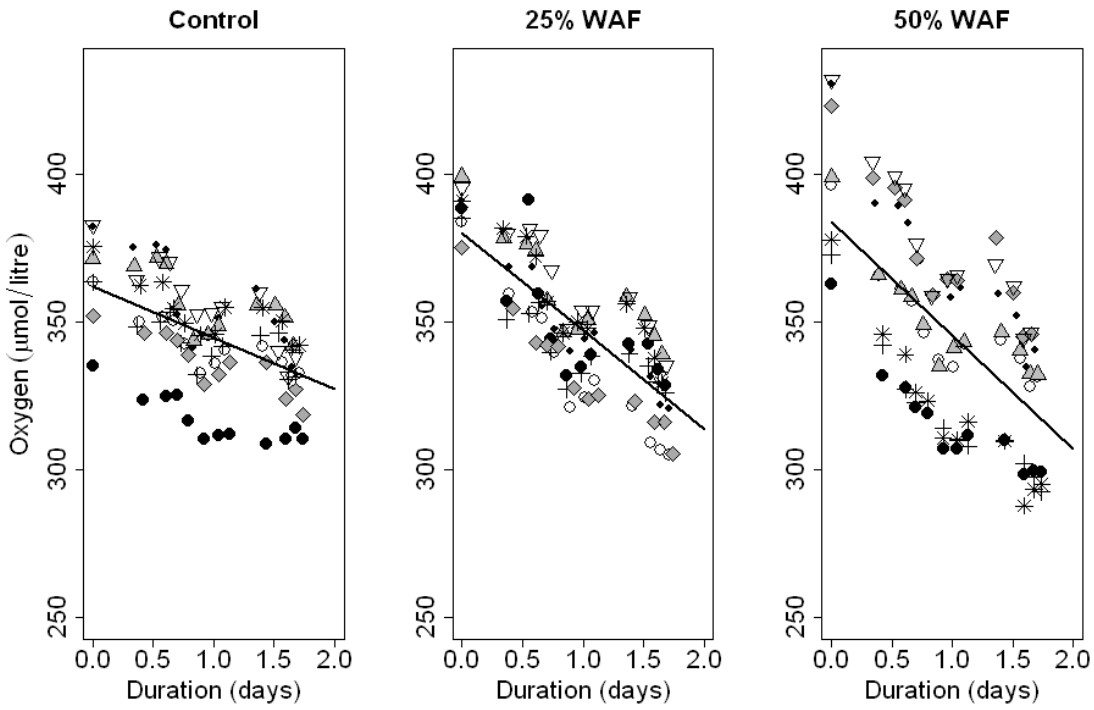

Figure 3.1. Oxygen concentration in cores overlying water over the 36-hour incubations. Cores are grouped by treatment in each panel, where symbols of same type show data from the same core. Lines show linear models fitted to the replicate data (n=8). Control cores had 25% of their water exchanged with uncontaminated bottom seawater at the start of the experiment.

Bacterial biomass present in the microcosms was over an order of magnitude greater than that of metazoans (Table 3.4). There was a significant treatment effect on bacterial biomass in both the 0-1 cm and 1-2 cm sediment layers (Tables 3.3, 3.4, A2.2, A2.3); increasing concentration of hydrocarbons typically resulted in a decrease in bacterial biomass. In contrast, macrofaunal biomass in the 0-1 and 1-2 cm sediment horizons remained unaffected by hydrocarbon contamination (Tables 3.3, 3.4, A2.4, A2.5).

Table 3.4. Bacterial and macrofaunal biomass in the sediment horizons investigated.

	Mean bacterial biomass (mmol C m^{-2} ± SE)		Mean macrofaunal biomass (mmol C m^{-2} ± SE)	
Depth Horizon	0-1 cm	1-2 cm	0-1 cm	1-2 cm
Control	68 ± 14	69 ± 7.7	2.9 ± 0.7	7.4 ± 4.0
25% WAF	43 ± 3.8	37 ± 4.1	8.5 ± 4.6	6.1 ± 2.6
50% WAF	28 ± 5.7	53 ± 10	7.7 ± 3.2	7.2 ± 2.6

The full set of PLFA compositional (mol%) and isotopic ($\delta^{13}C$) data from the 0-1 cm and 1-2 cm sediment horizons are presented in the Appendix in Tables A2.6-A2.7. Concentrations of PLFAs (0–1 cm) are presented in Figure A2.3. There was a significant effect of treatment on the relative composition of PLFAs in the surficial layer (Table 3.3; Figs. 3.2 a and b) and on PLFA concentration (df = 2; F = 3.39; p = 0.04, Figure A2.3). Control cores were discriminated from those in the 25% WAF treatment along the first axis (vertical axis) of Figure 3.2a and b, which explained 24.2% and had positive loadings of 18:1(n–7) and negative loadings of 14:0, 15:0i, 16:0, 16:0i, 17:0 and 17:0ai. The 50% WAF treatment was discriminated on the second axis (horizontal axis), which explained 7.0% of variation. This axis had positive loadings of 16:1(n-5), 19:1(n-5) and negative loadings of 18:1(n-9). Replicate observations of the composition of PLFAs in the 1-2 cm layer also grouped by treatment (Figs. 3.2c and d), although treatment effects were not statistically significant (Table 3.3). The first axis, which explained 14.4% of the variation, had positive loadings of 19:0cy and negative loadings of 17:0, 18:0 and 12Me16:0. The second axis explained 9.0% of the variation and had positive loadings of 18:1(n-9) and 16:1(n-5), and negative loadings of 16:1(n-7) and 19:1(n-6).

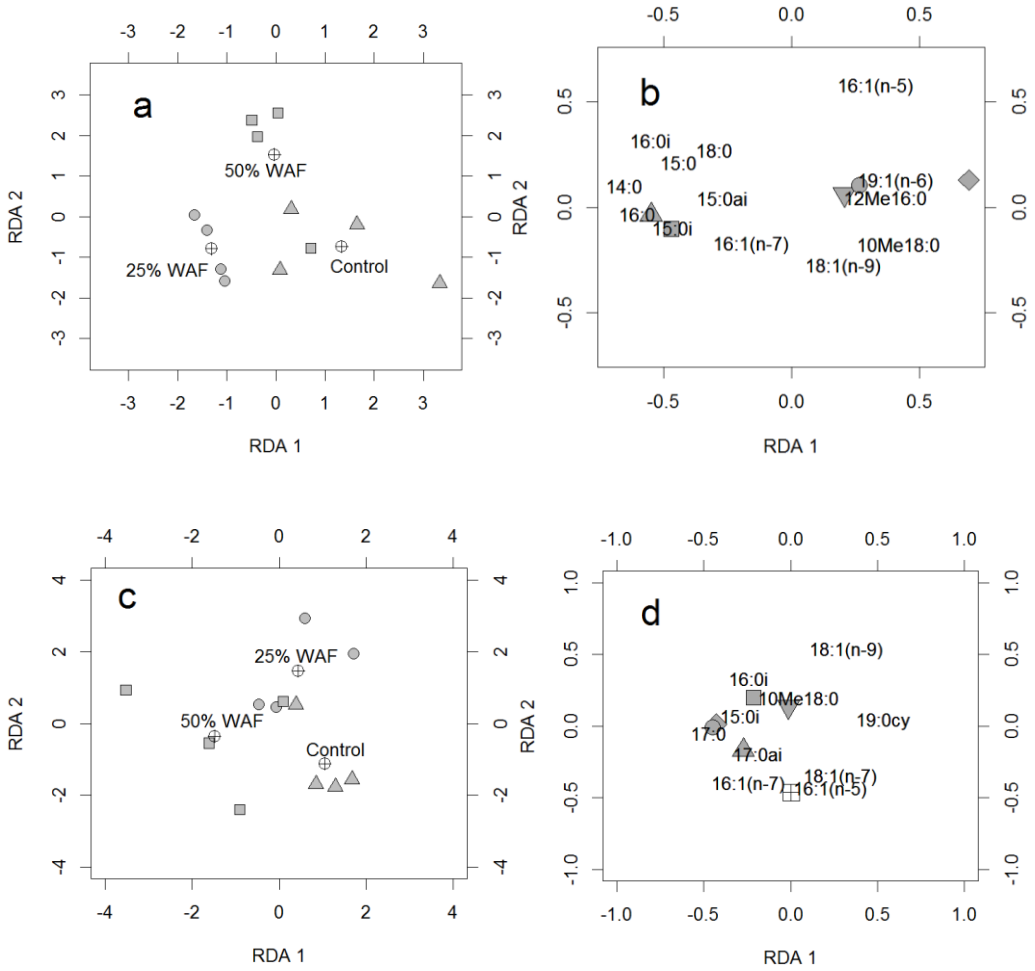

Figure 3.2. Redundancy analysis plots showing the effect of treatment on microbial PLFA proportion data in the top 0 - 1 cm (panels a and b) and 1 – 2 cm (panels c and d) of sediment at the experiment end. Ordination of individual cores is shown by plotting different symbols for each treatment (panels a and c). Triangles = controls; circles = 25% WAF; squares = 50% WAF. Effects of each treatment are shown by crossed circles. Ordination of individual PLFAs, indicated by their names (panels b and d). The following have been plotted with symbols for visual clarity: (b) square = 17:0; upward pointing triangle = 17:0:ai; downward pointing triangle = 17:1(n-8); circle = 19:0cy; diamond = 18:1(n-7). (d) square = 14:0; upward pointing triangle = 15:0; downward pointing triangle = 16:0; diamond = 12Me16:0; circle = 18:0; crossed square = 19:1(n-6).

The stable carbon isotopic composition ($\delta^{13}C$ value) of whole crude oil was -29.2‰. The $\delta^{13}C$ values of individual PLFAs in the 0-1 and 1-2 cm depth layers were not significantly affected by treatment (Table 3.3), although replicate observations in these horizons were visibly discernible by group (Fig. 3.3).

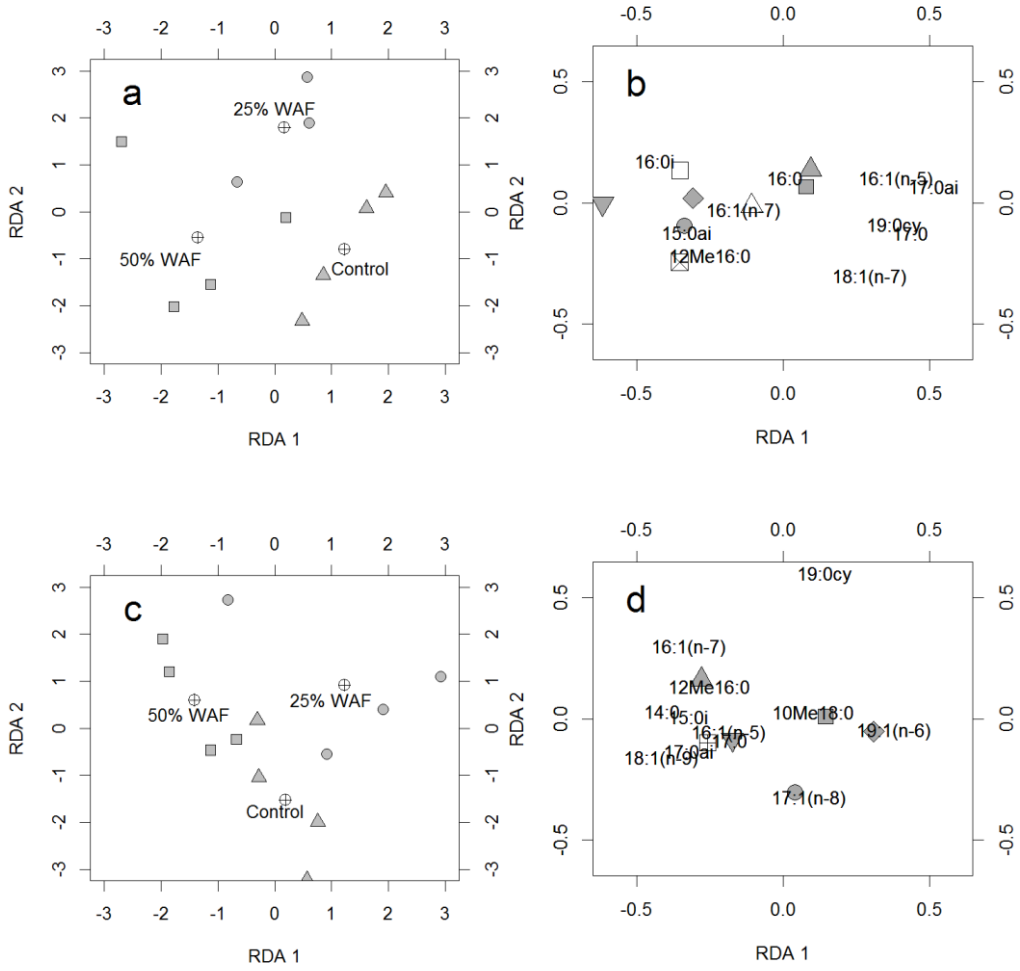

Figure 3.3. Redundancy analysis plots showing the effect of treatment on $\delta^{13}C$ values of microbial PLFAs at the end of the experiment in the 0-1cm (panels a and b) and 1-2 cm (panels c and d) layers. Ordination of individual cores is shown by plotting different symbols for each treatment (panels a and c). Triangles = controls; circles = 25% WAF; squares = 50% WAF. The effect of each treatment is shown by crossed circles. Ordination of PLFAs, is indicated by their names (panels b and d) with the following plotted with symbols for visual clarity: (b) crossed square = 14:0; downward pointing triangle = 15:0; circle = 15:0i; upward pointing triangle = 18:0; square = 18:1(n-9); diamond = 10Me18:0; open square = 19:1(n-6); open triangle = 17:1(n-8). (d) square =

15:0; upward pointing triangle = 15:0ai; downward pointing triangle = 16:0; circle = 16:0i; diamond = 18:0; crossed square = 18:1(n-7).

In the 0-1 cm layer (Figs. 3.3a and 3.3b) the first axis, which explained 15.4% of the variation, progressively discriminated the control cores from the WAF treated cores. This axis had positive loadings of 17:0ai, 17:0, 16:1(n-5) and 19:0cy and negative loadings of 15:0 and 16:0i. The second axis, which explained 3.14% of the variation, discriminated the replicate 25% WAF cores from all other cores. This axis had weak positive loadings of 16:0i, 18:0 and 19:1(n-6) and negative loadings of 18:1(n-7). In the 1-2 cm layer (Figs. 3.3c and 3.3d), only a low proportion of the variance was explained by the first and second axes; 8.9% and 5.5% respectively. Axis 1 had positive loadings of 19:1(n-6) and 18:0; axis 2 had a strong, positive loading of 19:0cy and negative loadings of 17:1(n-8)c and 16:0i.

Two compounds (17:0 and 17:0ai) became progressively depleted in ^{13}C in the surficial sediment, shifting from values of approximately -24‰ in the controls to < -27‰ in the 50% WAF treatment (Table A2.7). However, when investigated further, there was appreciable variance in the estimates at the 50% WAF level and treatment effects were not regarded as statistically significant (17:0ai: L. Ratio = 5.79, df = 2, p = 0.06; 17:0: L. Ratio = 5.10, df = 2, p = 0.08).

3.4 Discussion

This study demonstrated that SCOC rates and bacterial biomass (estimated using biomarker PLFAs) in a deep sea benthic community were significantly affected by exposure to increasing levels of WAF. The consistent grouping of the PLFA compositional and isotopic data by treatment suggests that the bacterial community composition and their metabolic functioning were also affected by exposure to WAF. The estimated rate of carbon remineralisation in the control cores, 1.5 mmol C m^{-2} d^{-1}, was very similar to the value of 1.8 mmol C m^{-2} d^{-1} reported previously at the experimental location (Heip *et al*., 2001) and the rate of carbon remineralisation in the upper WAF treatment level was approximately double that in controls. The significant increase in SCOC rate in response to WAF clearly demonstrates that exposure to these hydrocarbons affects deep-sea benthic organisms and hence the functioning of this environment, as has also been observed in shallower marine benthic habitats (Olsen *et al*., 2007a).

The present study was performed *ex situ* on sediments brought to the surface from ~1000 m water depth, and the effect of the change in pressure (e.g. barotrauma or stress) on the sediment microbial communities was assumed to be negligible. Effects of decompression have been observed to cause change in bacterial communities from abyssal depths (3170 m, Egan *et al*., 2012). However, oxygen consumption rates were not affected greatly by decompression for sediment communities collected from 1430 m (Graf, 1989) i.e. considerably deeper than the sediments used in the present study. Meyer-Reil and Köster (1992) also found no effect of pressure on the enzymatic performance of deep-sea bacteria from water depths of 1400 m – 2000 m.

Shifts in the stable carbon isotope values ($\delta^{13}C$) of some PLFAs lead to consistent grouping by treatments but these isotopic data were not found to be consistently or significantly different across the full range of PLFAs examined.

There were no clear effects of treatment on the quantity of macrofaunal biomass or its distribution in the 0 – 2 cm sediment depth horizons for which PLFA composition were obtained. A further hypothesis to assess the affect of treatment on macrofauna biomass down to 10 cm depth in the sediment also found no significant effect of treatment on the distribution of macrofauna biomass among depth horizons (see Chapter 2). Given the

short incubation time it is possible that mortality, which was not investigated as part of the study, may have contributed to the observed lack of either shoaling or burrowing into deeper layers. However, more targeted experiments would be required to further study the macrofauna as stress-induced behaviour caused by high concentrations of hydrocarbons could include, for example, burrowing avoidance behaviour and hence movement away from the stressor (Scarlett *et al*., 2007b). Since the sensitivity of different phyla and species to oil varies (Dauvin, 1998; Dauvin, 2000) enhanced taxonomic resolution would disentangle results that may be confounded by looking at biomass alone.

In contrast to the macrofauna biomass, bacterial biomass in the WAF-exposed cores was consistently lower than that in the controls, suggesting that the short-term exposure to hydrocarbons caused net mortality. This finding is consistent with results from a previous study: the PLFAs used to estimate microbial biomass here (15:0i, 15:0ai and 16:0i) decreased in a coastal marine benthic microbial community exposed to artificially weathered crude oil (Syakti *et al*., 2006). Lower bacterial biomass does not necessarily imply that the microbial contribution to SCOC was smaller. Instead, WAF exposure could have elicited stress responses in the fauna and the majority of active bacteria in the microcosms, resulting in increased respiration in both of these groups of organisms.

Oil-induced stimulation of hydrocarbon degrading bacteria results in increased oxygen consumption (Lee & Lin, 2013), even though these organisms potentially only represent a small component of the benthic community (Mazzella *et al*., 2005; Syakti *et al*., 2006). Little is known currently about how the physiology of deep-sea prokaryotic and eukaryotic organisms respond to oil exposure (Vevers *et al*., 2010). Hence it is not possible to predict how faunal and bacterial contributions of SCOC in our experiment changed from the biomass estimates alone. The relative contributions to increased oxygen consumption by stress-induced respiration and remineralisation of the introduced hydrocarbons are also not discernible.

Changes in the composition of sediment PLFAs and their isotopic signatures have previously been used to investigate how natural microbial communities respond to external stressors (e.g. Pelz *et al*., 2001; Mayor *et al*., 2013), and ^{13}C labeling techniques have traced the incorporation of oil-derived carbon into the biomass of hydrocarbon-degrading bacteria (Rodgers *et al*., 2000; Pelz *et al*., 2001).

Biodegredation in the field has been demonstrated for coastal microbial communities using isotopic analysis of ^{14}C (Slater *et al*., 2006; Mahmoudi *et al.,* 2013) and $\delta^{13}C$ values (Mahmoudi *et al*., 2013). The significant, oil-driven shift in the composition of PLFAs observed in surficial sediments here is consistent with the understanding that hydrocarbon exposure drives rapid changes in benthic microbial community structure (Hanson *et al*., 1999) and the composition of their PLFAs (Aries *et al*., 2001; Mazzella *et al*., 2005; Syakti *et al*., 2006).

Some consistent patterns emerged in PLFA composition. For example, the PLFAs that correlated positively with the WAF-treated sediments were typically saturated compounds, e.g. 14:0, 15:0, 16:0, 16:0i, 17:0, 17:0i and 18:0, many of which are frequently used as generic bacterial biomarkers. This observation agrees well with a range of studies that have investigated how the presence of hydrocarbons affects the PLFA composition of soils and sediments. For example, the PLFAs 15:0, 16:0, 17:0 and 18:0 have been reported to increase in soil microbial communities where hydrocarbon degradation was occurring via the activities of sulfate-reducing bacteria (Hanson *et al*., 1999; Pelz *et al*., 2001). Exposure to artificially weathered crude oil has also been reported to increase the prevalence of saturated PLFAs such as 15:0, 17:0 and 18:0 in a consortium of oil degrading marine bacteria (Aries *et al*., 2001), in a natural coastal benthic microbial community (Mazzella *et al*., 2005, Syakti *et al*., 2006) and in individual species extracted from therein (Mazzella *et al*., 2005). The monounsaturated PLFAs 16:1(n-5), 18:1(n-7) and 19:1(n-6) also contributed to significant discrimination between the treatments in our experiments, with 16:1(n-5) and 18:1(n-7) correlating positively with the control cores. These observations agree with the understanding that even-numbered chain length, monounsaturated PLFAs typically increase when hydrocarbon contaminants are removed (Aries *et al*., 2001; Syatki *et al*., 2006). The proportions of PLFAs in the surficial sediments did not always respond to the WAF treatment level in a linear manner; many of the saturated compounds increased in the 25% WAF treatment, whereas in the 50% WAF treatment they remained similar to values in the 25% WAF treatment or decreased towards control levels. This pattern of responses, and the association of these saturated compounds with hydrocarbon degrading bacteria (Hanson *et al*., 1999; Aries *et al*., 2001; Pelz *et al*., 2001) suggests that a component of the natural sediment microbial community was stimulated by the

presence of 25% WAF but inhibited (Muñoz *et al*., 2007) or even killed off in the highest, 50% WAF treatment.

Multivariate ordination of PLFAs $\delta^{13}C$ values revealed groupings by treatment in the 0-1 and 1-2 cm horizons (Fig. 3.3) but overall the result was not significant. The PLFAs 17:0 and 17:0ai in the surficial sediments became progressively depleted in ^{13}C, shifting from values of approximately -24 ‰ in the controls to ≤ -27 ‰ in the 50% WAF treatment (Fig. A2.3), and these compounds contributed strongly to discriminating the WAF-treated cores from the controls on the first axis (Fig. 3.3). Following the assumption that bacterial isotopic signatures reflect their nutrition source (Boschker & Middelburg, 2002) the isotopic signature ($\delta^{13}C$) of oil-degraders' PLFAs should eventually shift towards that of the oil (the bulk crude oil was measured as –29.2‰) as they incorporated the ^{13}C-depleted carbon into their lipids through the turnover of existing PLFAs and the production of new biomass (Lapham *et al*., 1999). However, there is evidence from previous studies on soils to suggest that such a rapid response might only happen in pre-exposed sediments (Zyakun *et al*., 2012). Non-significant effects of treatment on the isotopic composition of all PLFAs examined indicates either that the majority of PLFAs investigated did not respond consistently, or were not strongly affected by WAF. The progressive decrease in the $\delta^{13}C$ values of 17:0 and 17:0ai (Fig. A2.3), in contrast to the non-linear changes in the percentage abundance of these PLFAs (Fig. A2.1) may suggest a response by hydrocarbon degraders, but this cannot be concluded unequivocally. It is also likely that a range of other processes contributed to the observed shifts in the isotopic signatures of individual PLFAs, including the physiochemical conditions present (Teece *et al*., 1999) and the degradation of faunal biomass as a result of WAF-induced mortality (Mayor *et al*., 2013). The processes that govern the turnover rates of individual PLFAs, the microorganisms that produce them and the metabolic pathways that result in isotopic fractionation in natural sediment systems need further study (Lerch *et al*., 2010). Better understanding of these processes is required if we are to meaningfully interpret isotopic shifts in natural bacterial communities in response to accidental releases of hydrocarbons into the natural environment.

There is an emerging understanding that marine bacteria provide an intrinsic level of bioremediation in the event of hydrocarbons being released into surficial and deep

pelagic ecosystems (Slater *et al*., 2006; Hazen *et al*., 2010; Gutierrez *et al*., 2013). Benthic microbes also actively contribute to the removal of oil contaminants that reach the deep-seafloor (Kimes *et al*., 2013; Mason *et al*., 2014), but observations are currently scarce. This study showed that the contamination of deep-sea sediments with hydrocarbons will affect the structure and metabolic functioning of resident microbial communities. Since the microcosms used were formed from cohesive sediments taken directly from the seafloor they were a close emulation of what was naturally present. They therefore provide some initial insight into how a deep-sea benthic community responds to the presence of WAF. There is a clear need for more detailed information on how the physiology of deep-sea benthic organisms responds to hydrocarbon contamination so that the mechanisms underpinning these results can be more clearly understood. Future studies should not be limited to understanding the effects on sediment-dwelling microbes; benthic fauna contribute directly to SCOC and other ecosystem functions such as the recycling of nutrients. They also indirectly influence ecosystem functioning by mediating changes in the microbial community structure through their physical activities (e.g. Laverock *et al*., 2010; Mayor *et al*., 2013). Hence, the net, community-scale response to hydrocarbon contamination will likely reflect a range of interactive processes that are currently not possible to predict.

The deep-sea forms an important sink for carbon generated by surface production, with the processing of organic carbon at the seabed by benthos resulting in a fraction becoming buried. Understanding the carbon cycle, including disturbance-induced perturbations in benthic processes such as remineralisation give a measure of a whole-community response that will be a useful part of environmental assessment as our understanding of biogeochemical cycling continues to develop. As drilling operations currently continue to expand in the deep-sea, future large oil spills remain a possibility. Therefore, this work is of immediate relevance, because in order to predict the implications of future oil well blowouts, we need to build a better understanding of both benthic and pelagic processes following disturbance.

Chapter 4: Simulating trajectories of subsurface oil using a 3D GCM

4.1 Introduction

Following the Macondo 2010 oil well blowout, the ensuing leak of oil into the deep (~1600 m) Gulf of Mexico entered various transport pathways both below and at the ocean surface; contaminating deep-sea sediments (White *et al*., 2012; Montagna *et al*., 2013; Valentine *et al*., 2014) and the water column (Graham *et al*., 2010; Passow *et al*., 2012) as well as hitting widespread beaches (Aeppli *et al*., 2012) and evaporating to the atmosphere (Ryerson *et al*., 2011).

4.1.1 Subsurface oil and hydrocarbon plumes

The 1972 Ixtoc I oil well blowout in the Gulf of Mexico also showed that this type of incident leads to contamination across the entire water column. Water borne oil in concentrations of up to 10.6 mg L^{-1} were measured in close proximity (within several hundred metres) to the well head and a shallow water (~20 m) plume of suspended droplets was detected (Boehm & Fiest, 1982). Following the 2010 Gulf of Mexico spill, technology such as autonomous underwater vehicles (AUVs) and remotely operated vehicles (ROVs) was available that were able to sample and film the deep water environment. Hence, a new and advanced picture of what was going on beneath the surface emerged, yielding a more comprehensive understanding of how much oil remained subsurface and where it went.

The progression of oil leaking from an oil well blowout and the subsequent pathways it takes in the subsurface ocean depends on its buoyancy. The buoyancy of crude oil leaking from a well head depends on the proportion of gas emitted, subsequent gas hydrate formation, and oil droplet size and composition (Johansen, 2003; Yapa &

Dasanayaka, 2008; Dasanayaka & Yapa, 2009). Biological and chemical weathering processes change oil's composition in the environment and this also has an important effect on the behaviour of oil in seawater. Oil from the Macondo well blowout flowed as a hot (~100°C), high pressure jet into the much cooler (~4°C) surrounding ocean. Small droplets formed and a large proportion of the oil and gas dissolved (Reddy *et al*., 2011). The use of chemical dispersants at the Macondo well head further encouraged the formation of small oil droplets (National Research Council, 2005). Small droplets have less buoyancy, and following the Macondo blowout, droplets of < 100 µm diameter persisted in large, deep water plumes with dissolved monoaromatic hydrocarbons and methane (Camilli *et al*., 2010; Socolofsky *et al*., 2011).

In addition to these subsurface plumes, there are other mechanisms through which spilled oil is able to either remain subsurface, or become entrained there following an oil well blowout. The fact that bulk crude oil is less dense than seawater[6] naturally results in large quantities of oil quickly reaching the sea surface to form floating slicks. However, breaking waves at the surface can break the oil up into smaller droplets, and therefore encourage more oil to be mixed down into the water column. Oil in the water column can stick to particulates, forming aggregations of oil and sinking marine snow that transport oil downwards (Passow *et al*., 2012). The composition of oil in surface slicks changes quickly as lighter fractions evaporate or are preferentially removed by other weathering processes. This causes an increase in density of the remaining mixture, which can result in clumping and subsequent sinking of oil.

Subsurface oil was estimated to account for the largest proportion of the spilled Macondo oil that was detected and accounted for – in an estimate given by Ryerson *et al*. (2011). Beyond making direct measurements of the oil at the time of the spill, understanding the extent of the subsurface oil and its environmental impacts have since been dealt with largely using modelling (e.g. Adcroft *et al*., 2010; Liu *et al*., 2011b; Socolofsky *et al*., 2011; Valentine *et al*., 2012; Lindo-Atichati *et al*., 2014).

[6] Bulk crude oil is ~0.8 kg L^{-1} while seawater is > 1.0 kg L^{-1}

4.1.2 The use of models

As was demonstrated by the Gulf of Mexico spill, our access to observations of the subsurface ocean severely limits our understanding of oil spill dynamics over space and time. Datasets on ocean interior variables are by necessity based on limited sampling. Therefore, extrapolating from observations and using model simulations may provide essential tools for the study of ocean current dynamics. Models are also useful to test our understanding of ubiquitous processes or past events.

Modelling the fate of oil and gas from subsea blowouts considers, to varying degrees, the influence of various physical, chemical and biological factors on the transport of oil from a leaking well. Existing three-dimensional oil spill models such as the Oil Spill Contingency and Response Model, OSCAR (Reed *et al*., 1995), have proven successful in modelling spills on relatively small spatial scales, but the opportunities for validation against real spills or scenarios are rare (Johansen, 2003). Therefore, large or complex spills could benefit from the use of detailed models of ocean currents in order to help elucidate possible pathways. Oil well blowouts require the consideration of oil movement on a range of spatial scales that include near field plume modelling; plume transport and dispersal; surface slick transport and evaporation. All of these transport modes are influenced by weathering processes. Hence, the timescale of interest for modelling a spill is determined by the range of parameters considered.

4.1.3 Ocean circulation models

Three-dimensional ocean general circulation models (GCMs) have been developed to study ocean currents and patterns in transport on regional and global scales. Through testing of ideas and comparison with field observations, GCMs have enhanced our understanding of thermohaline circulation (e.g. Lohmann *et al*., 2014), transport pathways (e.g. Blanke *et al*., 1999) and bulk properties over ocean-basin scales (e.g. Marzocchi *et al*., 2015). Hindcast outputs of GCMs are able to resolve oceanic features

by solving equations of flow (Madec, 2008) and are forced with large datasets (Dussin & Barnier, 2013) to provide a simulation covering a period in the past.

The potential applications of GCMs are clearly far-reaching, including the study of physical oceanography, biogeochemical cycles, pollution and climate change. The ability of GCMs to capture variability on decadal time scales allows the study of circulation affected by cycles in climate (Persechino *et al*., 2012). Potential outcomes of climate change have also been investigated. For example, the (low) impact on circulation by increased freshwater fluxes caused by melting ice-sheets in Greenland was investigated by Marsh *et al*., (2010). Fully coupled models of the whole earth climate system were used to estimate possible changes in benthic biomass in response to climate change (Jones *et al*., 2014). Operational forecasting is possible with the adaptation of GCMs using up to date climatology data (Storkey *et al*., 2010).

Current dynamics have been studied using GCMs, with examples including the estimation of current strength in the Pacific and Atlantic subsurface ocean (Wacogne 1990) and variability in tropical Atlantic Ocean currents (Blanke & Delecluse, 1993). A multi-scale circulation model was produced for the Great Barrier Reef to study complex hydrodynamics in relation to subsurface topographical features, reefs and islands (Lambrechts *et al*., 2008).

Some high resolution GCMs have the advantage of providing global coverage. This makes them suitable for the study of processes on oceanic or planetary scales, e.g. assessing calculations of the influence of anthropogenic carbon emissions on variation in dissolved inorganic carbon on a global-scale, to distinguish these against background estimates (Yool *et al*., 2010). Nakano and Povinec (2012) used a GCM to model the distribution of radioactive isotopes of caesium from the 2011 Fukushima accident. A global sea ice model has been used to estimate changes in Southern Ocean sea ice thickness and volume for a recent period (1980 – 2008, Massonnet *et al*., 2013).

In the case of the DWH spill, ocean circulation models were utilised operationally to simulate the oil's transport, both at and below the surface (Liu *et al*., 2011a; Mariano *et al*., 2011). Circulation models were also used to study the potential extent of deep plumes of hydrocarbons following the DWH spill (Adcroft *et al*., 2010; Paris *et al*.,

2012; Lindo-Atichati *et al*., 2014), and to model their effects on resident pelagic microbial communities (Valentine *et al*., 2012). Hence, from a relatively early stage, models have played an important part in understanding the extent of the spill and its effects.

4.1.4 Lagrangian particle tracking algorithms

Full simulations of ocean physics and biogeochemistry using GCMs are 'expensive' in terms of both raw computational cost and output storage requirements, especially at high resolution. One alternative approach, particularly in the context of studying transport, is to use offline Lagrangian particle-tracking algorithms. These utilise existing model output to provide a means of studying the behaviour of the modelled circulation at a fraction of the cost of the full GCM. These tools also provide a technique for extracting positional information and bulk properties along pathways of current flow in GCMs. Lagrangian particle-tracking models release, and then trace, passive drifting 'particles' that can be applied to study the passage of the currents themselves (Blanke *et al*., 1999), or indeed anything that can be considered to passively drift with current flow, e.g. particulates (Jutzeler *et al*., 2014) or small (i.e. non-swimming) animals (Putman *et al*., 2012). Lagrangian particle tracking software (Connectivity Modeling System, or CMS, Paris *et al*., 2013) was used by Paris *et al*. (2012) to model distribution of oil following the 2010 Macondo oil well blowout. The use of CMS by Paris *et al*. (2012) allowed the inclusion of a range of particle sizes to represent distributions of oil droplet sizes, and therefore their buoyancy. This allowed a further level of complexity to the Lagrangian particle tracking simulations, with which questions on the effects of the different parameters could be addressed.

The Lagrangian particle-tracking algorithm, Ariane (Döös, 1995; Blanke & Raynaud, 1997; Blanke *et al*., 1999) has been developed for use with GCMs such as NEMO to aid the study of oceanic current flow. Ariane is a numerical, off-line tool written in Fortran that uses velocity fields from a GCM (e.g. NEMO, ROMS and others) to compute the three-dimensional trajectories of point 'particles' over time and space, following the assumption that water masses are conserved along trajectories. A full set of equations

that calculate how the point positions of particles are updated by Ariane is given by Döös (1995). In brief, velocities at the corners of the model grid are interpolated and used to calculate the displacement of particles through time in both the horizontal and vertical direction. Ariane is described as an 'offline' tool, since these ocean velocity fields are stored outputs from existing model simulations and there is therefore no need to run an expensive ocean circulation model each time Ariane is used.

Hence, the resultant paths and associated variables (e.g. temperature, nutrients) can be tracked by the particles following their release into the model's flow field at any location and time. Turbulent mixing of water along the particles' tracks is not explicitly considered in the calculations of velocity (Döös, 1995).

A clear advantage of Ariane is its computational speed, and the cost-saving use of pre-existing ocean GCMs. Its disadvantages include some inflexibility, for example, it is not configured to handle vertical convective mixing, and considerations involving biogeochemistry need to be addressed separately, with the use of other software, e.g. Matlab, to process the results.

Ariane has also been used to model the influence of ocean currents on lower level trophic dynamics in the Arctic by Popova *et al*. (2013) and to investigate the influence of mixed layer depth on the Southern Ocean's sequestration capacity for carbon (Robinson *et al*., 2014). The technique has been applied to map pathways in the north east Atlantic (NEA) and hence to validate a GCM (the Regional Oceanic Modelling System, ROMS) for that region (Sala *et al*., 2013). Various release sites were chosen, with particles released in order to map the main Lagrangian pathways in the NEA. Pathways were compared to fish stocks data, thus demonstrating connectedness of populations by water-borne larval transport. Also, trajectories of oil from the Prestige oil tanker spill that had been mapped with satellite imagery agreed with the model results of Sala *et al*. (2013). Hence the Lagrangian particle-tracking technique has been used previously in the context of mapping oil trajectories.

4.1.5 Oil exploitation in the Faroe Shetland Channel

Beyond the Gulf of Mexico, deepwater drilling is also being developed in various other regions worldwide, for example, the (at time of writing) United Kingdom (UK), New Zealand, Norway, Canada, Angola and Brazil all have, or are developing, plans for deep water drilling programmes (Leffer *et al*., 2011). The UK has been developing the Faroe-Shetland Channel (FSC, see Figures 4.1, 4.2) as an area for deepwater drilling since the 1990s (Smallwood & Kirk, 2005), and is an ocean area quite different to the Gulf of Mexico in terms of its temperature and circulation.

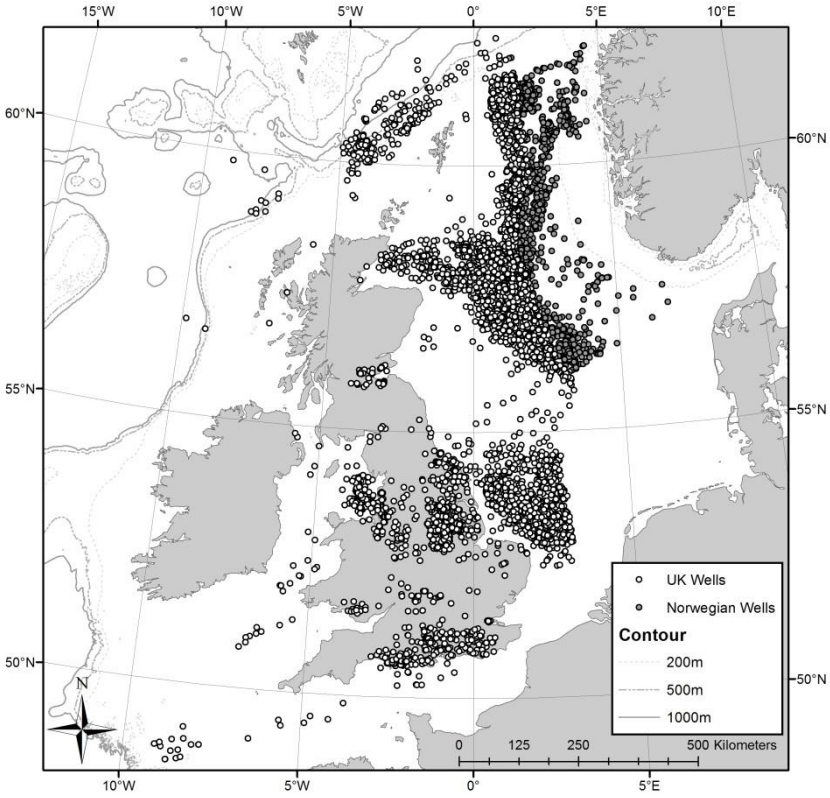

Figure 4.1. United Kingdom and Norwegian oil wells. Figure provided by the Serpent project.

If a prolonged oil spill were to happen in the FSC, complex ocean currents in the region would present challenges both to clean up operations and to understanding impacts there. The FSC is an oceanic region that forms important habitat for a diverse array of marine life (Bett, 2001; Jones *et al*., 2007). This is partly as a result of large vertical and

horizontal temperature gradients caused by the influence of cold Arctic bottom water underlying warmer currents at the surface (Figure 4.3). The FSC area also contains appreciable oil reserves, many of which fall within the exclusive economic zones of the UK and the Faroe Islands. Although exploration for oil began in the FSC in the 1970s, there was not a great amount of successful extraction in the region until 1992, with development of the Foinaven and Schiehallion fields. Interest subsequently picked up from that time, with licensing activity by the UK increasing from 1995 (Smallwood & Kirk, 2005). Border disputes between the UK and Faroe Island were cleared up in 1999, leading to the Faroe Islands granting licenses in large areas on the west side of the FSC in 2000 and 2004 (Faroese Petroleum Administration, 2004). Interest by oil companies continues in the area, with various new fields now under development e.g. the Lagavulin field recently drilled by Chevron, and the North Uist exploratory wells drilled by BP. There is clearly the potential for a large oil well blowout to happen in this region. An appreciation of the circulation characteristics here is therefore important.

4.1.6 Circulation in the Faroe Shetland Channel and Nordic Seas

The seabed topography of the Greenland-Scotland ridge gives rise to a complex exchange of water between Nordic seas and the North Atlantic (Figure 4.2). The area is important in terms of the meridional overturning circulation (MOC) in that the ridge feature represents a partial barrier across which deep water formed in the Nordic Seas must cross as it travels south to mix with deep water of the Atlantic.

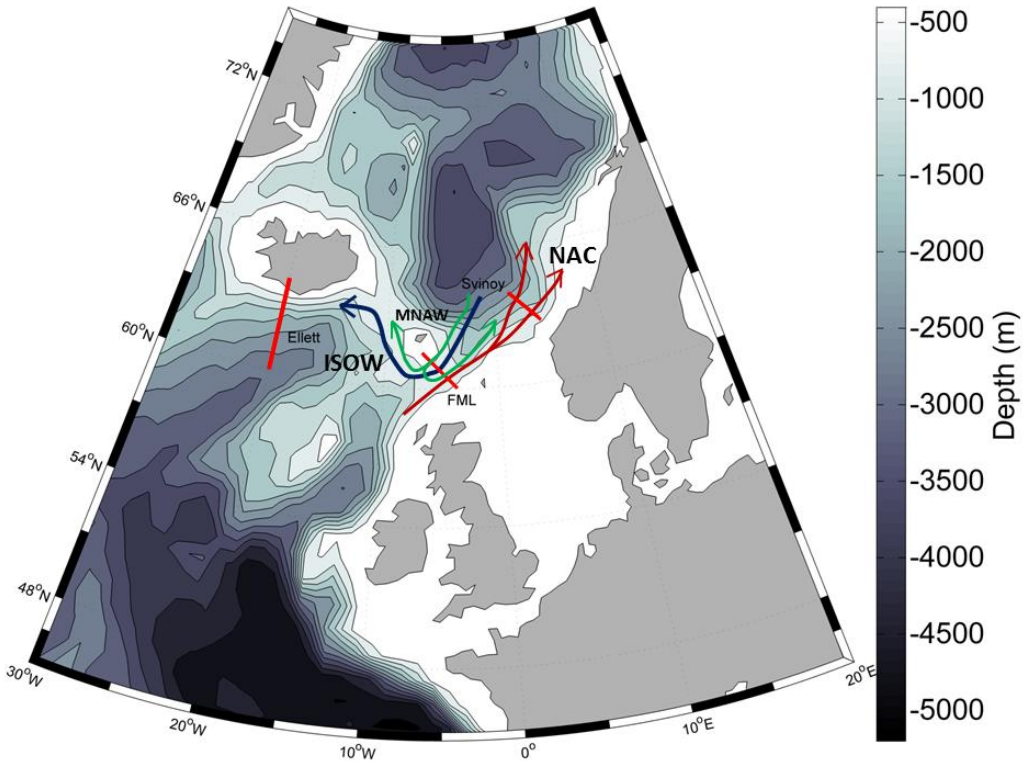

Figure 4.2. Map illustrating bottom topography, major ocean currents and linear sections through which these currents flow. Arrows show, schematically the major surface (red); intermediate (green) and deep water (blue) currents of interest to this study. NAC = Norwegian Atlantic current; MNAW = Modified North Atlantic Water; ISOW = Iceland Scotland Overflow Water. Red lines indicate the linear sections used in model validation (see Section 4.2.2). FML = Fair Isle – Munken Line. Ellet = Extended Ellet Line (part); Svinoy = Svinøy Section.

At and near the surface, water of the North Atlantic drift current, which originates from the Gulf Stream system, passes from the Atlantic northwards towards the Arctic in the Norwegian Atlantic Current (NAC). This current forms two main branches as it progresses north that have been mapped in Lagrangian drifter studies using subsurface RAFOS floats (Rossby *et al*., 2009). The other main near-surface current in the FSC is formed from Modified North Atlantic Water (MNAW), which dominates surface waters of the FSC in areal extent. This current originates from the Atlantic but enters the FSC from northeast of the Faroe Islands. It is then recirculated to join the NAC flowing into the Norwegian Sea (Turrell *et al*., 1999).

In deeper waters (1000 – 2000 m) over the continental slope west of Scotland, a current flows northwards year-round along the eastern boundary of the Rockall Channel The slope current has a velocity ranging between ~ 3 – 30 ms^{-1} and is thought to be driven largely as a result of N-S density gradients in the region (Huthnance, 1984, 1986).

Transport variability in the Nordic Seas has been the focus of previous oceanographic studies. For example, seasonal variability and pathways of the NAC have been studied with the use of surface drifting buoys (Andersson *et al*., 2011), indicating two main branches of the NAC, the strong, Norwegian coastal current (NCC) and a semi-permanent anticyclonic eddy in the Lofoten basin. Mork and Skagseth (2010) quantified mean flow and variability in the NAC, including its main branches. They used hydrographic data of the Svinøy section (running from ~65°N, 0°E to 62°N, 5°E) and sea surface topography for the period 1992 – 2009. The estimate of mean volume flux in the NAC was 5.1±0.3 Sv (1 Sverdrup, Sv = 10^6 m^3 s^{-1}). Both of these studies provided evidence of flow intensification in the winter, with the winter maximum almost twice as large as the summer minimum (Mork and Skagseth, 2010).

The warm surface waters of the NAC cool and lose buoyancy as they progress northwards to the Arctic. These sinking waters form a large proportion of the deep water formed in this region. Subsequently, bottom water formed in the Norwegian Arctic, flows southwards at depth, and Faroe Shetland Channel Bottom Water (FSCBW) is therefore a mix of intermediate water and deep water from Nordic seas (mainly Norwegian Sea Arctic Intermediate Water, NSAIW and Norwegian Sea deep water, NSDW). The Wyville Thomson Ridge (WTR), with a sill depth of ~450 m,

presents a barrier to mixing at depth between the cold water mass of the deep Faroe Shetland Channel to the north and the warmer water mass of North Atlantic Deep Water (NADW) to the south. Hence, although bottom water occasionally cascades over the WTR (Sherwin & Turrell, 2005), most is diverted to cross a sill at ~850 m to enter the Faroe Bank Channel. Volume transport of the water plume crossing this sill, known as Iceland Scotland Overflow Water (ISOW), has been estimated ~1000 km downstream as 3.8±0.6 Sv (Kanzow & Zenk, 2014). Average volume transport in the FSC has been estimated as 2.7±0.5 Sv (Berx *et al*., 2013), indicating entrainment of water into ISOW as a result of overflow at the FBC sill.

4.1.7 Research questions

There is a timely need to understand the effects of circulation on oil transport in regions such as the FSC, given the expansion of deepwater drilling in this region. Environmental impact statements (EIA), required by companies in order to gain a license to drill, provide estimates of potential oil distribution in the event of a spill. For example, the EIA for the BP North Uist exploratory field in the Faroe Shetland Channel has a section using available oil spill models to predict the potential coverage of a spill following an accidental blowout in this region (BP, 2011). However, the published results focus mainly on surface trajectories of oil, and do not deal in detail with possible impacts of oil on the deep water environment. The modelling scenarios[7] presented in the BP environmental statement for North Uist give 140 days of unrestricted flow as the maximum timescale of interest for a spill (BP, 2011) as this is the estimated total time required for the drilling of a relief well at the site to stem the flow from a leaking well head. The BP report briefly presents some results of underwater plume modelling, predicting concentrations of up to 5 mg L^{-1} with the main plume persisting at ~900 m water depth (BP, 2011).

---

[7] Modelling conducted with OSCAR and OSIS models: OSCAR is a commercial three-dimensional oil spill model operated by SINTEF (Reed *et al*., 1995); OSIS is a commercial two-dimensional oil spill model operated by BMT.

The fate and effects of oil in the water column depends on many factors including its own composition, but also the properties of the surrounding water such as temperature and the prevailing conditions at the time of the spill. Oceanic properties vary both seasonally and interannually and there is long-term (decadal) variability in circulation (Turrell *et al*., 1999). Based on our knowledge of the ocean currents in the Faroe Shetland Channel and Nordic Seas (Mork & Skagseth, 2010; Berx *et al*., 2013), it seems possible that a prolonged oil well blowout in the Faroe Shetland Channel could distribute oil to different ocean basins. In this chapter a novel approach is used to study the ocean circulation-influenced dispersal of hydrocarbons.

Here, hindcast output from a high resolution simulation of the Nucleus of European Modelling for the Oceans (NEMO) general circulation model (Madec, 2008) was used with the Ariane Lagrangian particle tracking algorithm (Blanke & Raynaud, 1997) to study patterns of potential near-surface and subsurface transport from a release in the FSC, considering the 16 year period between January 1994 and December 2009. Transport pathways and extent were considered in relation to depth, season and year of release of passive, drifting particles. The particles have no physical or chemical attribute directly representing oil and are instead used to represent the neutrally buoyant droplets and dissolved oil that have been documented following previous oil well blowouts (Boehm & Feist, 1982; Camilli *et al*., 2010).

The approach will elucidate the potential extremes of the transport range and allow the investigation of the relative importance of seasonal and interannual variability. The NEMO model was first validated against observational data for the region of interest so that its performance in showing transport pathways locally in the region can be assessed.

The following research questions were addressed to study the potential transport of oil from a deepwater blowout in the FSC, using passive particles to represent dissolved and neutrally buoyant hydrocarbons. The effect of release timing and depth was considered in each case.

1. Spread of oil with one year of transport.

How were drifting, neutrally buoyant particles distributed following a year of drift, considering both horizontal and vertical directions of travel?

2. The importance of temperature to limit spread.

What was the difference in spread when particles are decayed in relation to ambient temperatures, to simulate the effect of bacterial degradation of hydrocarbons?

3. The impact of bacterial respiration.

What was the areal extent of impact in terms of oxygen consumption, with an index estimated in relation to temperature-mediated decay rates?

4. The potential for seafloor contact beneath drifting oil.

What was the area impacted, assuming that seafloor contact could occur beneath plumes of drifting oil? Was there the potential for contamination of the Darwin Mounds, a unique habitat for cold water corals, *Lophelia pertusa*, located north of the Rockall trough and close to the FSC region?

4.2 Methods

4.2.1 The NEMO model

The Nucleus of European Modelling of the Oceans (NEMO) is a 'state-of-the-art' modelling framework with 5 major components, providing a simulation of ocean dynamics, sea-ice and ocean biogeochemistry (see: http://www.nemo-ocean.eu/). The general ocean circulation model (GCM) component, NEMO-OPA (Madec, 2008) for which the eddy-resolving 1/12 degree resolution for 1994 – 2009 has been used here, is described in full by Marzocchi *et al*. (2014). The model has 75 levels in the vertical dimension that increase in thickness from ~1m at the surface to ~200m at abyssal depths. The model ocean is forced at the surface by wind fields developed as part of the European DRAKKAR collaboration (1994 – 2007 uses DFS 4.1. Brodeau *et al*., 2010, and 2008 onwards uses DFS 5.1; Dussin & Barnier, 2013). The velocity fields for currents are subsequently output and stored as 5-day averages. The horizontal resolution is approximately 1/12 degree and is organised in a tripolar grid. The use of a tripolar grid avoids both the convergence of meridians to a single point at the North Pole, which could cause numerical instability, and long integration times caused by very small cell sizes at the highest latitudes. The three poles of the grid are instead on Canada and Siberia in the northern hemisphere, and on Antarctica (in the normal place) in the southern hemisphere.

4.2.2 Validation of NEMO in the study region

Pathways of the major currents were the main focus of this study (see section 4.1.5). Three key regions of interest were identified through which major currents flow (Figure 4.3, Table 4.1). Model output was compared to observational data for these sections. Cross sectional data (velocity normal to the section; temperature; salinity and density)

were extracted from the NEMO model output for the period 1992 – 2007. These data were used to calculate long term means.

The Fair Isle – Munken line lies across the Faroe Shetland Channel and is close to the drilled site chosen as the release location for the present study. Oceanographic measurements have been taken at intervals along this section between 1995 and 2009, allowing the estimation of long-term means of temperature, salinity, density and velocity (Berx *et al*., 2013). In the region relevant to this study, much of the surface flow is dominated by the Norwegian Atlantic current, which has been studied using a long-term dataset consisting of measurements along the Svinøy section (Mork and Skagseth, 2010). Thirdly, part of the Extended Ellett Line running south from Iceland at 20°W was chosen. This section was relevant because deep water from the Arctic passes through the FSC and much of it crosses a sill at 850 m water depth into the Faroe Bank Channel before heading west into the Iceland basin.

Table 4.1. Sections extracted from the NEMO model that were compared to published observational data

Section name	Currents of interest	Start Lat	Start Lon	End Lat	End Lon	Reference
Svinøy Section	Surface flow of Norwegian Atlantic current	65.0° N	0.0° E	62.0° N	5.0° E	Mork and Skagseth, 2010
Fair Isle – Munken Line	Circulation in the FSC	61.5° N	6.70° W	60.1° N	3.75° W	Berx *et al*., 2013
Ellett Line	Deep water flowing towards the Iceland basin	64.0° N	20.0° W	60.0° N	20.0° W	Holliday and Cunningham, 2014

4.2.2.1 Fair Isle – Munken Line comparison in the Faroe Shetland Channel

Long term monitoring of temperature, salinity and current flow has been carried out in the FSC in order to describe the flow field and water mass structure in the channel (Berx *et al*., 2013). The data have been collected by Acoustic Doppler Current Profilers (ADCPs) at moorings and from ship-borne conductivity temperature depth (CTD) equipment along several sections. There is bias in the sampling, with more measurements taken in winter than in summer (Berx *et al*., 2013). The data used here were from the Fair Isle – Munken Line (Figure 4 from Berx *et al*., 2013: reproduced here as Figure 4.4). Model output corresponding to the section is shown in Figure 4.5. Note that in the bottom panel of the Berx *et al*. (2013) figure, velocity contours are overlaid on the colour plot of temperature.

NEMO model output for the Fair Isle – Munken line generally corresponded adequately to the published data. Contours of temperature and density showed the closest agreement. Salinity contours in the model took a different shape at some depths. The magnitude of velocity was overestimated by the model in comparison to the data. Observed average annual temperature along the section ranged between temperatures just below 0°C in deep water (> 800 m) to those above 10°C at the surface. This range was represented well by the model output, although the variation in depth of some of the isotherms took a slightly different shape at some depths, looking more convex in the model output (Figure 4.5, top panel). While the surface water temperature appeared to be represented well by the model on the east side of the channel, on the west side it was ~ 1°C cooler than observations in the middle of the channel. Deep waters (> 700 m) were reported to be < 0 °C by Berx *et al*. (2013) whereas the model output was ~ 0 °C.

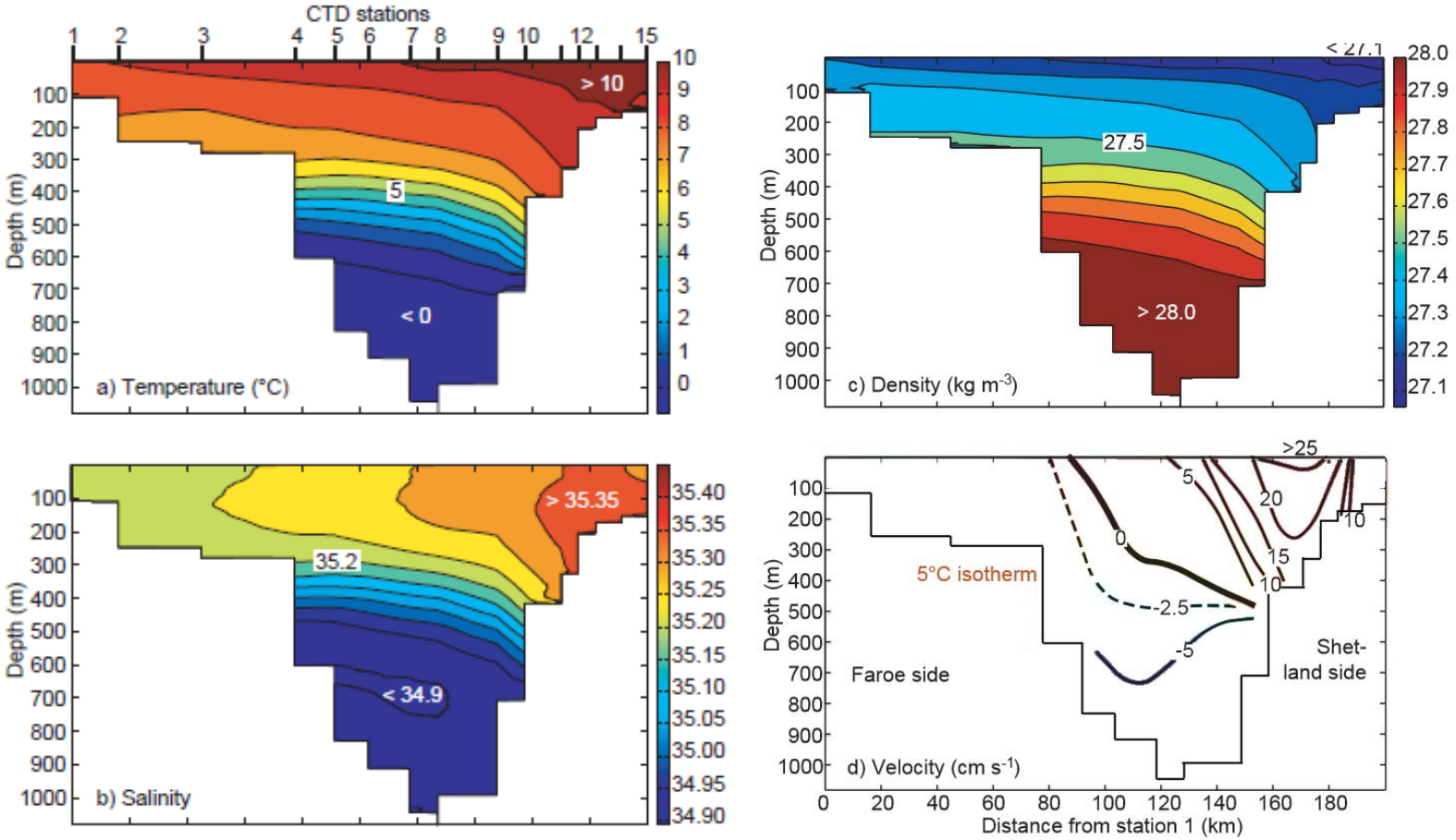

Figure 4.3. Observational data from the Fair Isle Munken line 1995 to 2009 showing annual means of temperature, salinity, density and velocity (Berx *et al*., 2013). Figure reproduced from Berx *et al*. (2013) under the Creative Commons License.

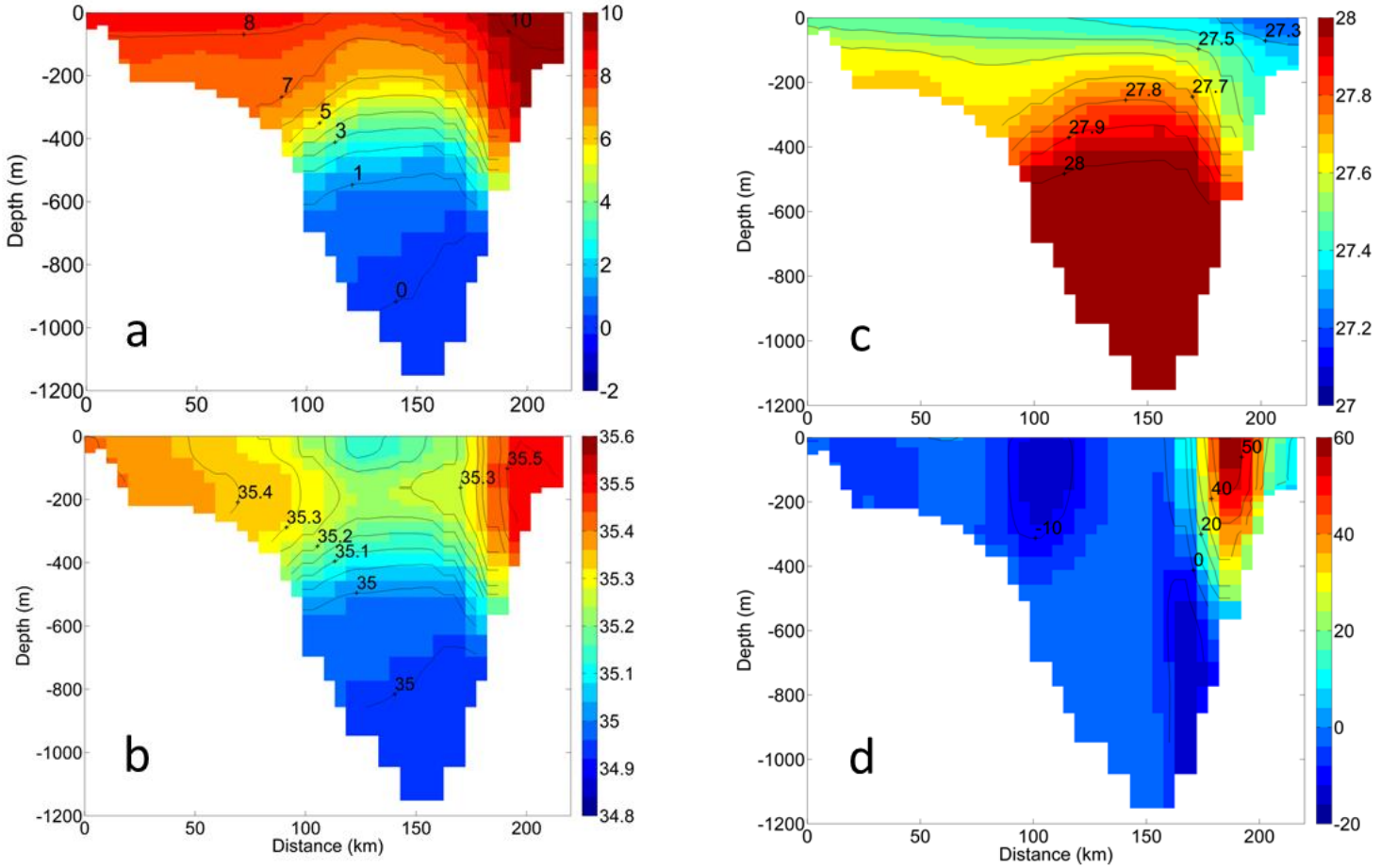

Figure 4.4. Annual means of (a) temperature (°C); (b) salinity; (c) density (σ); and (d) velocity (cm s^{-1}) calculated from the NEMO model output along the Fair Isle - Munken Line section, 1992 to 2007. Note that velocity here is plotted with a colour scale.

Observed salinity indicated an east-west gradient with the east side of the FSC more saline (> 35.35, Figure 4.3b). The gradient was not continuous in the model and although the magnitude of salinity was approximately equal at the east side of the channel, the west was more saline than the observations (Figure 4.4b). In the middle of the channel model salinity was low (35.15) with respect to observed salinity (35.25). In general, observed and modelled salinity was within 0.3 psu. A difference in the shape of salinity contours at ~ 400 m depth is also seen when comparing observational data to the model output. Density was overestimated in the model by ~0.3 kg m^{-3} at water depths down to ~ 600 m, where it agreed well (Figure 4.4c). The east-west gradient in density was estimated better by the model for shallower water depths (< 200 m) although the magnitude of model-estimated density was consistently ~ 0.1 kg m^{-3} greater in the top 200 m. The directional component of velocity was the same for observed and modelled for surface and deep currents (Figures 4.3d, 4.4d). Velocity magnitude was overestimated by the model in the northwards shallow water current flowing north, and agreed adequately for deep waters > 600m water depth. The agreement between horizontal density gradients and the presence of a strong (perpendicular) current (Figures 4.3, 4.4 panels c and d) indicates good agreement of the model with geostrophic balance.

4.2.2.2 Svinøy Section comparison in the Norwegian Sea

Mork and Skagseth (2010) used hydrographic data and sea surface topography from the Svinøy section in 1992 to 2009 to quantify the mean flow and variability in the two main branches of the Norwegian Atlantic Current, which flows northwards from the Atlantic into the Norwegian Sea. Mean temperature, salinity, density and velocity for winter (January to March) and summer (July to September) are reproduced here from Mork and Skagseth (2010, reproduced here as Figure 4.5) for the period 1992 to 2009, and compared to NEMO model output from the same section. Output was using the same months and the years 1992 to 2007 to produce averages for these variables (Figure 4.5).

Generally there was good agreement between observations and the model for both winter and summer means of temperature, salinity, density and velocity (Figures 4.5, 4.6). The model density gradients appeared to give an adequate representation of the main transport pathways through geostrophic balance (*cf* steep gradients in the inshore density in Figure 4.5 σ_t with Figure 4.6 c and g). The two branches of the Norwegian Atlantic current are visible in the top ~ 300 m. Velocity magnitude was over estimated by the model in these currents in both winter and summer (for example, by ~ 10 to 15 cm s^{-1} in winter in the offshore branch, Figure 4.6).

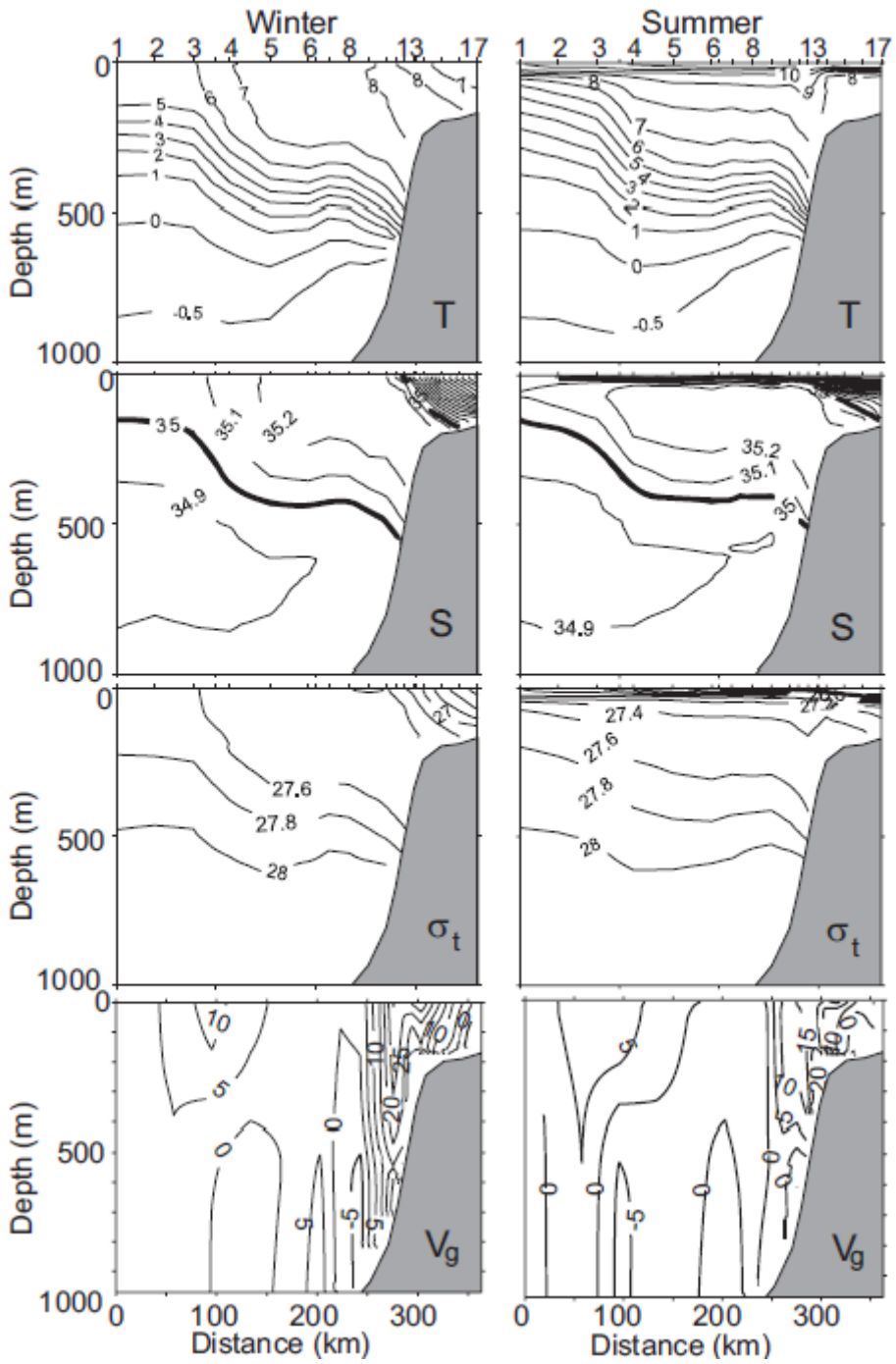

Figure 4.5. Observational data from the Svinøy Section 1992 to 2009 including winter (January to March) and summer (July to September). T = temperature (°C); S = salinity; σ_t = density; V_g = geostrophic velocity (cm s^{-1}). Figure reproduced from Mork and Skagseth (2010) under the Creative Commons License.

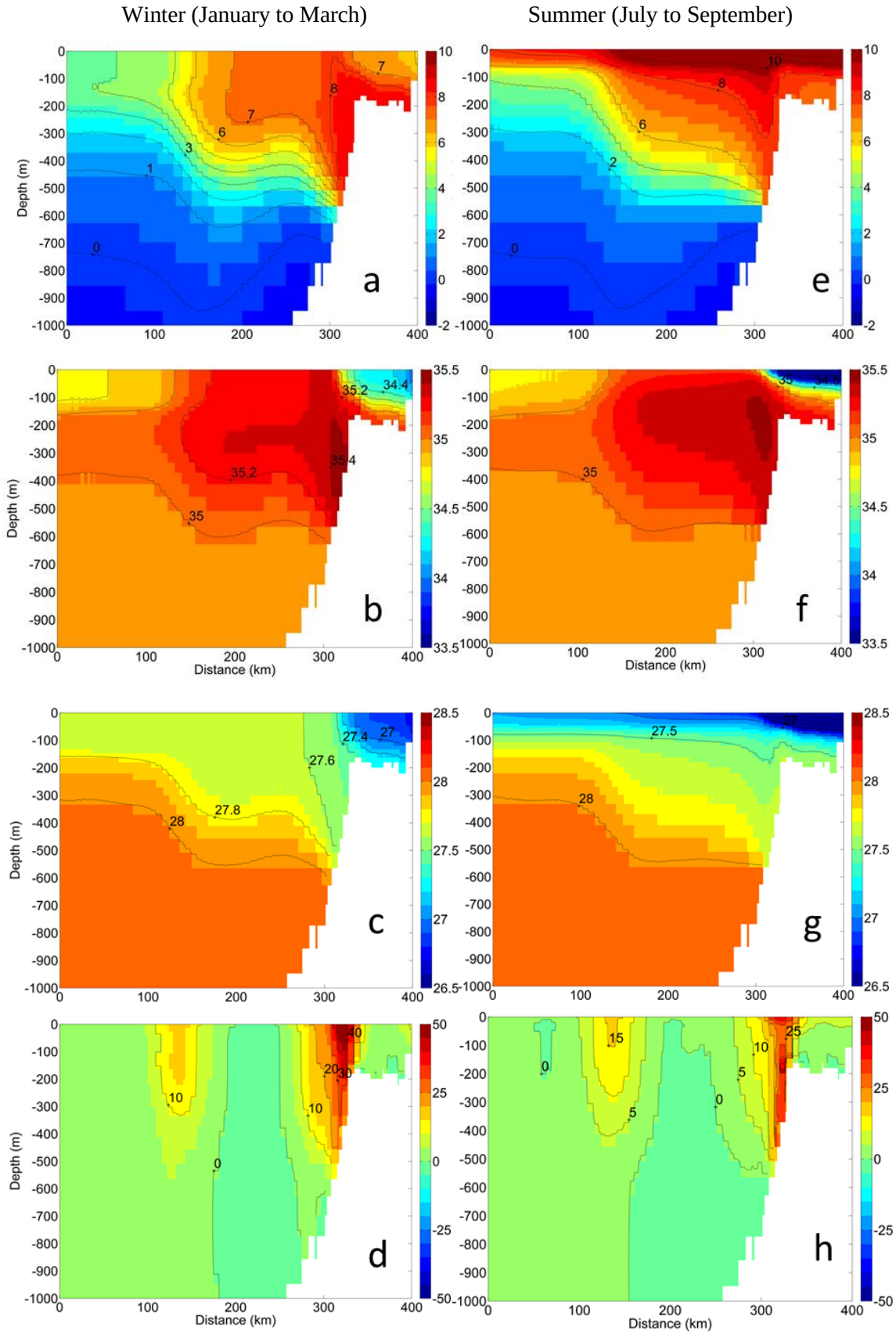

Figure 4.6. Means of temperature, °C (a, e); salinity (b, f) density, σ (c, g) and velocity, cm s^{-1} (d, h) calculated from NEMO model output along the Svinøy Section 1992 to 2007.

4.2.2.3 Extended Ellett Line section comparison

The Extended Ellett Line (EEL) has been sampled regularly between 1996 and 2013, using a Lowered Acoustic Doppler Current Profiler (LADCP) leading to recent estimates of velocity of the Iceland-Scotland overflow water (Holliday and Cunningham, 2014). Velocity data, obtained from Comer (2014) are presented here for a north section of the EEL (64.0 °N, 20.0 °W to 60.0 °N, 20.0 °W, Figure 4.7).

Data used by Comer covered the period 1996 – 2013, excluding 2002-4, 2008 and 2012. Sampling was carried out once along the transect of the EEL once in any year and was confined to spring, summer and autumn months varying between May and October.

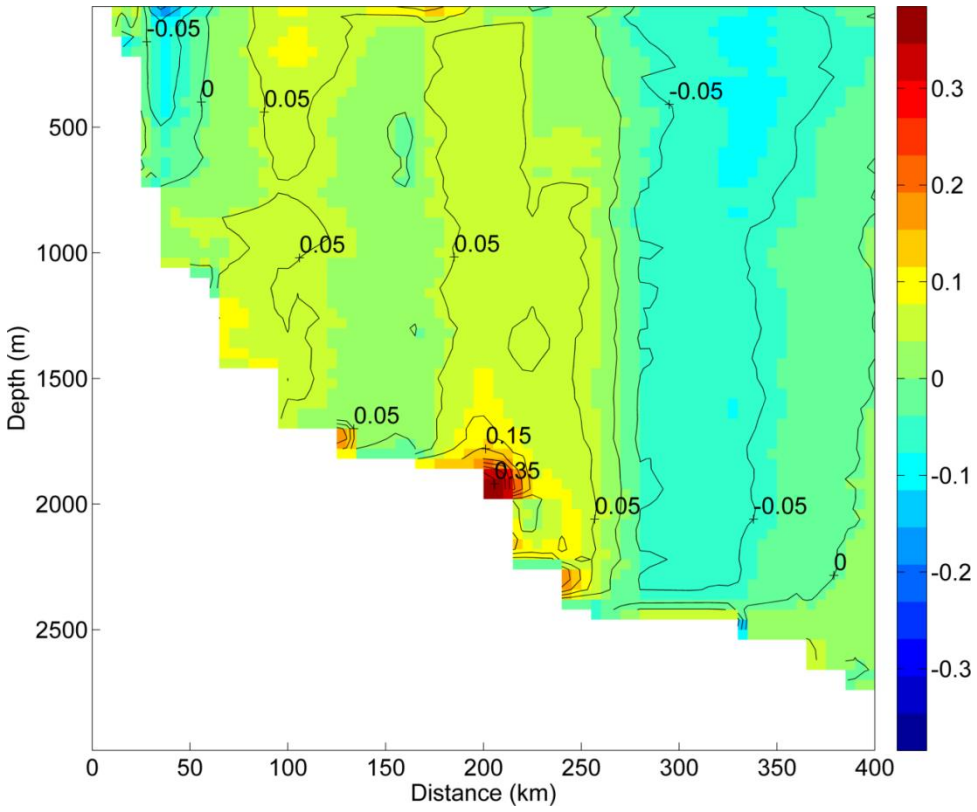

Figure 4.7. Observational (LADCP) data from the north part of the Extended Ellett Line running south from Iceland covering spring, summer and autumn months between 1996 and 2013. See text for full explanation of data coverage. Velocity units are m s^{-1}. Figure reproduced from data processed by Comer (2014).

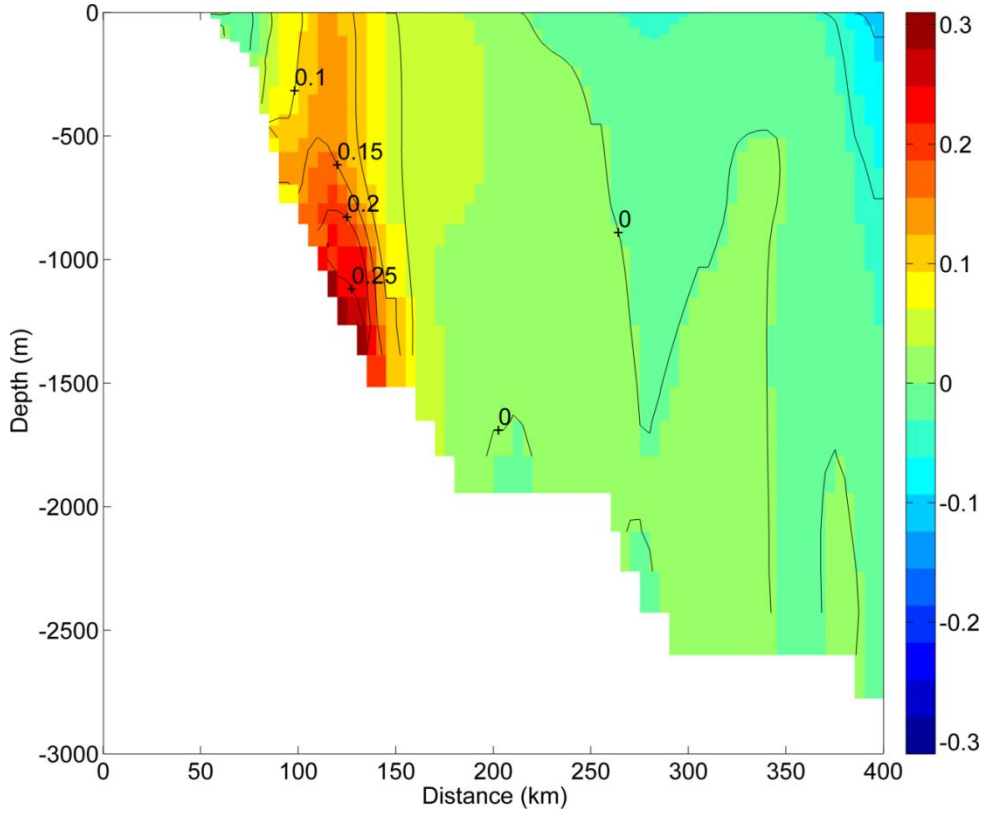

Figure 4.8. Annual means of westward velocity calculated from the NEMO model output for the north part of the Extended Ellett Line running south from Iceland, 1992 to 2007. Velocity units are m s^{-1}.

The model represented Iceland Scotland Overflow Water adequately, with the direction and magnitude close to observations. The depth of the flow was underestimated by the model since in the observational data the core of this current was around 500 m deeper (Figures 4.9, 4.10). Difficulties with maintaining high density in model overflow water are an acknowledged issue for z-level models because they tend to "over mix" the overflow water, reducing density and causing the flow to be anomalously shallow on the slope (Marzocchi *et al*., 2015). The shallow representation of ISOW by the model is therefore an accepted caveat of the present study.

4.2.3 Experiment design

A series of simulations were run spanning the period of interest (1994 – 2009), which allowed for the examination of both time and depth of oil release. Particles released were used to represent the possible subsurface trajectories of dissolved and neutrally buoyant oil and small droplets, following their emission from a hypothetical oil well blowout in the FSC. Using the Ariane Lagrangian particle tracking tool (Section 4.1.3), neutrally buoyant, passive 'particles,' representing hydrocarbons, were released in regularly spaced grids spanning approximately 0.5˚ latitude by 0.5˚ longitude at a location that has recently been drilled for oil in the FSC, (Lagavulin well: 1567 m depth, 62.66° N, 1.126° W). Grids of 20 x 20 particles were released at depth intervals spanning the water column from just below the surface (10 m), 50 m and then at 50 m intervals to 1500 m. A release of 400 particles at 31 depths was supplied to Ariane once every month from January 1994 until December 2009 and allowed to drift for 365 days (hereafter one year). Positions of particles were recorded by Ariane at 5 day intervals thus forming output results spanning 16 years of releases. Each particle position was therefore a representation of space occupied by 'oil' along trajectories. The final particle release date was December 2009, so Ariane simulations continued to December 2010 to permit this final release to drift for a full year. Hence, there were 12 releases per year for a total of 16 years, resulting in 192 releases and therefore 2,380,800 particles in total.

Output was subsequently processed and analysed with Matlab (The MathWorks, Inc., R2013a). The pathways of the released particles (described hereafter as particles, trajectories or oil) were used to study the possible transport pathways of oil and to analyse patterns in relation to year and season of release. Following analysis of year-long particle trajectories, a simple algorithm (see Section 4.2.4) was used (in Matlab) to decay particles in relation to ambient temperatures. This algorithm simulated the temperature-dependent biological weathering of oil by bacteria, allowing an examination of how the distribution of oil may be impacted by ambient conditions encountered along trajectory tracks.

4.2.4 Analyses

The distance travelled by particles was calculated for each release (400 particles). This included both: i) mean and median straight-line distance travelled from the release location after one year of drift, and ii) mean end-to-end trajectory length (with trajectory length calculated as the sum of all 5-day interval distances travelled by particles in one year). The effect of release depth on averages of depth, end depth and change in depth was also assessed for each release.

Particle densities were used to indicate the cumulative abundance of particle positions spatially so that two-dimensional maps could elucidate pathways in the model and patterns in relation to release timing. These maps were typically conventional geographical maps in latitude and longitude, but used alternative dimensions of depth, along-trajectory time or particle-release time according to their use. The output was visualised in this way for multiple depth layers summed, or for individual depth layers.

Starting with the most general visual representation available, a plot of particle density for the entire set of output particle positions allowed the identification of key pathways for further study (Figure 4.9). Key pathways of interest were regions where a large proportion of particles were transported, thus following the main currents in the model. Also of interest were regions at the far extent of the particles' range or regions close to an interesting oceanographic feature e.g. the Faroe Bank Channel sill. Note that the particle density plots shown here indicate the cumulative abundance of particles for each 5-day interval at each geographical location in the model grid. A value of 1 indicates a geographical position where a single particle was located within a single 5-day period, whereas a location with a value of 10000 had 10000 particle 'visits,' some of which could represent multiple visits by the same particle. Particle abundance at each location is plotted on a log scale.

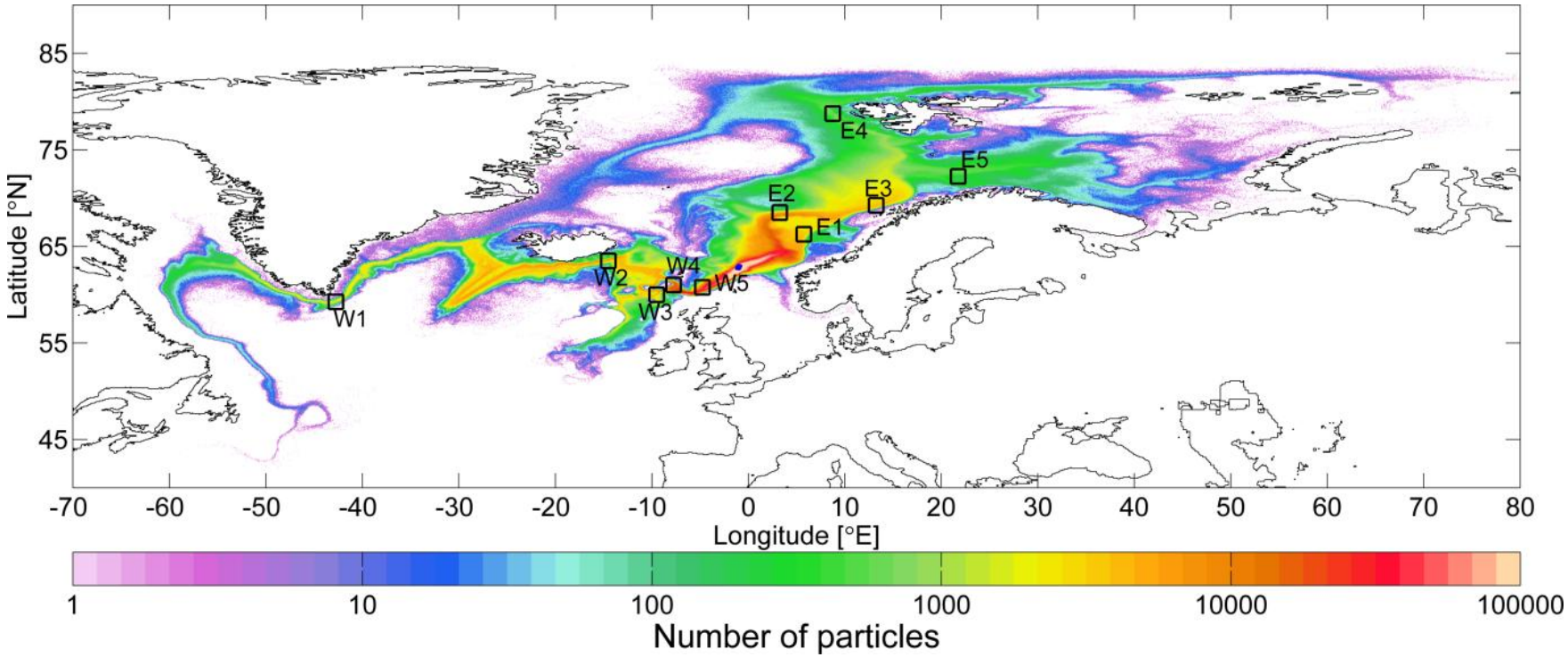

Figure 4.9. Traps used in the analysis, shown superimposed over a particle density plot of particles from all releases in the simulations (see text for description). The particle release locations are shown as blue dots at ~ 62.7° N; 1.13° W.

Particle arrival at these regions of interest was studied using defined 'traps' of 1.5 degrees latitude x 1.5 degrees longitude (Figure 4.9). Any particle that arrived at one of these traps was counted (once) and these particles were then summed at respective times and depths of release to create an array of 'hits' for each trap location, for which standard deviation, median and interquartile range were calculated. The traps were used to assess spread of oil, the importance of seasonal and interannual influences and the effect of temperature-mediated decay.

The traps were defined to study the proportion of particles reaching areas of interest, and to assess the frequency and regularity of patterns. Traps were positioned as indicated in Table 4.2 and Figure 4.9. The traps were located in order to cover the main transport pathways (traps W4, W5, E1, E2), and also areas at the extremes of transport following one year of drift by particles (traps W1, W2, E3, E4 and E5). A further trap (W3) was positioned over a bathymetric feature – the Wyville Thomson Ridge (WTR), to assess temporal patterns in particles arriving there. The traps were not intended to catch all of the particles released, but instead elucidate periods of significant flow to particular regions as well as the temporal patterns.

Trap W5 was located at the southern end of the Faroe Shetland Channel. Trap W4 was located over the sill connecting the Faroe Shetland Channel to the Faroe Bank Channel, with trap W3 covering another branch stemming from flow from the FSC, and covering the Wyville Thomson Ridge. Trap W2 was located to catch particles entering the Iceland basin. A further trap (W1) was located at the far extent of travel to the west (off Southeast Greenland). Two traps were located in the Norwegian Sea to capture the two main branches of flow: east (E1) and west (E2). Trap E3 was located towards the northern extent of the particles in the northern Norwegian Sea. Two further traps were situated in the Arctic: trap E4, to the west of Svalbard, and E5 in the Russian Arctic.

Table 4.2. Traps locations

Trap	Location	Coordinates
W1	Southeast Greenland	58.5 – 60.0 °N; 43.5 – 42.0 °W
W2	Iceland Basin	62.75 – 64.25 °N; 15.25 – 13.75 °W
W3	Wyville Thomson Ridge	59.25 – 60.75 °N; 10.25 – 8.75 °W
W4	Faroe Bank Channel sill	60.25 – 61.75 °N; 8.5 – 7.0 °W
W5	Faroe Shetland Channel	60.0 – 61.5 °N; 5.5 – 4.0 °W
E1	Norwegian Sea east	65.5 – 67.0 °N; 5.0 – 6.5 °E
E2	Norwegian Sea west	67.75 – 69.25 °N; 2.5 – 4.0 °E
E3	Sub-Arctic	68.5 – 70.0 °N; 12.5 – 14.0 °E
E4	Svalbard	78.0 – 79.5 °N; 8.0 – 9.5 °E
E5	Russian Arctic	71.5 – 73.0 °N; 21.0 – 22.5 °E

Having studied drift over one year, the importance of temperature to control decay, and therefore affect oil transport in the model, was assessed. As with other biogenic substances, oil is subject to biological breakdown. Hydrocarbon-degrading bacteria possess the enzymes necessary to be able to degrade oil as a source of organic carbon and energy. Like other biological processes, this breakdown is strongly influenced by ambient temperature, with higher temperatures typically accelerating the rate of oil degradation. This was examined here using a simple function to decay particles in relation to local temperature, and thus represent oil breakdown rate (1).

Decay in response to the temperature experienced by trajectories along their paths was simulated using this simple decay-rate equation. An example of how a particle released in either shallow or deep water might decay through time is shown in Figure 4.10. Starting with each whole particle, a decay rate, R^{-1}, was applied at each time interval in relation to the ambient temperature in the model. This set the proportion by which each particle would decrease by at each 5 day time interval, tending towards (but never reaching) zero. The decay rate equation (1) applied here has been used previously to model decay of oil (Adcroft *et al.*, 2010) to simulate observed rates of oil decay by bacteria (Atlas, 1981).

$$R^{-1} = 12 * 3^{(-T - 20) / 10} \quad (1)$$

Where T = ambient temperature (°C).

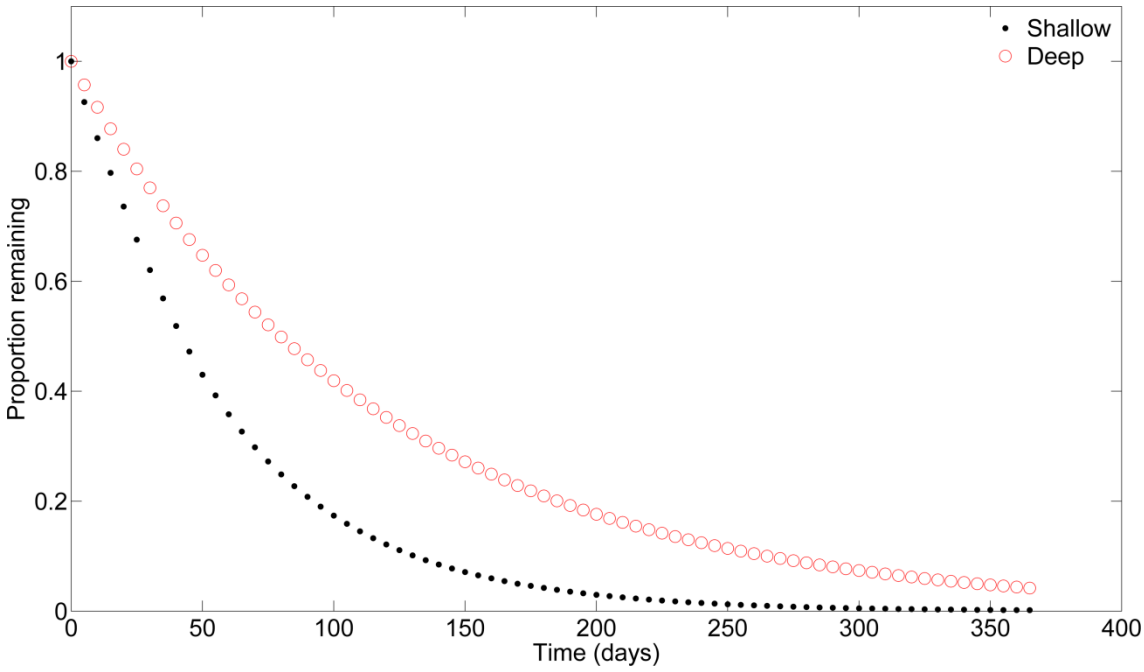

Figure 4.10. Example of how a simple decay equation reduces particles in the simulation from a starting proportion of one towards an asymptote of zero. Shallow = example of a particle released at 10 m; Deep = example of a particle released at 1500 m.

An arbitrary threshold of 10% of initial value was set at which to terminate the progress of particle trajectories. In the example here (Figure 4.10) this translates to the shallow particle trajectory (the first trajectory in the output in the shallowest depth level) being

terminated at 135 days. The deep trajectory (the first trajectory in the output in the deepest depth level) is terminated at 270 days. The effect of temperature-controlled decay on the oil's spread was investigated for these thresholds.

A proxy for oxygen consumption was used here to investigate the geographical spread of *represented* de-oxygenation impact caused by oil respiration. An index of oxygen consumption, or 'oil respired,' was represented by the amount of each particle that was *consumed* at each output position (as opposed to the amount of oil remaining). The proportion of each particle remaining after each time interval, in relation to ambient temperature (1) was multiplied by –1. This index of oxygen consumption does not have a quantitative amount of oxygen consumed associated with it (e.g. mol O_2 m^{-2} day^{-1}) since the Lagrangian particles used to represent oil do not have a specific quantity of hydrocarbons associated with them. The amount of oil respired at each estimation point was summed along trajectories for time periods of 1 month, 3 months, 6 months and 12 months, with comparisons made between releases from shallow, intermediate and deep water.

Evidence suggests that deep oil plumes formed from the leaking Macondo well in 2010, some of which were approximately 300 m off the seabed at their depth of establishment (Camilli *et al*., 2010), resulted in large areas (> 3200 km^2) where a footprint of oil contamination formed (Valentine *et al*., 2014). Contact with the seafloor was assessed here by summing the number of 'particle days' that were within 200 m of the seafloor, thus providing an arbitrary threshold below which it could be assumed that fallout from plumes could occur.

A combination of methods developed here were applied to investigate whether the particle tracking results indicated that oil could contaminate the area of the Darwin Mounds. The Darwin Mounds are sandy mounds (< 5 m tall, 75 – 100 m diameter) that provide habitat for cold water corals, *Lophelia pertusa*, and associated fauna (Kiriakoulakis *et al*., 2004). They are located in water of about 950 m depth at the northern end of the Rockall Trough (59.81°N, 7.38°W) and are considered to represent a globally important and ancient cold water coral community of international significance, having been designated as a Special Area for Conservation (SAC) in the European Union.

4.3 Results

4.3.1 Spread of oil

Pathways of particle trajectories were strongly determined by release depth, as indicated by particle densities from releases spanning depth horizons of 10 – 200 m, 250 – 550 m and 600 – 1500 m and allowed to drift for one year (Figure 4.11 a-c). Particles released at depths of 200 m or less tended to be transported northwards from the release location into offshore and coastal branches of the NAC (Figure 4.11 a). These particles were then in some cases carried north to the Arctic to Svalbard and into the Barents Sea. A further branch split off towards eastern Greenland to move again southwards close to the Greenland coast. Particles released in depths of 250 – 550 m also followed these pathways in many cases (Figure 4.11 b). However, these more intermediate-depth releases resulted also in particles being carried west through the FBC and on to the Iceland basin. Other particles entered the North Atlantic in a more southward-directed flow through the Rockall Trough (Figure 4.11 b). Particles from these intermediate-depth releases that travelled west beyond the mid-Atlantic ridge appeared to be channelled southwards, traversing the ridge at the Charlie Gibbs Fracture Zone (Figure 4.11 b). Particles released in deeper water (> 600 m) did not generally progress as far north as the shallow particles and were instead more likely to flow west over the FBC sill (Figure 4.11 c). Particles from deeper releases were able to reach as far west as southern Greenland, the Labrador Sea and on towards Newfoundland and the Grand Banks (Figure 4.11 b, c). A small number of particles from releases deeper than 250 m were advected around the southern Norwegian coast to enter the Skaggerak (Figure 4.11 b,c). Results of more detailed analyses will be described in sections dealing with the main research questions concerning oil spread, temperature-mediated decay, oil respiration and seafloor contact.

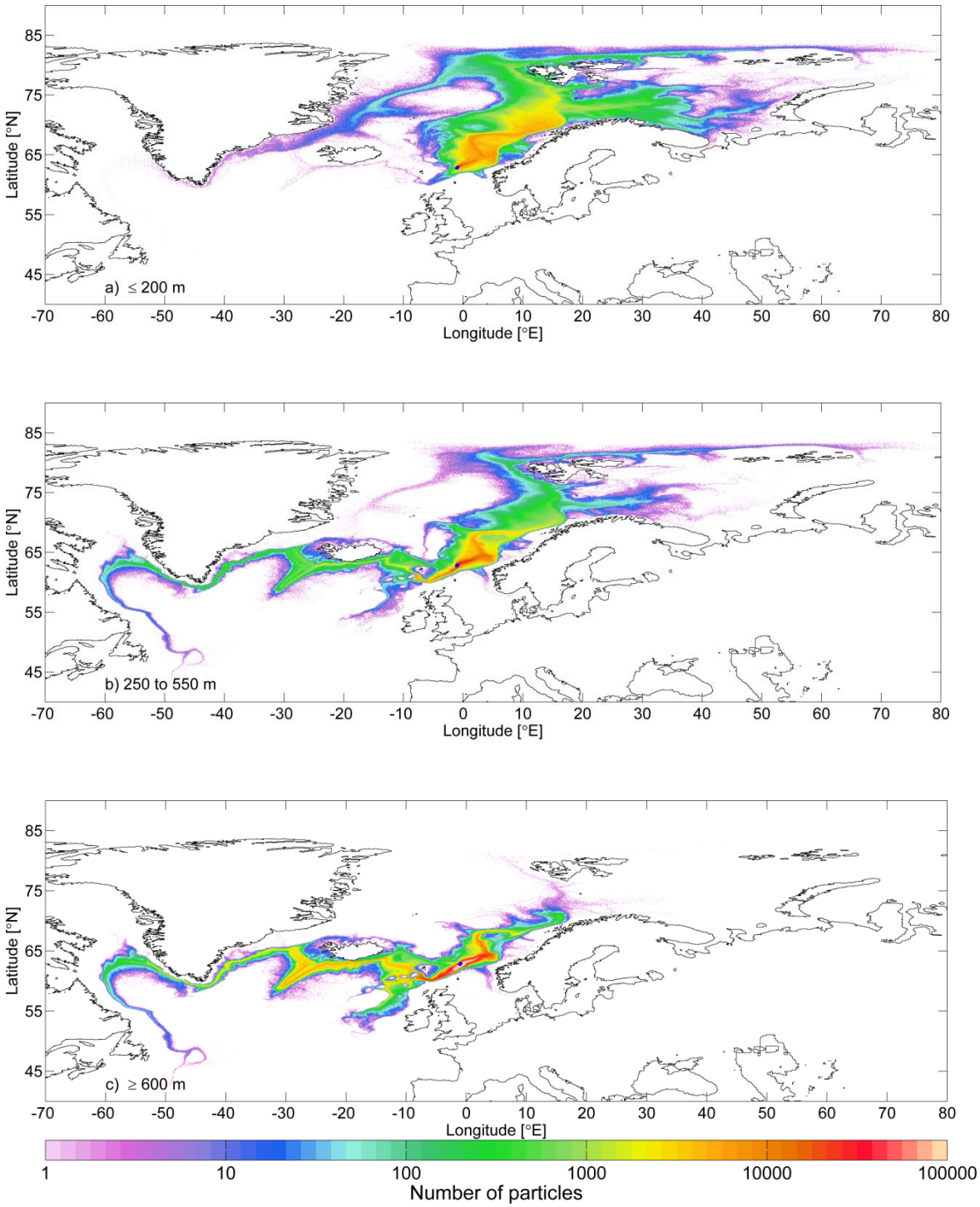

Figure 4.11. Particle density plot representing all particles released each month between 1994 and 2009 and allowed to drift for one year from release depths of: a) ≤ 200 m; b) 250 – 550 m, and c) ≥ 600 m. Particle release locations are shown as blue dots superimposed over the particle density output at 62.66° N; 1.126° W.

4.3.1.1 Horizontal spread

There were clear effects of release depth and timing on the resulting distance travelled by particles. There was both seasonal and interannual variation in distance travelled by particles (Figures 4.12 and 4.13).

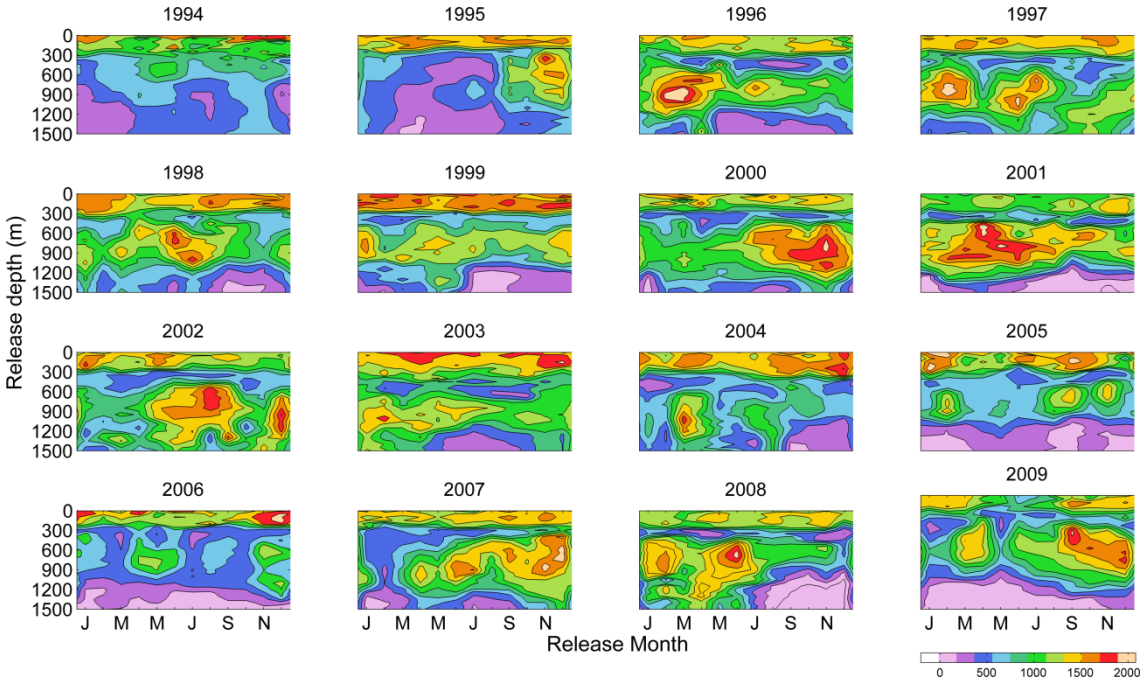

Figure 4.12. Contour plots of mean straight-line distance (km) travelled from particles' release location to their end point after one year. Distances travelled are shown for each release depth (vertical axis) and release month (horizontal axis) in the 16 year period 1994 – 2009. Each release was of 400 particles in a regularly spaced grid.

Particles released at shallow depths (10 – 300 m) were in many cases transported the furthest from their initial location by the end of one year, both in terms of: i) the straight line distance travelled between release location and end point (Figures 4.12 and 4.13) and; ii) total end-to-end distance of trajectories (Figure 4.14). However, particles released at 600 – 900 m were in some years (e.g. February 1996, June 1998, November 2000, June 2008, Figure 4.12) transported much further (> 2000 km), possibly as a result of entrainment into ISOW and subsequent increase in velocity. Particles released

deeper than ~1000 m were not transported as far, generally not travelling > 300 km away from the release location in one year (Figure 4.12).

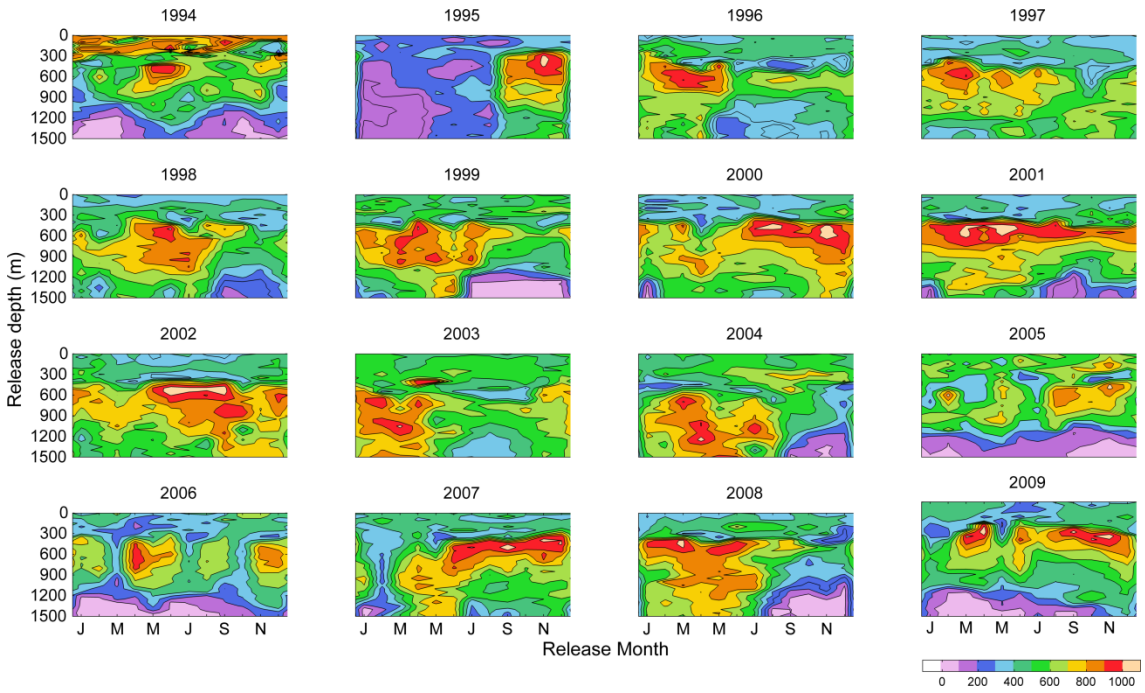

Figure 4.13. Contour plots of standard deviation in the mean straight-line distance travelled (km) by particles in one year for all releases in the 16 year period. Values are shown for each release depth (vertical axis) and release month (horizontal axis) in the 16 year period 1994 – 2009. Each release was of 400 particles in a regularly spaced grid.

Standard deviation of the mean distance travelled by particles (Figure 4.13) indicated that there was generally greater variability in distance travelled for intermediate releases (600 – 1000 m) of particles and consistently lower variability in this measure for particles released in both shallow (> 300 m) and deep (> 1000 m) water; both seasonally and between years. There was not a clear pattern in variability with respect to season and the maximum annual values of mean distance travelled and standard deviation occurred alternately in winter, spring and summer (Figure 4.13).

Measures of straight line distance travelled and end-to-end trajectory length were highly correlated (Figure 4.14). Therefore, all subsequent analyses concerned with horizontal distance used straight line distance travelled from the release location.

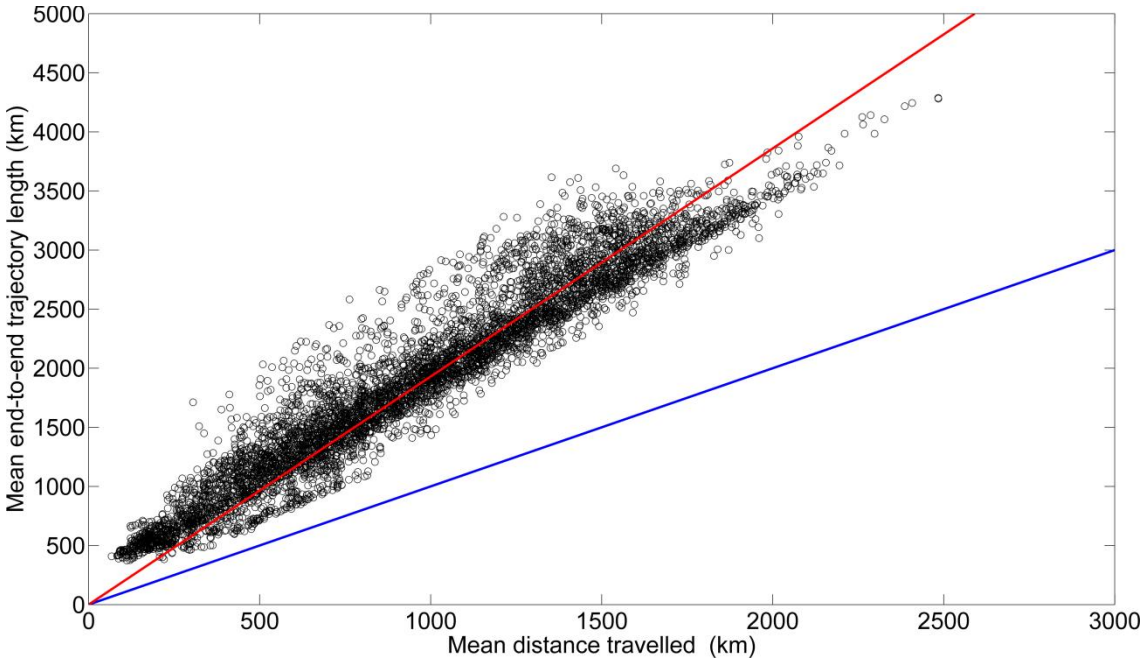

Figure 4.14. Mean straight line distance travelled from start location vs trajectory length. Blue line indicates x = y. Red line is the least squares regression fit to the points.

The maximum mean straight line distance travelled by particles (2484 km) occurred in the June 2008 release (650 m depth). Almost all of the particles (> 95%) from this release were transported westwards. A small minority (1%) of these particles were carried by the Labrador current to reach the North Atlantic in the area of the Grand Banks off Newfoundland (Figure 4.15 a) – over 2500 km from their release location at the end of one year of drift (Figure 4.15 b).

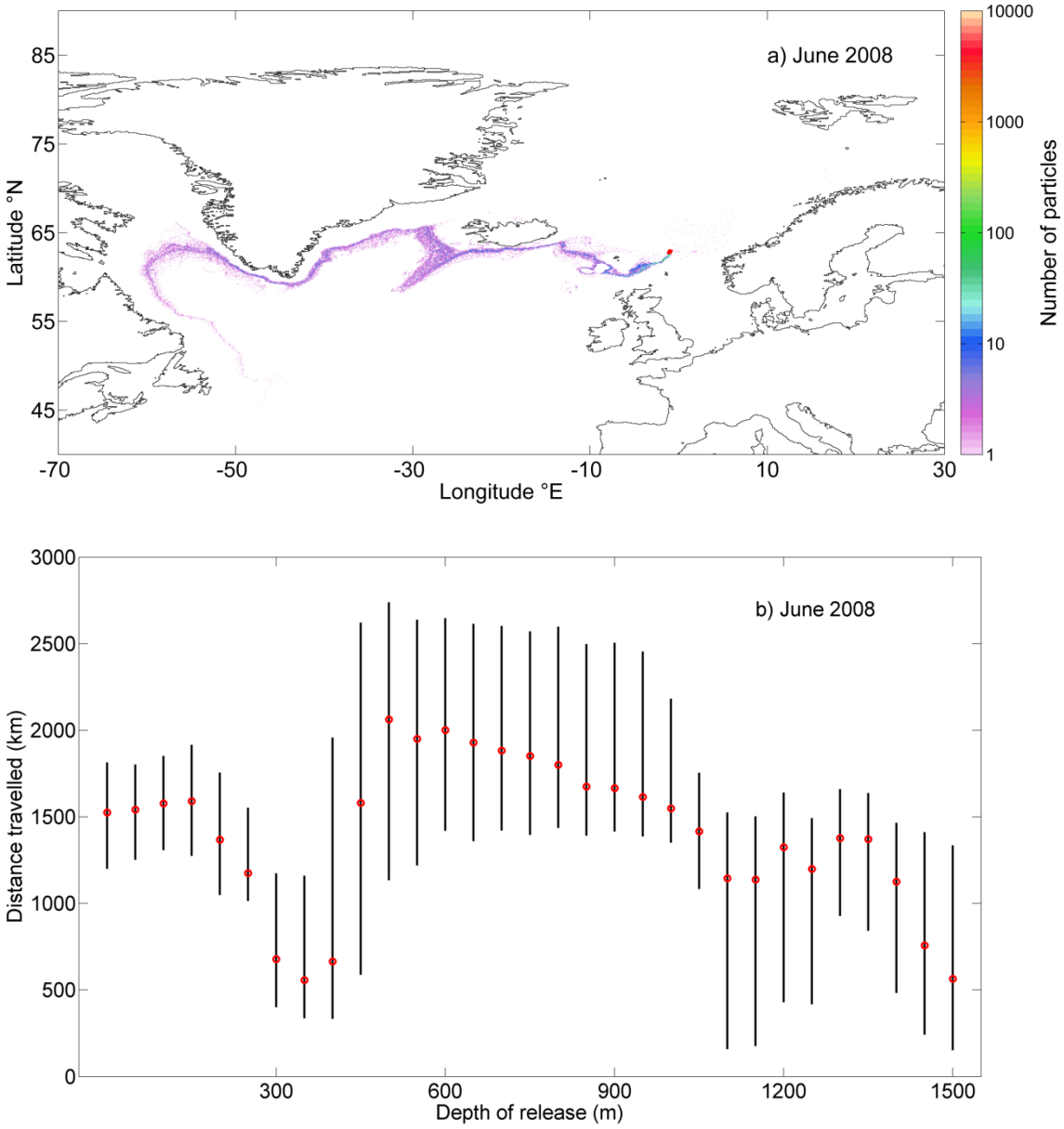

Figure 4.15. Particles released at 650 m in June 2008: a) Trajectories of the 400 particles. Release locations are indicated by red dot; b) Mean distance travelled from the release location for each release depth (error bars indicate ± standard deviation).

4.3.1.2 Transport to regions of interest

Release depth had a strong effect on particle counts at traps (Table 4.3, Figures 4.16 to 4.19. See Section 4.2.5 for explanation of the traps and their locations). Traps located to the west of the release location (W1–W5) received particles from < 20 % of all shallow (< 200 m) releases. In contrast, the eastern group of traps (E1–E5) received particles from 75 – 100 % of the releases from these shallow depths (Table 4.3).

The trap located in the FSC close to the release location (W5) received the highest number of particles, with 3.9 % of all particle releases resulting in 100% reaching this trap. High proportions (> 90% of each release from 500 – 1000 m depth) of the particles reaching W5 (FSC) trap were caught at the trap in prolonged periods between late 2000 and 2002. There was a further period of prolonged high capture-rate in late 2007 to early 2009. Interannual variability in the particle counts reaching trap W5 (FSC) was evident. For example, 2005 to 2007 resulted in lower proportions (< 80 %) of released particles reaching the trap.

Seasonality was evident at some of the traps, for example, at the traps situated towards the far western extent of particle travel (W1 – southeast Greenland and W2 – Iceland basin). At W1, higher particle counts (> 20 %) generally occurred in winter (11 of the 16 years studied). Trap W2 (Iceland basin) caught almost no particles from any release during 1994. However, from 1995 onwards, this trap received particles from most releases (20 – 50% of particles released at intermediate depths of 600 – 1000 m, Figure 4.16, lower panel).

Trap W3 was located over the Wyville Thomson Ridge, which forms a barrier to deep water circulation at 450 m water depth. Less than 10% of any release reached this trap from depths > 800 m. Most particles caught at W3 were from these deeper releases (Figure 4.17 upper panel). Shallower particles (released at 400 to 800 m) instead appeared to flow through the W4 trap, which was located at the FBC sill (Figure 4.17 middle panel).

Table 4.3. Percentage of all releases (1994 – 2009) from each release depth resulting in contamination (presence of any particles) at traps. Note that, because some particles never reach any traps, while others reach multiple traps, neither rows nor columns sum to 100%. Values ≥ 50% have been shaded.

Trap	W1	W2	W3	W4	W5	E1	E2	E3	E4	E5
Release depth (m)										
10	13				4	93	99	100	100	99
50	5			1	7	79	100	99	99	98
100	5	1	1	2	6	76	100	100	99	95
150		1	1	2	8	79	100	100	99	89
200	2	8	6	13	21	88	100	100	99	88
250	9	28	23	38	52	97	100	100	96	75
300	26	56	55	70	77	100	100	100	84	50
350	48	78	73	88	93	99	100	99	69	32
400	67	89	84	94	95	98	100	96	48	26
450	75	95	89	96	97	96	100	91	32	18
500	83	97	93	98	100	90	99	80	14	9
550	85	97	93	99	99	84	97	71	8	9
600	85	96	94	97	99	80	94	69	7	3
650	84	96	96	97	98	73	89	56	2	5
700	88	96	96	96	96	69	80	52	2	4
750	85	96	96	97	97	57	73	39	2	2
800	87	95	96	96	96	51	68	33	1	2
850	85	94	95	94	95	41	58	23		2
900	82	92	94	94	94	28	58	24	1	2
950	79	92	94	94	94	37	49	22		
1000	78	92	93	93	94	26	47	19		2
1050	72	91	93	92	93	32	41	14	1	
1100	65	91	92	92	93	20	40	17		1
1150	60	88	91	91	92	21	36	13	1	2
1200	57	85	90	90	90	22	30	8		1
1250	51	80	84	85	87	24	29	12	1	
1300	52	76	81	81	84	15	27	8	1	1
1350	46	75	77	80	81	19	20	8	1	1
1400	44	73	76	76	79	21	19	10	2	1
1450	46	70	74	75	78	18	17	7	1	2
1500	45	69	73	76	77	18	16	8	1	1

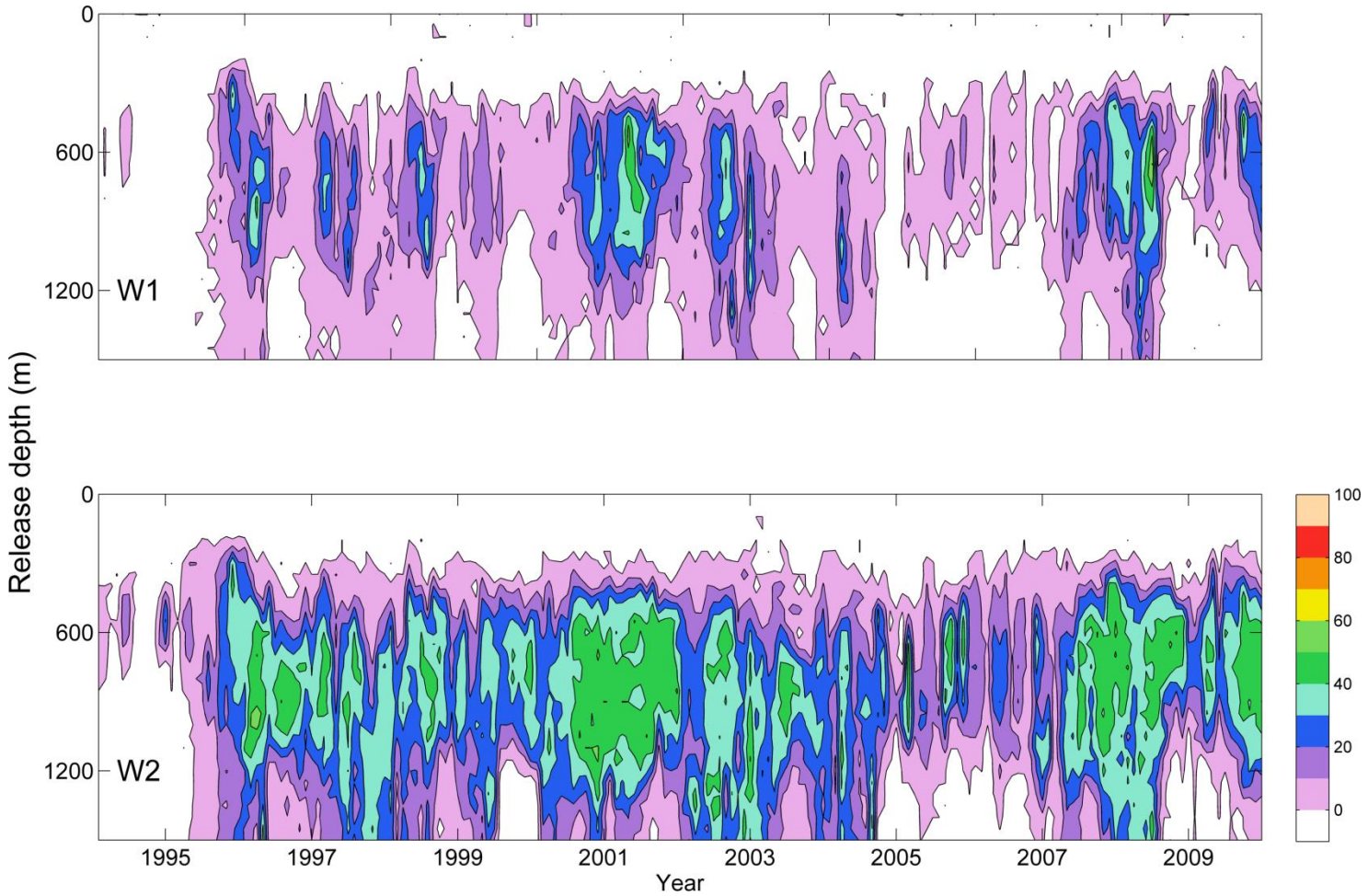

Figure 4.16. Percentage of particles from each release depth reaching traps. W1: Southeast Greenland; W2: Iceland basin. See text for explanation of traps and their locations.

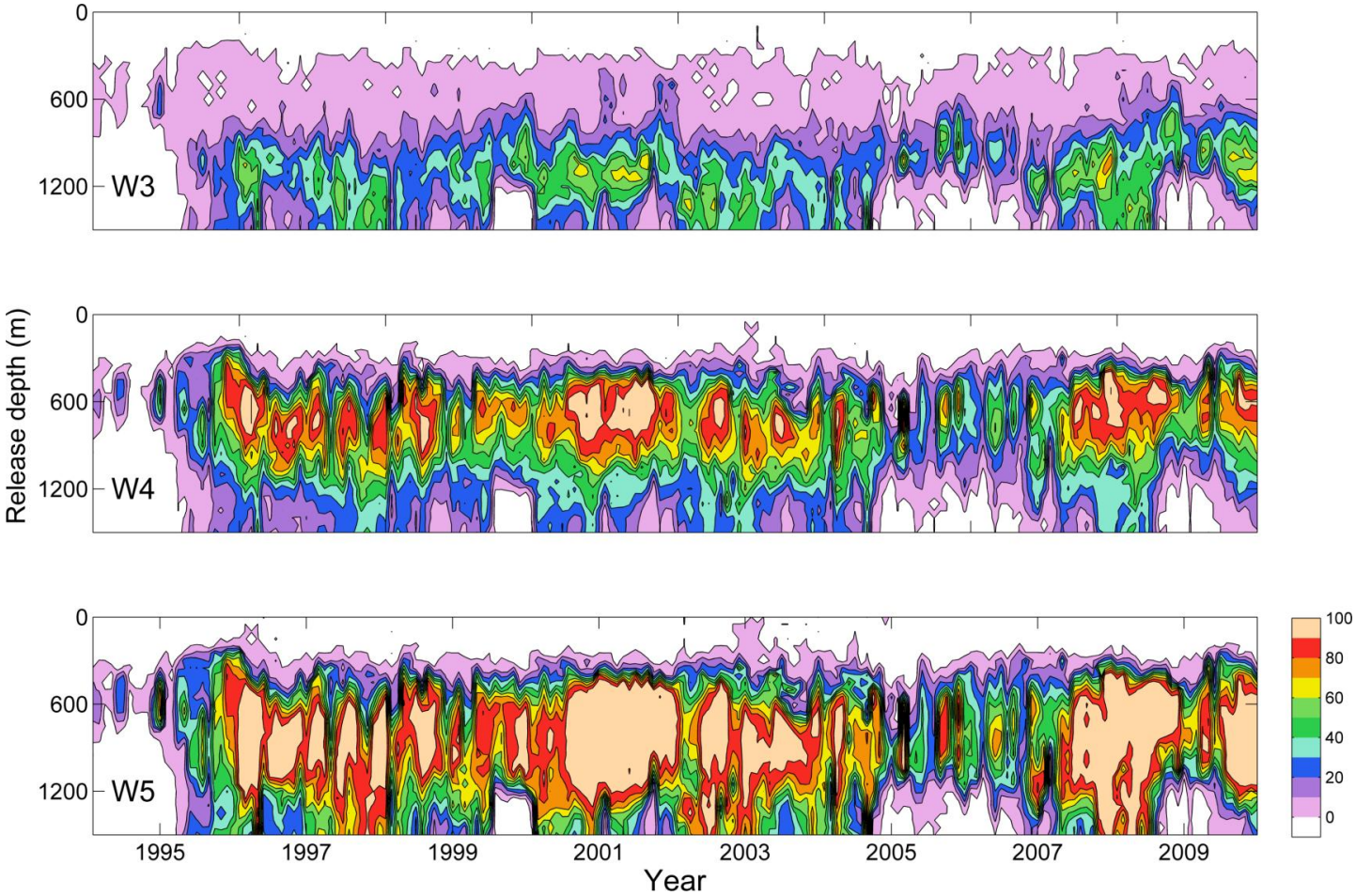

Figure 4.17. Percentage of particles from each release depth reaching traps. W3: Wyville Thomson Ridge; W4: Faroe Bank Channel; W5: Faroe Shetland Channel. See text for explanation of traps and their locations.

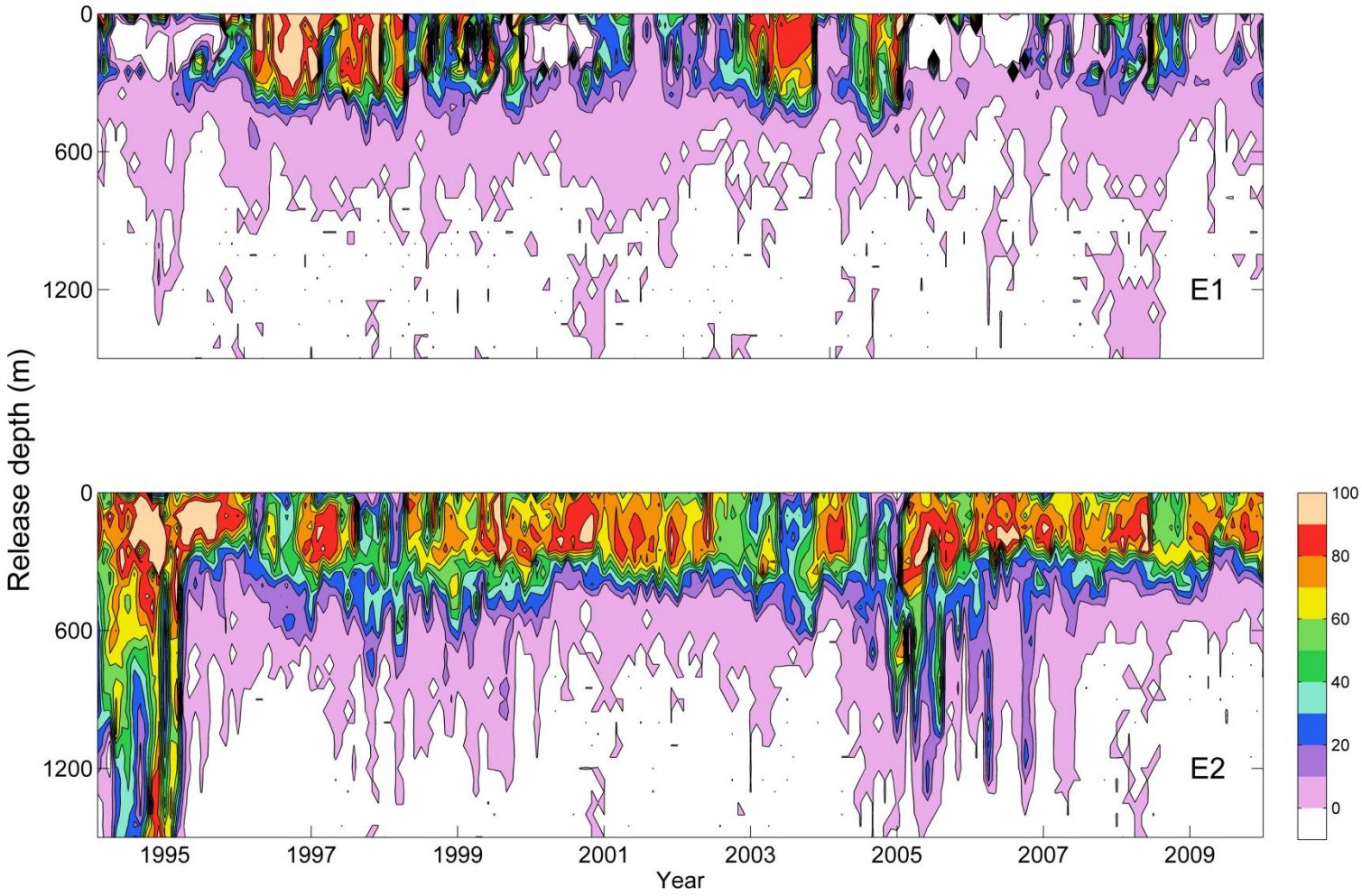

Figure 4.18. Percentage of particles from each release depth reaching traps. E1: Norwegian Sea east; E2: Norwegian Sea west. See text for explanation of traps and their locations.

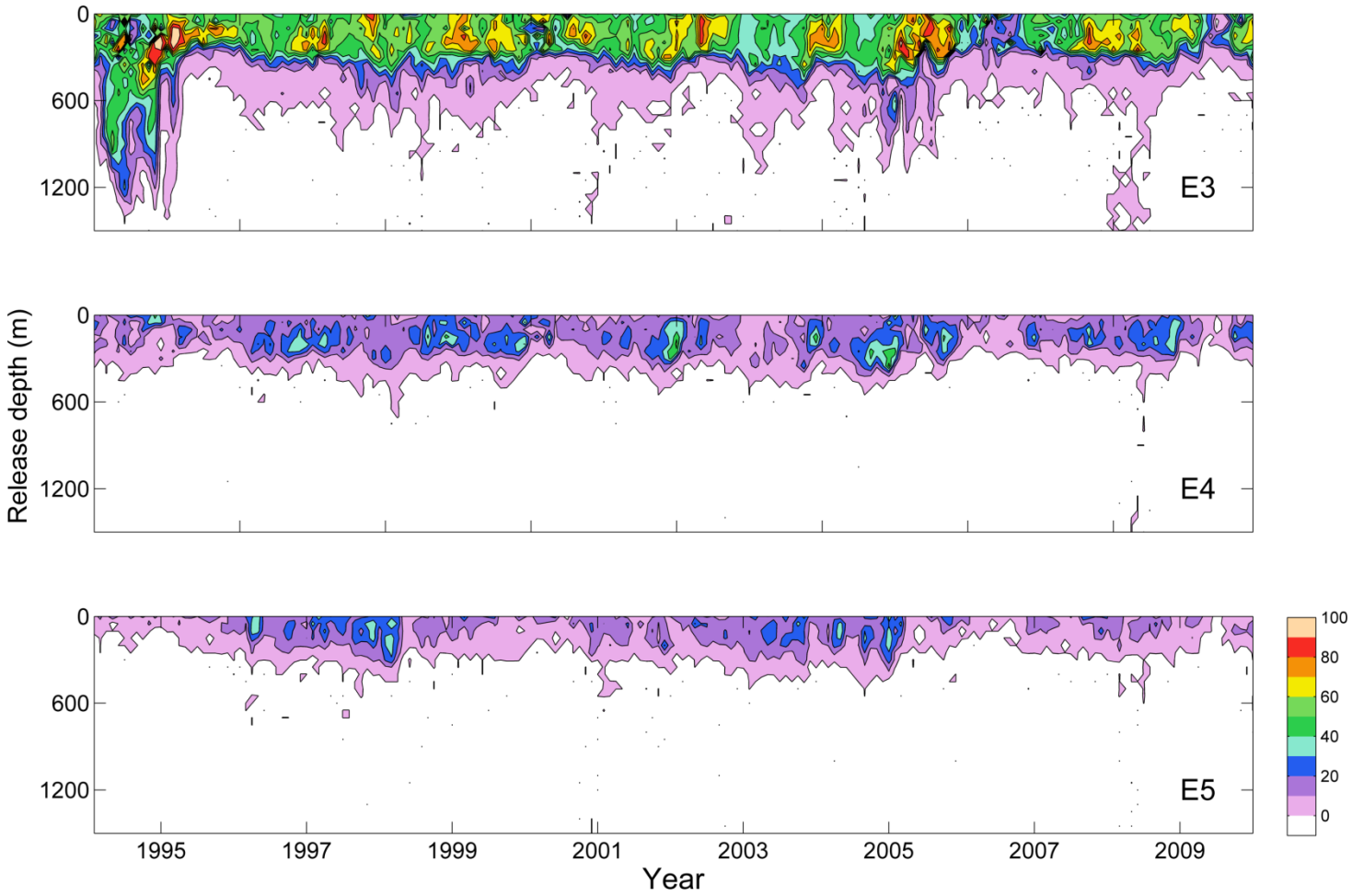

Figure 4.19. Percentage of particles from each release depth reaching traps. E3: Sub Arctic; E4: Svalbard. E5: Russian Arctic. See text for explanation of traps and their locations.

Particles reaching the Norwegian Sea (traps E1 and E2) were consistently from release depths < 400 m, year-round throughout the time series of releases, but with occasional gaps (Figure 4.18). Flow was stronger to offshore regions of the Norwegian Sea (trap E2) earlier in the time series (1994 to 1996). Subsequently, the more inshore areas of the Norwegian Sea (trap E1) generally received more particles throughout the periods 1996 to 2000 and 2000 to 2003. The more offshore trap (E2) received particles from releases spanning the water column for much of 1994 and 2005.

Particles travelling towards the sub-Arctic were caught by trap E3, with winter releases clearly resulting in higher proportions (> 70 %) of particles (Figure 4.19, upper panel). Traps E4 and E5 were located in the Arctic, and received relatively low proportions of particles (< 10 %) from many of the shallow water (< 300 m) releases (Figure 4.19). Some seasonality was evident, with winter releases resulting in higher proportions of particles reaching the Arctic (up to 50 % of releases in the winters of 2002 and 2005, for example).

4.3.1.3 Changes in depth

Release depth had a strong effect on end depth. Particles released from intermediate depths (600 – 900 m) experienced the greatest depth changes of up to 800 m. In contrast, both shallow (< 300 m) and deep (> 900 m) releases of particles tended to be within 100m of their release depth at the end of one year and the average change in depth (either positive or negative) was also smaller for shallower releases (Figure 4.20). Strong, repeating, seasonal patterns were not evident in the depth changes of released particles and here the effect of year resulted in more variation (Figure 4.20).

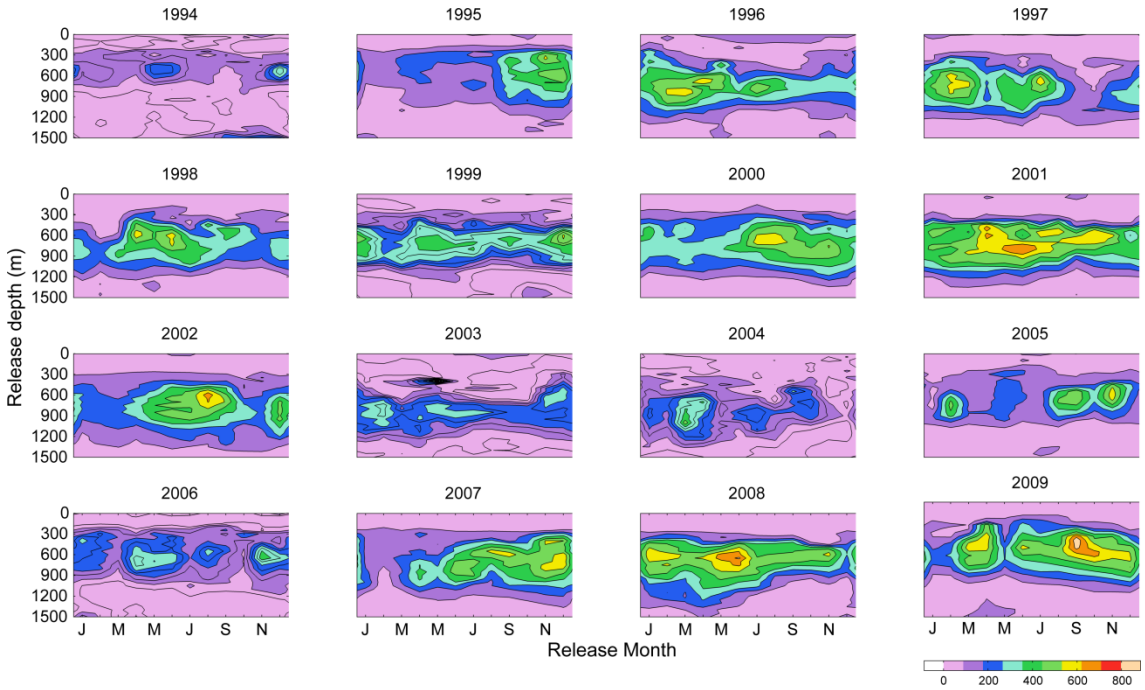

Figure 4.20. Average change in depth (m) for each release of 400 particles.

The depth change results further indicated that particles released in intermediate water depths could be entrained into ISOW. This was confirmed by plotting the particle trajectories of all particles released at 600 – 800 m (Figure 4.21).

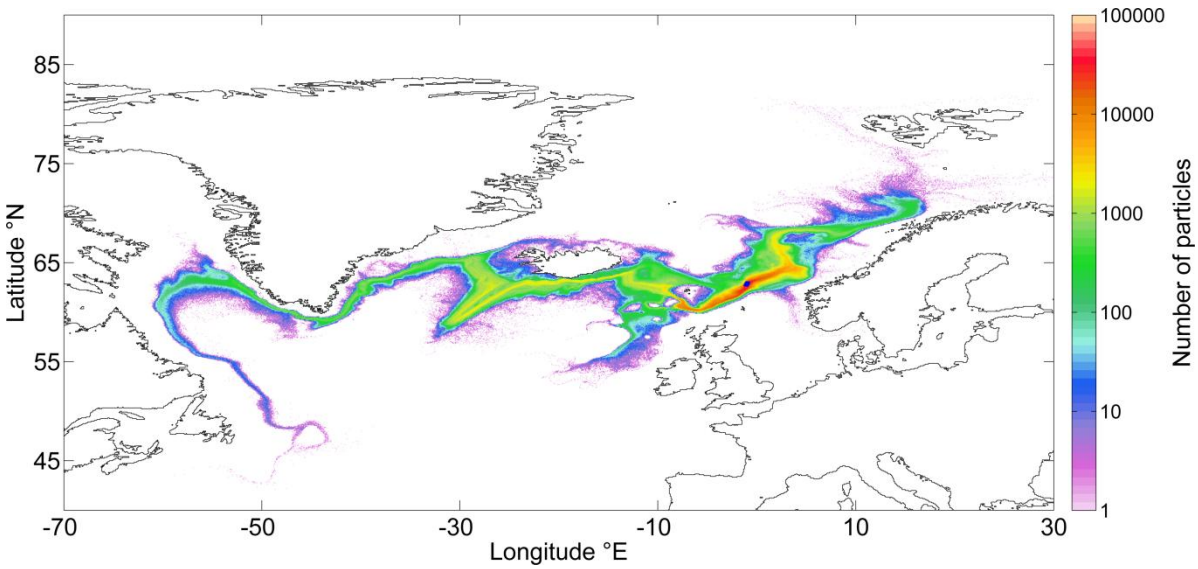

Figure 4.21. Pathways of all particles released at depths between 600 – 800 m.

4.3.2 Importance of temperature-controlled decay to limit spread

When a simple algorithm (Section 4.2.4) was applied to simulate temperature-controlled hydrocarbon degradation, release depth affected the time taken for the simulated oil to decay (Figure 4.22). Releases at the depth of the permanent thermocline (~600 m) reached the 10% decay threshold within 210 days on average (Figure 4.22).

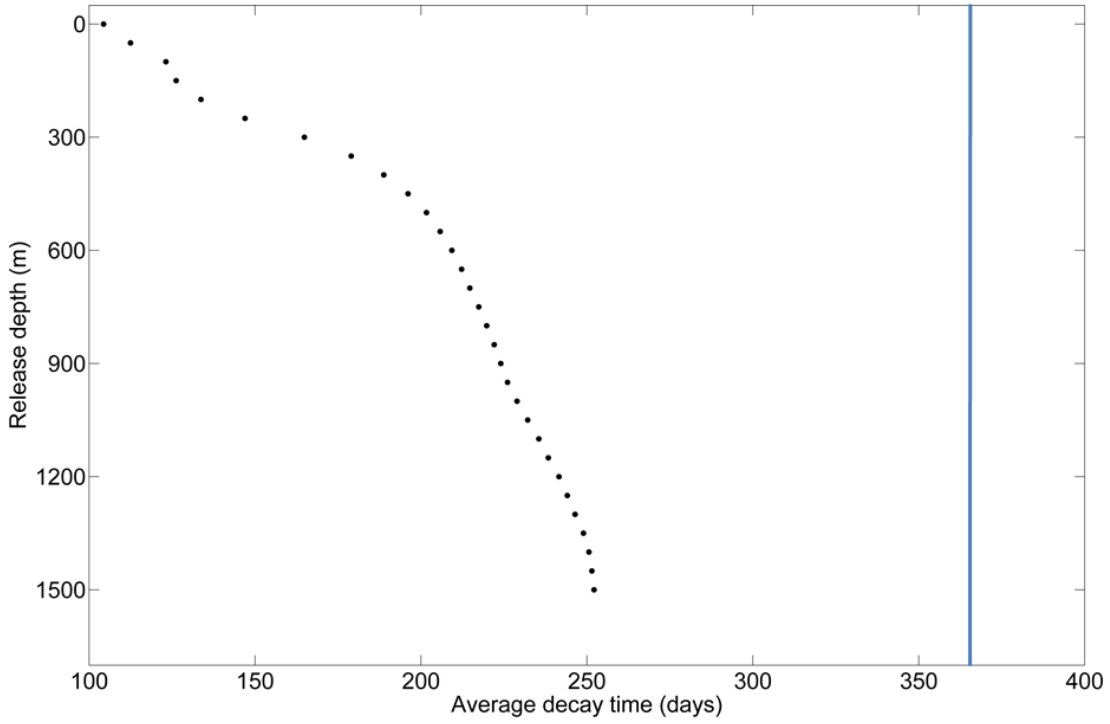

Figure 4.22. Average time taken by particles from each depth to reach the decay threshold of 10%. Vertical line at 365 days indicates that all particles decayed to 10% well before one year of drift.

4.3.2.1 Effect of decay on horizontal spread

Following particle decay, the horizontal area contaminated was reduced (Figure 4.23). Particles terminated on reaching 10% of their starting value were not transported nearly as far as undecayed particles in most cases, and some traps (see explanation of traps in Section 4.2.4) received few (E4, E5) or no particles (W1) from any release under this scenario (Figure 4.23, Table 4.4).

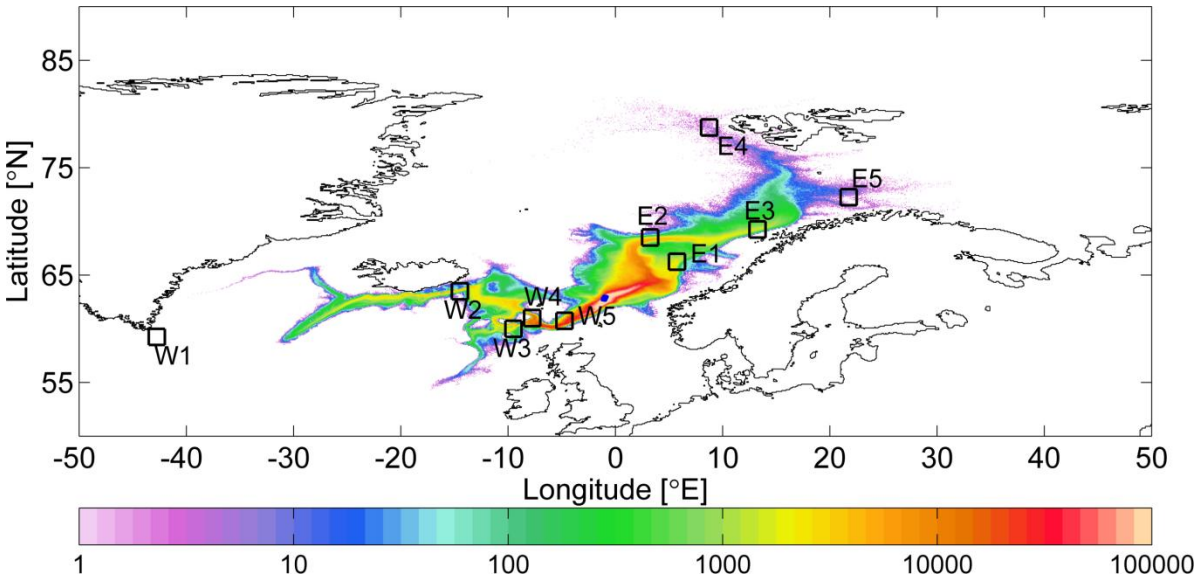

Figure 4.23. Particles terminated when decayed to 10% of starting value (all depths and times of release) with trap locations from previous sections superimposed.

Table 4.4. Percentage of all releases (1994 – 2009) resulting in contamination (presence of any particles) at traps following decay to 10%. No particles reached trap W1 under this scenario. Values > 50% have been shaded.

	W1	W2	W3	W4	W5	E1	E2	E3	E4	E5
Release depth (m)										
10					1	83	83	78	9	15
50					1	71	89	83	6	16
100						66	92	94	5	12
150				1	1	70	96	93	3	5
200		1		2	3	74	95	90	1	4
250		6	7	9	16	89	94	79	2	3
300		18	15	30	42	90	95	65	1	2
350		35	31	52	60	77	90	44	1	2
400		56	49	76	81	57	85	26		
450		70	57	83	87	40	72	18		
500		80	61	87	90	26	55	10		
550		83	61	89	91	15	44	6		
600		86	73	89	91	7	39	5		
650		86	81	90	91	4	30	4		
700		89	87	91	91	2	24	4		
750		89	91	91	91	2	24	3		
800		86	90	91	92	1	22	3		
850		85	90	91	92		19	3		
900		83	89	89	91	1	16	3		
950		81	90	90	91	2	16	3		
1000		75	88	90	90	1	16	2		
1050		72	88	89	90	1	16	2		
1100		68	84	85	89		13	1		
1150		62	78	81	84		11	1		
1200		57	75	77	82		8	1		
1250		54	69	70	76		7	1		
1300		52	65	67	73	1	6	1		
1350		48	63	63	70		5			
1400		47	61	63	69		4			
1450		45	61	61	69		4			
1500		48	61	63	67		4			

The effect of temperature-mediated decay on distance travelled was, for some releases, greater for particles released in shallower water (< 300 m) than those released in deep water (Figure 4.24). For deep water releases (> 1200 m) there was little effect of decay on the distance travelled from release location, except in intermittent cases (e.g. June 2008, Figure 4.24). There was less variability in the distance travelled for decayed particles than non-decayed particles at all release depths (Figure 4.24). Transport in the year and month that saw the greatest distances travelled for shallow water releases (> 2500 km, June 2008) was greatly reduced to ~1000 km following decay to 10 % (Figure 4.24).

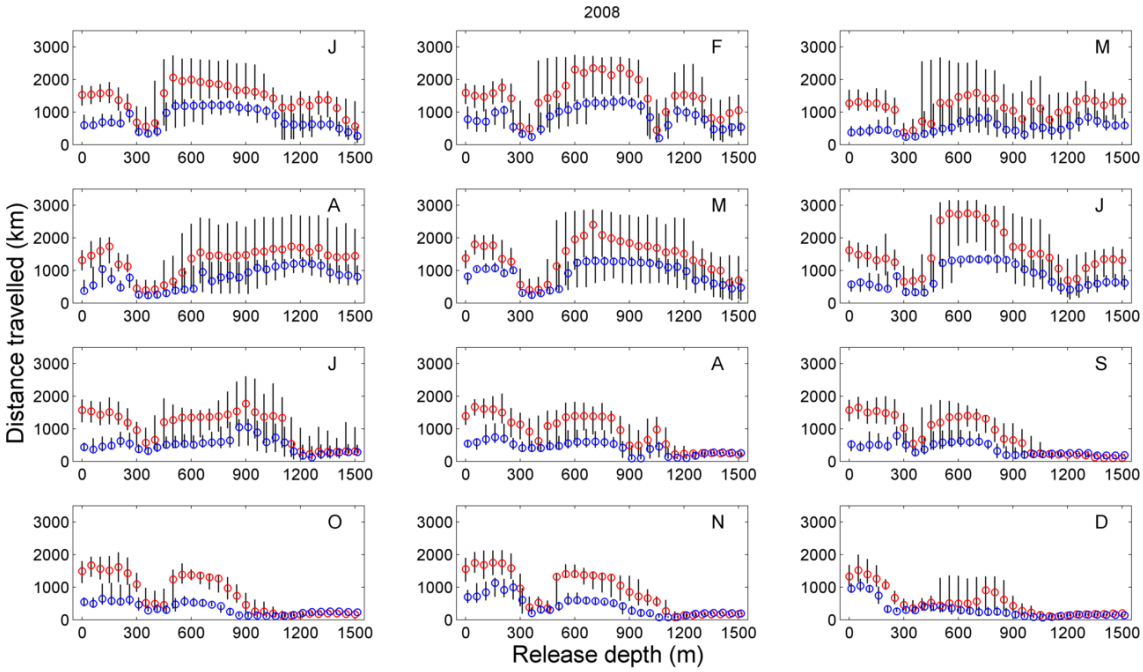

Figure 4.24. Median distance travelled from release location for undecayed (red circles) and decayed to 10 % (blue circles) particles released over every month in 2008. Error bars show interquartile range (25% and 75%). Letters J, F,…D indicate months January, February … December.

4.3.2.2 Effect of decay on temporal patterns

There was interannual variability in the effect of temperature-mediated decay on the length of time that particles remained drifting. For example, a comparison of January releases from three depths (300 m, 600 m and 1000 m) in two different years (1994 and 1998, Figure 4.25), indicated that shallow (300 m) releases were drifting for 200 days in January 1994 (Figure 4.25 a), but did not remain beyond 150 days in January 1998 (Figure 4.25 b).

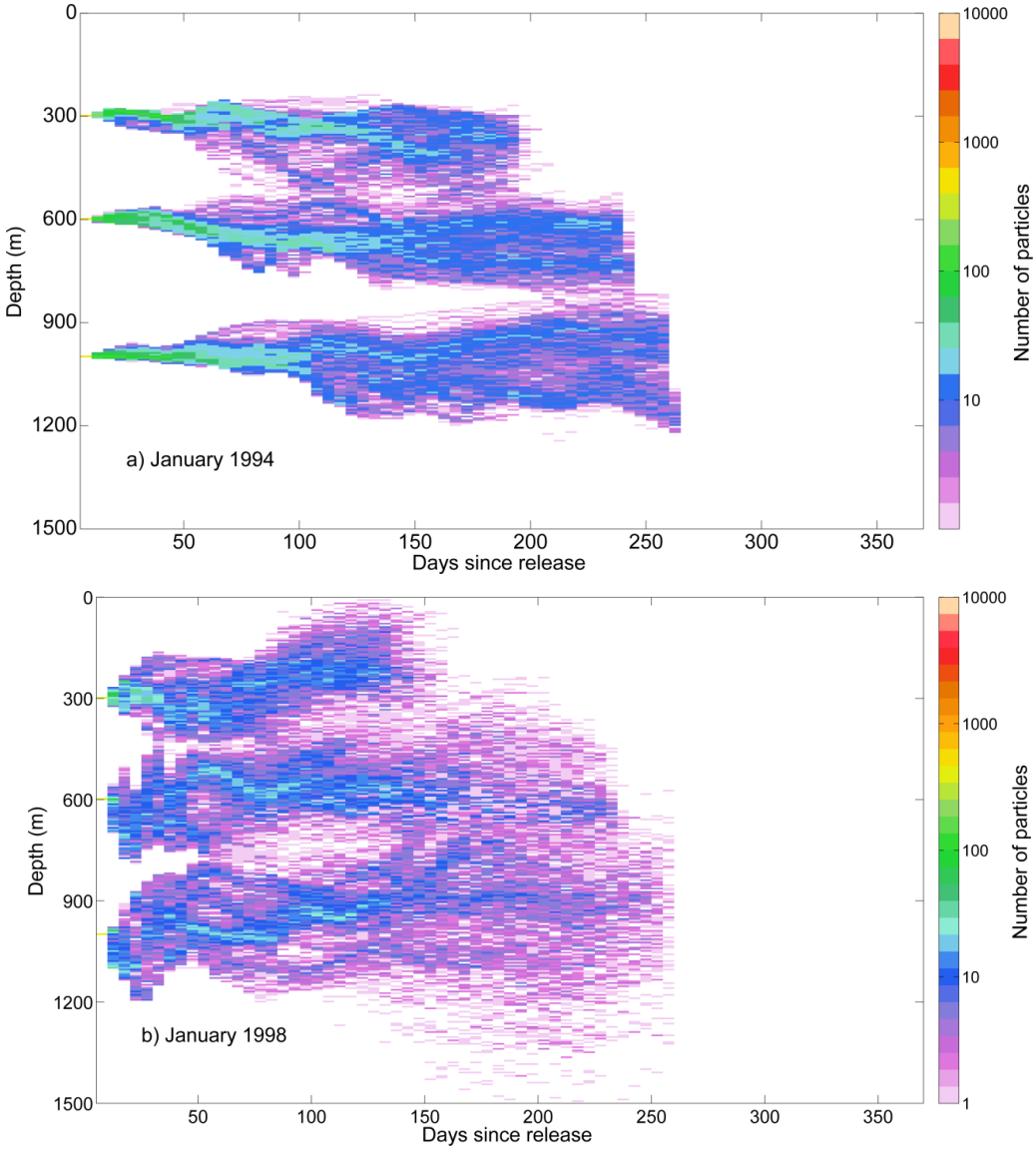

Figure 4.25. Particles released from 300 m, 600 m and 1000 m, terminated at the decay threshold of 10% in: a) January 1994, and b) January 1998.

Regardless of release time, particles released at the same depth tended to decay within a short time of one another (within 20 days). This indicates that particles released at the same depth experienced similar mean ranges of temperature along their trajectories, and that particles released from different depths experienced different temperatures (e.g. the model's average temperature for the deepest release at 1500 m was -0.4°C whereas for the shallowest release at 10 m this was 6.2°C).

4.3.3 Oil respiration

The amount of oil respired (interpreted here as an index of oxygen consumption) varied according to release depth. Particles released at shallower depths were more tied to seasonal cycles in temperature and ultimately consumed more oxygen, and more rapidly than those released in deep water (Figure 4.26). For example, particles released at 10 m water depth in summer had, on average, respired 50% of the total oil 'available' to them within one month (Figure 4.26 a) and close to 100% of the total oil available within 3 months (Figure 4.26 b). In contrast, particles released in deep water (1500 m) had respired little more than half of this amount in the same time frame, regardless of season (Figure 4.26 b) and particles released in deep water experienced very little change in their respiration rates, regardless of season. There was some interannual variability in oil respiration rate, particularly for particles released at 300 m. For example, in 1994 - 1995 the seasonal signal was absent for these particles, whereas from 1995 onwards there was a seasonal effect (Figure 4.26 a-d).

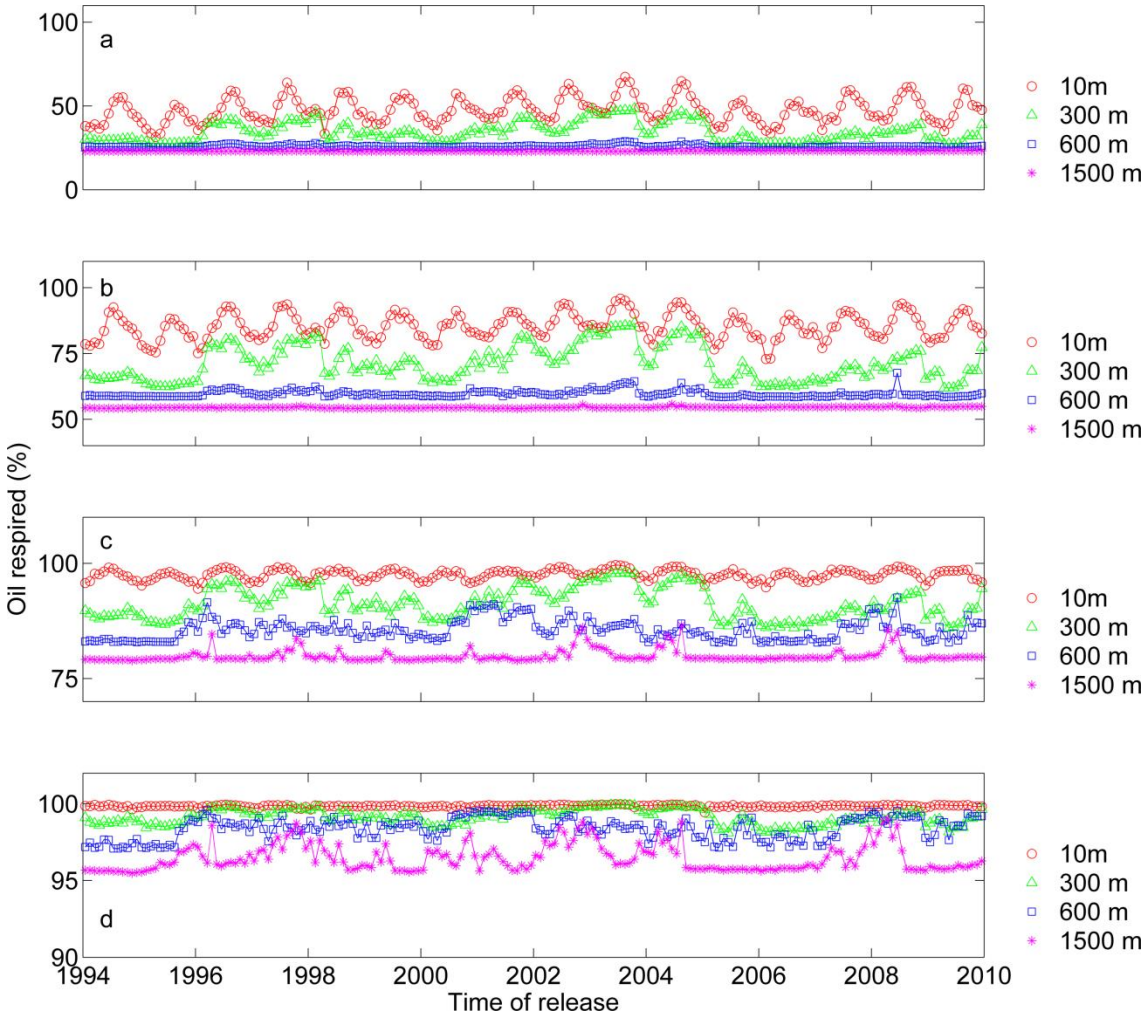

Figure 4.26. Average percentage of oil respired at four release depths (10 m; 300 m; 600 m and 1500 m) for each monthly release 1994 – 2009. The average amount of oil respired was integrated for drift times of: a) 1 month; b) 3 months; c) 6 months and d) 12 months. To improve visual clarity the scales of the vertical axes have been adjusted for each panel.

Spatially, oxygen consumption was spread over a wider area in shallow depths than in deep water (Table 4.5; Figures 4.27, 4.28). After one month, the total area affected was ten times greater in shallow waters (10 m) when compared to the deepest releases (1500 m, Table 4.5). This calculation assumed a threshold of 0.1 (arbitrary) units in order for a grid location to be recorded as experiencing enhanced oxygen consumption. Therefore, the area impacted depends on this threshold (which is arbitrary).

Table 4.5. Average area of grid squares (*1000 km^2) where oil respiration took place for releases from 1m; 300 m; 600 m and 1500 m with drift times of 1 month; 3 months; 6 months and 12 months. Grid squares were included where a threshold of 0.1 units of oxygen consumption was exceeded.

	1 month	3 months	6 months	12 months
10 m	101	202	245	246
300 m	50	138	181	199
600 m	21	70	123	158
1500 m	11	30	52	68

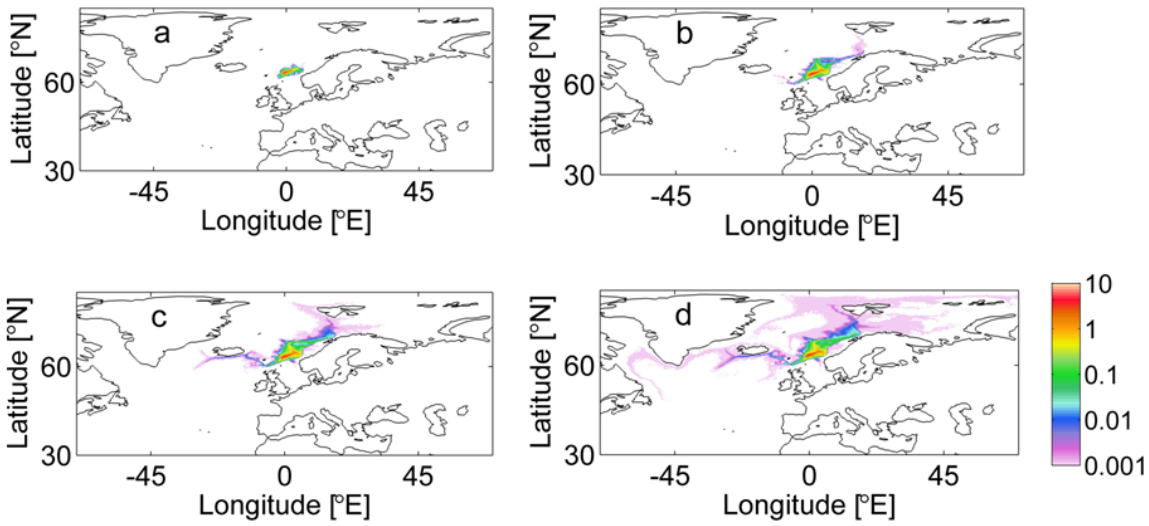

Figure 4.27. Spatial extent of oil respiration associated with 300 m water depth releases after: a) one month; b) three months; c) six months and d) twelve months. Colour scale represents number of particles consumed on average across all releases, with 400 (i.e. all those released at 300 m water depth) being the theoretical maximum.

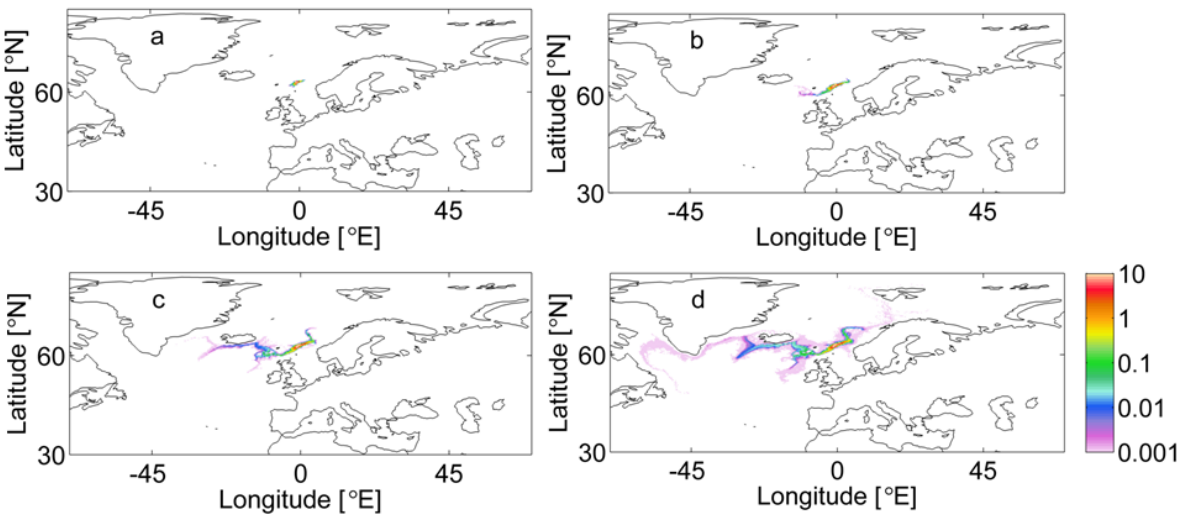

Figure 4.28. Spatial extent of oil respiration associated with 1500 m depth releases after: a) one month; b) three months; c) six months and d) twelve months. Colour scale represents number of particles consumed on average across all releases, with 400 (i.e. all those released at 1500 m water depth) being the theoretical maximum.

4.3.4 Seafloor contact

4.3.4.1 Release depth and timing effects on seafloor contact

Seafloor 'contact' was defined here as occurring when particles were within 200 m of the seabed. Deepwater (> 1400 m) releases resulted in the most seafloor contact (Figure 4.29). Considering the entire period of study (1994 – 2009), and firstly without temperature-controlled decay, a smaller proportion (35% on average) of particles released in depths less than 500 m were ever within 200 m of the seafloor (Figure 4.30; Table 4.6). Releases from depths > 500 m more often resulted in contact with the seafloor (74 % on average).

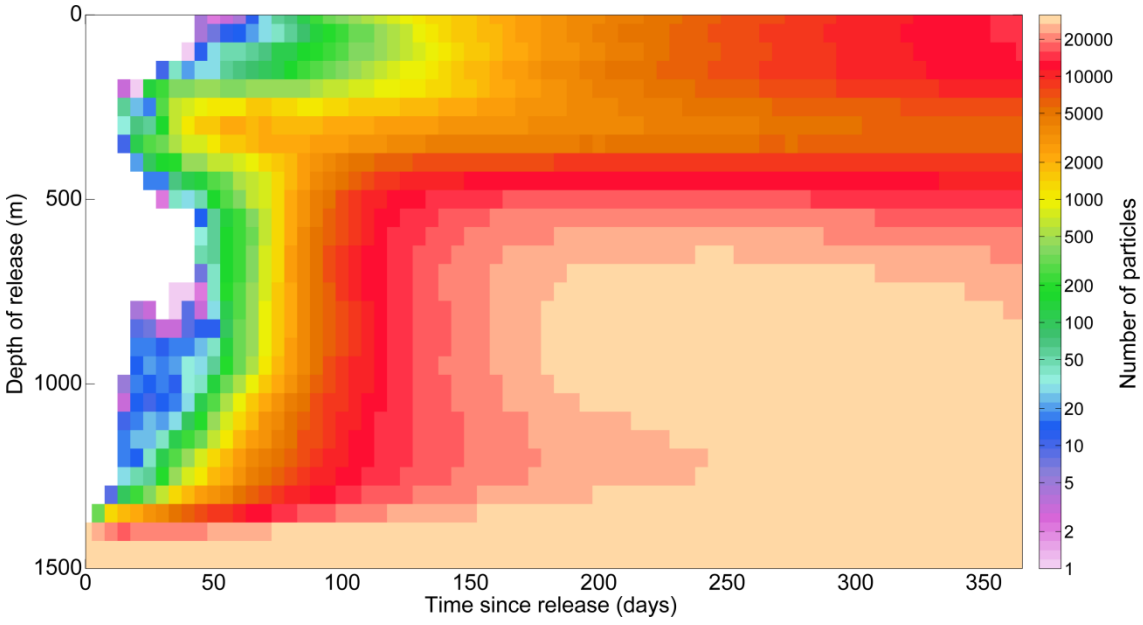

Figure 4.29. Number of particles within 200 m of seafloor for all releases 1994 – 2009.

From around 20 days into the simulations, particles released at shallower depths (300 – 500 m, Figure 4.30) were also transported to within 200 m of the seabed, in small numbers (< 1000 of the total) to begin with, This indicated the potential for particles to be advected over a slope, causing seafloor impact away from their initial location.

There was interannual variability in the average proportion of particle days (i.e. the amount of time in the year-long simulations) that oil was within 200 m of the seafloor (Table 4.6). For example, in both 1994 and 1995, < 50 % of the total number of particle days from from intermediate releases (500 – 1250 m) resulted in seafloor contact.

Table 4.6. Average percentage of particle days from each release that were within 200 m of seafloor. Values > 50% have been shaded grey.

Release depth (m)	1994	1995	1996	1997	1998	1999	2000	2001
10	27	20	32	44	31	33	25	19
50	15	14	33	41	42	27	26	30
100	8	16	37	40	43	23	19	32
150	3	14	34	41	44	27	19	35
200	5	18	32	39	42	26	18	35
250	9	34	42	41	41	31	29	32
300	9	38	54	51	38	34	36	23
350	11	39	53	51	35	26	29	29
400	14	37	41	40	38	29	36	45
450	17	35	41	38	51	36	54	74
500	19	35	51	44	56	45	66	92
550	19	35	64	52	62	59	74	96
600	19	37	74	61	67	70	79	98
650	19	40	83	68	72	76	84	98
700	16	41	90	76	77	78	87	99
750	15	42	92	80	79	78	89	99
800	13	42	94	82	82	79	90	99
850	8	42	95	85	85	81	90	99
900	6	43	94	86	87	82	90	99
950	5	45	94	87	86	81	90	97
1000	5	47	93	88	84	82	90	95
1050	5	47	92	86	82	77	89	92
1100	10	46	90	88	77	74	89	89
1150	19	43	81	88	73	67	89	85
1200	31	44	73	88	73	57	88	80
1250	41	45	67	90	74	48	86	76
1300	53	49	68	92	79	51	85	78
1350	67	61	72	94	87	72	86	84
1400	82	81	87	97	95	88	92	92
1450	91	89	95	99	98	96	96	98
1500	98	95	99	100	99	100	100	100

Table continues

Table 4.6. continued. Average percentage of particle days from each release that were within 200 m of seafloor. Values > 50% have been shaded grey.

Release depth (m)	2002	2003	2004	2005	2006	2007	2008	2009
10	24	38	40	34	18	26	23	13
50	35	38	39	29	13	26	32	14
100	35	36	44	22	10	24	28	19
150	38	41	48	22	9	23	29	16
200	38	43	47	17	14	17	26	15
250	34	46	45	18	20	21	25	17
300	38	55	48	18	18	27	28	27
350	39	63	54	13	17	29	28	33
400	36	65	47	17	21	38	46	42
450	45	54	41	22	26	47	71	51
500	53	49	41	27	31	55	86	61
550	62	41	48	37	36	64	92	72
600	71	48	52	43	41	70	93	79
650	77	56	56	46	46	75	93	83
700	82	71	58	47	47	77	94	85
750	84	83	62	49	47	78	94	86
800	86	88	67	51	47	79	93	86
850	87	90	68	54	47	80	91	86
900	87	91	70	58	47	82	86	84
950	87	92	71	59	48	81	84	81
1000	87	90	68	60	47	82	85	80
1050	85	90	66	57	47	82	85	77
1100	84	87	62	49	52	83	84	73
1150	87	84	60	40	53	83	84	67
1200	88	82	58	37	55	81	85	62
1250	93	80	62	39	61	80	86	63
1300	97	86	65	47	70	81	89	70
1350	99	90	74	60	77	85	94	78
1400	99	96	89	74	82	90	99	89
1450	100	99	97	87	89	95	99	96
1500	100	100	99	94	96	98	100	99

Particles released in shallow water (≤ 200 m) were transported to within 200 m of the seafloor in all of the years studied, but the maximum proportion of particle days for which seafloor contact occurred was only 48% (in 2004, Table 4.6).

When particles were decayed to 10 %, < 1% of shallow water releases (< 300 m) came within 200 m of the seafloor (Figure 4.30). All particles had decayed within 275 days, indicating that the areal extent contacted by particles would not expand beyond that length of drift time.

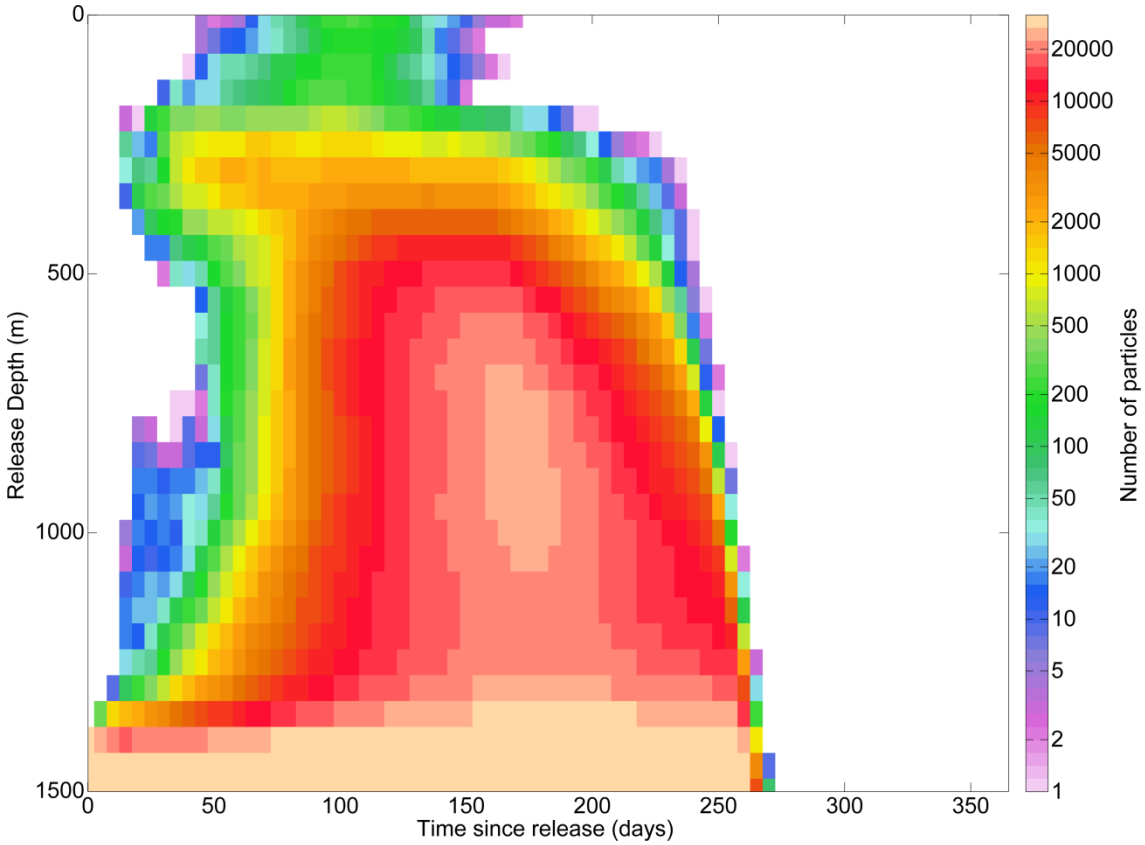

Figure 4.30. Number of particles terminated at threshold of 10% within 200 m of seafloor over all releases 1994 – 2009.

4.3.4.2 Spatial and temporal variability in seafloor contact

Release depth affected the geographical areas of the seabed that were contaminated by particles (again, within 200 m of the seafloor, Figures 4.31, 4.32). Particles released from shallow depths (300 m) contacted the seabed along the shelf edge break of the FSC and Norwegian Sea and covered vast areas of the Barents Sea and the Arctic around Svalbard (Figure 4.31 a).

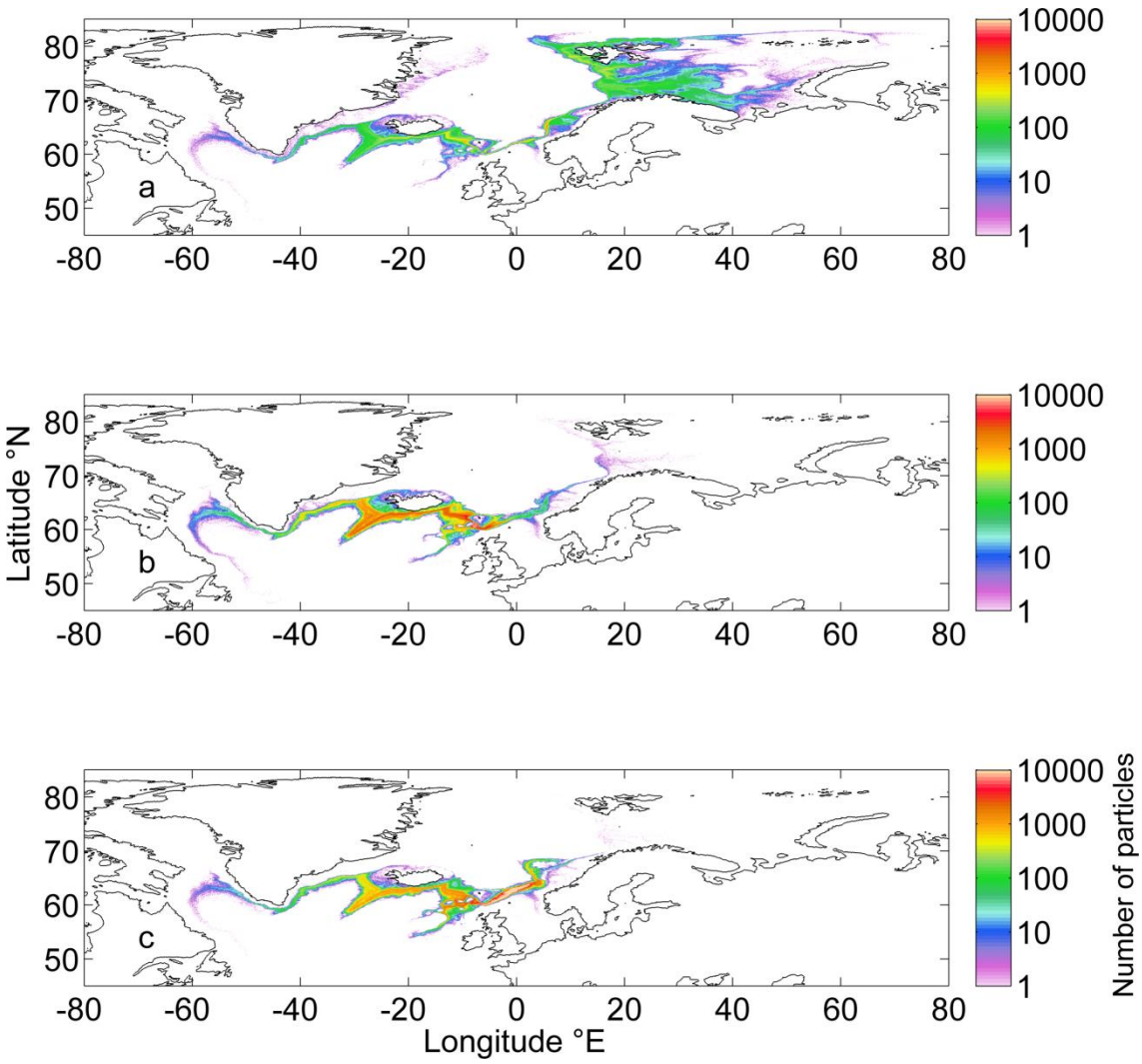

Figure 4.31. Particle densities of releases from: a) 10 – 450 m; b) 500 – 950 m; c) 1000 – 1500 m releases (1994 – 2009) that were within 200 m of the seabed.

In contrast, particles released at intermediate depths (600 m) were transported west, and areas of the FSC, FBC, Iceland basin and the mid-Atlantic ridge were instead impacted

(Figure 4.31 b). Particles released in deep water (1500 m) contaminated large areas of the FSC and also these western areas of the Iceland basin etc (Figure 4.31 c).

Particle decay (Section 4.3.2) limited the average area of seafloor contact considerably (Figure 4.32, Table 4.7). However, deep releases still reached as far as the mid-Atlantic ridge and a small minority of shallow particles (< 1%) still reached the Arctic.

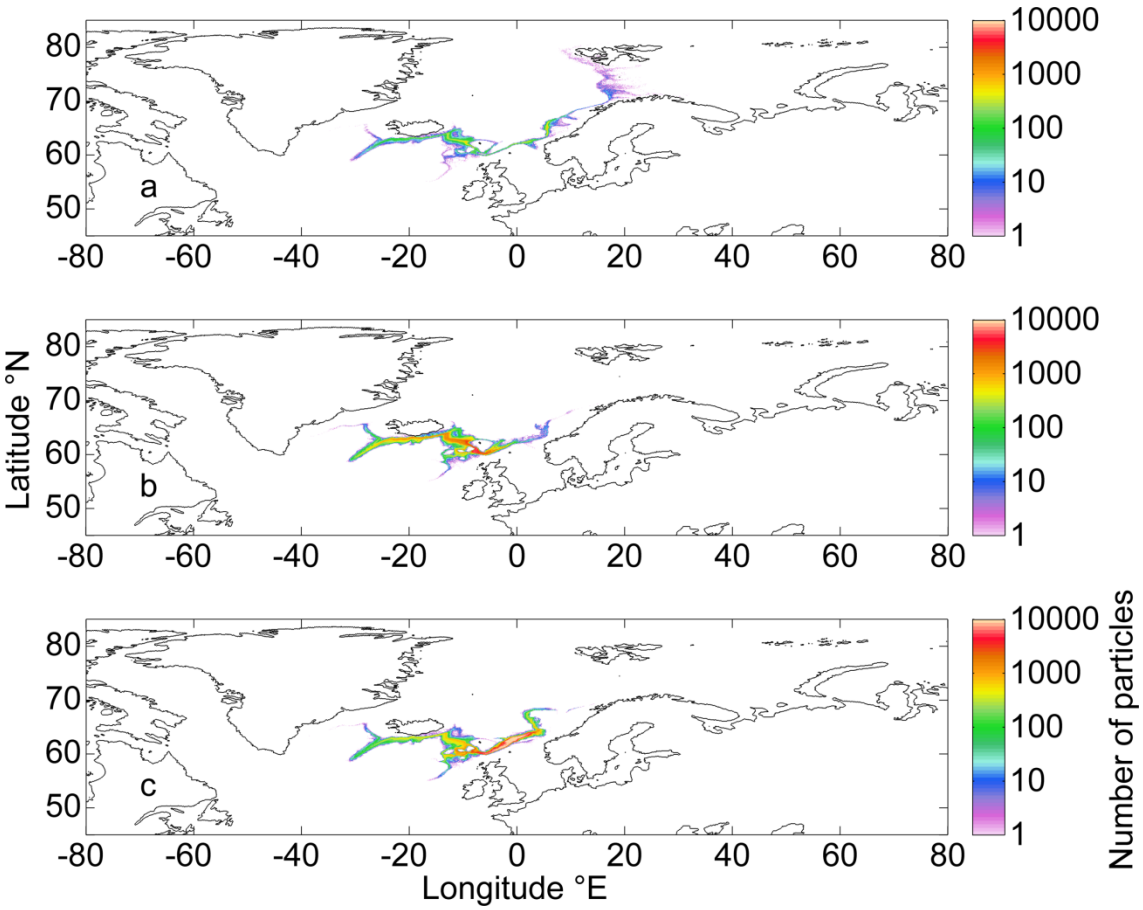

Figure 4.32. Particle densities of decayed releases from (a) 10 – 450 m; b) 500 – 950 m; c) 1000 – 1500 m releases that were within 200 m of the seabed. Chosen decay threshold was 10%.

There was seasonal variability between releases for all estimations of seafloor area contacted, with maxima in both summer and winter (Table 4.7). There was also considerable interannual variability in the amount of seafloor contact and the

geographical locations affected (Figures 4.33 – 4.38). The maximum seafloor area contacted from a single release was in June 2008 (31,307 km^2, for undecayed particles).

Table 4.7. Estimated average seafloor area (*1000 km^2) contaminated by particles from three release depths (10 – 450 m, 500 – 950 m and 1000 – 1500 m) for each month in the series of simulations, and with particles decayed to 10% threshold.

	Not decayed			Decayed to 10%		
	10 – 450 m	500 – 950 m	1000 – 1500 m	10 – 450 m	500 – 950 m	1000 – 1500 m
Jan	270.7	373.2	315.7	39.9	110.6	102.7
Feb	267.9	372.5	311.6	33.5	115.4	109.0
Mar	241.3	385.2	345.5	27.3	125.5	130.1
Apr	279.3	404.3	365.2	37.1	139.6	137.7
May	267.3	431.1	367.6	36.2	144.4	137.1
Jun	285.3	448.6	364.5	41.6	155.9	142.7
Jul	263.1	427.2	343.1	33.5	150.4	131.6
Aug	327.1	427.6	327.5	48.3	146.8	113.4
Sep	348.1	440.2	294.1	48.2	149.3	99.9
Oct	298.7	399.2	303.7	34.4	126.2	100.8
Nov	329.9	436.1	330.9	44.7	139.6	112.3
Dec	292.8	419.1	336.7	39.1	128.8	118.0

Table 4.8. Standard deviation in mean seafloor area (*1000 km^2) contacted for each month in the series of simulations, with particles decayed to 10% threshold.

	Not decayed			Decayed to 10%		
	10 – 450 m	500 – 950 m	1000 – 1500 m	10 – 450 m	500 – 950 m	1000 – 1500 m
Jan	149.1	164.7	147.2	39.4	74.5	62.7
Feb	148.2	155.2	161.7	34.5	72.0	72.7
Mar	126.4	173.7	172.6	27.6	76.1	80.2
Apr	117.6	152.1	162.1	33.5	67.6	82.8
May	128.5	123.7	142.9	24.1	66.4	74.2
Jun	102.7	134.4	148.9	31.5	70.5	80.4
Jul	112.6	166.8	134.2	27.0	75.9	72.5
Aug	148.4	152.1	123.8	35.0	66.8	62.0
Sep	122.2	138.3	151.2	35.0	58.3	66.7
Oct	95.9	146.7	151.6	25.7	65.4	68.9
Nov	123.7	121.5	150.0	38.1	65.5	79.5
Dec	118.8	131.6	163.6	35.0	77.1	78.2

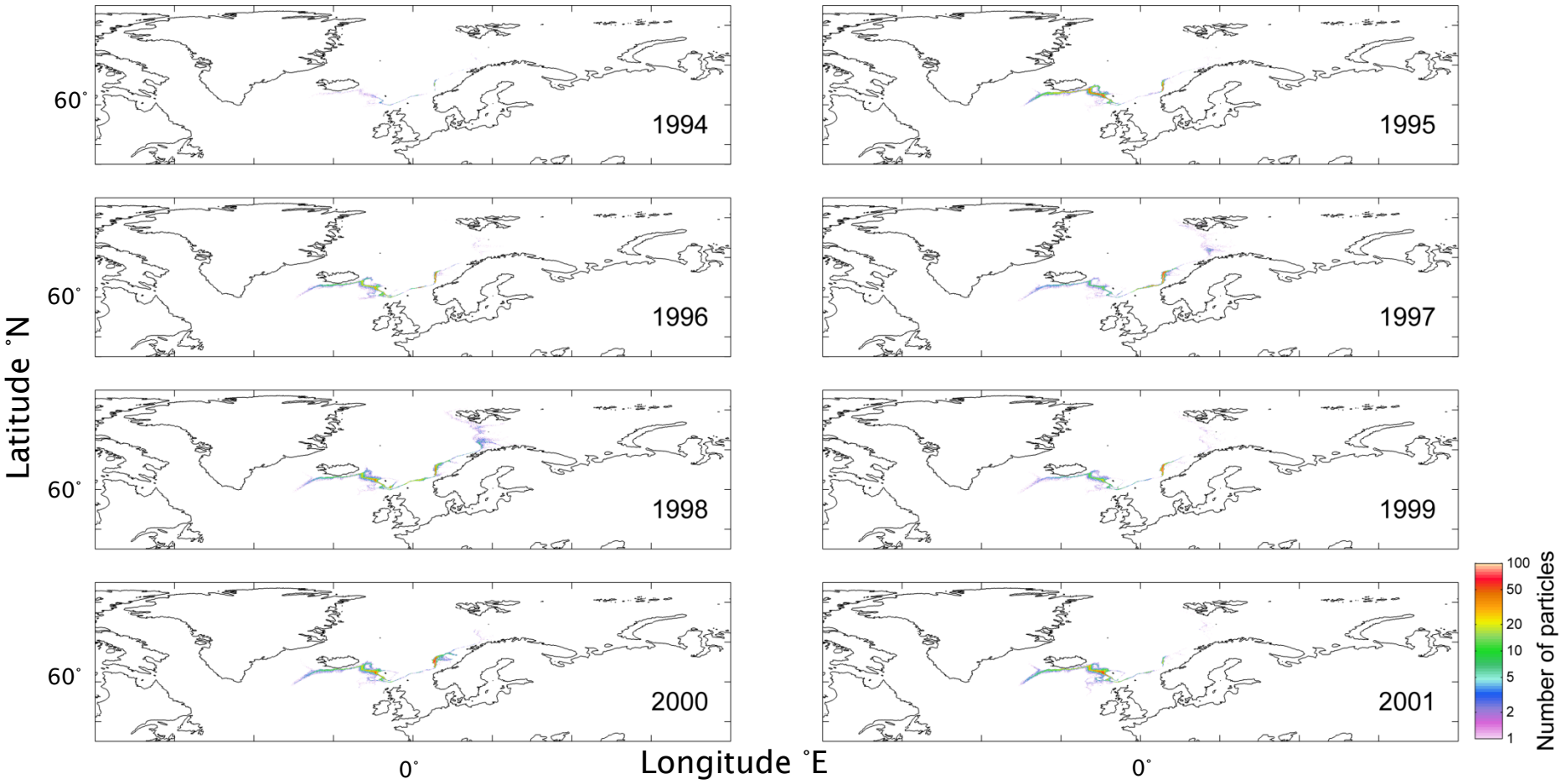

Figure 4.33. Contact with seafloor by decayed particles released at 10 - 450 m summed for all releases in each year 1994 – 2001.

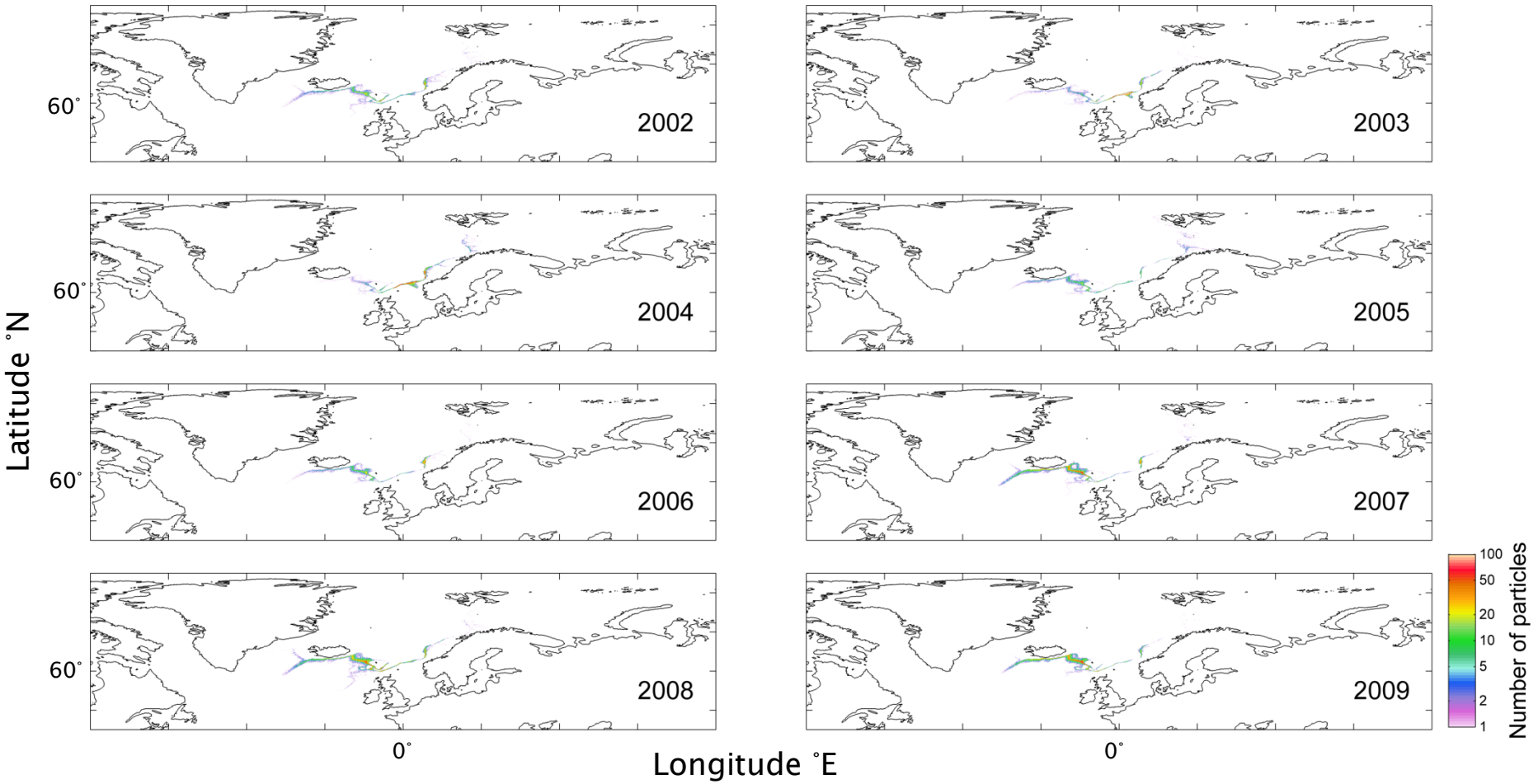

Figure 4.34. Contact with seafloor by decayed particles released at 10 - 450 m summed for all releases in each year 2002 – 2009.

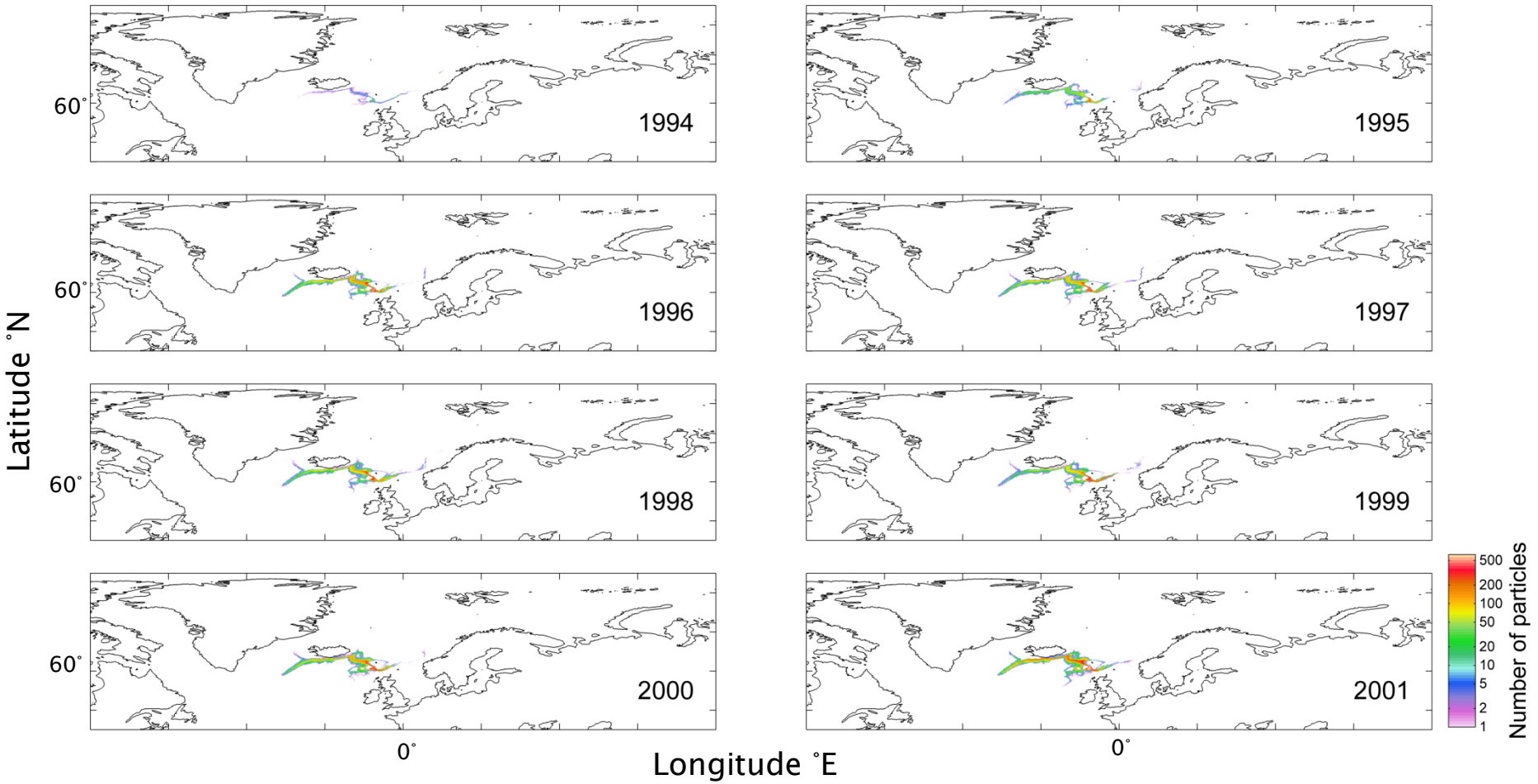

Figure 4.35. Contact with seafloor by decayed particles released at 500 - 950 m summed for all releases in each year 1994 – 2001.

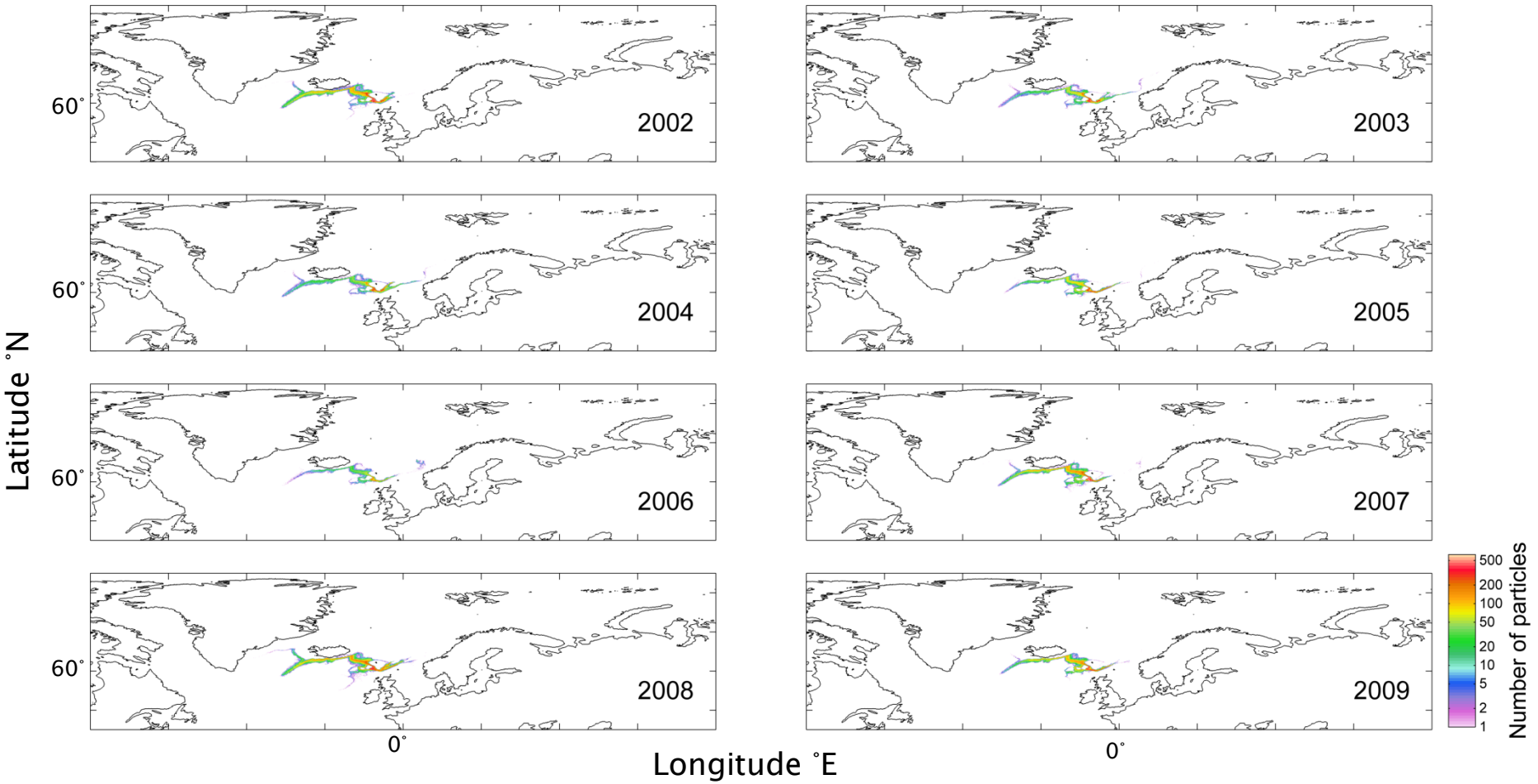

Figure 4.36. Contact with seafloor by decayed particles released at 500 - 950 m summed for all releases in each year 2002 – 2009.

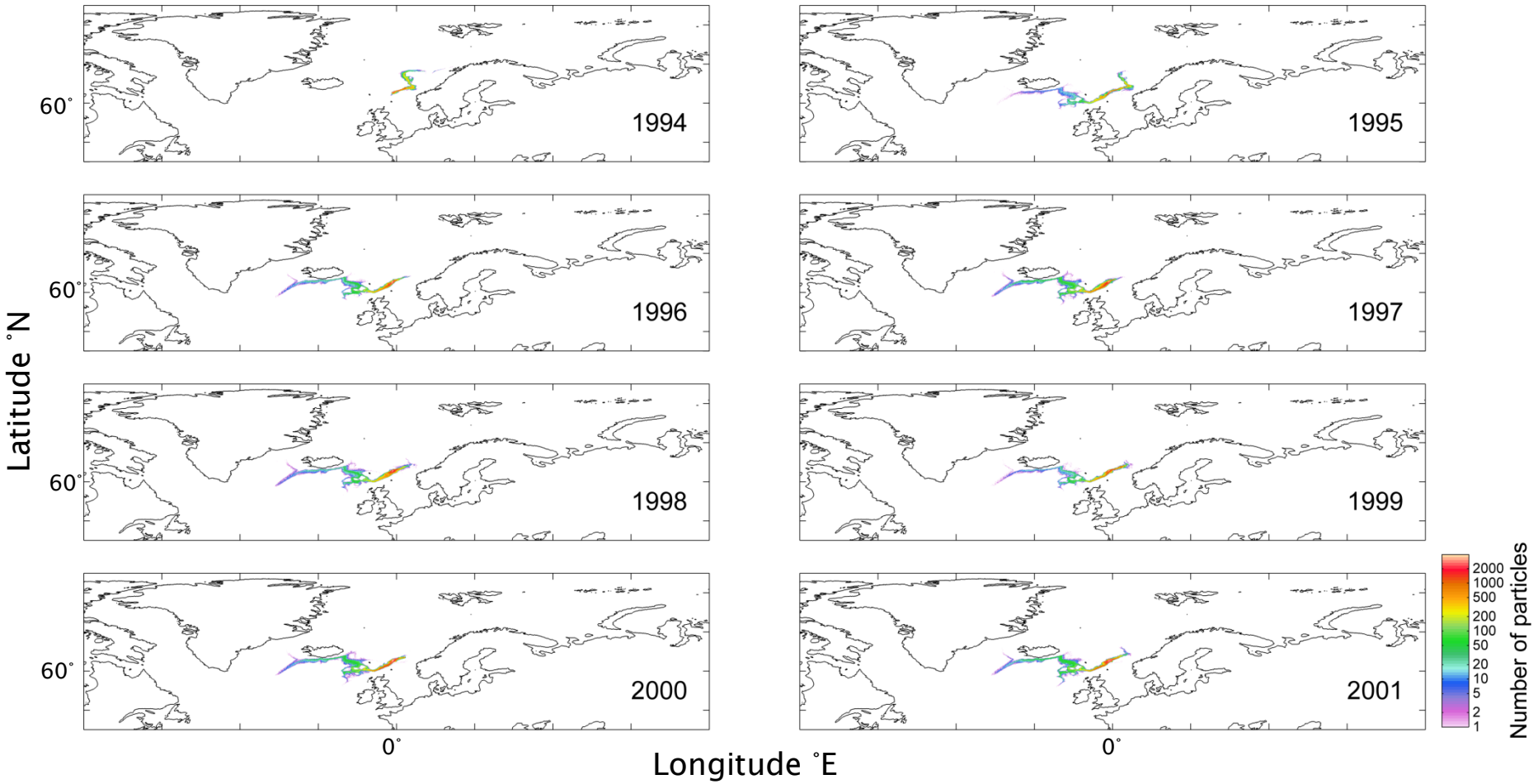

Figure 4.37. Contact with seafloor by decayed particles released at 1000 - 1500 m summed for all releases in each year 1994 – 2001.

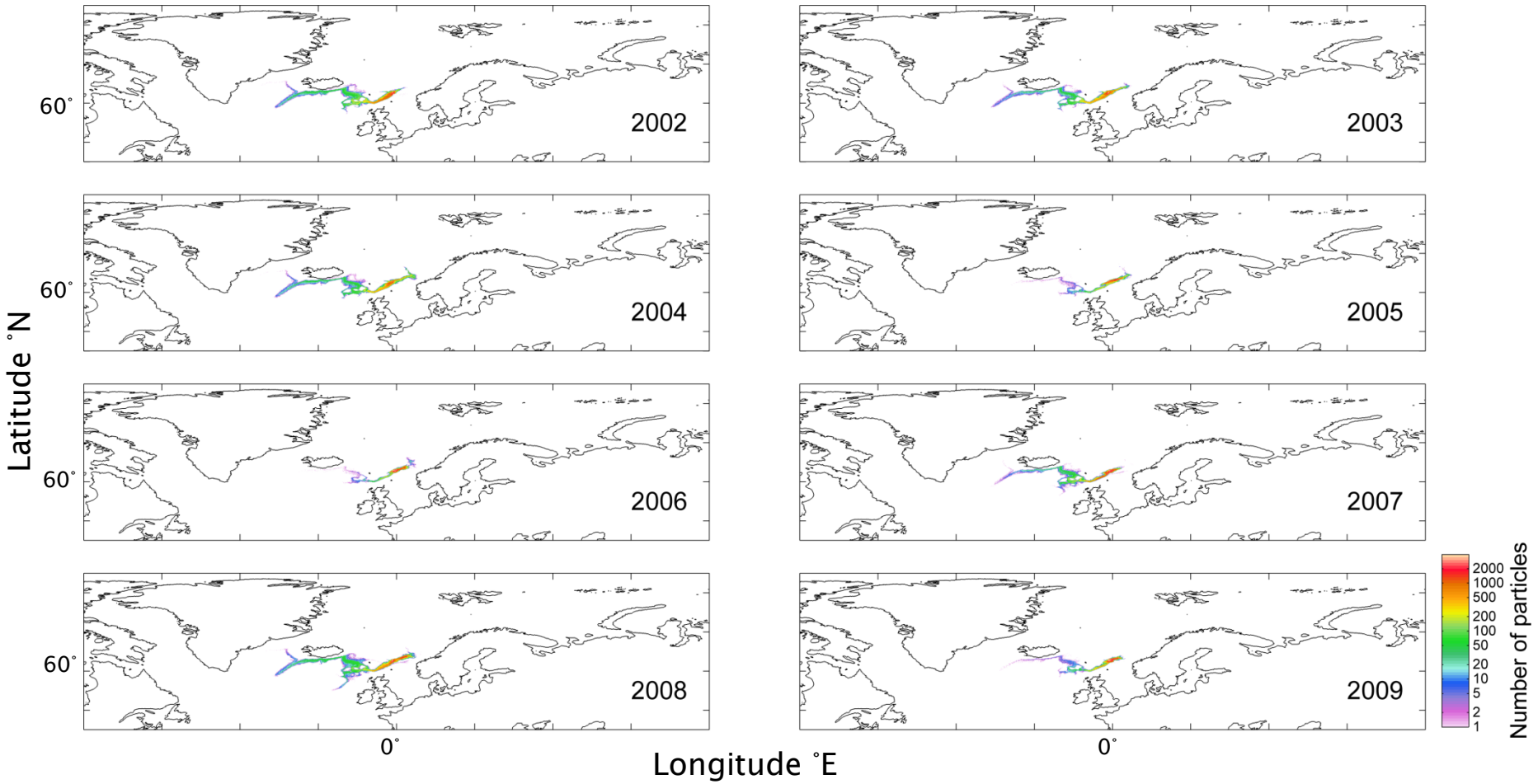

Figure 4.38. Contact with seafloor by decayed particles released at 1000 - 1500 m summed for all releases in each year 2002 – 2009.

4.3.4.3 Contamination of the Darwin Mounds

Particle releases from > 800 m water depth were transported to the region where the Darwin Mounds (DM) are located, even when the decaying algorithm was applied (Figure 4.39). However, the main 'flow' of particles was 30 km to the north.

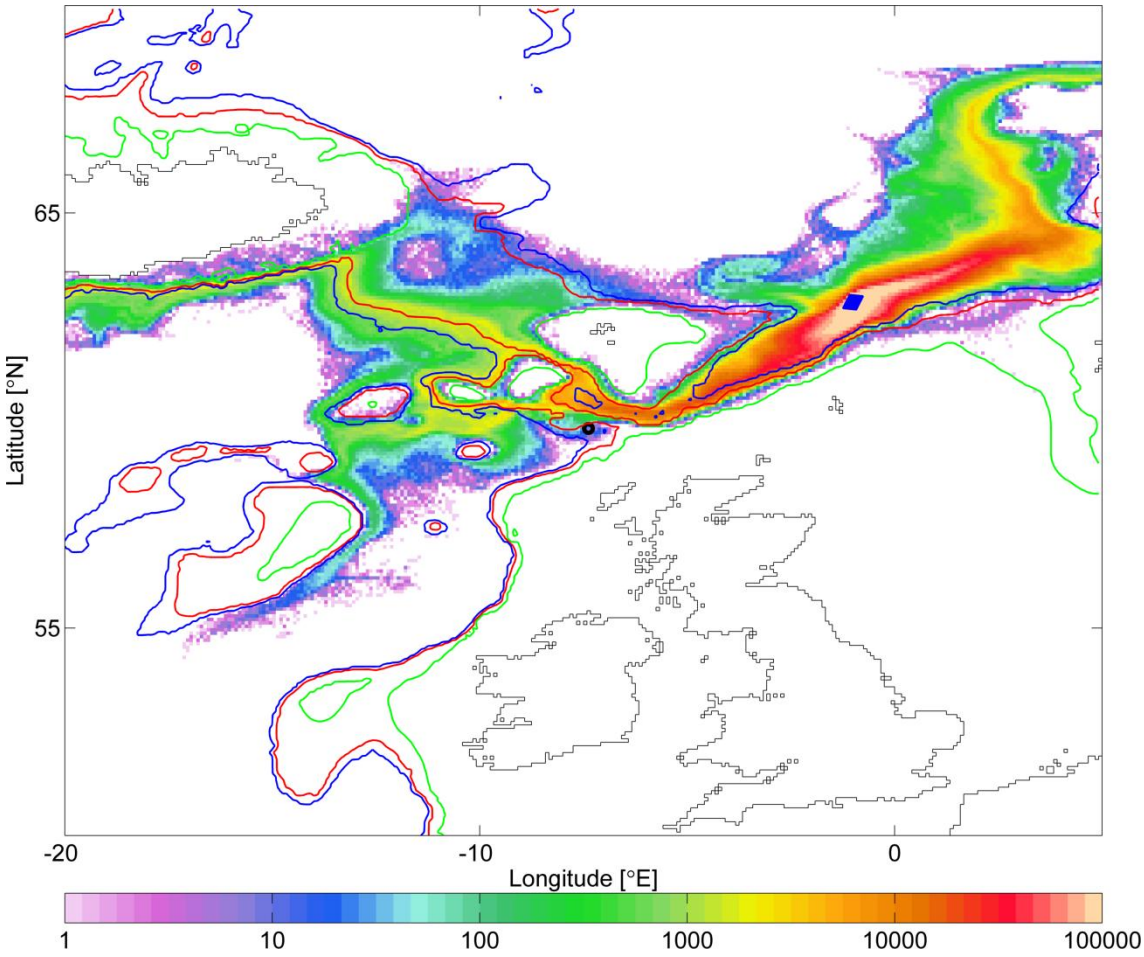

Figure 4.39. Particles released from depths > 800m with decay algorithm applied and termination threshold set at 10%. The location of the Darwin Mounds is indicated at 59.8° N, 7.81°W (black circle). Depth contours are indicated by lines: green = 500 m; red = 600 m; red = 900 m; blue = 1000 m. Release locations of particles are indicated by the blue diamond. Colour scale indicates count of particles.

Release year did not, in most cases, reduce the potential for contamination at the DM (Figure 4.40). In the event of a prolonged oil well blowout in the FSC, results here

indicate that contamination at DM would occur, since in only one year (1994) no particles released in depths > 800 m were transported in their direction. From 1995 onwards there was increased potential for contamination, indicated by a large density of particles travelling to the west (Figure 4.40).

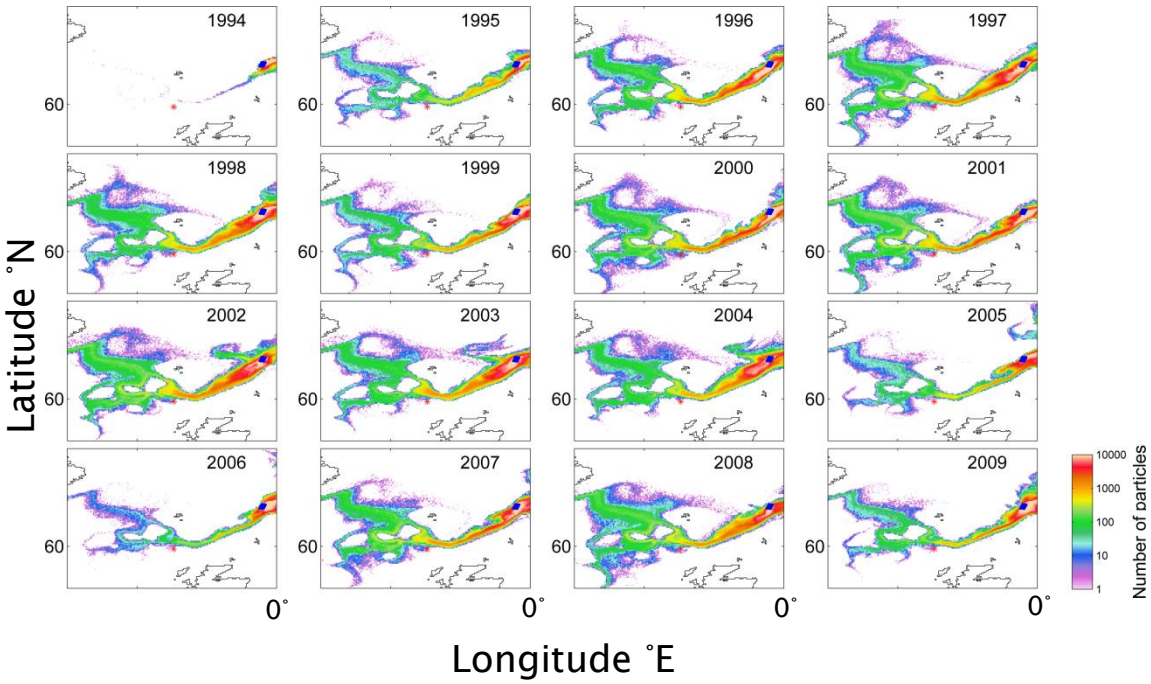

Figure 4.40. Particles released from depths > 800m for years 1994 – 2009 with decay algorithm applied and termination threshold set at 10%. The location of the Darwin Mounds is indicated at 59.8° N, 7.81°W (red star). Release locations of particles are indicated by a blue diamond.

4.4 Discussion

In the simulations, particle release depth had a strong directional effect on their spread, and also on extent of spread. Near to the surface (< 300 m depth) most of the released particles were advected northwards in the model's two branches of the relatively warm (~10°C average) Norwegian Atlantic Current (NAC). Deeper (> 600 m) releases were more likely to be advected to the west in cold (< 0°C) bottom water, with most of the flow travelling over a sill into the Faroe Bank Channel.

These results (and model validation, Section 4.2.2) reflect previous observations of the circulation in the region. For example, long term oceanographic measurements in the FSC have shown that much of the bottom water formed in the Arctic must traverse the Greenland-Scotland ridge in order to enter the north Atlantic (Turrell *et al*., 1999; Sherwin *et al*., 2006). While much of this crosses the sill at ~850 m depth into the Faroe Bank Channel, occasionally, cascades over the Wyville Thomson Ridge are caused by internal waves (Sherwin & Turrell, 2005). Well-studied surface currents in the region include the NAC, which has a strong flow (5.1±0.3 Sv) that separates into two main branches, the strongest of which (3.4±0.3 Sv) is the inshore, eastern branch (Mork and Skagseth, 2010). In agreement with these observations, the modelling results also showed that shallow (< 300 m depth) releases of particles flowed in two main branches to traverse the Norwegian Sea. These shallow releases were most likely to be carried furthest from their release location, with some reaching almost as far as the Arctic Ocean. Volume transport at the FBC sill has been estimated from instrumental measurements as 2.1±0.5 Sv (Hansen & Osterhus, 2007) which is ~0.5 Sv greater than that of the model (1.5 Sv; Marzocchi *et al*., 2015).

There was seasonal and interannual variability in the strength of the flow of these currents as depicted by the Lagrangian particles. For example, there is evidence of seasonality in volume transport at the FBC (Lake & Lundberg, 2006) and this was also captured here in analysis using particle counts at the sill (Section 4.3.1.2). Data from the instrumental record has also found interannual variability in the currents of the FSC (Berx *et al*., 2013) and the Norwegian Sea (Mork and Skagseth, 2010). Circulation in

the FSC may be affected by changes in strength of the North Atlantic Oscillation (NAO, Chafik, 2012). However, for the 16 years studied here, there was not a clear indication that the model results demonstrated this. Years which seemed exceptional in terms of some of the measures here included: 1998 (maximum distance travelled); 2004 and 2008 (largest seafloor area impacted) and the annual mean NAO values for these years included both positive (0.25 in 1998; 0.05 in 2004) and negative (-0.73 in 2008) values.[8]

Temperature-controlled decay is important for the consideration of subsurface oil transport. It is well established that the biodegradation of hydrocarbons by bacteria is strongly temperature-dependent (Atlas, 1975; Atlas, 1981; Atlas & Hazen, 2011). Temperature in the model agreed well with observations from the literature (Section 4.2.2), and temperature-mediated decay of particles, representing the biodegradation of hydrocarbons, affected the oil's spread in the simulations. Particles released in cold, deep water experienced slower decay and persisted for a longer period of time than those released in shallow water, but did not travel as far. Since results here indicate that oil released in the deep ocean of the FSC may persist for considerably longer than the oil that is present at the surface, the implication is that large areas of the deep ocean would experience prolonged exposure in the event of a spill. The cold, Arctic influence in the FSC region means that biodegradation rates in deep water there would be relatively slow. This increases the potential for exposure, and therefore the harm done by oil pollution. Indeed, Reddy *et al*. (2011) suggested that, in fact, there was limited biodegradation in the deepwater plumes following the Macondo blowout, which further suggests that oil in the colder, more Arctic-influenced FSC might be metabolised even more slowly. Even after temperature-mediated decay was considered, the shallow releases of particles were transported the furthest (up to ~ 700 km to the north). This implies that a larger area of the shallow ocean would be affected, but probably for a shorter time period than in the deep ocean. Close to the surface, processes affecting the oil composition and buoyancy would be impacted by the action of weather and waves, but these influences were not considered here.

[8] Source: National Oceanic and Atmospheric Administration: http://www.cpc.ncep.noaa.gov/

Modelling results here showed that the horizontal area with an elevated index of oxygen consumption was greatest for shallow water depths. Exposure of living organisms to oil results in increased oxygen consumption rate (Chapter 3), either through metabolism of oil by hydrocarbon-degrading bacteria, or through stress, for example as organisms (including invertebrates and bacteria) use energy to up-regulate their de-toxification mechanisms. However, since oil is likely to be broken down much slower in cold water, the intensity of effect could be greater for the deep sea.

Water-borne hydrocarbons that remained in the deep ocean of the Gulf of Mexico after the 'Deepwater Horizon' spill triggered blooms of oil-degrading bacteria (Hazen *et al*., 2011) and created a higher demand for oxygen in the area of deep water oil plumes (Valentine *et al*., 2010). Coral communities that were directly beneath the path of the deep hydrocarbon plumes were observed to become stressed, probably resulting from contact with oily sludge that was traced to the Macondo oil (White *et al*., 2012) and therefore may have resulted from fallout from the midwater oil. The affected coral communities from the Gulf of Mexico provide important evidence that seabed biota are impacted by subsurface oil released from oil well blowouts. It is therefore important to consider the progress of oil on subsurface currents. In an EIA for the North Uist exploratory well, BP presented information from a modelling exercise designed to model subsurface plumes of oil (BP, 2011). However, there was not an obvious comparison of interannual or seasonal variability in the extent of the flow, despite the project being forecast to commence at any time within an eleven month period: hence, in theory an oil well blowout could have occurred in any season throughout 2012, when the drilling took place.

Modelling results here found that the drifting particles did not experience large changes in depth over the course of their trajectories. Results showing seafloor contact in shallow provides theoretical evidence for the so-called 'toxic bathtub ring' hypothesis, another mechanism that was proposed as a route through which dissolved or neutrally buoyant oil could contact the seafloor from a prolonged oil well blowout (Hollander *et al*., 2013).

There are various factors that affect oil's buoyancy in water (and hence its depth). Monoaromatic hydrocarbons (e.g. benzene and toluene) are slightly soluble in water, and were major constituents of the Gulf of Mexico deep water plumes measured by Camilli *et al*. (2010). Droplet size is also important in determining the depth of establishment of subsurface plumes of oil (Ryerson *et al*., 2012; Socolofsky *et al*., 2011; Lindo-Atachati *et al*., 2014). As the chemical composition of crude oil changes through weathering processes (biodegradation, dissolution, etc.) the proportion of lighter compounds present decreases. Hence the oil's density increases and it can lose buoyancy. Subsurface oil also adheres to particulate organic matter (e.g. marine snow) forming aggregates of oil with these particulates (Passow *et al*., 2012). The oil is then transported to the seabed with the already sinking material. This 'dirty blizzard' of oil was observed following DWH in the Gulf of Mexico (Deepwater Horizon Principal Investigator Workshop, 2011), and resulted in large quantities of oil impacting the seabed within 25 km of the well head (Montagna *et al*., 2012).

Some particles were transported further north than 70°N to the sub-Arctic. If oil from a blowout in the FSC were to reach the Arctic, this is an environment that, because of its cold temperatures, may be particularly sensitive to oil pollution, as indicated by toxicological studies on Arctic species (Olsen *et al*., 2007; Camus *et al*., 2002; 2003). Processes relating to the functioning of Arctic environments, e.g. sediment community oxygen consumption, are also altered by exposure to oil pollution (Olsen *et al*., 2007, see also Chapter 3).

4.4.1 Caveats

The NEMO GCM was not designed to model oil and hence the results here should not be treated as a true and complete representation of the subsurface transport of oil, or parameters associated with oil respiration. Furthermore, the model is designed to consider the open ocean and omits many, near-shore processes such as wave formation and breaking. Tides, which would influence transport in shelf seas, are also excluded. However, the FSC and Norwegian Sea is an open ocean area and observational data and

validation (Marzocchi *et al*., 2015) suggest that the model represented pathways adequately.

The releases of particles were not continuous and were initiated by the same grid of regularly particles i.e. there were single, monthly release of particles. The effect of the size and shape of grid on particle transport was not considered but could be carried out as a sensitivity analysis.

The particles tracked here by Ariane were considered as index of transport, particularly for the dissolved oil compounds and small, neutrally buoyant droplets. Oil composition and behaviour were not considered here and these would undoubtedly have an effect on the true transport, including the potential for effects on fluid dynamics caused by the presence of liquids with different density and temperature. This should definitely be considered in future studies developing this approach. The areas estimated in terms of impact (oxygen consumption and seafloor footprint) were all horizontal only, and there was no treatment of impacts spread over three dimensions through the water column. This could also be considered for future plume mapping studies using the model, though ideally with a treatment, also of oil's behaviour in seawater.

Oil degradation was considered, albeit with a very simple decay-rate implementation. Similar decay rate approaches have been used to study the DWH spill (Adcroft *et al*., 2010). However, this could potentially be improved by considering species of bacteria present; their abundance, or the effects of nutrient limitation on bacteria populations.

The time series used here covered only 16 years (1994 to 2009). Using a longer set of years would allow us to better understand the role and importance of repeating phenomena, such as the NAO, and decadal shifts in circulation strength. Variations in conditions and transport in the region are known to result in circulation changes (Turrell *et al*., 1999) and GCMs have the ability to represent decadal cycles in the Atlantic meridional overturning circulation (Persechino *et al*., 2012).

4.4.2 Conclusions

The implications of this work are that if ocean-basin scale transport of subsurface oil took place from a blowout in the FSC, the major impacts would spread in different directions according to the depths maintained by subsurface plumes of oil. For example, the deep water environments of the FSC and west towards the Iceland basin are more likely to be heavily impacted than deep waters further north. Conversely, faster, shallow water and surface currents would transport oil the furthest north into the Norwegian Sea and towards the Arctic, even though the warmer water of these currents would increase rates of breakdown by biodegradation.

General circulation models such as NEMO are powerful tools with many potential applications. The surface forcing datasets are realistic (Dussin & Barnier, 2013; Marzocchi *et al*., 2015) and this reduces uncertainty when applying the model to address questions. The hindcast output of NEMO is clearly not a forecasting tool. However, as shown here, it can be used quickly and cheaply to ask questions relating the transport of oil, and to do so using historically realistic patterns of ocean circulation.

As was highlighted by the DWH spill, there remain large gaps in our understanding of the transport of subsurface oil on ocean currents. As such, there is a timely need to understand the full implications of deep water spills in regions currently being explored or exploited, such as the FSC.

Chapter 5: Concluding Discussion

5.1 Summary of research aims

Little is known about the fate of subsurface plumes of hydrocarbons from prolonged oil well blowouts, and their effects on deep-sea sediment communities. This was brought into focus by the 2010 DWH spill in the Gulf of Mexico and its subsequent research findings. So, as deepwater drilling continues to expand globally, momentum has been gathering in understanding the fate and effects of oil plumes in other deep-sea environments (through, for example, the Gulf of Mexico Research Initiative). However, areas like the FSC have received relatively little attention. Furthermore, the effects of seasonal variability on the outcome of such an event are clearly important, and need to be further investigated.

The aims of this study were twofold. These followed routes in both observational and modelling disciplines to:

1. Study the effects of crude oil on deep-sea sediment communities from a non-drilled site, using experimental incubations (Chapters 2 and 3);

The effects of oil on deep-sea communities need to be studied with the focus on impacts, behaviour and recovery. Both macrofauna and bacteria are important components of deep-sea sediment communities. Given the known importance of bacteria in hydrocarbon degradation following shallow water oil spills (Slater *et al*., 2005) these organisms also need to be studied in the deep-sea.

Null hypotheses were tested to assess whether there was an effect of WAF on SCOC (Chapters 2 and 3), distribution of macrofaunal biomass among sediment horizons (Chapter 2) and changes in microbial community structure, biomass and isotopic signature (Chapter 3).

2. Investigate temporal and depth-related influences on patterns of sub-surface oil transport in a model ocean (Chapter 4).

The FSC is an area of complex and variable circulation and is part of an important region for the processes relating to meridional overturning circulation (Turrell *et al*., 1999; Berx *et al*., 2013). Deepwater drilling is expanding in this region and the potential for transport of plumes on ocean basin scales has remained unstudied for both the water column and seafloor. The NEMO GCM shows good agreement to observational data for the FSC (Chapter 4; Marzocchi *et al*., 2015) and is therefore a suitable tool for studying patterns of subsurface transport in relation to an oil well blowout.

5.2 Effects of oil on deep-sea sediment communities and SCOC

5.2.1 Effects of oil on deep-sea bacteria

The relative abundance and stable carbon isotope ratios ($\delta^{13}C$ values) of microbial phospholipid fatty acids (PLFAs) were used to study effects of oil on a community of deep-sea bacteria (Chapter 3). Addition of hydrocarbons caused the composition of the resident microbial community to alter significantly. A response within 36 hours of incubation was indicated by significant concentration changes in PLFAs in the 0 – 1 cm layer, and hence also the estimate of bacterial biomass, which significantly decreased in the presence of oil over the incubation period.

Changes in the composition of sediment microbial PLFAs in response to crude oil have been measured previously in the laboratory. For example, a complex profile of PLFAs resulted from exposure of hydrocarbon-degrading bacteria to oil, with the apparent synthesis of certain bacterial biomarkers such as 15:0 and 17:0 (Aries *et al*., 2001). Fatty acids with the same chain length as their n-alkane substrate were synthesised by a

marine hydrocarbon degrading bacteria, *Marinobacter hydrocarbonoclasticus* (Doumenq *et al*., 2001).

The stable carbon isotope ratios ($\delta^{13}C$ values) of microbial lipids have been shown to reflect nutritional substrate, and the response is not the same for each fatty acid (Abraham *et al*., 1998). In a study of biodegradation by bacteria collected from a toluene-contaminated aquifer, Pelz *et al*. (2001) found that the isotope ratio of certain fatty acids including 16:1(n-5) and cy17:0 shifted towards that of their carbon substrate (^{13}C-labelled toluene). Small depletions (reductions in the δ-value) were also observed here in these fatty acids in oil-treated microcosms and there were groupings of PLFAs $\delta^{13}C$ values by treatment as shown by multivariate ordination. However, the results were not found to be statistically significant. It cannot be proved that hydrocarbon degradation had begun in experimental microcosms here. However, the results can in part be related to those of Hanson *et al*. (1999), who used ^{13}C-labelled toluene to study hydrocarbon uptake by bacteria, resulting in a small subset of the community's PLFAs including 15:0 (as observed in the present study) to shift towards the isotope ratio of the carbon source. The uptake rate of tracer in experiments by Hanson *et al*. (1999; their Figure 4) suggests that a significant change in isotope ratio of microbial PLFAs would probably take > 100 hours, although small shifts would be detectable within 30 hours (comparable with the 36 hour incubations of the present study). Evidence from experimentation on soils further indicates that significant hydrocarbon breakdown would not necessarily occur within the short time of the incubations here (36 hours) unless the sediment had been pre-exposed to hydrocarbons (Zyakun *et al*., 2012).

Oil is known to cause stress in some bacteria (Griffin & Calder, 1977). Therefore, a possible explanation underpinning the observed differences in estimated bacterial biomass between oil-treated and control cores is that there was inhibition of growth in some groups of bacteria. This implies that bacteria biomass in oil-treated cores could be preferentially made up from hydrocarbon-tolerant bacteria. However, although the growth of these bacteria may not have been inhibited, the measured stable carbon isotope ratios ($\delta^{13}C$ values) did not provide unequivocal evidence that they were carrying out hydrocarbon degradation. This was because although there were groupings by treatment shown by multivariate ordination, there was not statistical significance to support any observed differences.

The use of PLFAs to study microbial communities is not without its disadvantages (Frostegård *et al*., 2011). The techniques involved in the identification and quantification of PLFAs require that part of the original molecule is cleaved and lost, leaving information only in the triglyceride fatty acid chains. Also, of the many thousands of species of bacteria, only a small proportion of them have been successfully cultured in the lab and hence described fully, so identification is challenging regardless of technique. Fatty acid profiles can be difficult to link to individual species because many are common to various groups of bacteria and also fungus (Zelles, 1999). The technique discriminates against Archaea because their fatty acids are ether-linked, not ester-linked as in other bacteria (Woese & Fox, 1977), and so the lipids of Archaea are not captured by the technique of extracting PLFAs.

Nevertheless, the characterisation of microbial communities using PLFAs has been in wide use since it was pioneered to study soil bacteria and estimate living biomass – using the attribute that PLFAs degrade quickly from non-living cells (White *et al*., 1979; Frostegard *et al*., 1991; Moodley *et al*., 2005). Extraction of total lipid can be done relatively easily and cheaply (Bligh & Dyer, 1959). Subsequently, and with cleavage of the glycerol and attached groups, the fatty acid chain parts of the parent molecule can then be produced by trans esterification with methanol to produce fatty acid methyl esters (FAMEs). Since FAMEs can be volatilised they can therefore be quantified by gas chromatography.

The function of bacteria groups has been linked to some PLFAs e.g. 18:1(n-9) and 16:1(n-7) and 16:0 are the most abundant fatty acids in the hydrocarbon-degrading bacteria, *Marinobacter hydrocarbonoclasticus* (previously named *Psudomonas nautica*; Doumenq *et al*., 1999). These fatty acids were identified here as making up appreciable proportions of the community total, though there were not significant differences between treatments and controls.

5.2.2 Effects of oil on SCOC

The effect of hydrocarbons on sediment community oxygen consumption rates was studied in natural sediment communities collected from the continental slope (~1000 m water depth). Sediment community oxygen consumption was not significantly altered in the presence of low treatment levels of WAF, and instead the effects of temperature and the macrofaunal biomass present in the sediment surficial layer explained more of the variance in oxygen concentration in this case (Chapter 2). At higher treatment levels (Chapter 3) addition of hydrocarbons significantly increased oxygen consumption rates. In this case the change in SCOC could have been driven by changes in the microbial community (Section 5.2.1) but could also have included stress of either macrofauna or bacteria.

Macrofauna and bacteria are both important contributors to the total oxygen consumption of sediment communities on the continental slope, accounting each for approximately half of total biological oxygen demand (Heip *et al*., 2001). The effect of oil on sediment oxygen community consumption has also been studied by Olsen *et al*. (2007a), who found that oxygen demand in Arctic sediments increased more in response to oil, than that of temperate sediments.

Oxygen consumption rate changes in response to stress, as organisms mobilise resources to up-regulate detoxifying mechanisms. This has been studied in invertebrates, with respiration rate commonly increasing in response to oil-induced stress, e.g. in the amphipod *Gammarus wilkitzkii* (Hatlen *et al*., 2009); spider crabs (*Hyas araneus*, Camus *et al*., 2002) and other Arctic invertebrates (Olsen *et al*., 2007b).

The toxicity of hydrocarbons at the concentrations present in the WAF used here in Chapters 2 and 3 (1.6 mg L^{-1} BTEX; 2.7 mg L^{-1} total petroleum hydrocarbons, TPH) is not well known. Studies on shallow water invertebrates indicate a range of acute toxicity levels for hydrocarbons: between, for example, 0.8 mg L^{-1} TPH for the amphipod *Gammarus oceanicus* (Linden, 1976) to over 14 mg L^{-1} TPH in the polychaete *Capitella capitata* (Rossi *et al*., 1976). Deep-sea animals have evolved in an environment of high hydrostatic pressure in relation to their shallow water counterparts, but it is not known whether this would make them more or less susceptible to oil, and unfortunately there is a lack of studies relating hydrostatic pressure to toxicity (Vevers

et al., 2010). Stress in response to contaminants has previously been investigated by measuring the expression of certain 'heat shock proteins' that can be expressed in response to a variety of stressors (e.g. Werner & Nagel, 1997).

5.3 Modelling oil transport with a 3D GCM

Temporal and spatial patterns of subsurface oil plume transport from a hypothetical release in the FSC were studied using the NEMO GCM in conjunction with Ariane, a Lagrangian particle-tracking algorithm (Chapter 4). This framework allowed a thorough investigation of simulated oil spills occurring at times within and between different years, and for plumes spanning a full range of depths from near the surface to the seafloor. Plume depth had a strong effect on the resulting pathways followed by subsurface dissolved and neutrally buoyant oil. Release timing also affected the direction and extent of travel.

The fast surface currents such as the NAC tended to transport oil further than those at depth, even following the simulation of temperature-mediated decay. This is also linked to a large area being affected by increased oxygen consumption in surface waters. However, the simulated slow biodegradation rates of oil in the deep-sea would result in longer time of exposure for any given parcel of water, meaning that the intensity of impact felt at depth may be greater.

The NEMO model does not deal explicitly with the seabed. However, it is important to study the potential for oil contact with the seafloor, given that it is known that this occurs following an oil well blowout (Boehm & Feist, 1982; White *et al*., 2012; Montagna *et al*., 2012). Results here (Section 4.3.4.1) provided theoretical evidence to support the 'toxic bathtub ring hypothesis' that was discussed following DWH as a possible mechanism for oil from the oil well blowout to reach the seabed (Hollander *et al*., 2012). Results here further indicated that the main flow of oil plumes from an oil well blowout in the FSC could contaminate large areas of the deep ocean seafloor and contaminate, for example, the Darwin Mounds, a designated SAC, and a habitat of global significance (Kiriakoulakis *et al*., 2004).

5.4 Future work on the fate and effects of deep-sea oil plumes

The experiments performed here addressed hydrocarbon contamination at a non-drilled site. It is essential to carry out such work using deep-sea sediments from the FSC, where oil drilling is taking place. The experiments could be carried out at sea at a non-drilled site (unpolluted sediments), and compared to those carried out on an oil platform or drill ship (chronically disturbed sediments). The next step beyond these *ex situ* experiments would be *in situ* ones. These would need the use of an ROV (or divers if performed elsewhere in shallow water) to manipulate chambers at the seabed. A known quantity of crude oil could be injected into *in situ* microcosms with resulting changes in SCOC subsequently measured. The sediments could be retrieved to the surface for sampling at the end of the experimental period (comparing treatments to controls to mitigate for the effects of bringing them to the surface, which in itself would be stressful). Heat shock proteins could be sought in macrofauna as indicators of stress (Lewis *et al*., 2000). Experiments should be done across multiple seasons and sediment types to provide a more comprehensive look at how communities change on an annual basis. Also, the interactive effects of treatment, temperature, pressure and sediment type could be studied, potentially using multivariate statistical analysis and linear model fitting procedures outlined here in Chapters 2 and 3.

Future work should also look in more detail at the specific effects of low to high levels of contamination on deep-sea macrofauna. This will not be easy, as any animal from the deep-sea needs to be handled carefully to avoid artefacts caused by the removal of the animal from its native high-pressure environment. Experiments could be done in pressurised chambers to mitigate this (*sensu* Mestre *et al*., 2009; Brown & Thatje, 2011). A more detailed look at behaviour of macrofauna could be studied in relation to oil, by gaining more detailed taxonomic information and comparing biomass, abundance and diversity at different sediment depths across treatments and controls. This would also provide an opportunity to study effects along a pollution gradient (Pearson & Rosenberg, 1978) by having more treatments from low to high concentrations of oil.

Future studies should also identify and characterise the deep-sea bacteria that respond to oil, possibly using molecular techniques to sequence 16S ribosomal RNA to determine their phylogeny (*sensu* Moeseneder *et al*., 2001). Furthermore, stable isotope probing has been used to identify bacteria and link them to the function of hydrocarbon bacteria, using organisms collected in surface and deepwater slicks of the DWH spill (Gutierrez *et al*., 2013). Using PLFAs to study the lipids of membrane bilayers is a relatively accessible and inexpensive technique, but quantifying intact polar lipids could provide more information and therefore enhance the study of identity and function of bacteria communities (Sturt *et al*., 2004).

Given that hydrocarbons represent a food source for some bacteria, it would be interesting to investigate experimentally how rapidly oil could be degraded in the deep-sea. This could be addressed by running longer incubations with either a through-flow of WAF or with water exchanges with fresh WAF daily over ~14 days. Based on previous research (Hanson *et al*., 1999) this could allow sufficient time for significant hydrocarbon degradation to take place. Keeping a consistent mixture of WAF would represent a significant challenge to this approach, so alternatively, use of a single compound, e.g. toluene, could serve as an index for crude oil. Isotope (^{13}C) labelling of toluene, as has been used previously (Hanson *et al*., 1999; Pelz *et al*., 2001) could allow the quantification of carbon uptake by bacteria to synthesise PLFAs, as well as conclusive evidence that a particular compound had been used as a substrate. This kind of study would provide quantification on biodegradation rates by deep-sea bacteria and hence provide an initial estimate for the speed of recovery for deep-sea environments following a spill.

Once rates of biodegradation are obtained for the deep sea, models will help to extrapolate findings over larger areas. Furthermore, effects of temperature on biodegradation, measured experimentally, could lead to estimates of impacts in different seasons. Seasonal impacts could be studied in relation to existing carbon sources (e.g. following the spring phytoplankton bloom). Additional carbon (oil) could be simulated as a supplementary carbon source to a bacteria community. With the use of a model of benthic biomass size structure of macrofauna (for example Kelly-Gerreyn *et al*., 2014), estimates of the effects of large scale mortality on the size class distribution could help study succession and recovery following a spill.

Further work using Ariane as a tool to model oil should incorporate an algorithms for particle buoyancy, that could represent oil plume's (changing) behaviour in seawater as chemical composition and modal droplet size evolves. Recent laboratory experiments on oil droplet interactions with suspended particulate matter (Sørensen et al., 2013) could help inform this.

Using approaches similar to those developed here, further experiments could be run using NEMO with Ariane. One possibility would be to seed particles more frequently than was done here. This would make the most of the 5 day means for current flows that are present in the model and so enhance temporal resolution in the results as well as spatial resolution in choosing a 1/12 degree grid.

The effect of release location could affect the results of experiments as performed here, since particles released in different locations might make it into different water masses. Locations further afield that are undergoing deep water drilling development e.g. the Falkland Islands, New Zealand and Angola all possess unique oceanic conditions that could affect transport. The NEMO model could also be comprehensively validated for the specific region of interest with a large Lagrangian drifters experiment: releasing subsurface buoys such as RAFOS floats (Rossby *et al*., 2009) to provide more data on subsurface pathways. In the FSC and Nordic seas region release depth clearly affects how much makes it into fast-flowing overflow water. Since Ariane can be run in 'backwards mode,' the likelihood that particular areas of interest could be contaminated could be addressed.

Finally, more could be done to enhance the relationship between academia and industry and hence perform knowledge exchange between these groups of institutions and people. A logical progression from this study would be to work with an industry contact, either through a consultancy that use oil spill models or directly with an oil company. Results here could be compared with simulations from existing oil spill models that have been used to provide information for EIAs and oil pollution emergency plans (OPEPs). The various existing oil spill models have different forcing and parameters so could not be expected to give the same results for a given scenario. However, it would benefit the community to start working together well before a large spill incident in the FSC and it might help with the review process of existing oil spill models, which OSPRAG has decided is necessary.

5.5 Conclusions

- Deep-sea sediment communities respond rapidly to oil pollution, with significant changes to microbial communities and the potential for stress in invertebrates;
- An oil well blowout in the FSC would result in subsurface oil plumes that could persist for long periods, especially in cold waters where biodegradation rates are likely to be slow;
- Furthermore, deep plumes (> 600 m) are likely to be transported in a different direction to shallow plumes, potentially resulting in the contamination of different ocean basins;
- Modelling can indicate the geographical locations and extents of seafloor area that could be impacted by a spill in the FSC;
- Oxygen consumption rates increase in response to oil, with large areas affected, especially in shallow water;
- Modelling can indicate the geographical locations and horizontal extents of either midwater or seafloor areas that could be contaminated, or be subject to increased oxygen consumption;
- The results highlight the need to review the efficacy of existing oil spill models to elucidate the extent of subsurface oil transport and impacts from an oil well blowout.

5.6 Perspective

Industrialisation of the sea, including the drilling for oil in deep water, is progressing at an alarmsing rate, despite recent unprecedented rises in atmospheric CO_2 as a result of the burning of fossil fuels (Keeling *et al*., 1976; 2005). One of the benefits of publicly funded research such as that presented here, is that the impartial findings of the work will be in the public domain from the outset. This will hopefully contribute to our understanding of the impacts of deepwater oil spills. Comprehensive, commercially produced modelling scenarios of subsurface oil transport have not so far been readily or publicly presented in existing environmental impact statements produced prior to the issue of commercial drilling licenses. It is of great importance to understand the implications of a prolonged deep-sea oil well blowout in the FSC before it happens.

Appendices

Appendix 1

Chapter 2 Supplementary Information

Supplementary Figures

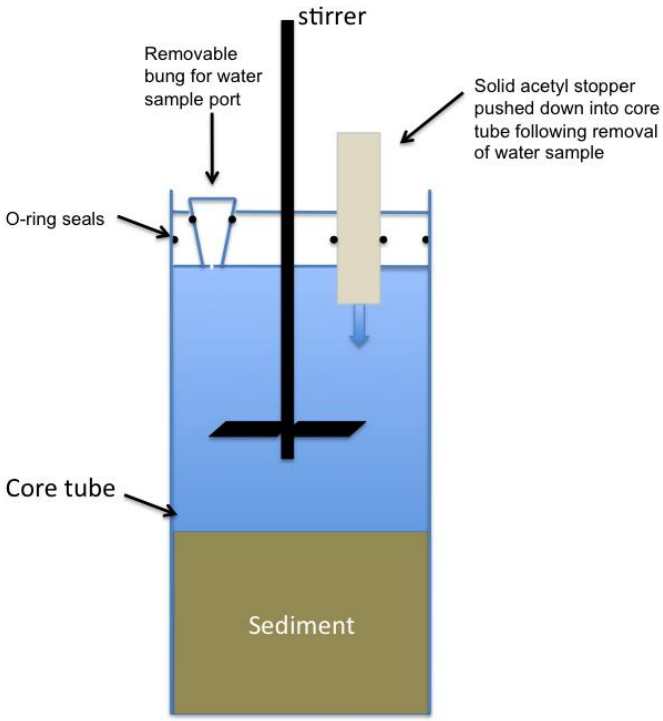

Figure A1.1 Diagram of microcosm set-up

Figures A1.2 – A1.9. Photographs of cores sediment surface at the start and end of the end of the experiment

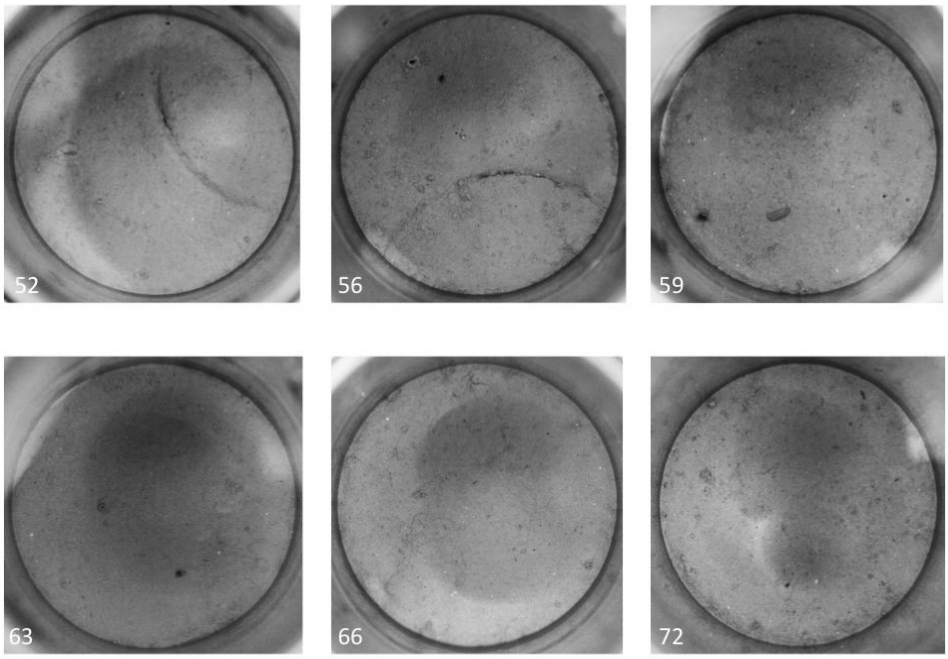

Figure A1.2. Photographs of control cores before treatment and incubation. Numbers show core ID.

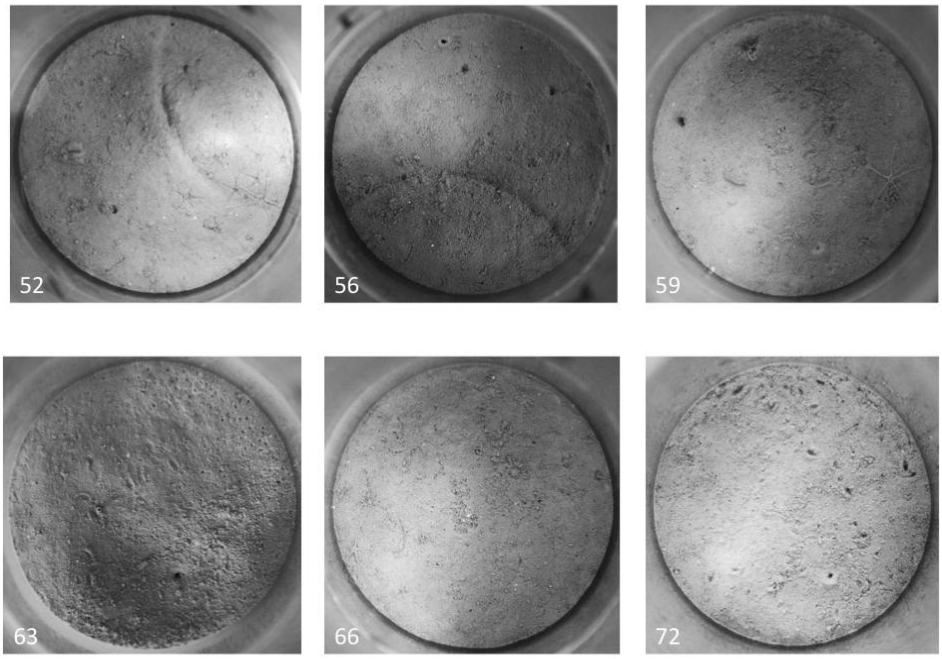

Figure A1.3. Photographs of control cores at end of incubation. Numbers show core ID.

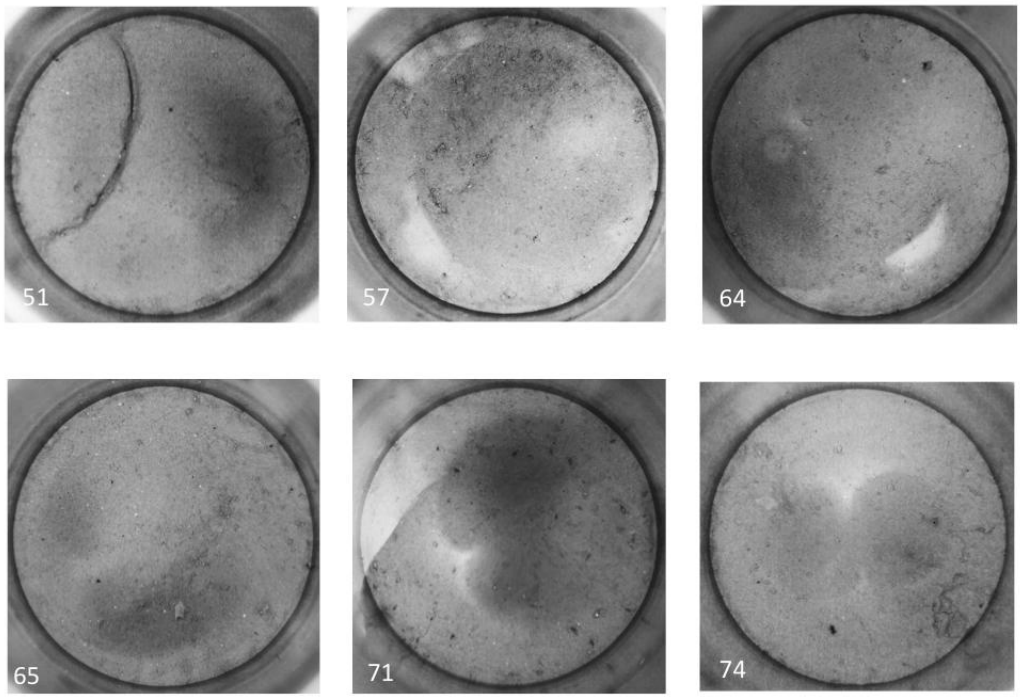

Figure A1.4. Photographs of 5% WAF treatment cores before treatment and incubation. Numbers show core ID.

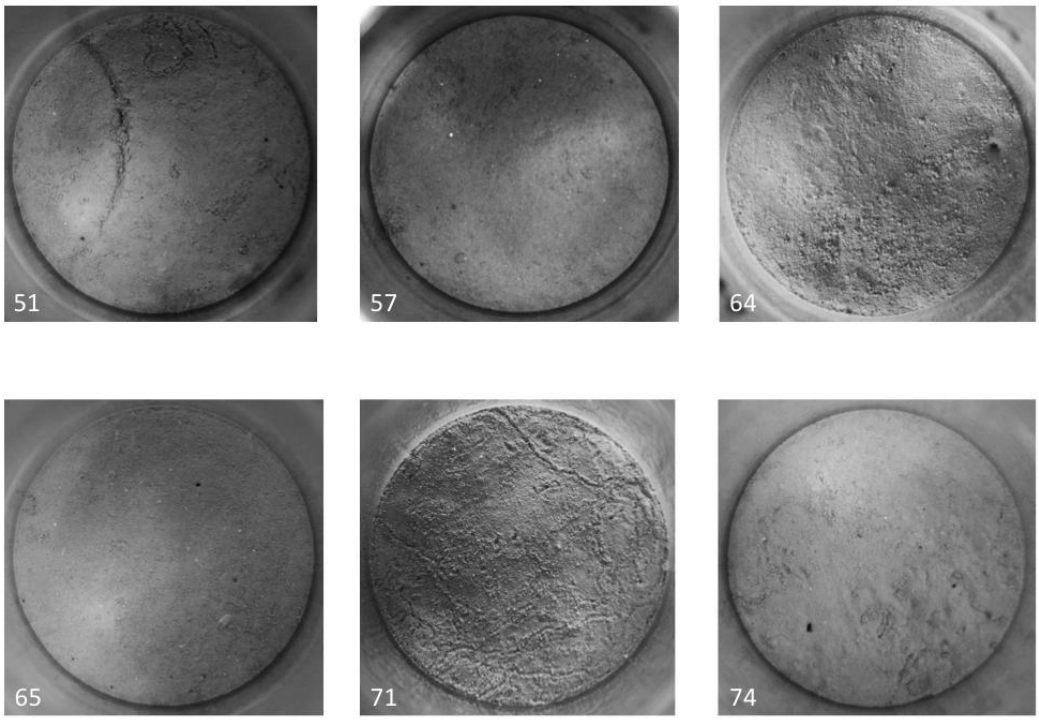

Figure A1.5. Photographs of 5% WAF treatment cores at end of incubation. Numbers show core ID.

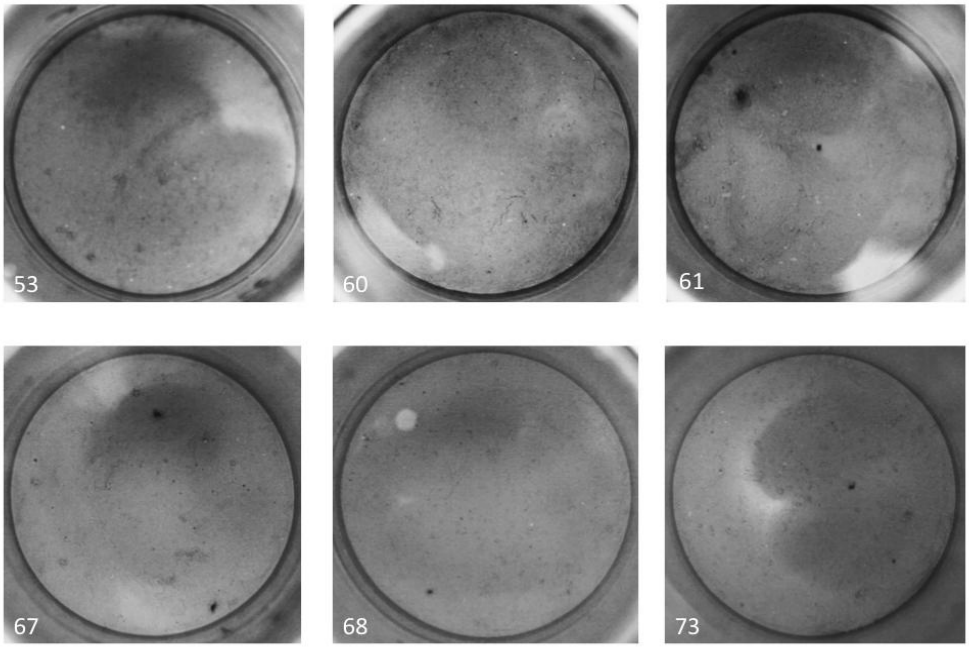

Figure A1.6. Photographs of 15% WAF treatment cores before treatment and incubation. Numbers show core ID.

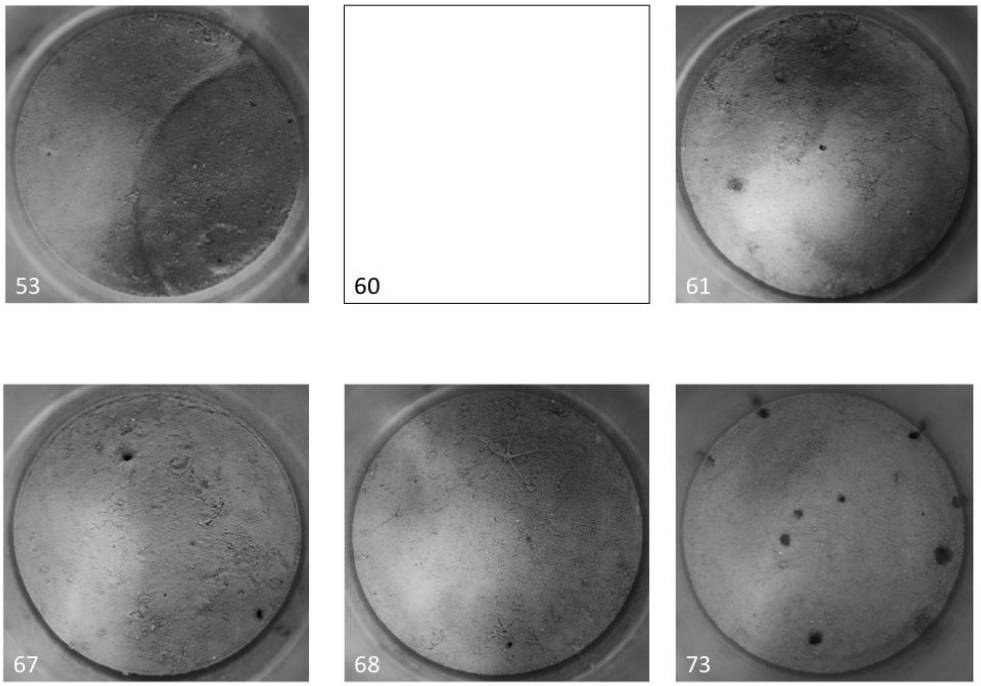

Figure A1.7. Photographs of 15% WAF treatment cores at end of incubation. Numbers show core ID. No file for core 60.

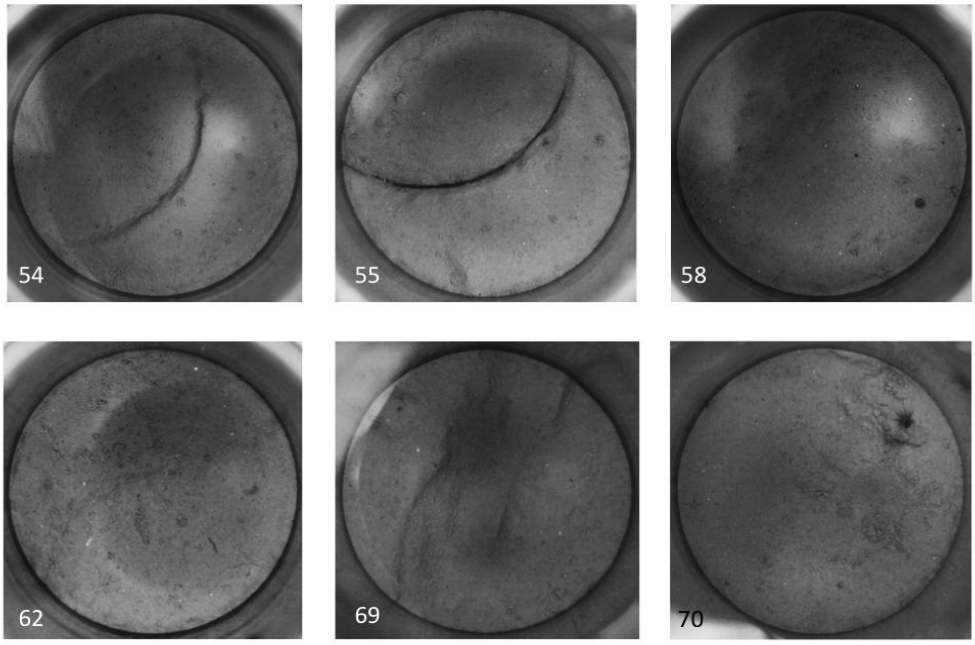

Figure A1.8. Photographs of 25% WAF treatment cores before treatment and incubation. Numbers show core ID.

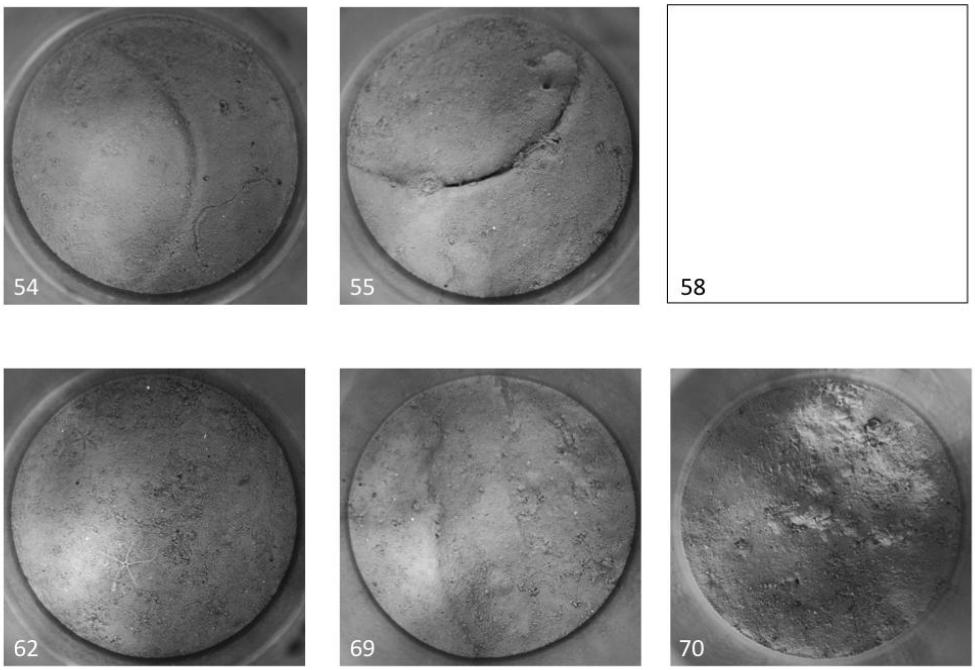

Figure A1.9. Photographs of 25% WAF treatment cores at end of incubation. Numbers show core ID. No file for core 58.

Linear modelling: parameter estimates

Table A1.1 Model parameter estimates: linear mixed effects model of oxygen concentration and time fit by REML

Model:
Oxygen concentration ~ time
Model coefficients:

	Value	Std.Error	DF	t-value	p-value
Intercept	274	0.71	1	387	< 0.0001
Time	-20.1	0.85	1	-23.7	< 0.0001

Table A.1.2. Model parameter estimates: linear mixed effects model of oxygen concentration, biomass, temperature and interaction

Model:
Oxygen ~ biomass + temperature + biomass : temperature
Model coefficients:

	Value	Std.Error	DF	t-value	p-value
Intercept	308	7.93	1	38.9	< 0.0001
Time	-24.9	0.68	1	-36.7	< 0.0001
Macrofauna biomass	-2.70	0.99	1	-2.73	0.0258
Temperature	-6.57	1.62	1	-4.04	0.0037
Biomass : Temperature	0.540	0.194	1	2.78	0.0240

Appendix 2

Supplementary information for Chapter 3

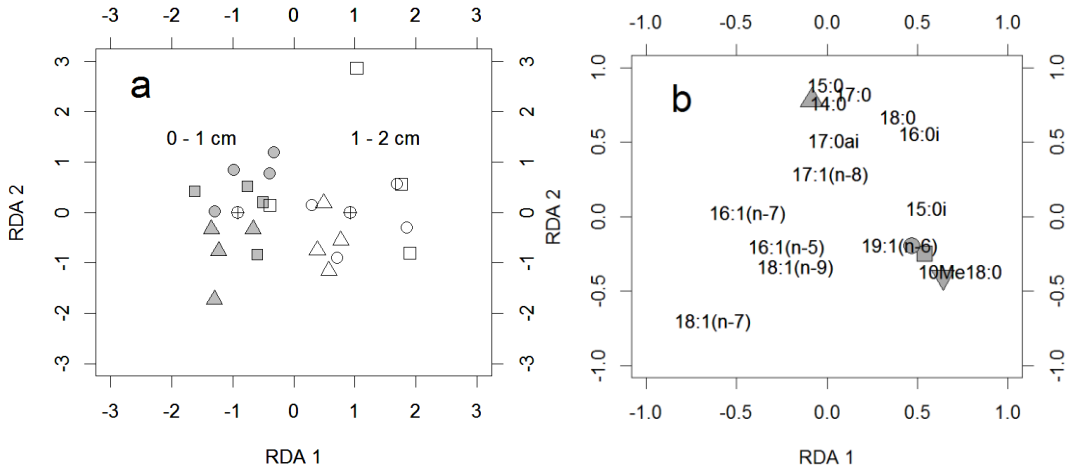

Figure A2.1: Redundancy analysis plot showing the significant effect of sediment depth on PLFA percentage composition data ($F = 3.88$, $df = 1$, $p < 0.001$). Filled and open symbols represent replicate observations of the 0-1 cm (filled symbols) and 1-2 cm (open symbols) sediment horizons respectively at the end of the experiment. (a) Individual cores are plotted with symbols by treatment: triangles = controls; circles = 25% WAF; squares = 50% WAF. The effect of sediment depth is shown by crossed circles with labels offset. Treatment was not considered an explanatory variable in this analysis. (b) Ordination of PLFAs is indicated by their names. The following PLFAs have been plotted with filled symbols for visual clarity: square = 15:0ai; upward pointing triangle = 16:0; downward pointing triangle = 19:0cy; circle = 12Me16:0.

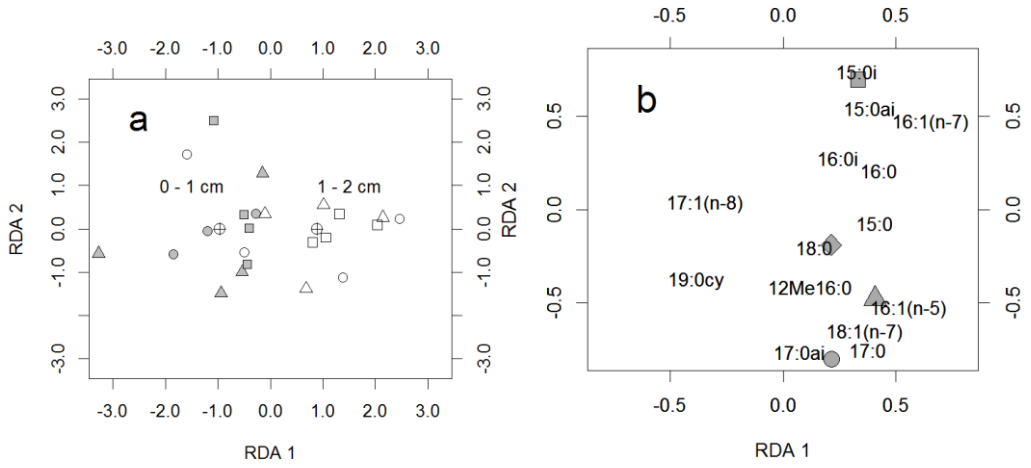

Figure A2.2. Redundancy analysis plot showing the significant effect of sediment depth on PLFA $\delta^{13}C$ values (F = 2.75, df = 1, p = 0.006). Filled and open symbols represent replicate observations of the 0-1 cm (filled symbols) and 1-2 cm (open symbols) sediment horizons respectively at the end of the experiment. (a) Individual cores are plotted with symbols by treatment: triangles = controls; circles = 25% WAF; squares = 50% WAF. The effect of sediment depth is shown by crossed circles with labels offset. (b) Ordination of PLFAs is indicated by their names. The following PLFAs have been plotted with filled symbols for visual clarity: square = 14:0; upward pointing triangle = 10Me18:0; circle = 18:1(n-9); diamond = 19:1(n-6).

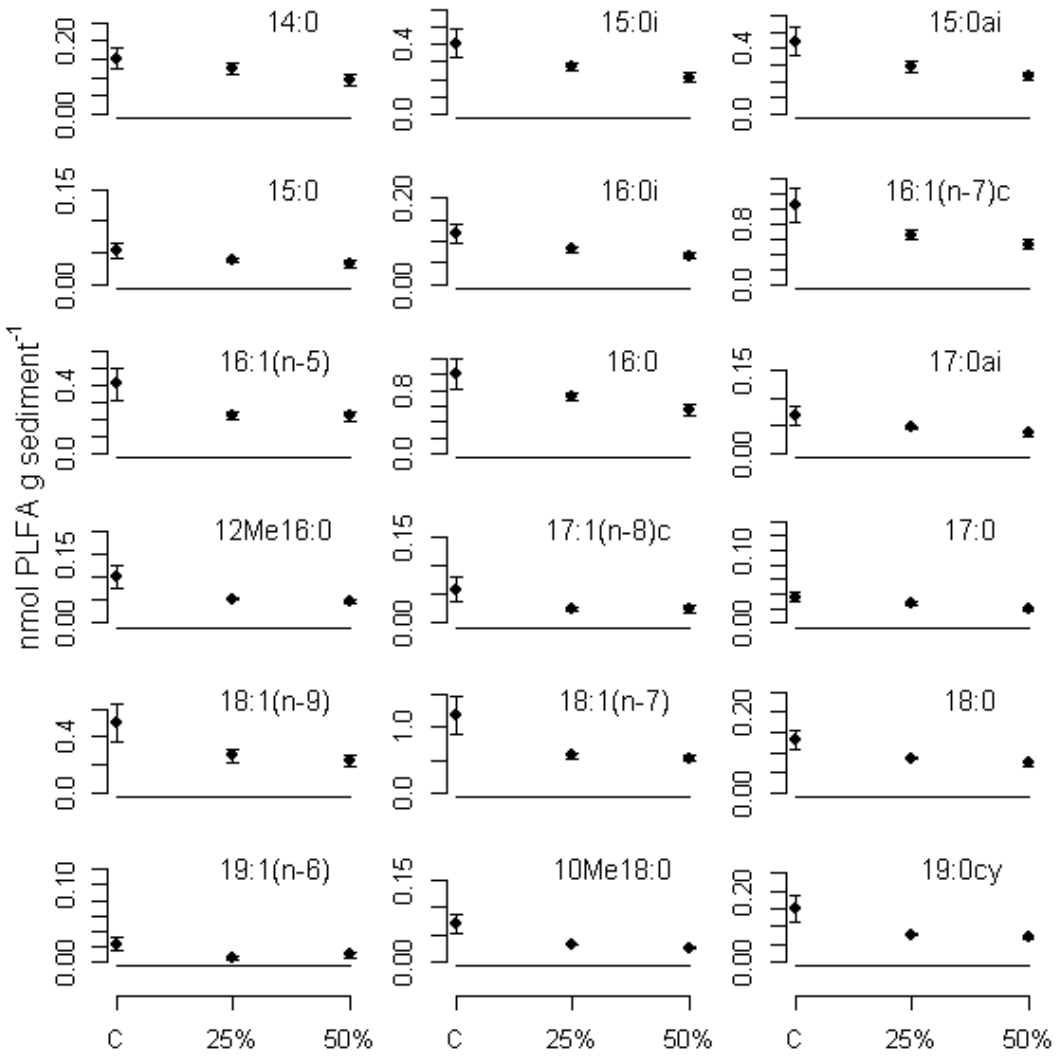

Figure A2.3. Mean concentration (± standard error) of PLFAs in the 0 – 1 cm sediment layer in controls (= C) and 25 % and 50 % WAF treatment levels.

Table A2.1 Model parameter estimates: linear mixed effects model of oxygen concentration, treatment and interaction fit by REML

Model:

Oxygen concentration ~ treatment + time + treatment × time

Model coefficients:

	Value	Std.Error	DF	t-value	p-value
Control (intercept)	362.1749	6.341864	261	57.10859	< 0.0001
25% WAF treatment	18.1305	8.967595	21	2.02178	0.0561
50% WAF treatment	21.7842	8.970278	21	2.42849	0.0242
Time	-17.4226	1.745992	261	-9.97863	< 0.0001
25% WAF treatment × time	-15.9431	2.471649	261	-6.45039	< 0.0001
50% WAF treatment × time	-20.9484	2.466641	261	-8.4927	< 0.0001

Table A2.2. Model parameter estimates for generalised least squares model fit by REML of treatment effects on bacteria biomass (0-1cm)

Model:

Bacteria biomass (0-1cm) ~ treatment

Model coefficients:

	Value	Std.Error	t-value	p-value
Control (Intercept)	67.48505	13.92023	4.847982	0.0007
25% WAF treatment	-23.23784	14.29657	-1.625414	0.1351
50% WAF treatment	-39.44303	15.03745	-2.622987	0.0255

Table A2.3. Model parameter estimates for generalised least squares model fit by REML of treatment effects on bacteria biomass (1-2 cm)

Model:

Bacteria biomass (1-2 cm) ~ treatment

Model coefficients:

	Value	Std.Error	t-value	p-value
Control (Intercept)	69.29666	7.71269	8.98476	< 0.0001
25% WAF treatment	-32.19032	8.726737	-3.688701	0.0050
50% WAF treatment	-16.62593	12.89496	-1.289336	0.2294

Table A2.4. Model parameter estimates for generalised least squares model fit by REML of treatment effects on macrofaunal biomass (0-1cm)

Model:

Macrofaunal biomass (0-1cm) ~ treatment

Model coefficients:

	Value	Std.Error	t-value	p-value
Control (Intercept)	2.876319	0.692902	4.151116	0.0025
25% WAF treatment	5.570464	4.688356	1.188149	0.2652
50% WAF treatment	4.827718	3.305126	1.460676	0.1781

Table A2.5. Model parameter estimates for generalised least squares model fit by REML of treatment effects on macrofaunal biomass (1-2 cm)

Model:

Macrofaunal biomass (1-2 cm) ~ treatment

Model coefficients:

	Value	Std.Error	t-value	p-value
Control (Intercept)	7.390869	4.028387	1.834697	0.0997
25% WAF treatment	-1.337527	4.813012	-0.277898	0.7874
50% WAF treatment	-0.229639	4.811431	-0.0477278	0.9630

Table A2.6. Mean percentage composition (mol % ± SE) of PLFAs present in the sediment at the end of the experiment

	0-1cm			1-2cm		
	Control	25% WAF	50% WAF	Control	25% WAF	50% WAF
14:0	2.6	3.4	3.1	2.7	3.2	3.2
	± 0.2	± 0.1	± 0.2	± 0.2	± 0.5	± 0.3
15:0i	6.4	7.0	6.6	7.2	7.7	8.2
	± 0.2	± 0.1	± 0.3	± 0.2	± 0.5	± 1.0
15:ai	7.4	7.9	7.7	8.8	8.4	8.0
	± 0.3	± 0.3	± 0.4	± 0.2	± 0.2	± 0.4
15:0	0.9	1.0	1.0	1.0	0.9	1.1
	± 0.1	± 0.0	± 0.1	± 0.1	± 0.1	± 0.1
16:0i	2.0	2.2	2.2	2.2	2.5	2.4
	± 0.1	± 0.0	± 0.0	± 0.1	± 0.1	± 0.1
16:1(n-7)	17.9	18.3	17.6	16.8	14.7	17.5
	± 0.9	± 0.3	± 0.3	± 0.8	± 1.3	± 1.1
16:1(n-5)	6.9	6.3	7.4	7.0	6.3	6.5
	± 0.2	± 0.1	± 0.3	± 0.2	± 0.2	± 0.4
16:0	17.4	20.0	18.6	18.0	18.8	18.3
	± 0.9	± 0.4	± 0.6	± 0.6	± 0.8	± 1.6
17:0ai	1.1	1.4	1.2	1.3	1.2	1.3
	± 0.1	± 0.1	± 0.0	± 0.0	± 0.0	± 0.0
12Me16:0	1.6	1.5	1.6	1.7	1.9	2.4
	± 0.1	± 0.1	± 0.0	± 0.1	± 0.0	± 0.5
17:1(n-8)	0.9	0.7	0.8	0.6	0.7	1.0
	± 0.2	± 0.1	± 0.2	± 0.1	± 0.1	± 0.1
17:0	0.6	0.8	0.7	0.6	0.7	0.9
	± 0.0	± 0.1	± 0.0	± 0.0	± 0.0	± 0.2
18:1(n-9)	8.4	7.4	6.6	6.1	9.1	5.0
	± 1.1	± 1.0	± 0.8	± 0.2	± 1.7	± 0.5
18:1(n-7)	19.6	16.3	18.4	16.8	14.8	15.0
	± 1.0	± 0.2	± 0.3	± 0.2	± 0.6	± 1.3
18:0	2.3	2.5	2.6	2.5	2.8	3.7
	± 0.1	± 0.2	± 0.1	± 0.1	± 0.1	± 0.8
19:1(n-6)	0.3	0.2	0.3	0.4	0.3	0.4
	± 0.1	± 0.1	± 0.1	± 0.1	± 0.0	± 0.0
10Me18:0	1.2	0.9	1.0	1.6	1.8	1.6
	± 0.1	± 0.1	± 0.1	± 0.1	± 0.3	± 0.3
19:0cy	2.6	2.3	2.5	3.6	3.5	2.7
	± 0.2	± 0.2	± 0.3	± 0.2	± 0.3	± 0.4

Table A2.7. Mean isotopic composition ($\delta^{13}C$, ± SE) for each of the 18 identified and quantified microbial PLFAs measured at the end of the experiment

	0-1cm			1-2cm		
	Control	25% WAF	50% WAF	Control	25% WAF	50% WAF
14:0	-24.3	-24.8	-22.7	-23.0	-23.6	-21.8
	± 1.2	± 1.0	± 0.7	± 1.1	± 0.9	± 0.3
15:0i	-23.9	-23.7	-22.5	-22.5	-22.9	-21.9
	± 1.1	± 0.9	± 0.3	± 0.7	± 0.8	± 0.2
15:ai	-23.4	-23.4	-22.1	-22.3	-22.2	-21.4
	± 1.1	± 0.9	± 0.3	± 0.8	± 0.5	± 0.3
15:0	-27.2	-26.1	-24.4	-24.1	-23.7	-24.7
	± 1.0	± 0.6	± 0.3	± 0.8	± 1.9	± 1.1
16:0i	-25.8	-24.6	-24.3	-23.4	-24.6	-24.6
	± 0.8	± 0.8	± 0.1	± 0.2	± 0.6	± 1.4
16:1(n-7)	-23.5	-23.4	-23.2	-22.4	-22.1	-21.4
	± 0.7	± 0.1	± 0.5	± 0.4	± 0.5	± 0.3
16:1(n-5)	-25.8	-26.0	-27.0	-24.6	-25.1	-24.3
	± 0.4	± 0.8	± 0.7	± 0.2	± 1.4	± 0.4
16:0	-24.9	-24.6	-24.9	-23.9	-24.2	-23.8
	± 0.4	± 0.4	± 0.9	± 0.3	± 0.6	± 0.3
17:0ai	-24.2	-24.9	-26.5	-24.7	-26.1	-24.2
	± 0.2	± 0.3	± 1.2	± 0.7	± 1.7	± 0.6
12Me16:0	-25.4	-25.7	-24.8	-25.3	-25.2	-24.6
	± 0.6	± 0.2	± 0.7	± 0.9	± 0.3	± 0.3
17:1(n-8)	-24.8	-24.6	-24.0	-24.8	-27.6	-28.0
	± 0.6	± 3.6	± 1.2	± 2.8	± 1.7	± 0.9
17:0	-24.5	-27.4	-28.8	-24.1	-25.3	-23.8
	± 0.8	± 1.5	± 2.5	± 1.3	± 2.0	± 1.4
18:1(n-9)	-26.0	-25.8	-26.4	-24.8	-26.6	-24.2
	± 1.0	± 1.1	± 1.5	± 0.7	± 1.5	± 0.5
18:1(n-7)	-25.1	-26.0	-25.7	-24.9	-25.3	-24.7
	± 0.3	± 0.3	± 0.5	± 0.5	± 0.6	± 0.3
18:0	-26.1	-25.9	-26.2	-25.7	-25.6	-26.3
	± 0.7	± 0.3	± 0.1	± 0.5	± 0.2	± 0.5
19:1(n-6)	-32.0	-29.7	-28.9	-28.3	-27.3	-30.9
	± 2.4	± 1.8	± 0.3	± 1.4	± 1.7	± 2.3
10Me18:0	-26.5	-25.3	-23.9	-23.0	-22.5	-23.2
	± 2.4	± 0.7	± 1.2	± 1.5	± 1.1	± 1.7
19:0cy	-27.8	-28.4	-28.8	-30.1	-28.3	-28.9
	± 0.6	± 0.4	± 0.3	± 0.5	± 0.3	± 0.6

List of References

Abraham, W., Hesse, C., & Pelz, O. (1998). Ratios of Carbon Isotopes in microbial lipids as an indicator of substrate usage. *Applied and Environmental Microbiology*, *64*(11), 4202–4209.

Adcroft, A., Hallberg, R., Dunne, J. P., Samuels, B. L., Galt, J. A., Barker, C. H., & Payton, D. (2010). Simulations of underwater plumes of dissolved oil in the Gulf of Mexico. *Geophysical Research Letters*, *37*(18), 1–5.

Aeppli, C., Carmichael, C. A., Nelson, R. K., Lemkau, K. L., Graham, W. M., Redmond, M. C., Valentine, D. L. & Reddy, C. M. (2012). Oil weathering after the *Deepwater Horizon* disaster led to the formation of oxygenated residues. *Environmental Science & Technology*, *46*(16), 8799–807.

Anderson, J.W., Neff, J.M., Cox, B.A., Tatem, H.E. and Hightower, G.N. (1974) Characteristics of dispersions and water soluble extracts of crude and refined oils and their toxicity to estuarine crustaceans and fish. *Marine Biology*, 27, 75-88.

Andersson, M., Orvik, K. a., LaCasce, J. H., Koszalka, I., & Mauritzen, C. (2011). Variability of the Norwegian Atlantic Current and associated eddy field from surface drifters. *Journal of Geophysical Research*, *116*(C8), C08032.

Aries, E., Doumenq, P., Artaud, J., Acquaviva, M., & Bertrand, J. (2001). Effects of petroleum hydrocarbons on the phospholipid fatty acid composition of a consortium composed of marine hydrocarbon-degrading bacteria. *Organic Geochemistry*, *32*(7), 891–903.

Ashforth, E., Olive, P., & Ward, A. (2011). Phylogenetic characterisation of bacterial assemblages and the role of sulphur-cycle bacteria in an *Arenicola marina* bioturbated mesocosm. *Marine Ecology Progress Series*, *439*, 19–30.

Atlas, R. M. (1975). Effects of temperature and crude oil composition on petroleum biodegradation. *Applied Microbiology*, *30*(3), 396–403.

Atlas, R. M. (1981). Microbial degradation of petroleum hydrocarbons: an environmental perspective. *Microbiological Reviews*, *45*(1), 180–209.

Atlas, R. M., & Hazen, T. C. (2011). Oil biodegradation and bioremediation: a tale of the two worst spills in U.S. history. *Environmental Science & Technology*, *45*(16), 6709–15.

Aunaas, T., Olsen, A., & Zachariassen, K. E. (1991). The effects of oil and oil dispersants on the amphipod *Gammarus oceanicus* from Arctic waters. *Polar Research*, *10*(2), 619–630.

Azam, F., & Graf, J. S. (1983). The Ecological Role of Water-Column Microbes in the Sea. *Marine Ecology*, *10*, 257–263.

BP (2011). North Uist Exploration Well Environmental Statement, (August 2011).

Bælum, J., Borglin, S., Chakraborty, R., Fortney, J. L., Lamendella, R., Mason, O. U., Auer, M., Zemla, M., Bill, M., Conrad, M. E., Malfatti, S. A., Tringe,S. G., Holman,H., Hazen, T. C. & Jansson, J. K. (2012). Deep-sea bacteria enriched by oil and dispersant from the Deepwater Horizon spill. *Environmental Microbiology*, 14(9), 2405–2416.

Barnett, P. R. O., Watson, J., Connelly, D., & Marine, D. (1984). A multiple corer for taking virtually undisturbed samples from shelf , bathyal and abyssal sediments. *Oceanologica Acta*, *7*(4), 399–408.

Bejarano, A., Chandler, G., He, L., & Coull, B. (2006). Individual to population level effects of South Louisiana crude oil water accommodated hydrocarbon fraction (WAF) on a marine meiobenthic copepod. *Journal of Experimental Marine Biology and Ecology*, *332*(1), 49–59.

Berx, B., Hansen, B., Østerhus, S., Larsen, K. M., Sherwin, T., & Jochumsen, K. (2013). Combining in situ measurements and altimetry to estimate volume, heat and salt transport variability through the Faroe–Shetland Channel. *Ocean Science*, *9*(4), 639–654.

Bett, B. J. (2001). UK Atlantic Margin Environmental Survey: Introduction and overview of bathyal benthic ecology. *Continental Shelf Research*, *21*(8-10), 917–956.

Biles, C. L., Paterson, D. M., Ford, R. B., Solan, M., & Raffaelli, D. G. (2002). Bioturbation, ecosystem functioning and community structure. *Hydrology and Earth System Sciences*, *6*(6), 999–1005.

Billett, D. S. M., Lampitt, R. S., Rice' A. L. & Mantoura R. F. C. (1983) Seasonal sedimentation of phytoplankton to the deep-sea benthos *Nature 302*, 520–522.

Blair, N. E., Leu, A., Muñoz, E., Olsen, J., Kwong, E., & Des Marais, D. (1985). Carbon isotopic fractionation in heterotrophic microbial metabolism. *Applied and Environmental Microbiology*, *50*(4), 996–1001.

Blair, N. E., Levin, L. A., Demaster, D. J., & Plaia, G. (1996). The short-term fate of fresh algal carbon in continental slope sediments, *Limnology and Oceanography, 41*(6), 1208–1219.

Blanke, B., Arhan, M., Madec, G., & Roche, S. (1999). Warm Water Paths in the Equatorial Atlantic as Diagnosed with a General Circulation Model. *Journal of Physical Oceanography*, *29*, 2753–2768.

Blanke, B., & Delecluse, P. (1993). Variability of the tropical Atlantic ocean simulated by a general circulation model with two different mixed-layer physics. *Journal of Physical Oceanography*, *23*, 1363–1388.

Blanke, B., & Raynaud, S. (1997). Kinematics of the Pacific Equatorial Undercurrent : An Eulerian and Lagrangian Approach from GCM Results. *Journal of Physical Oceanography*, *27*, 1038–1053.

Bligh, E. G. & Dyer, W. J. (1959) A rapid method of total lipid extraction and purification. *Canadian Journal of Biochemistry and Physiology 37*(8), 911-917.

Boehm, P. D., & Fiest, D. L. (1982). Subsurface distributions of petroleum from an offshore well blowout. The Ixtoc I blowout, Bay of Campeche. *Environmental Science & Technology*, *16*(2), 67–74.

Boschker, H. T. S., & Middelburg, J. J. (2002). Stable isotopes and biomarkers in microbial ecology. *FEMS Microbiology Ecology*, *40*(2), 85–95.

Brinch-Inversen, J. & King, G. M. (1990) Effects of substrate concentration, growth state, and oxygen availability on relationships among bacterial carbon, nitrogen and phospholipid phosphorus content. *FEMS Microbiology Letters*, 74, 345-355.

Brodeau, L., Barnier, B., Treguier, A.-M., Pendu, T., Gulev, S., 2010. An ERA40-based atmospheric forcing for global ocean circulation models. *Ocean Modelling* 31 (3-4), 88-104.

Brodersen, C. (1987). Rapid narcosis and delayed mortality in larvae of king crabs and kelp shrimp exposed to the water-soluble fraction of crude oil. *Marine Environmental Research*, *22*(3), 233–239.

Brown, A., & Thatje, S. (2011). Respiratory response of the deep-sea amphipod *Stephonyx biscayensis* indicates bathymetric range limitation by temperature and hydrostatic pressure. *PLoS ONE*, *6*(12), 1–12.

Brown, J., Gillooly, J., Allen, A., Savage, V., & West, G. (2004). Toward a metabolic theory of ecology. *Ecology*, *85*(7), 1771–1789.

Camilli, R., Reddy, C. M., Yoerger, D. R., Van Mooy, B. A. S., Jakuba, M. V, Kinsey, J. C., McIntyre, C. P., Sylva, S. P. & Maloney, J. V. (2010). Tracking hydrocarbon plume transport and biodegradation at Deepwater Horizon. *Science, 330*(6001), 201–204.

Camus, L., Birkely, S. R., Jones, M. B., Børseth, J. F., Grøsvik, B. E., Gulliksen, B., Lønne, O. J. Regoli, F. & Depledge, M. H. (2003). Biomarker responses and PAH uptake in *Mya truncata* following exposure to oil-contaminated sediment in an Arctic fjord (Svalbard). *The Science of the Total Environment*, *308*(1-3), 221–34.

Camus, L., Jones, M. B., Børseth, J. F., Grøsvik, B. E., Regoli, F., & Depledge, M. H. (2002). Total oxyradical scavenging capacity and cell membrane stability of haemocytes of the Arctic scallop, *Chlamys islandicus*, following benzo(a)pyrene exposure. *Marine Environmental Research*, *54*(3-5), 425–430.

Camus, L., Jones, M. B., Børseth, J. F., Regoli, F., & Depledge, M. H. (2002). Heart rate, respiration and total oxyradical scavenging capacity of the Arctic spider crab, *Hyas araneus*, following exposure to polycyclic aromatic compounds via sediment and injection. *Aquatic Toxicology, 61*, 1–13.

Carpenter, S. (1996). Microcosm experiments have limited relevance for community and ecosystem ecology. *Ecology*, *77*(3), 677–680.

Chafik, L. (2012). The response of the circulation in the Faroe-Shetland Channel to the North Atlantic Oscillation. *Tellus*, *1*, 1–12.

Cifuentes, L. A., & Salata, G. G. (2001). Significance of carbon isotope discrimination between bulk carbon and extracted phospholipid fatty acids in selected terrestrial and marine environments. *Organic Geochemistry*, *32*, 613–621.

Coelho, G., & Aurand, D. (1997). *Proceedings of the Seventh Meeting of the Chemical Response to Oil Spills*. Ecological Effects Research Forum Santa Cruz, CA.

Coffin, R. B., Velinsky, D. J., Devereux, R., Price, W. A., & Cifuentest, L. A. (1990). Stable carbon isotope analysis of nucleic acids to trace sources of dissolved substrates used by estuarine bacteria. *Applied and Environmental Microbiology*, *56*(7), 2012–2020.

Comer, E. (2014). Estimating the mean transport of components of the Meridional Overturning Circulation between Iceland and Scotland. Thesis. University of Southampton. Master of Oceanography.

Cowie, B. R., Greenberg, B. M., & Slater, G. F. (2010). Determination of microbial carbon sources and cycling during remediation of petroleum hydrocarbon impacted soil using natural abundance ^{14}C analysis of PLFA. *Environmental Science & Technology*, *44*(7), 2322–2327.

Daan, R. M., (1994). Differential sensitivity of macrozoobenthic species to discharges of oil-contaminated drill cuttings in the North Sea. *Netherlands Journal of Sea Research*, *33*(1), 113–127.

Daan, R., & Mulder, M. (1996). On the short-term and long-term impact of drilling activities in the Dutch sector of the North Sea. *ICES Journal of Marine Science*, *53*(6), 1036–1044.

Danovaro, R., Gambi, C., Anno, A. D., Corinaldesi, C., Fraschetti, S., Vanreusel, A., Vincx, M. & Gooday, A. J. (2008). Exponential Decline of Deep-Sea Ecosystem Functioning Linked to Benthic Biodiversity Loss. *Current Biology*, *18*, 1–8.

Dasanayaka, L. K., & Yapa, P. D. (2009). Role of plume dynamics phase in a deepwater oil and gas release model. *Journal of Hydro-Environment Research*, *2*(4), 243–253.

Dauvin, J.-C. (1998). The fine sand *Abra alba* community of the Bay of Morlaix twenty years after the Amoco Cadiz oil spill. *Marine Pollution Bulletin*, *36*(9), 669–676.

Dauvin, J.-C. (2000). The muddy fine sand *Abra alba–Melinna palmata* community of the Bay of Morlaix twenty years after the Amoco Cadiz oil spill. *Marine Pollution Bulletin*, *40*(6), 528–536.

Delore P. & Borgomano, C. (1928) Leucemie aigue au cours de l'intoxication benzenique. Sur l'origine toxique de certaines leucemies aigues et leurs relations avec les anemies graves. *Journal de Medecine de Lyon*, 9, 227-33.

DeNiro, M., & Epstein, S. (1977). Mechanism of carbon isotope fractionation associated with lipid synthesis. *Science*, *197*(4300), 261–263.

Denoyelle, M., Jorissen, F. J., Martin, D., Galgani, F., & Miné, J. (2010). Comparison of benthic foraminifera and macrofaunal indicators of the impact of oil-based drill mud disposal. *Marine Pollution Bulletin*, *60*(11), 2007–21.

DHSG (2011) Final report on the investigation of the Macondo well blowout. *Deepwater Horizon Study Group*, March 2011. 124pp.

Doherty, V. F., & Otitoloju, A. A. (2013). Monitoring of soil and groundwater contamination following a pipeline explosion and petroleum product spillage in Ijegun, Lagos Nigeria. *Environmental Monitoring and Assessment*, *185*(5), 4159–4170.

Döös, K. (1995). Interocean exchange of water masses. *Journal of Geophysical Research*, *100*(C7), 13499–13514.

Doumenq, P., Mille, G., & Bertrand, J. C. (1999). Changes in fatty acids of *Pseudomonas nautica*, a marine denitrifying bacterium, in response to n-eicosane as carbon source and various culture conditions. *FEMS Microbiology Ecology*, *28*, 151–161.

Doumenq, P., Mille, G., & Bertrand, J. C. (2001). Influence of n-alkanes and petroleum on fatty acid composition of a hydrocarbonoclastic bacterium: *Marinobacter hydrocarbonoclasticus* strain 617. *Chemosphere*, *44*, 519–528.

Duineveld, G., Lavaleye, M., Berghuis, E., & Wilde, P. De. (2001). Activity and composition of the benthic fauna in the Whittard Canyon and the adjacent continental slope (NE Atlantic). *Oceanologica Acta*, *24*(1), 69–83.

Dussin, R., & Barnier, B. (2013). The Making of DFS 5.1. *DRAKKAR Collaboration*, 39pp.

Egan, S. T., McCarthy, D. M., Patching, J. W., & Fleming, G. T. A. (2012). An investigation of the physiology and potential role of components of the deep ocean bacterial community (of the NE Atlantic) by enrichments carried out under minimal environmental change. *Deep Sea Research Part I: Oceanographic Research Papers*, *61*, 11–20.

Faksness, L.-G., Brandvik, P. J., & Sydnes, L. K. (2008). Composition of the water accommodated fractions as a function of exposure times and temperatures. *Marine Pollution Bulletin*, *56*(10), 1746–1754.

Faksness, L.-G., Hansen, B. H., Altin, D., & Brandvik, P. J. (2012). Chemical composition and acute toxicity in the water after in situ burning - a laboratory experiment. *Marine Pollution Bulletin*, *64*(1), 49–55.

Faroese Petroleum Administration, (2004). Second Faroese Licencing Round. 40pp.

Feder, H. M., & Blanchard, A. (1998). The deep benthos of Prince William Sound, Alaska, 16 months after the Exxon Valdez oil spill. *Marine Pollution Bulletin*, *36*(2), 118–130.

Fernández, N., Cesar, A., Salamanca, M. J., & DelValls, T. A. (2006). Toxicological characterisation of the aqueous soluble phase of the Prestige fuel-oil using the sea-urchin embryo bioassay. *Ecotoxicology*, *15*(7), 593–9.

Fisher, C. R., Demopoulos, A. W. J., Cordes, E. E., Baums, I. B., White, H. K., & Bourque, J. R. (2014). Coral Communities as Indicators of Ecosystem-Level Impacts of the Deepwater Horizon Spill. *BioScience*, *64*(9), 796–807.

Flach, E., Lavaleye, M., de Stigter, H., & Thomsen, L. (1998). Feeding types of the benthic community and particle transport across the slope of the N.W. European continental margin (Goban Spur). *Progress in Oceanography*, *42*(1-4), 209–231.

Flach, E., & Bruin, W. de. (1999). Diversity patterns in macrobenthos across a continental slope in the NE Atlantic. *Journal of Sea Research*, *42*, 303–323.

Frostegård, Å., Tunlid, A., & Bååth, E. (1991). Microbial biomass measured as total lipid phosphate in soils of different organic content. *Journal of Microbiological Methods*, *4*, 151–163.

Frostegård, Å., Tunlid, A., & Bååth, E. (2011). Use and misuse of PLFA measurements in soils. *Soil Biology and Biochemistry*, *43*(8), 1621–1625.

Gates, A. R., & Jones, D. O. B. (2012). Recovery of benthic megafauna from anthropogenic disturbance at a hydrocarbon drilling well (380 m depth in the Norwegian Sea). *PloS One*, *7*(10), 1–14.

Georgiades, E. T., Holdway, D. A., Brennan, S. E., Butty, J. S., & Temara, A. (2003). The impact of oil-derived products on the behaviour and biochemistry of the eleven-armed asteroid *Coscinasterias muricata* (Echinodermata). *Marine Environmental Research*, *55*(3), 257–276.

Glud, R. N. (2008). Oxygen dynamics of marine sediments. *Marine Biology Research*, *4*(4), 243–289.

Gontikaki, E., Mayor, D., Thornton, B., Black, K., & Witte, U. (2011a). Processing of 13C-labelled diatoms by a bathyal community at sub-zero temperatures. *Marine Ecology Progress Series*, *421*, 39–50.

Gontikaki, E., van Oevelen, D., Soetaert, K., & Witte, U. (2011b). Food web flows through a sub-arctic deep-sea benthic community. *Progress In Oceanography*, *91*(3), 245–259.

Gooday, A. J. (1988) A response by benthic Foraminifera to the deposition of phytodetritus in the deep sea. *Nature, 332*, 70-73.

Graf, G. (1989) Benthic-pelagic coupling in a deep-sea benthic community *Nature, 341*, 437-439.

Graham, W. M., Condon, R. H., Carmichael, R. H., D'Ambra, I., Patterson, H. K., Linn, L. J., & Hernandez Jr, F. J. (2010). Oil carbon entered the coastal planktonic food web during the Deepwater Horizon oil spill. *Environmental Research Letters*, *5*(4), 045301.

Gray, J., Larke, K., Warwick, R., & Hobbs, G. (1990). Detection of initial effects of pollution on marine benthos: an example from the Ekofisk and Eldfisk oilfields, North Sea. *Marine Ecology Progress Series*, *66*, 285–299.

Gray, J., Wu, R., & Or, Y. (2002). Effects of hypoxia and organic enrichment on the coastal marine environment. *Marine Ecology Progress Series*, *238*, 249–279.

Grassle, J. F. & Grassle J. P. (1974) Opportunistic life histories and genetic systems in marine benthic polychaetes. *Journal of Marine Research, 32*, 253-284 .

Griffin, L. F., & Calder, J. A. (1977). Toxic effect of water-soluble fractions of crude, refined, and weathered oils on the growth of a marine bacterium. *Applied and Environmental Microbiology*, *33*(5), 1092–1096.

Guckert, J. B., Antworth, C. P., Nichols, P. D., & White, D. C. (1985). Phospholipid, ester-linked fatty acid profiles as reproducible assays for changes in prokaryotic community structure of estuarine sediments. *FEMS Microbiology Letters*, *31*(3), 147–158.

Guezennec, J., & Fiala-Medioni, A. (1996). Bacterial abundance and diversity in the Barbados Trench determined by phospholipid analysis. *FEMS Microbiology Ecology*, *19*(2), 83–93.

Gutierrez, T., Singleton, D. R., Berry, D., Yang, T., Aitken, M. D., & Teske, A. (2013). Hydrocarbon-degrading bacteria enriched by the Deepwater Horizon oil spill identified by cultivation and DNA-SIP. *The ISME Journal*, *7*(11), 2091–104.

Hahn, M. E. (2011). Mechanistic research in aquatic toxicology: perspectives and future directions. *Aquatic Toxicology*, *105*(3-4 Suppl), 67–71.

Hahn-Weinheimer, P., & Hirner, A. (1980). Chemical composition and stable isotopic ratios of crude oils from southern Germany. *Organic Geochemistry*, *2*, 45–53.

Hansen, B., & Osterhus, S. (2007). Faroe Bank Channel overflow 1995 – 2005. *Progress in Oceanography*, *75*, 817–856.

Hanson, J. R., Macalady, J. L., Harris, D., & Scow, K. M. (1999). Linking toluene degradation with specific microbial populations in soil. *Applied and Environmental Microbiology*, *65*(12), 5403 – 5408.

Hargrave, B. T. (1973). Coupling carbon flow through somep and benthic communities. *Journal of the Fisheries Research Board of Canada*, *30*, 1317–1326.

Hatlen, K., Camus, L., Berge, J., Olsen, G. H., & Baussant, T. (2009). Biological effects of water soluble fraction of crude oil on the Arctic sea ice amphipod *Gammarus wilkitzkii*. *Chemistry and Ecology*, *25*(3), 151–162.

Hazen, T. C., Dubinsky, E. A., Desantis, T. Z., Andersen, G. L., Piceno, Y. M., Singh, N., Jansson, J.K., Probst, A., Borglin,S. E., Fortney, J. L., Stringfellow, W. T., Bill, M., Conrad, M. E., Tom, L. M., Chavarria, K. L., Alusi,T. R., Lamendella, R., Joyner, D. C., Spier, C., Baelum, J., Auer, M., Zemla, M. L., Chakraborty, R., Sonnenthal,E. L., D'haeseleer, P., Holman, H. N., Osman, S., Lu, Z., Van Nostrand, J. D., Deng, Y., Zhou, J., & Mason, O. U. (2010). Deep-sea oil plume enriches indigenous oil-degrading bacteria. *Science*, *330*, 204–208.

Hedman, J., Bradshaw, C., Thorsson, M., Gilek, M., & Gunnarsson, J. (2008). Fate of contaminants in Baltic Sea sediments: role of bioturbation and settling organic matter. *Marine Ecology Progress Series*, *356*, 25–38.

Hess, S., Alve, E., Trannum, H. C., & Norling, K. (2013). Benthic foraminiferal responses to water-based drill cuttings and natural sediment burial: Results from a mesocosm experiment. *Marine Micropaleontology*, *101*, 1–9.

Heip, C., Duineveld, G., Flach, E., Graf, G., Helder, W., Herman, P., Lavaleye, M., Middelburg, J., Pfannkuche, O., Soetaert, K., Soltwedel, T., de Stigter, H., Thomsen, L. & de Wilde, P. (2001). The role of the benthic biota in sedimentary metabolism and sediment-water exchange processes in the Goban Spur area (NE Atlantic). *Deep Sea Research Part II: Topical Studies in Oceanography*, *48*(14-15), 3223–3243.

Hokstad, J., Daling, P., Buffagni, M., & Johnsen, S. (1999). Chemical and ecotoxicological characterisation of oil - water systems. *Spill Science & Technology Bulletin*, *5*(1), 75–80.

Hollander, D. J., Brooks, G. R., Larson, R., Romero, I., Schwing, P., & Watson, K. (2013). Testing the Mechanisms of Sedimentary Oil Deposition in Deep-Sea. *Gulf of Mexico Oil Spill & Ecosystem Science Conference*. New Orleans, LA, January 21-23, 2013.

Holliday, N., & Cunningham, S. (2013). The Extended Ellett Line: discoveries from 65 years of marine observations west of the UK. *Oceanography*, *26*(2), 156–163.

Hughes, S. J. M., Jones, D. O. B., Hauton, C., Gates, A. R., & Hawkins, L. E. (2010). An assessment of drilling disturbance on *Echinus acutus* var*. norvegicus* based on *in-situ* observations and experiments using a remotely operated vehicle (ROV). *Journal of Experimental Marine Biology and Ecology*, *395*(1-2), 37–47.

Hullar, M., Fry, B., Peterson, B. J., & Wright, R. T. (1996). Microbial utilization of estuarine dissolved organic carbon: a stable isotope tracer approach tested by mass balance. *Applied and Environmental Microbiology*, *62*(7), 2489–2493.

Hunter, W. R., Veuger, B., & Witte, U. (2012). Macrofauna regulate heterotrophic bacterial carbon and nitrogen incorporation in low-oxygen sediments. *The ISME Journal*, *6*(11), 2140–2151.

Huthnance, J. M. (1984) Slope currents and 'JEBAR.' *Journal of Physical Oceanography, 14*, 795–810.

Huthnance, J. M. (1986) The Rockall slope current and shelf-edge processes. *Proceedings of the Royal Society of Edinburgh. Section B. Biological Sciences,* 88, 83-101.

Hyland, J., Balthis, L., Karakassis, I., Magni, P., Petrov, A., Shine, J., Vestergaard, O. & Warwick, R.. (2005). Organic carbon content of sediments as an indicator of stress in the marine benthos. *Marine Ecology Progress Series*, *295*, 91–103.

IPCC (2014) Summary for Policymakers. In: *Climate Change 2014: Impacts, Adaptation, and Vulnerability. Part A: Global and Sectoral Aspects. Contribution of Working Group II to the Fifth Assessment Report of the Intergovernmental Panel on Climate Change.* Field, C.B., V.R. Barros, D.J. Dokken, K.J. Mach, M.D. Mastrandrea, T.E. Bilir, M. Chatterjee, K.L. Ebi,

Y.O. Estrada, R.C. Genova, B. Girma, E.S. Kissel, A.N. Levy, S. MacCracken, P.R. Mastrandrea, and L.L. White (eds.). Cambridge University Press, Cambridge, United Kingdom and New York, NY, USA, 32pp.

Jahnke, R. A. (1996). The global ocean flux of particulate organic carbon: Areal distribution and magnitude. *Global Biogeochemical Cycles*, *10*(1), 71–88.

Jechalke, S., Franchini, A. G., Bastida, F., Bombach, P., Bergen, M. Von, Vogt, C., & Richnow, H. H. (2013). Analysis of structure, function, and activity of a benzene-degrading microbial community. *FEMS Microbiology Ecology*, *85*, 14–26.

Jensen, P (1984) Measuring carbon content in nematodes. *Helgolander Meeresuntersuchungen 38*(1), 83-86.

Jobson, A., Cook, F. D., & Westlake, D. W. S. (1972). Microbial utilization of crude oil. *Applied Microbiology*, *23*(6), 1082–1089.

Johansen, Ø. (2000). DeepBlow – a Lagrangian plume model for deep water blowouts. *Spill Science & Technology Bulletin*, *6*(2), 103–111.

Johansen, Ø. (2003). Development and verification of deep-water blowout models. *Marine Pollution Bulletin*, *47*(9-12), 360–368.

Jones, D. O. B., Yool, A., Wei, C., & Henson, S. A. (2014). Global reductions in seafloor biomass in response to climate change. *Global Change Biology*, *20*, 1861–1872.

Jones D. O. B., Wigham, B., & Hudson, I. (2007). Anthropogenic disturbance of deep-sea megabenthic assemblages: a study with remotely operated vehicles in the Faroe-Shetland Channel, NE Atlantic. *Marine Biology*, *151*(5), 1731–1741.

Joint Analysis Group (2010). *Review of Preliminary Data to Examine Oxygen Levels In the Vicinity of MC252 1 May 8 to August 9, 2010.* National Incident Command Report. 95pp.

Jutzeler, M., Marsh, R., Carey, R. J., White, J. D. L., Talling, P. J., & Karlstrom, L. (2014). On the fate of pumice rafts formed during the 2012 Havre submarine eruption. *Nature Communications*, *5*, 3660.

Kanzow, T., & Zenk, W. (2014). Structure and transport of the Iceland Scotland overflow plume along the Reykjanes Ridge in the Iceland Basin. *Deep Sea Research Part I: Oceanographic Research Papers*, *86*, 82–93.

Keeling, B. C. D., Bacastow, R. B., Bainbridge, A. E., Ekdahl, C. A., Guenther, P. R., & Waterman, L. E. E. S. (1976). Atmospheric carbon dioxide variations at Mauna Loa Observatory , Hawaii. *Tellus*, (6), 538–551.

Keeling, B. C. D., Piper, S. C., Bacastow, R. B., Wahlen, M., Whorf, T. P., Heimann, M. and Meijer, H. A. (2005) Atmospheric CO_2 and $^{13}CO_2$ exchange with the terrestrial biosphere and oceans from 1978 to 2000: observations and carbon cycle implications, pages 83-113, In: Ehleringer, J.R., T. E. Cerling, M. D. Dearing (eds) *A History of Atmospheric CO_2 and its effects on Plants, Animals, and Ecosystems*, Springer Verlag, New York, 2005

Kelly-Gerreyn, B. A., Martin, A. P., Bett, B. J., Anderson, T. R., Kaariainen, J. I., Main, C. E., Marcinko, C. & Yool, A. (2014). Benthic biomass size spectra in shelf and deep-sea sediments. *Biogeosciences*, *11*(22), 6401–6416.

Kessler, J. D., Valentine, D. L., Redmond, M. C., Du, M., Chan, E. W., Mendes, S. D., Quiroz, E. W., Villanueva, C. J., Shusta, S. S., Werra, L. M., Yvon-Lewis, S. A. & Weber, T. C. (2011). A persistent oxygen anomaly reveals the fate of spilled methane in the deep Gulf of Mexico. *Science*, *331*(6015), 312–315.

Kimes, N. E., Callaghan, A. V, Aktas, D. F., Smith, W. L., Sunner, J., Golding, B. T., Drozdowska, M., Hazen, T. C., Suflita, J. M. & Morris, P. J. (2013). Metagenomic analysis and metabolite profiling of deep-sea sediments from the Gulf of Mexico following the Deepwater Horizon oil spill. *Frontiers in Microbiology*, *4*, 1–17.

Kiriakoulakis, K., Bett, B. J., White, M., & Wolff, G. A. (2004). Organic biogeochemistry of the Darwin Mounds, a deep-water coral ecosystem of the NE Atlantic. *Deep-Sea Research Part I*, *51*, 1937–1954.

Koch-Larrouy, A., Madec, G., Blanke, B., & Molcard, R. (2008). Water mass transformation along the Indonesian throughflow in an OGCM. *Ocean Dynamics*, *58*, 289–309.

Lake, I., & Lundberg, P. (2006). Seasonal barotropic modulation of the deep-water overflow through the Faroe Bank Channel. *Journal of Physical Oceanography*, *36*, 2328–2339.

Lambrechts, J., Hanert, E., Deleersnijder, E., Bernard, P., Legat, V., Remacle, J., & Wolanski, E. (2008). A multi-scale model of the hydrodynamics of the whole Great Barrier Reef. *Estuarine, Coastal and Shelf Science*, *79*, 143–151.

Lapham, L., Proctor, L., & Chanton, J. (1999). Using respiration rates and stable carbon isotopes to monitor the biodegradation of orimulsion by marine benthic bacteria. *Environmental Science & Technology*, *33*(12), 2035–2039.

Laureillard, J., Méjanelle, L., & Sibuet, M. (2004). Use of lipids to study the trophic ecology of deep-sea xenophyophores, *Marine Ecology Progress Series*, *270*, 129–140.

Laverock, B., Smith, C. J., Tait, K., Osborn, A. M., Widdicombe, S., & Gilbert, J. A. (2010). Bioturbating shrimp alter the structure and diversity of bacterial communities in coastal marine sediments. *The ISME Journal*, *4*(12), 1531–44.

Leahy, J. G. and Colwell, R. R. (1990) Microbial degradation of hydrocrbons in the environment. Microbiology and Molecular Biology Reviews, 54(3), 305-315.

Lechevalier, M. P., Bievre, C. D. E., & Lechevalier, H. (1977). Chemotaxonomy of aerobic Actinomycetes : phospholipid composition. *Biochemical Systematics and Ecology*, *5*, 249–259.

Lee, L.-H., & Lin, H.-J. (2013). Effects of an oil spill on benthic community production and respiration on subtropical intertidal sandflats. *Marine Pollution Bulletin*, *73*(1), 291–299.

Leffer, W. L., Pattarozzi, R. and Sterling, G. (2011) Deepwater petroleum exploration & production a nontechnical guide (2nd Edition). Penwell. 351 pp.

Lerch, T. Z., Nunan, N., Dignac, M.-F., Chenu, C., & Mariotti, A. (2011). Variations in microbial isotopic fractionation during soil organic matter decomposition. *Biogeochemistry*, *106*(1), 5–21.

Lewis, C., Pook, C., & Galloway, T. (2008). Reproductive toxicity of the water accommodated fraction (WAF) of crude oil in the polychaetes *Arenicola marina* (L.) and *Nereis virens* (Sars). *Aquatic Toxicology*, *90*(1), 73–81.

Lewis, S., Handy, R. D., Cordi, U. B., Billinghurst, Z., & Depledge, M. H. (2000). Stress proteins (HSP 's): Methods of detection and their use as an environmental biomarker. *Ecotoxicology*, *8*, 351–368.

Li, K., Jing, Y., Yang, C., Liu, S., Zhao, Y., He, X., Li, F., Han, J. & Li, G. (2014). Increased leukemia-associated gene expression in benzene-exposed workers. *Nature Scientific Reports*, *4*, 5369.

Lindo-Atichati, D., Paris, C. B., Le Hénaff, M., Schedler, M., Valladares Juárez, A. G., & Müller, R. (2014). Simulating the effects of droplet size, high-pressure biodegradation, and variable flow rate on the subsea evolution of deep plumes from the Macondo blowout. *Deep Sea Research Part II: Topical Studies in Oceanography*. doi:10.1016/j.dsr2.2014.01.011

Liu, Y., Weisberg, R. H., Hu, C., & Zheng, L. (2011a). Tracking the Deepwater Horizon Oil Spill: A Modeling Perspective. *Ocean Modelling*, *92*(6), 2010–2012.

Liu, Y., Weisberg, R. H., Hu, C., & Zheng, L. (2011b). Trajectory forecast as a rapid response to the Deepwater Horizon oil spill. *Geophysical Monograph Series 195*, 153–165.

Lochte, K. & Turley, C. M. (1988) Bacteria and cyanobacteria associated with phytodetritus in the deep sea. *Nature, 333*, 67 – 69.

Lohmann, K., Jungclaus, J. H., Matei, D., Mignot, J., Menary, M., Langehaug, H. R., Ba, J., Gao, Y., Ottera, O. H., Park, W. & Lorenz, S. (2014). The role of subpolar deep water formation and Nordic Seas overflows in simulated multidecadal variability of the Atlantic meridional overturning circulation. *Ocean Science*, *10*(2), 227–241.

Lohse, L., Helder, W., Epping, E. H. G., & Balzer, W. (1998). Recycling of organic matter along a shelf-slope transect across the N.W. European Continental Margin (Goban Spur). *Progress In Oceanography*, *42*(1-4), 77–110.

Londry, K. L., Jahnke, L. L., & Des Marais, D. J. (2004). Stable carbon isotope ratios of lipid biomarkers of sulfate-reducing bacteria. *Applied and Environmental Microbiology*, *70*(2), 745–751.

Long, S. M., & Holdway, D. A. (2002). Acute toxicity of crude and dispersed oil to *Octopus palldus*. *Water Research*, *36*, 2769–2776.

Madec, G. (2008). *NEMO ocean engine*. 2011pp.

Magni, P., Tagliapietra, D., Lardicci, C., Balthis, L., Castelli, A., Como, S., Frangipane, G., et al. (2009). Animal-sediment relationships: evaluating the “Pearson-Rosenberg paradigm” in Mediterranean coastal lagoons. *Marine Pollution Bulletin*, *58*(4), 478–86.

Mahmoudi, N., Porter, T. M., Zimmerman, A. R., Fulthorpe, R. R., Kasozi, G. N., Silliman, B. R., & Slater, G. F. (2013). Rapid Degradation of Deepwater Horizon Spilled Oil by Indigenous Microbial Communities in Louisiana Saltmarsh Sediments. *Environmental Science and Technology*, *47*, 13303–13312.

Mair, J. (1987). Offshore macrobenthic recovery in the Murchison field following the termination of drill-cuttings discharges. *Marine Pollution Bulletin*, *18*(12), 628–634.

Mariano, a. J., Kourafalou, V. H., Srinivasan, a., Kang, H., Halliwell, G. R., Ryan, E. H., & Roffer, M. (2011). On the modeling of the 2010 Gulf of Mexico Oil Spill. *Dynamics of Atmospheres and Oceans*, *52*(1-2), 322–340.

Marsh, R., Desbruyères, D., Bamber, J. L., de Cuevas, B. A., Coward, A. C., & Aksenov, Y. (2010). Short-term impacts of enhanced Greenland freshwater fluxes in an eddy-permitting ocean model. *Ocean Science*, *6*(3), 749–760.

Marzocchi, A., Hirschi, J. J.-M., Holliday, N. P., Cunningham, S. A., Blaker, A. T., & Coward, A. C. (2015). The North Atlantic subpolar circulation in an eddy-resolving global ocean model. *Journal of Marine Systems*, *142*, 126–143.

Mason, O. U., Scott, N. M., Gonzalez, A., Robbins-Pianka, A., Bælum, J., Kimbrel, J., Bouskill, N. J., Prestat, E., Borglin, S., Joyner, D. C., Fortney, J. L., Jurelevicius, D., Stringfellow, W. T., Alvarez-Cohen, L., Hazen, T. C., Knight, R. Gilbert, J. A., & Jansson, J. K. (2014). Metagenomics reveals sediment microbial community response to Deepwater Horizon oil spill. *The ISME Journal*, 1–12.

Massonnet, F., Mathiot, P., Fichefet, T., Goosse, H., König, C., Vancoppenolle, M., & Lavergne, T. (2013). A model reconstruction of the Antarctic sea ice thickness and volume changes over 1980 – 2008 using data assimilation. *Ocean Modelling*, *64*, 67–75.

Maurer, D. (1993). San Pedro Shelf California: testing the Pearson-Rosenberg model (PRM). *Marine Environmental Research*, *35*(4), 303–321.

Mayor, D. J., Gray, N. B., Elver-Evans, J., Midwood, A. J., & Thornton, B. (2013). Metal-macrofauna interactions determine microbial community structure and function in copper contaminated sediments. *PLoS ONE*, *8*(5), 1 – 9.

Mayor, D. J., Thornton, B., Hay, S., Zuur, A. F., Nicol, G. W., Mcwilliam, J. M., & Witte, U. F. M. (2012). Resource quality affects carbon cycling in deep-sea sediments. *The ISME Journal*, 1–9.

Mazzella, N., Syakti, A. D., Molinet, J., Gilewicz, M., Doumenq, P., Artaud, J., & Bertrand, J.-C. (2005). Effects of crude oil on phospholipid fatty acid compositions of marine hydrocarbon degraders: estimation of the bacterial membrane fluidity. *Environmental Research*, *97*(3), 300–311.

McNutt, M, R. Camilli, G. Guthrie, P. Hsieh, V. Labson, B. Lehr, D. Maclay, A. Ratzel, and M. Sogge. (2011). Assessment of Flow Rate Estimates for the Deepwater Horizon / Macondo Well Oil Spill. *Flow Rate Technical Group report to the National Incident Command, Interagency Solutions Group*, March 10, 2011. 30pp

Mestre, N. C., Thatje, S., & Tyler, P. A. (2009). The ocean is not deep enough: pressure tolerances during early ontogeny of the blue mussel *Mytilus edulis*. *Proceedings of the Royal Society B*, *276*(1657), 717–26.

Meyer-Reil, L.-A., & Koster, M. (1991). Microbial life in pelagic sediments: the impact of environmental parameters on enzymatic degradation of organic material. *Marine Ecology Progress Series*, *81*, 65–72.

Middelburg, J. J., & Meysman, F. J. R. (2007). Burial at sea. *Science*, *316*(5829), 1294–1295.

Moeseneder, M. M., Winter, C., & Herndl, G. J. (2001). Horizontal and vertical complexity of attached and free-living bacteria of the eastern Mediterranean Sea, determined by 16S rDNA and 16S rRNA fingerprints. *Limnology and Oceanography*, *46*(1), 95–107.

Moles, A. (2000). Changing perspectives on oil toxicity evaluation. In *2001 International Oil Spill Conference* (Vol. 50).

Montagna, P. A., Baguley, J. G., Cooksey, C., Hartwell, I., Hyde, L. J., Hyland, J. L., Kalke, R. D., Kracker, L. M. Reuscher, M & Rhodes, A. C. E. (2013). Deep-sea benthic footprint of the Deepwater Horizon blowout. *PLoS ONE*, *8*(8), e70540.

Moodley, L., Middelburg, J. J., Soetaert, K., Boschker, H. T. S., Herman, P. M. J., & Heip, C. H. R. (2005). Similar rapid response to phytodetritus deposition in shallow and deep-sea sediments. *Journal of Marine Research*, *63*(2), 457–469.

Mork, K. A., & Skagseth, Ø. (2010). A quantitative description of the Norwegian Atlantic Current by combining altimetry and hydrography. *Ocean Science*, *6*(4), 901–911.

Muñoz, R., Díaz, L. F., Bordel, S., & Villaverde, S. (2007). Inhibitory effects of catechol accumulation on benzene biodegradation in *Pseudomonas putida* F1 cultures. *Chemosphere*, *68*(2), 244–52.

Naeem, S., Thompson, L. J., Lawler, S. P., Lawton J.H. & Woodfin, R. M. (1994) Declining biodiversity can alter the performance of ecosystems *Nature, 368*, 734 – 737.

Nakano, M., Povinec, P. P., & Agency, E. (2012). Long-term simulations of the in the world ocean ^{137}Cs dispersion from the Fukushima accident. *Journal of Environmental Radioactivity*, *111*, 109–115.

National Research Council (2005) Dispersant-oil interactions and effectiveness testing. In: *Oil spill dispersants: efficacy and effects.* National Academies Press. 395 pp.

National Science and Technology Council (2012). *Deepwater Horizon Oil Spill Principal Investigator Workshop Report*, 91pp.

Neff, J. M., Ostazeski, S., Gardiner, W., & Stejskal, I. (2000). Effects of weathering on the toxicity of three offshore Australian crude oils and a diesel fuel to marine animals. *Environmental Toxicology and Chemistry*, *19*(7), 1809–1821.

Negri, A. P., & Heyward, A. J. (2000). Inhibition of fertilization and larval metamorphosis of the coral *Acropora millepora* (Ehrenberg, 1834) by petroleum products. *Marine Pollution Bulletin*, *41*, 420–427.

Oevelen, D. Van, Soetaert, K., & Heip, C. (2012). Carbon flows in the benthic food web of the Porcupine Abyssal Plain : The (un) importance of labile detritus in supporting microbial and faunal carbon demands. *Limnology & Oceanography*, *57*(2), 645–664.

Olsen, G. H., Carroll, M. L., Renaud, P. E., Ambrose, W. G., Olssøn, R., & Carroll, J. (2007a). Benthic community response to petroleum-associated components in Arctic versus temperate marine sediments. *Marine Biology*, *151*(6), 2167–2176.

Olsen, G. H., Sva, E., Carroll, J., Camus, L., De Coen, W., Smolders, R., Olsen, G. H., Sva, E., Carroll, J., Camus, L., De Coen, W., Smolders, R., Overaas, H., & Hylland, K. (2007b). Alterations in the energy budget of Arctic benthic species exposed to oil-related compounds. *Aquatic Toxicology*, *83*(2), 85–92.

Olsgard, F., Somerfield, P., & Carr, M. (1997). Relationships between taxonomic resolution and data transformations in analyses of a macrobenthic community along an established pollution gradient. *Marine Ecology Progress Series*, *149*, 173–181.

Oksanen, J., Blanchet, G., Kindt, R., Legedre, P., Minchin, P. R., O'Hara, R. B., Simpson, G., Solymos, P., Stevens, M. H. H. & Wagner, H. (2013). *vegan* R package version 2.0-10. http://cran.r-project.org/package=vegan

Oudot, J. (1984). Rates of microbial degradation of petroleum components as determined by computerized capillary gas chromatography and computerized mass spectrometry. *Marine Environmental Research*, *13*(4), 277–302.

Paris, C. B., Le, M., Aman, Z. M., Subramaniam, A., Helgers, J., Wang, D., Kourafalou, V. H. & Srinivasan, A. (2012). Evolution of the Macondo well blowout: simulating the effects of the circulation and synthetic dispersants on the subsea oil transport. *Environmental Science and Technology*, *46*, 13293–13302.

Paris, C. B., Helgers, J., van Sebille, E., & Srinivasan, A. (2013). Connectivity Modeling System: A probabilistic modeling tool for the multi-scale tracking of biotic and abiotic variability in the ocean. *Environmental Modelling & Software*, *42*, 47–54.

Passow, U., Ziervogel, K., Asper, V., & Diercks, A. (2012). Marine snow formation in the aftermath of the Deepwater Horizon oil spill in the Gulf of Mexico. *Environmental Research Letters*, *7*(3), 035301 (11 pp).

Pearson, T.H. & Rosenberg, R., (1978). Macrobenthic succession in relation to organic enrichment and pollution of the marine environment. *Oceanography and Marine Biology: an Annual Review*, 16, 229-311.

Peters, K. E., Walters, C. C. and Moldowan, M. (eds) (2005) The Biomarker Guide. Volume I Biomarkers and Isotopes in the Environment and Human History. Cambridge University Press, 471pp.

Peterson, B. J., & Fry, B. (1987). Stable isotopes in ecosystem studies. *Annual Reviews in Ecology and Systems*, *18*, 293–320.

Pelz, O., Chatzinotas, A., Zarda-Hess, A., Abraham, W.-R., & Zeyer, J. (2001). Tracing toluene-assimilating sulfate-reducing bacteria using ^{13}C-incorporation in fatty acids and whole-cell hybridization. *FEMS Microbiology Ecology*, *38*(2-3), 123–131.

Persechino, A., Marsh, R., Sinha, B., Megann, A. P., Blaker, A. T., & New, A. L. (2012). Decadal-timescale changes of the Atlantic overturning circulation and climate in a coupled climate model with a hybrid-coordinate ocean component. *Climate Dynamics*, *39*(3-4), 1021–1042.

Pinheiro, J. C. and Bates, D. M. (2000) Mixed-Effects Models in S and S-PLUS, José C. Pinheiro and Douglas M. Bates, *Statistics and Computing Series*, Springer-Verlag, New York, NY, 2000.

Pinheiro J, Bates D, DebRoy S, Sarkar D & R Core Team (2014). *nlme: Linear and Nonlinear Mixed Effects Models*. R package version 3.1-117, http://cran.r-project.org/package=nlme

Popova, E. E., Yool, A., Aksenov, Y., & Coward, A. C. (2013). Role of advection in Arctic Ocean lower trophic dynamics: A modeling perspective. *Journal of Geophysical Research: Oceans*, *118*(3), 1571–1586.

Popova, E. E., Yool, A., Coward, A. C., Aksenov, Y. K., Alderson, S. G., de Cuevas, B. A., & Anderson, T. R. (2010). Control of primary production in the Arctic by nutrients and light: insights from a high resolution ocean general circulation model. *Biogeosciences*, *7*(11), 3569–3591.

Putman, N. F., Scott, R., Verley, P., Marsh, R., & Hays, G. C. (2012). Natal site and offshore swimming influence fitness and long-distance ocean transport in young sea turtles. *Marine Biology*, *159*(10), 2117–2126.

R Core Team (2013) R: A language and environment for statistical computing. *R Foundation for Statistical Computing, Vienna, Austria*. ISBN 3-900051-07-0, URL http://www.R-project.org/.

Raj, R. P., Chafik, L., Nilsen, J. E. Ø., Eldevik, T., & Halo, I. (2015). The Lofoten Vortex of the Nordic Seas. *Deep Sea Research Part I: Oceanographic Research Papers*, *96*, 1–14.

Ramirez-Llodra, E., Tyler, P. A, Baker, M. C., Bergstad, O. A., Clark, M. R., Escobar, E., Levin, L. A., Menot, L., Rowden, A. A., Smith, C. R & Van Dover, C. L. (2011). Man and the last great wilderness: human impact on the deep sea. *PloS One*, *6*(8), e22588.

Reddy, C. M., Arey, J. S., Seewald, J. S., Sylva, S. P., Lemkau, K. L., Nelson, R. K., Carmicheal, C. A., MacIntyre, C. P., Fenwick, J., Ventura, G. T., Van Mooy, B. A. S. & Camilli, R. (2011). Composition and fate of gas and oil released to the water column during the Deepwater

Horizon oil spill. *Proceedings of the National Academy of Sciences, 109(50),* 20229 – 20234.

Redmond, M. C., & Valentine, D. L. (2011). Natural gas and temperature structured a microbial community response to the Deepwater Horizon oil spill. *Proceedings of the National Academy of Sciences*, *109(50),* 20292-20297.

Reed, M., French, D., Rines, H., & Rye, H. (1995). A three-dimensional oil and chemical spill model for environmental impact assessment. *Proceedings of the 1995 International Oil Spill Conference,* pp.61-66.

Reineke, V., Rullkotter, J., Smith, E., & Rowland, S. (2006). Toxicity and compositional analysis of aromatic hydrocarbon fractions of two pairs of undegraded and biodegraded crude oils from the Santa Maria (California) and Vienna basins. *Organic Geochemistry*, *37*(12), 1885–1899.

Robinson, J., Popova, E., Yool, A., Lampitt, R., & Blundell, J. (2014). How deep is deep enough? Ocean iron fertilization and carbon sequestration in the Southern Ocean. *Geophysical Research Letters*, 2489–2495.

Rodgers, R. P., Blumer, E. N., & Emmett, M. R. (2000). Efficacy of bacterial bioremediation: demonstration of complete incorporation of hydrocarbons into membrane phospholipids from *Rhodococcus* hydrocarbon degrading bacteria by electrospray ionization Fourier transform ion cyclotron resonance mass spectrometry. *Environmental Science & Technology*, *34*(3), 535–540.

Rossby, T., Prater, M. D., & Søiland, H. (2009). Pathways of inflow and dispersion of warm waters in the Nordic seas. *Journal of Geophysical Research*, *114*(C4), C04011.

Rossi, V., Van Sebille, E., Sen Gupta, A., Garçon, V., & England, M. H. (2013). Multi-decadal projections of surface and interior pathways of the Fukushima Cesium-137 radioactive plume. *Deep Sea Research I*, *80*, 37–46.

Rowe, G. T. (ed) (1983) *The sea (ideas and observations on progress in the study of the seas). Vol.8: Deep-sea biology*. John Wiley and Sons, New York. 560 pp.

Rowe G. T., Morse, J., Nunnally, C., & Boland, G. S. (2008). Sediment community oxygen consumption in the deep Gulf of Mexico. *Deep-Sea Research II*, *55*, 2686–2691.

Rowe, G. T., & Deming, J. W. (2011). An alternative view of the role of heterotrophic microbes in the cycling of organic matter in deep-sea sediments. *Marine Biology Research*, *7*, 629–636

Rowe, G. T., Elizabeth, M., Kaegi, C., Morse, J. W., Boland, G. S., Briones, E. G. E., & Gregory, S. (2013). Sediment Community Metabolism Associated with Continental Shelf Hypoxia , Northern Gulf of Mexico. *Deep Sea Research Part II*, *26*(6), 1097–1106.

Rowland, S., Donkin, P., Smith, E., & Wraige, E. (2001). Aromatic hydrocarbon “humps” in the marine environment : unrecognized toxins ? *Environmental Science & Technology*, *35*(13), 2640–2644.

Ruhl, H. A, & Smith, K. L. (2004). Shifts in deep-sea community structure linked to climate and food supply. *Science*, *305*(5683), 513–515.

Ryerson, T. B., Camilli, R., Kessler, J. D., Kujawinski, E. B., Reddy, C. M., Valentine, D. L., Atlas, E., Blake, D. R., de Gou, J., Meinardi, S., Parrish, D. D., Peischl, J., Seewald, J. S. and Warneke, C. (2012). Chemical data quantify Deepwater Horizon hydrocarbon flow rate and environmental distribution. *Proceedings of the National Academy of Sciences*, *109(50),* 20246-20253.

Sala, I., Caldeira, R. M. A., Estrada-Allis, S. N., Froufe, E., & Couvelard, X. (2013). Lagrangian transport pathways in the northeast Atlantic and their environmental impact. *Limnology & Oceanography: Fluids & Environments*, *3*, 40–60.

Scarlett, A., Galloway, T. S., & Rowland, S. J. (2007a). Chronic Toxicity of Unresolved Complex Mixtures (UCM) of Hydrocarbons in Marine Sediments. *Journal of Soils and Sediments*, *7*(4), 200 – 206.

Scarlett, A., Rowland, S., Canty, M., & Smith, E. (2007b). Method for assessing the chronic toxicity of marine and estuarine sediment-associated contaminants using the amphipod *Corophium volutator*. *Marine Environmental Research*, *63*(5), 457–70.

Scarlett, A., Canty, M. N., Smith, E. L., Rowland, S. J., & Galloway, T. S. (2007c). Can amphipod behavior help to predict chronic toxicity of sediments? *Human and Ecological Risk Assessment: An International Journal*, *13*(3), 506–518.

Schaanning, M., Trannum, H., Oxnevad, S., Carroll, J., & Bakke, T. (2008). Effects of drill cuttings on biogeochemical fluxes and macrobenthos of marine sediments. *Journal of Experimental Marine Biology and Ecology*, *361*(1), 49–57.

Shafir, S., Van Rijn, J., & Rinkevich, B. (2007). Short and long term toxicity of crude oil and oil dispersants to two representative coral species. *Environmental Science & Technology*, *41*, 5571–5574.

Sherwin, T. J., & Turrell, W. R. (2005). Mixing and advection of a cold water cascade over the Wyville Thomson Ridge. *Deep Sea Research Part I: Oceanographic Research Papers*, *52*(8), 1392–1413.

Sherwin, T. J., Williams, M. O., Turrell, W. R., Hughes, S. L., & Miller, P. I. (2006). A description and analysis of mesoscale variability in the Färoe-Shetland Channel. *Journal of Geophysical Research*, *111*(C3), C03003.

Singer, M. M., Aurand, D., Bragin, G. E., Clark, J. R., Coelho, G. M., & Sowby, M. L. (2000). Standardization of the preparation and quantitation of water-accommodated fractions of petroleum for toxicity testing. *Marine Pollution Bulletin*, *40*(11), 1007–1016.

Slater, G. F., White, H. K., Eglinton, T. I., & Reddy, C. M. (2005). Determination of microbial carbon sources in petroleum contaminated sediments using molecular ^{14}C analysis. *Environmental Science & Technology*, *39*(8), 2552–2558.

Slater, G., Nelson, R., Kile, B., & Reddy, C. (2006). Intrinsic bacterial biodegradation of petroleum contamination demonstrated in situ using natural abundance, molecular-level ^{14}C analysis. *Organic Geochemistry*, *37*(9), 981–989.

Smallwood, J. R., & Kirk, W. J. (2005). Paleocene exploration in the Faroe − Shetland Channel: disappointments and discoveries. In: *Dore, A. G. and Vining, B. A. (eds) Petroleum Geology: North-West Europe and Global Perspectives—Proceedings of the 6th Petroleum Geology Conference*.

Smith, K. L., & Teal, J. (1973). Deep-sea benthic community respiration: an *in situ* study at 1850 meters. *Science*, *179*, 282–283.

Smith, K. L. Jr (1992). Benthic boundary layer communities and carbon cycling at abyssal depths in the central North Pacific. *Limnology and Oceanography*, *37*(5), 1034–1056

Smith, K.L., Kaufman, R., Baldwin, R., Carlucci, A., (2001). Pelagic–benthic coupling in the abyssal eastern North Pacific: an eight-year time-series study of food supply. *Limnology and Oceanography, 46*, 543–556.

Socolofsky, S. A., Adams, E. E., & Sherwood, C. R. (2011). Formation dynamics of subsurface hydrocarbon intrusions following the Deepwater Horizon blowout. *Geophysical Research Letters*, *38*(9), 2–7.

Sørensen, L., Melbye, A. G., & Booth, A. M. (2013). Oil droplet interaction with suspended sediment in the seawater column: Influence of physical parameters and chemical dispersants. *Marine Pollution Bulletin, 78*(1-2), 146-152.

Storkey, D., Furner, R., Lea, D., Hines, A., & Hyder, P. (2010). Forecasting the ocean state using NEMO: The new FOAM system. *Jounal of Operational Oceanography*, *3*(1), 3–16.

Sturt, H. F., Summons, R. E., Smith, K., Elvert, M., & Hinrichs, K.-U. (2004). Intact polar membrane lipids in prokaryotes and sediments deciphered by high-performance liquid chromatography/electrospray ionization multistage mass spectrometry - new biomarkers for biogeochemistry and microbial ecology. *Rapid Communications in Mass Spectrometry*, *18*(6), 617–28.

Syakti, A. D., Mazzella, N., Nerini, D., Guiliano, M., Bertrand, J. C., & Doumenq, P. (2006). Phospholipid fatty acids of a marine sedimentary microbial community in a laboratory microcosm: responses to petroleum hydrocarbon contamination. *Organic Geochemistry*, *37*(11), 1617–1628.

Sun, M.-Y., Aller, R. C., Lee, C., & Wakeham, S. G. (1999). Enhanced degradation of algal lipids by benthic macrofaunal activity: Effect of *Yoldia limatula*. *Journal of Marine Research*, *57*(5), 775–804.

Teece, M. A., Fogel, M. L., Dollhopf, M. E., & Nealson, K. H. (1999). Isotopic fractionation associated with biosynthesis of fatty acids by a marine bacterium under oxic and anoxic conditions. *Organic Geochemistry*, *30*(12), 1571–1579.

Thornton, B., Zhang, Z., Mayes, R. W., Högberg, M. N., & Midwood, A. J. (2011). Can gas chromatography combustion isotope ratio mass spectrometry be used to quantify organic compound abundance? *Rapid Communications in Mass Spectrometry*, *25*(17), 2433–2438.

Trannum, C., Setvik, Å., Norling, K., & Nilsson, H. (2011). Rapid macrofaunal colonization of water-based drill cuttings on different sediments. *Marine Pollution Bulletin*, *62*(10), 2145–2156.

Trannum, H. C., Nilsson, H. C., Schaanning, M. T., & Øxnevad, S. (2010). Effects of sedimentation from water-based drill cuttings and natural sediment on benthic macrofaunal community structure and ecosystem processes. *Journal of Experimental Marine Biology and Ecology*, *383*(2), 111–121.

Trannum, H. C., Nilsson, H. C., Schaanning, M. T., & Norling, K. (2011). Biological and biogeochemical effects of organic matter and drilling discharges in two sediment communities. *Marine Ecology Progress Series*, *442*, 23–36.

Turrell, W. R., Slesser, G., Adams, R. D., Payne, R., & Gillibrand, P. A. (1999). Decadal variability in the composition of Faroe Shetland Channel bottom water. *Deep Sea Research Part I: Oceanographic Research Papers*, *46*(1), 1–25.

Valentine, D. L., Kessler, J. D., Redmond, M. C., Mendes, S. D., Heintz, M. B., Farwell, C., Hu, L., Kinnaman, F. S., Yvon-Lewis, S., Mengran, D., Chan, E. W., Garcia Tigreros, F. & Villanueva, C. J. (2010). Propane respiration jump-starts microbial response to a deep oil spill. *Science*, *330*, 208–211.

Valentine, D. L., Mezic, I., Macesic, S., Crnjaric-Zic, N., Ivic, S., Hogan, P. J., Fonoberov, V. A. & Loire, S. (2012). Dynamic autoinoculation and the microbial ecology of a deep water hydrocarbon irruption. *Proceedings of the National Academy of Sciences*, 1–6.

Valentine, D. L., Fisher, G. B., Bagby, S. C., Nelson, R. K., Reddy, C. M., Sylva, S. P., and Woo, M. A. (2014) Fallout plume of submerged oil from *Deepwater Horizon Proceedings of the National Academy of Sciences, 111 (45) 15906-15911.*

Van Nugteren, P., Herman, P. M. J., Moodley, L., Middelburg, J. J., Vos, M., & Heip, C. H. R. (2009). Spatial distribution of detrital resources determines the outcome of competition between bacteria and a facultative detritivorous worm. *Limnology and Oceanography*, *54*(5), 1413–1419.

Van Weering, T., Hall, I., de Stigter, H., McCave, I., & Thomsen, L. (1998). Recent sediments, sediment accumulation and carbon burial at Goban Spur, N. W. European continental margin (47 – 50 ° N). *Progress in Oceanography*, *42*, 5–35.

Vevers, W. F., Dixon, D. R., & Dixon, L. R. J. (2010). The role of hydrostatic pressure on developmental stages of *Pomatoceros lamarcki* (Polychaeta : Serpulidae) exposed to water accommodated fractions of crude oil and positive genotoxins at simulated depths of 1000 – 3000 m. *Environmental Pollution*, *158*(5), 1702–1709.

Wacogne, S. (1989). On the difference in strength between Atlantic and Pacific undercurrents. *Journal of Physical Oceanography*, *20*, 792–799.

Wells, P., & Sprague, J. (1976). Effects of crude oil on American lobster (*Homarus americanus*) larvae in the laboratory. *Journal of the Fisheries Research Board of Canada*, *33*(7), 1604–1614.

Werner, I., & Nagel, R. (1997). Stress proyteins hsp60 and hsp70 in three species of amphipods exposed to cadmium, diazinon, dieldrin and fluoranthene. *Environmental Toxicology and Chemistry*, *16*(11), 2393–2403.

White, D. C., Davis, W. M., Nickels, J. S., King, J. D. & Bobbie, R. J. (1979) Determination of the sedimentary microbial biomass by extractable lipid phosphate. *Oecologia, 40*, 51 – 62.

White, H. K., Hsing, P.-Y., Cho, W., Shank, T. M., Cordes, E. E., Quattrini, A. M., Nelson, R. K., Camilli, R., Demopolous, A. W. J., German, C. R., Brooks, J. M., Roberts, H. H., Shedd, W., Reddy, C. M. & Fisher, C. R. (2012). Impact of the Deepwater Horizon oil spill on a deep-water coral community in the Gulf of Mexico. *Proceedings of the National Academy of Sciences*, 109(50), 20303-20308 .

Widdows, J., Donkin, P., Brinsley, M. D., Evans, S. V, Salkeld, P. N., Franklin, A., Law, R. J. & Waldock, M. J. (1995). Scope for growth and contaminant levels in North Sea mussels *Mytilus edulis*. *Marine Ecology Progress Series*, *127*, 131–148.

Witte, U., Aberle, N., Sand, M., & Wenzhöfer, F. (2003). Rapid response of a deep-sea benthic community to POM enrichment: an in situ experimental study. *Marine Ecology Progress Series*, *251*, 27–36.

Woese, C. R., & Fox, G. E. (1977). Phylogenetic structure of the prokaryotic domain: The primary kingdoms. *Proceedings of the National Academy of Sciences*, *74*(11), 5088–5090.

Word, J. Q. 1979. The infaunal trophic index. Pages 19–41 *in* Annual Report 1978 Southern California Coastal Water Research Project, Los Angeles, California, USA.

Yakimov, M. M., Timmis, K. N., & Golyshin, P. N. (2007). Obligate oil-degrading marine bacteria. *Current Opinion in Biotechnology*, *18*(3), 257–66.

Yapa, P. D., Dasanayaka, L. K., Bandara, U. C. & Nakata, K. (2008). Modeling the Impact of an Accidental Release of Methane Gas in Deepwater. *Oceans 2008. 15-18 Sept 2008*, 1–10.

Yardley-Jones, A., Anderson, D., & Parke, D. V. (1991). The toxicity of benzene and its metabolism and molecular pathology in human risk assessment. *British Journal of Industrial Medicine*, *48*, 437–444.

Yool, A., Oschlies, A., Nurser, a. J. G., & Gruber, N. (2010). A model-based assessment of the TrOCA approach for estimating anthropogenic carbon in the ocean. *Biogeosciences*, *7*(2), 723–751.

Yool, A., Popova, E., Coward, A., Bernie, D., & Anderson, T. (2013). Climate change and ocean acidification impacts on lower trophic levels and the export of organic carbon to the deep ocean. *Biogeosciences*, *10*, 5831–5854.

Zelles, L., Bai, Q., Beck, T., & Beese, F. (1992). Fatty acid patterns of phospholipids and lipopolysaccharides in the characterisation of microbial communities in soil: a review. *Soil Biology and Biochemistry*, *24*(4), 317–323.

Zelles, L. (1999). Fatty acid patterns of phospholipids and lipopolysaccharides in the characterisation of microbial communities in soil: a review. *Biology and Fertility of Soils*, *29*(2), 111–129.

Ziervogel, K., Joye, S. B., & Arnosti, C. (2014). Microbial enzymatic activity and secondary production in sediments affected by the sedimentation pulse following the Deepwater Horizon oil spill. *Deep Sea Research Part II: Topical Studies in Oceanography*, 1–8.

Zink, K.-G., & Rabus, R. (2010). Stress-induced changes of phospholipids in betaproteobacterium *Aromatoleum aromaticum* strain EbN1 due to alkylbenzene growth substrates. *Journal of Molecular Microbiology and Biotechnology*, *18*(2), 92–101.

Zuur, A. F., Ieno, E. N., and Smith, G. M. (2007) *Analysing Ecological Data (statistics for biology and health).* Springer. 672pp.

Zuur, A. F., Ieno, E. N., Walker, N. and Saveliev, A. A. (2009) *Mixed effects models and extensions in ecology with R (statistics for biology and health).* Springer. 574pp.

Zuur, A. F., Ieno, E. N., & Elphick, C. S. (2010). A protocol for data exploration to avoid common statistical problems. *Methods in Ecology and Evolution*, *1*(1), 3–14.

Zyakun, A., Nii-Annang, S., Franke, G., Fischer, T., Buegger, F., & Dilly, O. (2012). Microbial Activity and ^{13}C / ^{12}C Ratio as Evidence of N- Hexadecane and N-Hexadecanoic Acid Biodegradation in Agricultural and Forest Soils. *Geomicrobiology Journal*, *28*(7), 632-647.